RV SONNE
CRUISE REPORT SO143

TECFLUX - I - 1999
TECTONICALLY-INDUCED MATERIAL FLUXES

HONOLULU - ASTORIA - SAN DIEGO
JUNE 29 - SEPTEMBER 6, 1999

Leg SO143-1a: Honolulu - Astoria
June 29 - July 12, 1999

Leg SO143-1b: Astoria - Astoria
July 14 - July 30, 1999

Leg SO143-2: Astoria - Astoria
July 31 - August 25, 1999

Leg SO143-3: Astoria - San Diego
August 26 - September 6, 1999

Edited by
Gerhard Bohrmann, Peter Linke, Erwin Suess, and Olaf Pfannkuche
with contributions of cruise participants

Table of Contents

Preface

E. Suess, G. Bohrmann, P. Linke, O. Pfannkuche

The TECFLUX program (= TECtonically induced FLUXes) addresses geophysical, biogeochemical, and hydrographic processes associated with fluid venting from the Cascadia continental margin, specifically the processes resulting from the methane hydrate dynamics at Hydrate Ridge. An international group of scientists from institutions in Germany, the USA, Canada, and Japan (Table 1 and list of Participating Institutions) established a long-term research program based on the initial discovery in 1996 of methane hydrate exposures. At this margin site mixed methane-sulfide hydrates and carbonates form a pavement along the crest of the ridge at water depths between 600–1000 m. Vent fields from which methane-charged, low-salinity fluids containing sulfide, ammonia, ^{4}He, and isotopically light CO_2 escape, are associated with these exposures. The fluid emissions characterize a newly recognized mechanism of dewatering at convergent margins. However, the rates of discharge, the fluctuations and frequency of pulses, as well as the mechanisms responsible for the modulations of flow are totally unknown. Also immediate and intriguing questions concerning the composition, depth distribution, interlayering with sediment, and physical properties of these near-surface gas hydrates were to be addressed during SO Cruise 143.

Table 1: Current Research Programs in TECFLUX.

„Geochemical Consequences of Extensive Gas Hydrate Formation in Sediments of the Cascadia Accretionary Prism" funded by NSF to M.E. Torres, J. McManus, and K. Brown

„High- Resolution Analysis of the Nature and Volume of Gas Hydrate and Carbonate Mineralization Across the Oregon Margin Accretionary Complex" funded by NSF to Ch. Goldfinger, A. Trehu, and M.E. Torres

„Chemical distributions and fluxes in the water column above an emerging hydrate field on the Cascadia accretionary prism" funded by NSF to W.R. Collier, G. Klinkhammer, and M. de Angelis

„Long-term impact of methane hydrate on the deep-sea ecosystem at the Cascadia subduction zone" funded by BMBF to E. Suess, G. Bohrmann, P. Linke, O. Pfannkuche, K. Wallmann, L. Thomsen, N. Kukowski and R. Zahn

„Developing a Paleoceanographic Tracer of Methane Venting" funded to NSF to A. Mix and M.E. Torres

Initial results suggest that hydrate-related fluid emissions lead to local dewatering rates that are much higher than at other margins in the absence of hydrate. Discharge of fluids stimulates benthic oxygen consumption that is orders of magnitude higher than is normally found at comparable ocean depths. Extensive coverage of the seafloor by bacterial mats and hydrogen sulfide immediately below the seafloor suggest an intimate relationship between hydrate exposure, fluid discharge, biological community structure and activity, and total sediment respiration. From previous

investigations (SO 110 and ROPOS) vigorous discharge of methane bubbles was observed at the northern summit of the ridge at depths where hydrates are actually stable. The injection of methane from the ridge generates a plume hundreds of meters high and several kilometers wide. A large fraction of the methane appears to be oxidized within the water column and generates $\partial^{13}C$ anomalies of the dissolved inorganic carbon pool, although it remains unclear if, where, and how much methane escapes to the atmosphere. Hence of considerable importance to the success of the SO 143 cruises were the seasonal data on methane distributions in the water column overlying Hydrate Ridge obtained during the RV WECOMA cruises (Table 2) in preceding and following the SONNE cruises.

The wide spread carbonate pavement as well as the chemoherms result from bacterial methane oxidation and subsequent precipitation of a variety of carbonate mineral phases and fabrics leading to the recognition of a class of carbonates with considerable diagnostic features related to gas hydrates. The subsurface extent of the chemoherms, the detailed petrographic, isotopic, and structural relationship of the carbonates are presently unknown but contain enough information from which -in conjunction with rates of biogeochemical turnover- a budget of past and present carbon emissions may be derived.

The project TECFLUX '99 is a multiple and interdisciplinary effort addressing these open questions resulting from the initial discovery of gas hydrate exposures. In doing so TECFLUX brings together separately funded-projects and was able to stage eight cruises between May-October of 1999 (Table 2). The following cruise report should be seen in conjunction with the report by M.E. Torres on the RV ATLANTIS Cruise AT3-35b Geochemical observations on Hydrate Ridge. During this cruise which preceded SO 143, the deep submersible ALVIN conducted 10 dives to the northern and southern summits of Hydrate Ridge. The dives provided valuable observations as did the other cruises (Table 2) for the SONNE work documented here.

Table 2: TECFLUX Expeditions in 1999.

Expedition	Date	Ports	Chief scientist
RV NEW HORIZON 1	01.06. - 11.06.	Newport - Newport	C. Goldfinger, OSU
RV NEW HORIZON 2	13.06. - 23.06.	Newport - San Francisco	B. Collier, OSU
RV ATLANTIS/ALVIN	30.06. - 13.07.	Newport - Astoria	M. Torres, OSU
FS SONNE 143-1a	29.06. - 13.07.	Honolulu - Astoria	P. Linke, GEOMAR
FS SONNE 143-1a	14.07. - 30.07.	Astoria - Astoria	E. Suess, GEOMAR
FS SONNE 143-2	31.07. - 25.08.	Astoria - Astoria	O. Pfannkuche, GEOMAR
FS SONNE 143-3	26.08. - 06.09.	Astoria - San Diego	G. Bohrmann, GEOMAR
RV WECOMA	03.10. - 07.10.	Newport - Newport	B. Collier, OSU

The expeditions and programs of TECFLUX were jointly planned, coordinated and carried out by the GEOMAR Research Centre for Marine Geosciences at Kiel and the College of Ocean and Atmospheric Sciences of Oregon State University, Corvallis with a large number of investigator groups from different institutions (see list of Participating Institutions). The projects were financed in Germany by the Federal Ministry of Science and Technlogy, Bonn and in the USA by the National Science Foundation, Washington (Table 1). Project review and scheduling of the SONNE Cruise 143 was handled efficiently by the Projektträger Biologie, Energie und Umwelt, Jülich-Warnemünde. On behalf of all participants we wish to thank these agencies, departments, and staff for their support. The Reedereigemeinschaft Forschungsschifffahrt, RF Bremen, as always, provided technical support on the vessel in order to accommodate the variety of technological, electronic, and navigational challenges required for the complex sea-going operations. We would like to especially acknowledge the vessel's masters H. Andresen (SO 143-1a/1b) and H. Papenhagen (SO 143-2 and –3) and their crews for their continued interest, flexibility, patience, and their contribution to provide an always pleasant and professional atmosphere aboard.

Scientific crew

Leg SO143-1a: 29 June – 13 July, Honolulu/Hawaii – Astoria/Oregon

Aberle, Nicole	GEOMAR Forschungszentrum, Kiel
Appel, Frank	OKTOPUS, Hohenwestedt
Bannert, Bernhard	OKTOPUS, Hohenwestedt
Bohnert, Jens	GEOMAR Forschungszentrum, Kiel
Domeyer, Bettina	GEOMAR Forschungszentrum, Kiel
Floridnova, Hana	GEOMAR Forschungszentrum, Kiel
Freyenhagen, Jörn	Journalist, Kiel
Jung, Carmen	GEOMAR Forschungszentrum, Kiel
Linke, Peter (chief scientist)	GEOMAR Forschungszentrum, Kiel
Petersen, Asmus	K.U.M. Meerestechnik GmbH, Kiel
Teichert, Barbara	GEOMAR Forschungszentrum, Kiel

Leg SO143-1b: 14 July – 29 July, Astoria/Oregon – Astoria/Oregon

Aberle, Nicole	GEOMAR Forschungszentrum, Kiel
Barrazoul, Lisa	UVIC, Victoria
Bohnert, Jens	GEOMAR Forschungszentrum, Kiel
Bollwerk, Sandra	GEOMAR Forschungszentrum, Kiel
Brooksforce, Kathryn	OSU, Corvallis
Cumberland, Bronwen	OSU, Corvallis
Domeyer, Bettina	GEOMAR Forschungszentrum, Kiel
Eisenhauer, Anton	GEOMAR Forschungszentrum, Kiel
Florianova, Hana	GEOMAR Forschungszentrum, Kiel
Heeschen, Katja	GEOMAR Forschungszentrum, Kiel
Heitmann, Birte	GEOMAR Forschungszentrum, Kiel
Heuser, Alexander	GEOMAR Forschungszentrum, Kiel

Jung, Carmen	GEOMAR Forschungszentrum, Kiel
Klinkhammer, Gary	OSU, Corvallis
Naehr, Thomas	MBARI, Moss Landing
Petersen, Asmus	K.U.M. Meerestechnik GmbH, Kiel
Prins, John C.	OSU, Corvallis
Rehder, Gregor	GEOMAR Forschungszentrum, Kiel
Rickert, Dirk	GEOMAR Forschungszentrum, Kiel
Sahling, Heiko	GEOMAR Forschungszentrum, Kiel
Suess, Erwin (chief scientist)	GEOMAR Forschungszentrum, Kiel
Teichert, Barbara	GEOMAR Forschungszentrum, Kiel
Whiticar, Michael	UVIC, Victoria

Leg SO143-2: 30 July – 25 August, Astoria/Oregon – Astoria/Oregon

Appel, Frank	GEOMAR Technologie GmbH, Kiel
Boetius, Antje	MPI, Bremen
Colbert, Steven	USC, Los Angeles
Collier, Robert (departed 19 Aug.)	OSU, Corvallis
Cremer, Axel	OKTOPUS, Hohenwestedt
Eek, Magnus	UVIC, Victoria
Getzlaff, Klaus	GEOMAR Forschungszentrum, Kiel
Gutthann, Franziska	GEOMAR Forschungszentrum, Kiel
Heeschen, Katja	GEOMAR Forschungszentrum, Kiel
Heuser, Alexander	GEOMAR Forschungszentrum, Kiel
Kähler, Anja	GEOMAR Forschungszentrum, Kiel
Linke, Peter	GEOMAR Forschungszentrum, Kiel
Meyer, Stephan	MPI, Bremen
Nakamura, Koichi	GSJ, Ibaraki
Nimser, Michael	GEOMAR Forschungszentrum, Kiel
Pfannkuche, O. (chief scientist)	GEOMAR Forschungszentrum, Kiel
Poser, Michael	GEOMAR Forschungszentrum, Kiel
Queisser, Wolfgang	GEOMAR Forschungszentrum, Kiel
Rickert, Dirk	GEOMAR Forschungszentrum, Kiel
Sahling, Jens	GEOMAR Forschungszentrum, Kiel
Schäfer, Hinrich	UVIC, Victoria
Sommer, Stefan	GEOMAR Forschungszentrum, Kiel
Treude, Tina	GEOMAR Forschungszentrum, Kiel
Tryon, Michael (arrived 19 Aug.)	SIO, La Jolla
Witte, Ursula	MPI, Bremen

Leg SO143-3: 26 August – 06 September, Astoria/Oregon – San Diego/California

Bartlett, Cindy	OSU, Corvallis
Bohrmann, G. (chief scientist)	GEOMAR Forschungszentrum, Kiel
Bracker, Eggo	GEOMAR Forschungszentrum, Kiel
Domeyer, Bettina	GEOMAR Forschungszentrum, Kiel
Elvert, Marcus	GEOMAR Forschungszentrum, Kiel
Fausten, Armin (departed 30 Aug.)	Kick Film, Berlin
Goergens, Rainer	BGR, Hannover

Hohenberg, Hans-Jürgen	TU Berlin, Berlin
Johnson, Joel	OSU, Corvallis
Jung, Carmen	GEOMAR Forschungszentrum, Kiel
Kawohl, Helmut	BGR, Hannover
Klaus, Oliver	GEOMAR Forschungszentrum, Kiel
Kopf, Achim	Géosciences Azur, Villefranche s/Mer
Kudraß, Hermann	BGR, Hannover
Kukowski, Nina	GFZ, Potsdam
Rickert, Dirk (departed 30 Aug.)	GEOMAR Forschungszentrum, Kiel
Steinmetz, Marc (departed 30 Aug.)	MARE, Hamburg
Stüber, Arndt	GEOMAR Forschungszentrum, Kiel
Stuckmann, Harald (departed 30 Aug.)	Kick Film, Berlin
Surberg, Regina	GEOMAR Forschungszentrum, Kiel
Suttinger, Manfred (departed 30 Aug.)	Kick Film, Berlin
Teichert, Barbara	GEOMAR Forschungszentrum, Kiel
Weinrebe, Reimer	GEOMAR Forschungszentrum, Kiel
Worm, Thomas (departed 30 Aug.)	MARE, Hamburg

Reedereigemeinschaft Forschungsschiffahrt GmbH, Bremen

Personnel aboard RV SONNE during Cruise 143

Leg SO143-1a/b	Leg SO143-2	Leg SO143-3
Andresen, Hartmut, Master	Angermann, Rudolf	Angermann, Rudolf
Bochnik, Eberhard G.	Baschek, Walter	Baschek, Walter
Bosselmann, Norbert M.	Bochnik, Eberhard G.	Blohm, Volker
Buxel, Heiko X.	Boldt, Harald	Bochnik, Eberhard G.
Cwienk, Adolf P.	Bosselmann, Norbert M.	Boldt, Harald
Dracopoulos, Eugenius	Buxel, Heiko X.	Bosselmann, Norbert M.
Duthel, Rainer	Cwienk, Adolf P.	Braatz, Willy
Eller, Peter	Drakopoulos, Evgenios	Buxel, Heiko X.
Freitag, Rudolf	Evers, Fridtjof	Evers, Fridtjof
Grund, Helmut F.	Grund, Helmut F.	Grund, Helmut F.
Hasler, Justine	Hasler, Justine	Hasler, Justine
Hermann, Klaus Otto	Hermann, Klaus Otto	Hermann, Klaus Otto
Horzella, Ernst	Horzella, Ernst	Hoffmann, Werner M.
Jahns, Winfried	Klein, Andreas	Horzella, Ernst
Klein, Andreas	Konrath, Rolf	Kähler, Erhard
Köthe, Wolfgang	Meyer, Helmut S.	Klein, Andreas
Mallon, Lutz	**Papenhagen, Henning, Master**	Konrath, Rolf
Meyer, Helmut	Röpti, Hermann H.	Meyer, Helmut S.
Prinz, Udo	Rost, Peter	**Papenhagen, Henning, Master**
Röpti, Hermann	Scheller, Werner	Röpti, Hermann H.
Schrapel, Andreas M. K.	Schrapel, Andreas M.K.	Rost, Peter
Sebastian, Frank	Sebastian, Frank	Scheller, Werner
Siewert, Manfred O.G.	Siewert, Manfred O.G.	Schrapel, Andreas M.K.
Stängl, Günter M.	Sosnowski, Werner	Sebastian, Frank
Stammer, Kurt R.	Stammer, Kurt R.	Sosnowski, Werner
Szymanski, Leszek T.	Stängl, Günter M.	Stammer, Kurt R.
Thaysen, Uwe	Szymanski, Leszek T.	Stängl, Günter M.
Tscharntke, Rudolf	Thaysen, Uwe	Szymanski, Leszek T.
Vor, Hans-Jürgen	Tscharntke, Rudolf	Thaysen, Uwe
Walther, Anke	Vor, Hans-Jürgen	Tscharntke, Rudolf

Participating institutions

GEOMAR Forschungszentrum für marine
Geowissenschaften der Christian-Albrechts-
Universität zu Kiel
Wischhofstraße 1-3
24148 Kiel, Germany

College of Oceanic and Atmospheric Sciences
Oregon State University
Ocean Admin. Bldg. 104
Corvallis, Oregon 97331-5503
U.S.A.

School of Earth and Ocean Sciences
University of Victoria
P.O. Box 3050
Victoria, BC
V8W 2Y2, Canada

Marine Geology Department
Geological Survey of Japan
1-1-3 Higashi
Tsukuba, Ibaraki 305, Japan

Monterey Bay Aquarium Research Institute
7700 Sandholdt Road
Moss Landing, California 95039, U.S.A.

Scripps Institutions of Oceanography
University of California at San Diego
La Jolla, California 92093-0220, U.S.A.

Departement of Earth Sciences
University of Southern California
Los Angeles, California 90089-0742, U.S.A

Geoforschungszentrum-Potsdam
Telegrafenberg
14473 Potsdam, Germany

Technische Universität Berlin
Maritime Technik
Müller-Breslau-Str.
10623 Berlin, Germany

K.U.M. Umwelt- und Meerestechnik Kiel GmbH
Wischhofstraße 1-3, Geb. D5
24148 Kiel, Germany

Bundesanstalt für Geowissenschaften und
Rohstoffe
Stilleweg 2
30161 Hannover, Germany

OKTOPUS GmbH
Kieler Straße 51
24594 Hohenweststedt, Germany

Géosciences Azur
BP 48
Quai de la Darse
06235 Villefranche-sur-Mer Cédex, France

Max Planck Institut für Marine Mikrobiologie
Celsiusstr.1
28359 Bremen, Germany

Kick Film
Otto-Suhr-Allee 59
10585 Berlin-Charlottenburg, Germany

MARE, Dreiviertel Verlag GmbH
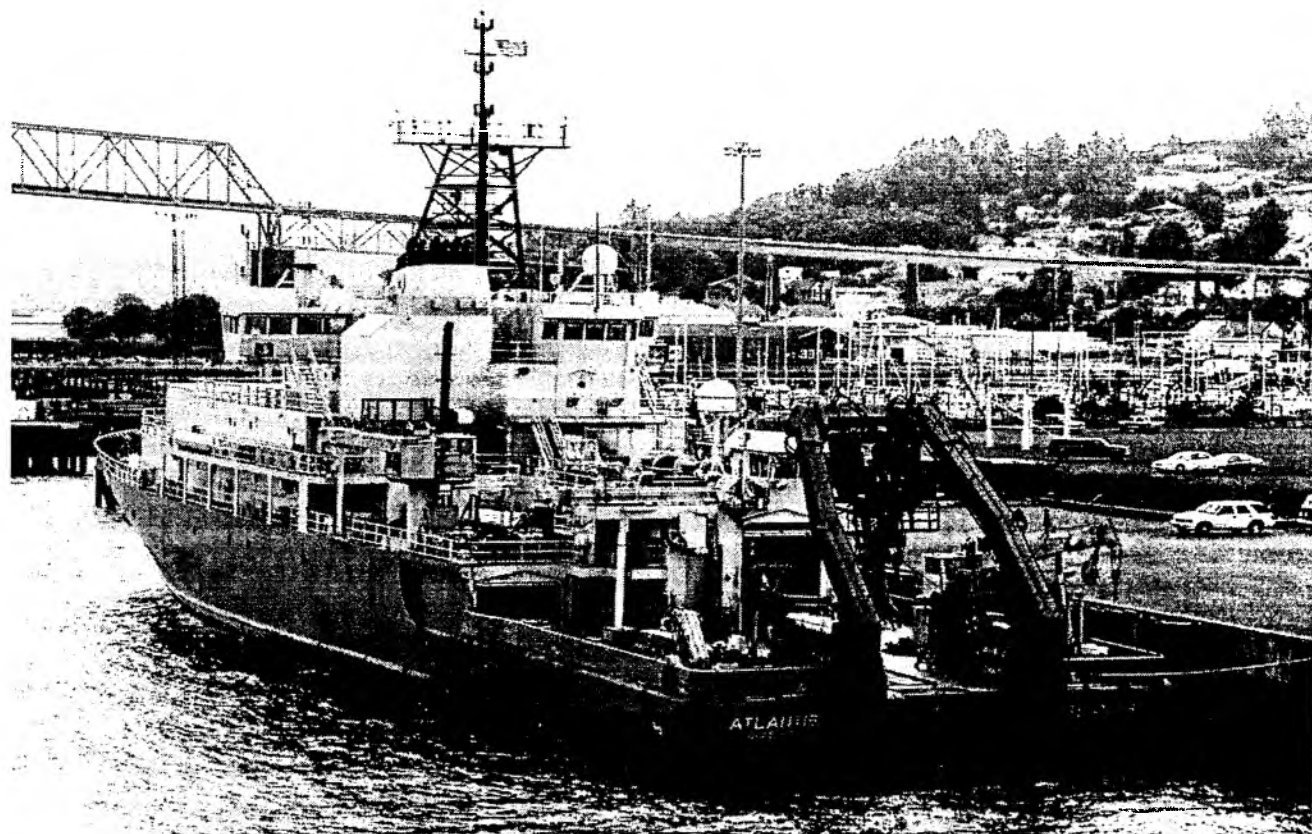Am Sandtorkai 1
20457 Hamburg, Germany

Fig.1: RV ATLANTIS (above) and RV SONNE (below).

1 Introduction

E. Suess

1.1 Objectives

On the crest of Hydrate Ridge, vent fields, extensive communities of vent biota, methane hydrate exposures, and authigenic carbonates were discovered in 1996 (Suess et al., 1996; 1999; Bohrmann et al., 1998; Trehu et al., 1999). Water depth and temperature place these hydrate occurrences close to their stability limit, hence minor changes in environmental parameters along the tectonically active margin may release large quantities of methane and hydrate water. Portions of the methane are injected into the water column to form extensive plumes. The behavior of methane plumes appears critical in order to evaluate how much, if any, of this potent green house gas escapes into the atmosphere. Equally, the near-surface exposure of hydrates and the venting process are important, because they provide an enormous nutrient and energy reservoir for benthic life. Efficient methane turnover by highly specialized methane-oxidizing communities at the seafloor coupled to microbial sulfate reduction generate wide-spread authigenic carbonates along the ridge crest.

These phenomena lead to the following new general objectives which were addressed during the FS SONNE Cruise 143 as part of the TECFLUX '99 field work:

- Mapping of vent fields, carbonate pavements, and hydrate exposures for eventual regional extrapolation of total material vent transport;
- Sampling of the complete gas hydrate–pore water–sediment–carbonate system in order to characterize the major geochemical controls;
- Investigations on the biologic/oxidative erosion of exposed gas hydrates;
- Long-term recordings of fluid flow rates for the quantification of the fluid and heat budgets;
- Quantification of the benthic material turn over from selected tectonic and morphologic settings of the accretionary ridge;
- Sampling along transects crossing currently active and dead vent sites as well as "background" environments in order to establish biologic, chemical, isotopic, sedimentologic and other criteria to diagnose hydrate-driven venting;
- Evaluation of the elemental input to the bottom water via hydrate decomposition and its significance to the overall geochemical fluxes at the ocean floor;
- Assessment of the magnitude of spatial and temporal variability of hydrate decomposition and benthic fluxes.

1.2 Background

Gas hydrates are solids composed of rigid cages of water that enclose molecules of a low-weight molecular gases, mainly methane and traces of hydrogen sulfide and carbon dioxide. Natural gas hydrates of the marine environment occur within sediments and at the seafloor on continental margins worldwide where water depths exceed apprx. 500 m. Estimates on the amount of carbon contained in gas hydrates range from 10^{15} to 10^{16}

kg of carbon, such that they may constitute the largest single form of fossil fuel hydrocarbons on the planet (e.g. Kvenvolden 1995). Data on which these estimates are based include the distribution of the "bottom simulating reflector" (BSR) as evident in seismic reflection profiles (Shipley et al., 1979; Hyndman and Spence, 1992) and the approximation of the amount of methane contained in sediments exhibiting BSRs. Destabilized gas hydrate beneath the seafloor could have broad implications for regional sediment stability, as well as for global climate change. If the methane is released into the atmosphere, it's "greenhouse effect" will have a positive feedback on atmospheric warming (MacDonald, 1990: Gornitz and Fung, 1994).

A decade of research in the Cascadia convergent margin (Fig. 2) has documented active venting of fluids, gases, and gas hydrates at the seafloor. Hydrates were recognized in seismic reflection data (McKay et al., 1992; Trehu et al., 1995). Hydrates were directly sampled below the sea floor by deep sea drilling (ODP Leg 146; Kastner et al., 1995a) and from exposures at the sea floor during the FS SONNE expedition (SO110; Suess et al., 1996). The importance of hydrate dynamics on benthic fluxes and diagenetic pathways of carbon and trace elements in the Cascadia margin could ultimately shed light on broader issues such as climate-forcing on a global scale or the development of mega-slumps and slides on continental margins.

Tectonic uplift and thrusting by convergence between the Juan de Fuca and the North American plate cause thrust faults, extensional fractures, and breached folds to develop along the accretionary ridges. The faults extend through the accreted sediments to below the gas hydrate phase transition. At depth, they tap a fluid reservoir that contains in part fresh water from hydrate destabilization and free methane gas. The faults serve as conduits and channel water and methane up to the seafloor where secondary gas hydrates in equilibrium with their surrounding geochemical enviornment. The secondary hydrate exposure and vents constitute a distinct tectonically-generated deep-sea ecosystem which impacts the carbon cycle to an as yet unknown degree.

In sediments of Hydrate Ridge secondary gas hydrate occurs in layers or faults, generally oriented parallel to bedding, but sometimes cutting the bedding planes obliquely. The internal fabric of the pure hydrate shows a peculiar structure (bubble-fabric) with large pores imaging bubbles of free methane apparently frozen in place. The fabric is similar to that experimentally produced by releasing methane bubbles at depth in the ocean to form gas hydrate (Brewer et al., 1997). Thin carbonate layers are intergrown with massive hydrates; sometimes they contained casts of the characteristic bubble fabric (Bohrmann et al., 1998). Such gas hydrate cemented sediments or layers of hydrate exposed at the seafloor as well the associated carbonate crusts will act as a barrier for fluid and gas exchange or otherwise modulate transport of methane to the bottom water. Thus, hydrate composition and distribution in the sediments has a strong control on hydrologic process within accretionary margins and hence material exchange with the ocean. There is a current consensus that research on the biogeochemical processes associated with gas hydrate dynamics and fluid venting in continental margins constitutes a first order scientific objective (Suess and Thiede; eds. 1999).
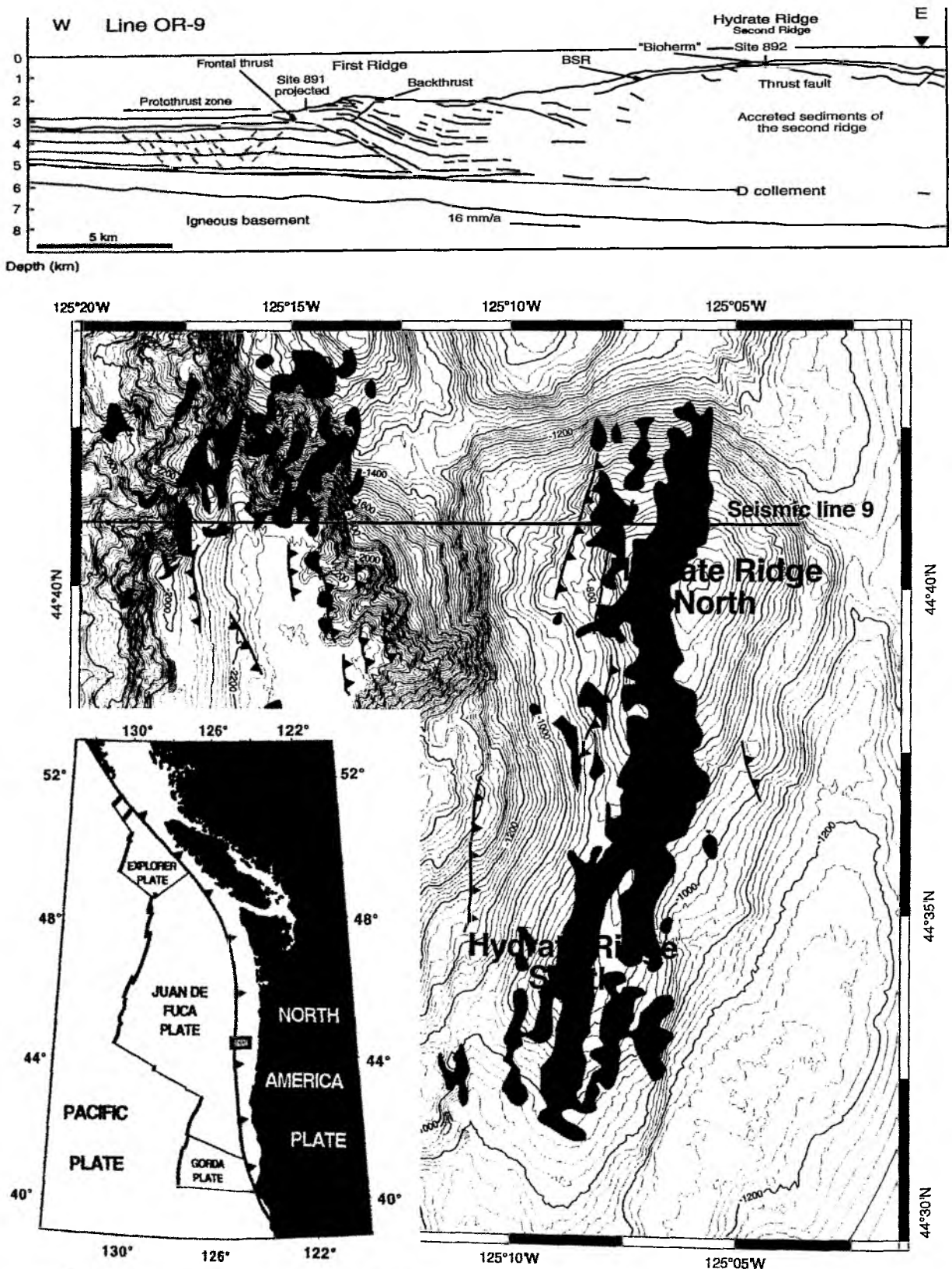
Fig. 2: Plate tectonic setting of the Cascadia convergent margin and map showing bathymetry and areas of high side-scan-sonar reflectivity at seafloor (from Carson et al. 1994); on top line drawing of seismic profile 9 crossing first and second Ridge which is known as Hydrate Ridge.

1.3   Methane hydrates and their manifestations at Hydrate Ridge

The pavement on Hydrate Ridge was imaged by a video-survey during the FS SONNE cruises SO109 and SO110 and then sampled by TV-guided grab at the northern and the southern summits. Massive hydrate was observed just beneath the smooth, thinly sediment-covered surface or occurred in tensional fractures between blocks of the chemoherm carbonates. The formation of a secondary hydrogen sulfide-containing hydrate near the sediment/water interface has previously been described, but the properties of this secondary hydrate, i.e. its fabric, trace gas content, isotope signature of water and gas, and its seawater salt inclusions are poorly known but could provide a spectrum of environmental indicators.

These indicators can be applied for environmental characterization if it can be shown that the hydrate phases co-exist and equilibrate with their immediate chemical and physical environment.   Geochemical and isotopic work on hydrates recovered during SO143 would provide a major step towards this objective.

Side-scan sonar survey of the area (RV New Horizon 1; 1-11 June 1999; Table 2) showed that the ridge flank, the saddle, and crestal region are covered by acoustically hard, highly reflective materials. In addition several targets were identified, either as "white spots", "scars", "pock marks" or "mud volcanoes", which indicated anomalous environments or manifestations of hydrates and fluid venting. Particularly in the eastern basin, at considerable distance from Hydrate Ridge,"anomalous acoustic patches" of unknown origin characterize the sea floor images obtained by side-scan sonar.

Several of these targets were investigated by DSV ALVIN (RV ATLANTIS 35b; 30 June – 13 July, Table 2); i.e. documentation by DSV ALVIN showed an enormous carbonate chimney (50 m high; 100 x 100 m at the base) near the southern summit and vigorous methane bubble escaping on both summits. Previously we had assumed that the entire high reflectivity area delimits the extent of a large mixed carbonate-hydrate pavement but the relative distribution of hydrate and carbonate and the relationship between tectonics and vigorous venting remained to be determined during SO143.

1.4   Flux rates and effects on water column chemistry

Immediately preceding FS SONNE cruises 143, DSV ALVIN surveyed and sampled active gas vents and deployed a variety of in situ instruments designed to measure fluid flux rates. The deployment of vent samplers was at the northern and southern summit. Hydro-acoustic imaging of plumes from RV ATLANTIS (35b) showed for the first time a strong tidal signal related to plume intensities. This information served as the basis for hydro-acoustic, hydrostatic pressure, bottom current surveys (RV NEW HORIZON 2; 13-26 June, Table 2) and also for the first time of continuous deployment of methane sensors. The data were complemented by hydrocast samples taken over the active vent fields for calibration of the continuously recorded data. Injection of methane-charged fluids from vents at the summit of the gas hydrate ridge generates a plume hundreds of meters high and several kilometers wide. The mechanism for transport of gases through

the methane stability zone is, at present, not clearly understood and remains to be solved during SO143.

The implications of injection of methane from vents for the carbon budget and carbon isotope inventory of the water column is profound. Previous data from CTD-casts show a significant decrease in the $\delta^{13}C_{DIC}$, and a small increase in the dissolved inorganic ΣCO_2, both of which may be derived from vent water injection, either by in situ oxidation of vent methane or the concurrent injection of dissolved ΣCO_2 from vents, or both. This question is to be pursued during SO143.

1.5   Enhanced benthic turnover

The biogeochemical reactions at the sediment-water interface are stimulated by the injection of reduced chemical species, i.e. methane, hydrogen sulfide, and ammonia. Their oxidation requires oxygen that far exceeds the sediment oxygen demand normally recorded at the deep seafloor. From previous VESP-deployment time-dependent changes of dissolved reduced species from the vent water could be related to decrease in bottom water oxygen. The overall stoichiometry and rates of the oxidation reactions and material fluxes was derived from the initial decrease in oxygen and the increase in reduced chemical species. So far we found a very close agreement between the stoichiometric oxygen demand (-1600 ± 300 mmol m^{-2} d^{-1}) and the combined oxidation equivalents needed to consume all reduced species; i.e. the sum of CH_4, H_2S, and NH_4 emitted. For comparison the sediment oxygen demand for the deep-sea is > 10,000-times lower. The reactor for this process is the benthic interface of as yet unknown thickness, but most probably including free bottom water as well. This interface is populated by macro- and micro-organisms which, either free-living or in symbiosis, efficiently sweep out the sulfide, ammonia and methane by utilizing bottom water oxygen. The rate of turnover by benthic communities at the hydrate vents is a first order objective of the FS SONNE cruises 143.

1.6   Carbonate mineral formation

Authigenic carbonates derived from methane-carbon are most likely responsible for the large areal coverage of the carbonate chemoherm on the crest of Hydrate Ridge. An important previous finding is that the rapid oxidation of chemical species is coupled to the precipitation of calcium carbonate. This reaction fixes considerable amounts of methane-carbon at the sediment-water interface. The chemoherm that forms on top of Hydrate Ridge is such a residual methane-carbon sink. It represents an as yet unknown portion of the total hydrate-generated methane-carbon flux from venting. There is a feed-back between tectonic convergence, uplift of accretionary ridges, discharge of methane from destabilized hydrate, and the magnitude of carbonate formation. Such a feed-back has implications for the modulation of greenhouse gases emitted globally from active margins. The history of formation of the carbonate cap as seen on Hydrate Ridge records this feed-back relationship over geologic time. This question will be pursued during FS SONNE cruises 143.

2   Leg SO143-1a/b: HONOLULU – ASTORIA (29 June – 29 July)

2.1   Cruise narrative Leg SO143-1

The cruise tracks and ports of operation are shown in Fig. 3; underway to and from the area of investigation only data for multi-beam surveys were collected and no station work performed.
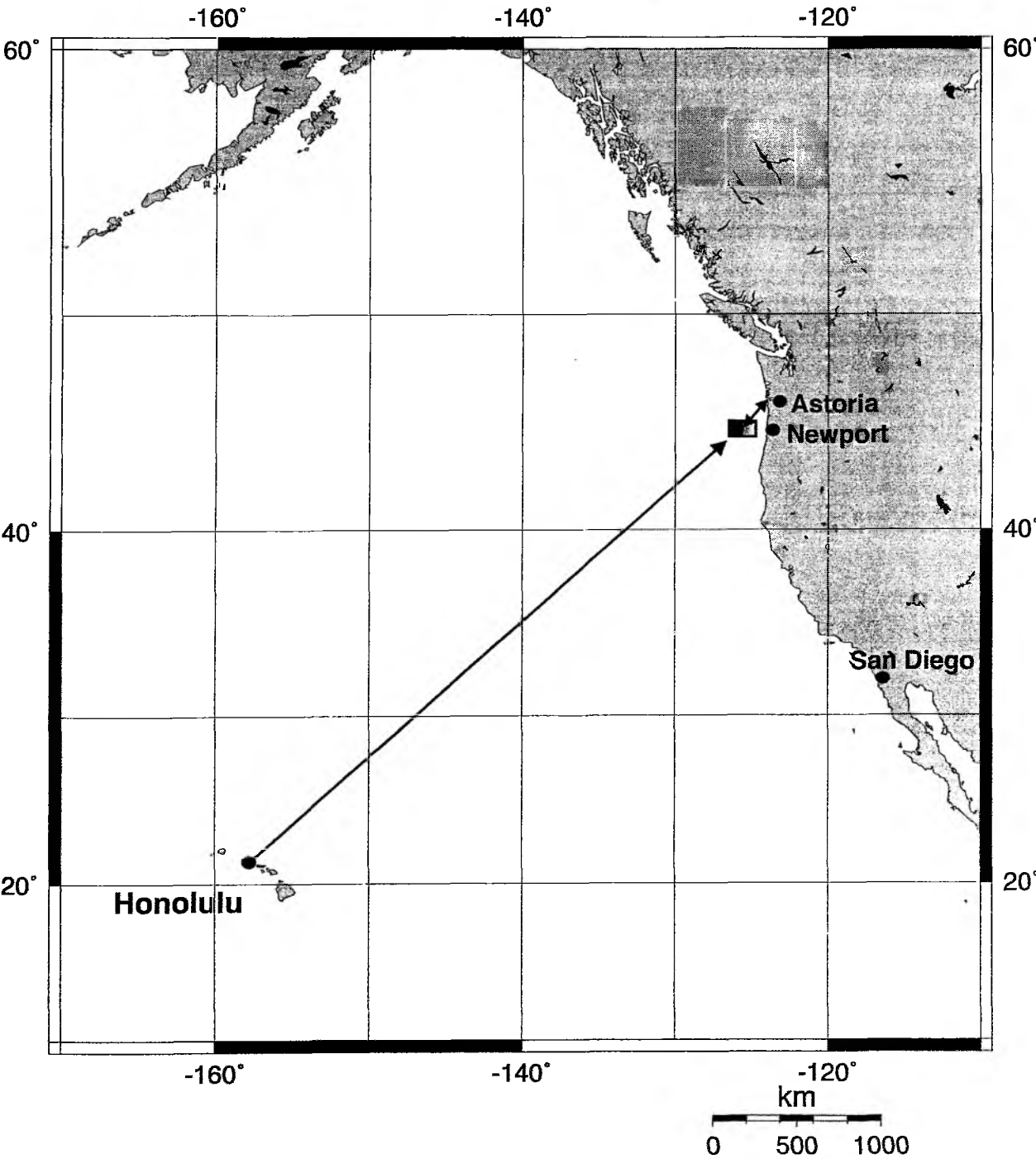
Fig. 3: Cruise tracks and working area of SO143-1 (29 June – 30 July 1999).

The areas selected for the specific objectives of the SONNE-work are shown separately for Leg SO143-1 (Fig. 4). In order to facilitate orientation and station/profile identification these selected areas for Leg 143-1 were asigned descriptive names and are shown as individual maps as follows:

> Fig. 4 A: Seismic line 100 map
> Fig. 4 B: BSR-outcrop map
> Fig. 4 C: Northwest knoll map
> Fig. 4 D: Northern summit map
> Fig. 4 E: Mud mound north map
> Fig. 4 F: Mud mound central map
> Fig. 4 G: Southern summit map
> Fig. 4 H: Southeast patch map
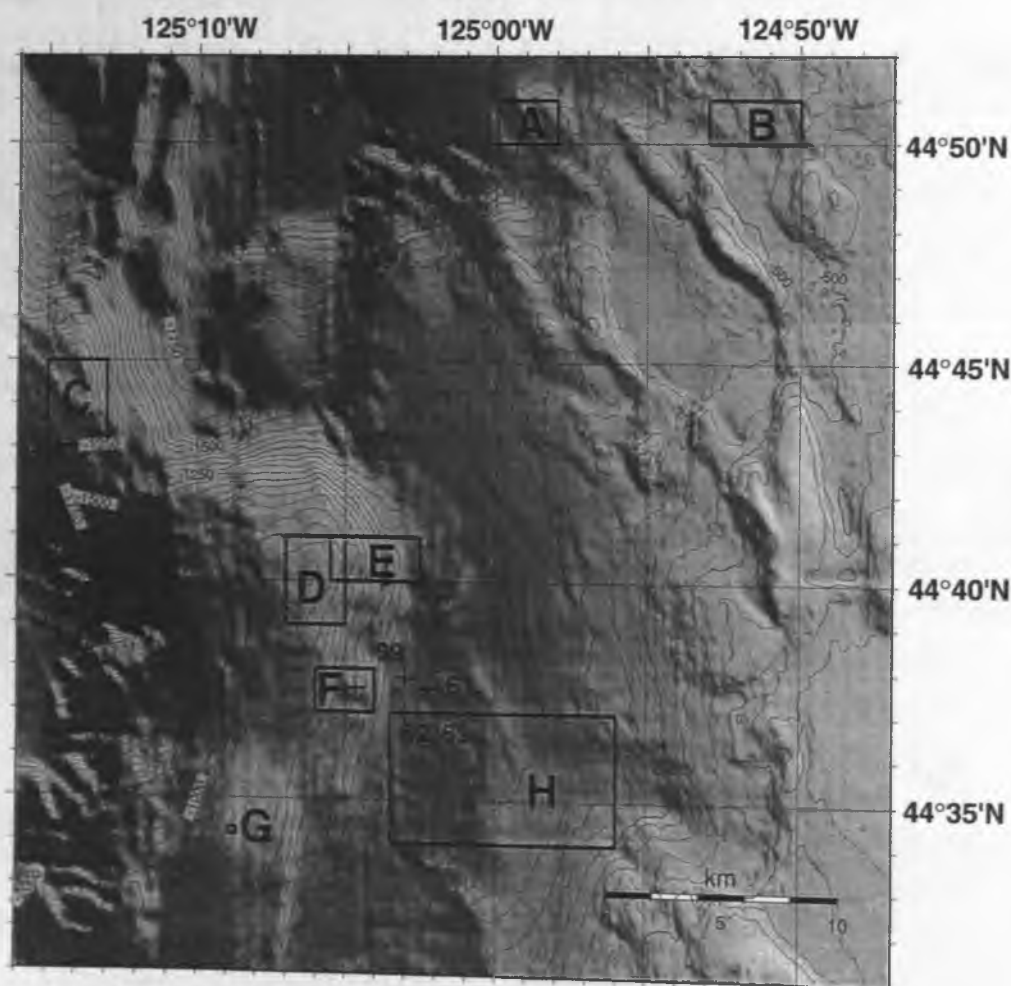
Fig. 4: Map of the research area; boxes cover areas of individual maps.

Fig. 4 A: Seismic line100
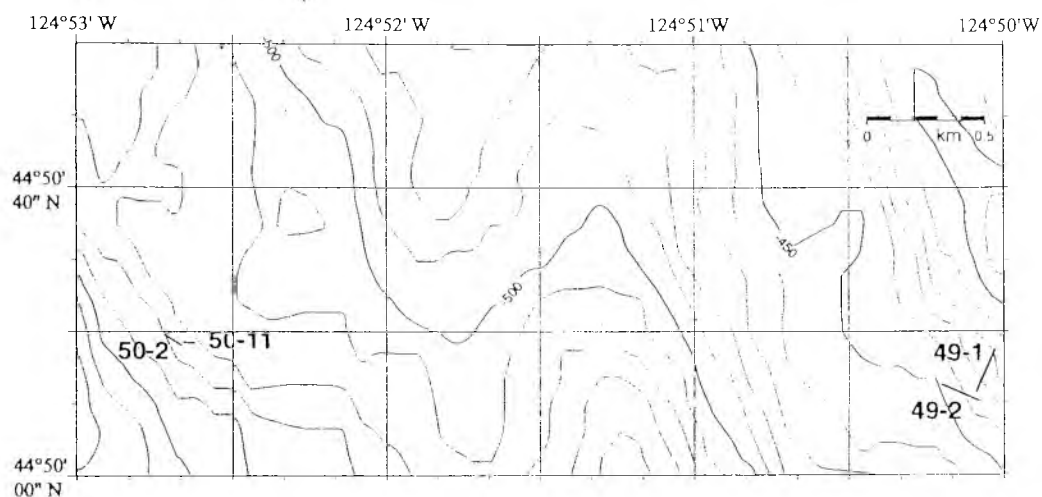
Fig. 4 B: BSR-outcrop
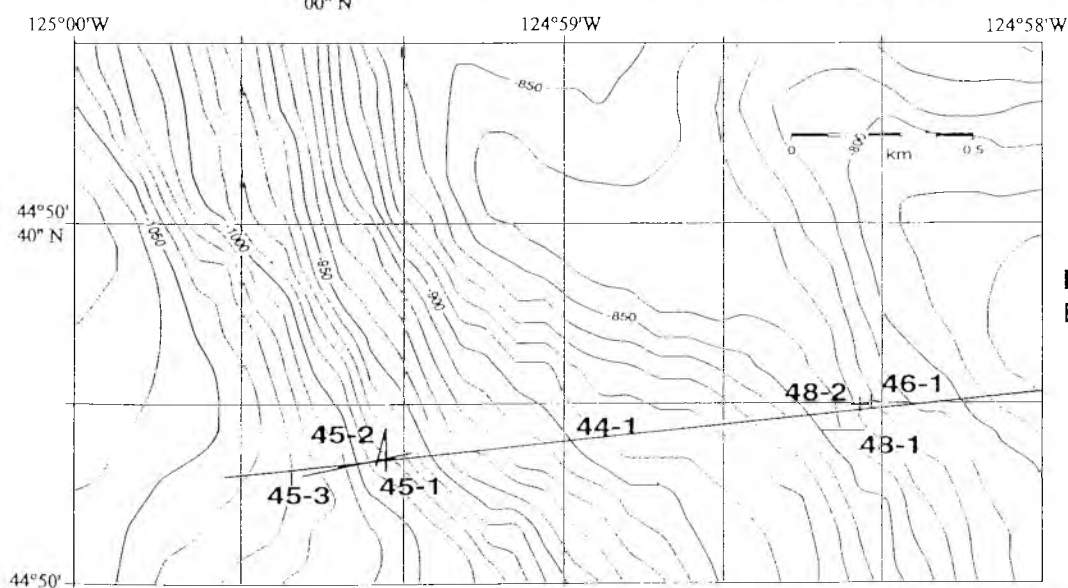
Fig. 4 C: Northwest knoll
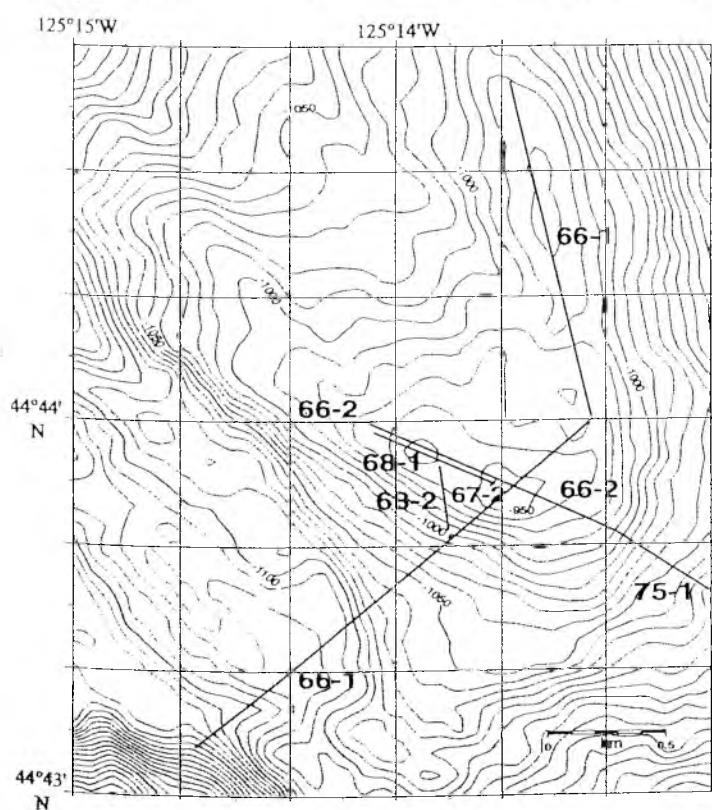
Fig. 4 D: Northern summit
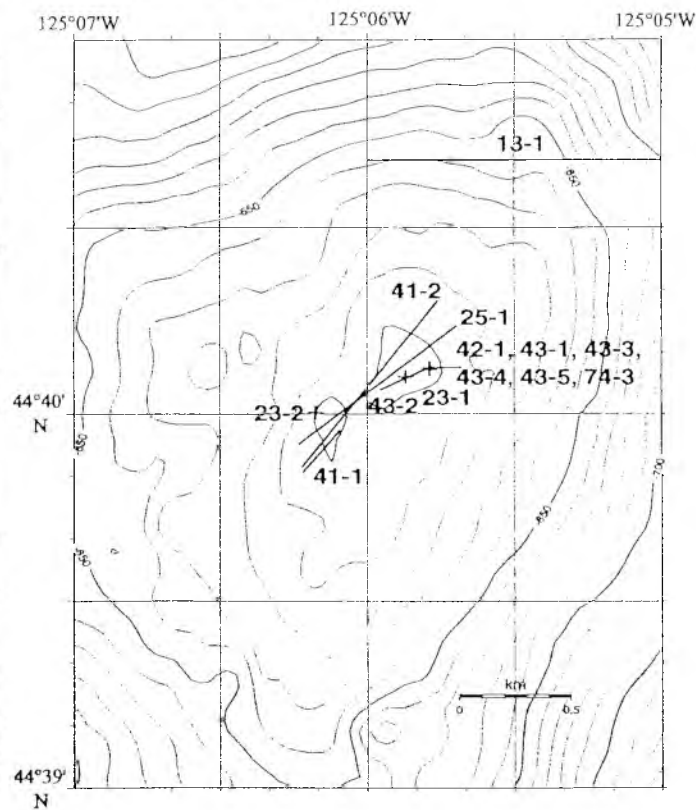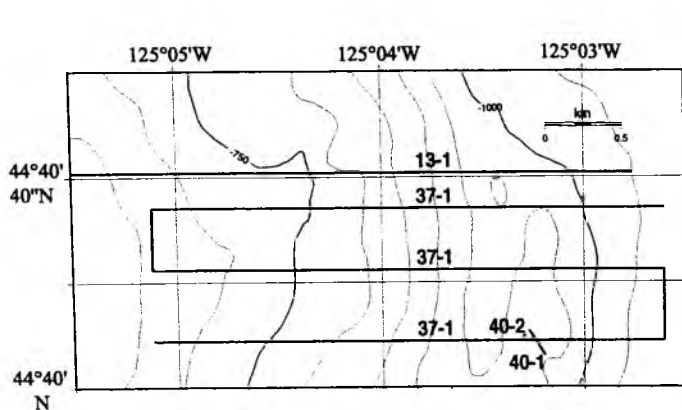
Fig. 4 E: Mud mound north
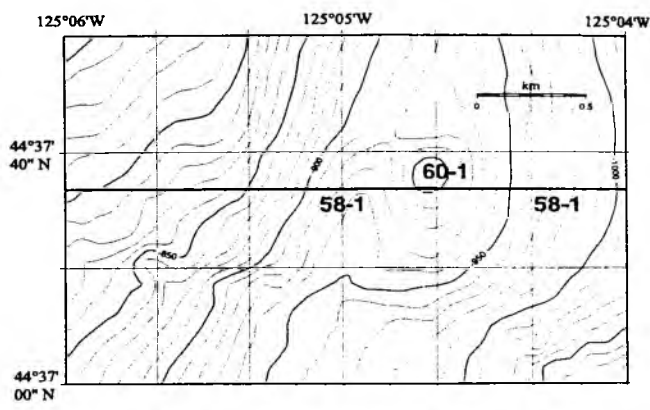
Fig. 4 F: Mud mound central
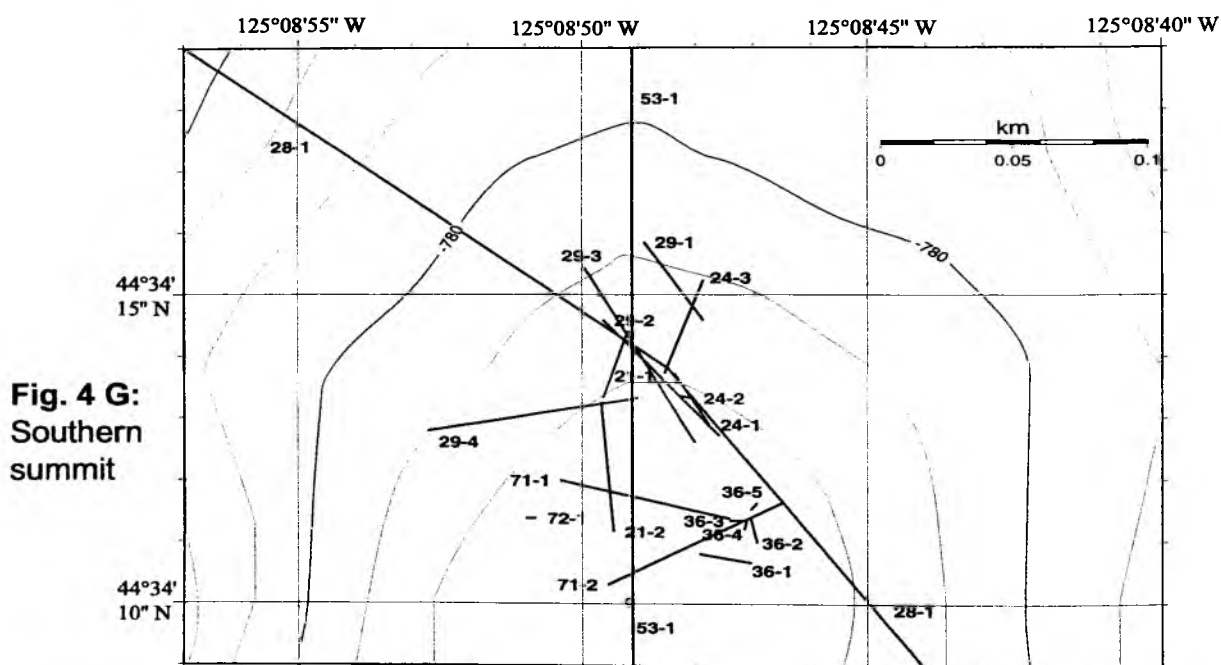
Fig. 4 G: Southern summit
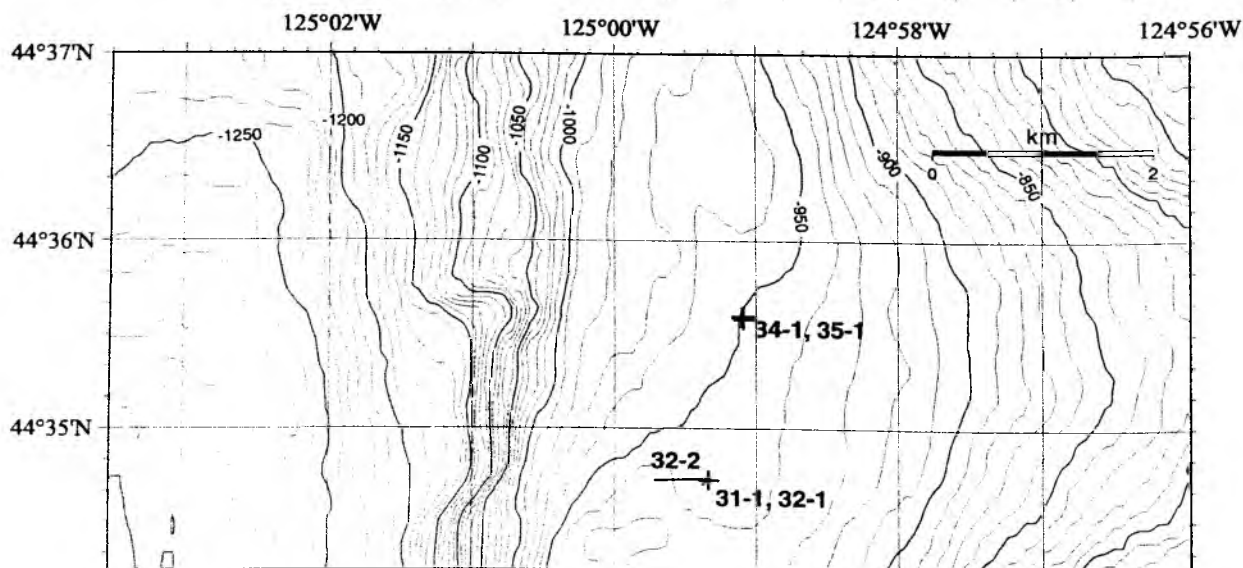
Fig. 4 H: Southeast patch

2.1.1   Leg SO143-1a: 28 June – 30 July 1999, Honololu – Astoria

P. Linke

On June 28, 10:00 RV SONNE departed Honolulu after loading containers and fuel to start transit to the working area at the Cascadia margin off Oregon (Fig. 3). During transit laboratories and complex sampling instruments were readied. The latter consist of a video-guided multiple corer, VESP, and two VESP-lander which will be deployed for several weeks as a long-term observatory by a video-guided laucher on a suspected seep site. On July 7 close to midnight, RV SONNE reached the working area where RV ATLANTIS was conducting the ALVIN dive program (RV ATLANTIS 35b; 30 June – 13 July, Table 2). Radio communication was used for coordination of the working schedules during day and night to optimize the capabilities of the both vessels. RV SONNE started with a CTD-cast to calibrate the hydro-acoustic measurements with the actual sound velocity. During the following nights Hydrosweep and Parasound mapping was used to fill the gaps of the mapping conducted in 1996.

On July 8, an OFOS track on the seismic line 100 traversing a BSR-outcrop (Fig. 4B) was conducted which revealed carbonate rock, clam fields and bacterial mats. After this profile, the 2 VESP-landers were tested and proved functional in all respects. On the next morning a new OFOS-profile was conducted which revealed no signs of active venting but showed carbonate and hard rock which might be the reason for the enhanced back scatter in the side scan sonar survey of the RV New Horizon. In the afternoon the first VESP-lander was deployed for search of an active seep site at the first marginal ridge of the accretionary prism (Fig. 1). During 9 hours of search the drop weights of former ALVIN dives and some single clams but no suitable deployment site was found. Since this site is very close to a steep cliff the search was finished. On the morning of July 10 another OFOS profile was conducted in between the two summits of Hydrate Ridge which revealed massive carbonates pavements covered only by a thin and fine layer of sediment. After contacting the scientists on Atlantis it was suggested to change plan and deploy the lander at the northern summit of Hydrate Ridge (Fig. 4D). We succeeded to deploy it successfully on a large bacterial mat in between 6 other moorings deployed with ALVIN. On the next day, July 11, two OFOS-Profiles were conducted. The first track in the northeast of the northern summit (Fig. 4 E) revealed extended carbonate crusts and clam fields as well as a large field of huge sponges. The second OFOS-profile confirmed sediments which seemed to be upfolded like small pockmarks possibly by emerging fluids as suggested from former side scan surveys. In the late evening a transponder net was established and calibrated on the southern summit after Atlantis had retrieved her transponders and moved north for the night program. This region has proved to be extremely active with a massive gas hydrates on the seafloor as well a large gas plume emerging from tidal pulsed vents extending more than 100 m off the bottom.

Unfortunately, the weather deteriorated requiring to stop all work for the day. The last ALVIN dive in the north had to be cancelled and RV ATLANTIS left the working area after retrieval of the last transponders. Winds stronger than 7 Bft. did not allow the deployment of the second VESP-lander which was supposed to be deployed in very close vicinity of other instrument moored before by ALVIN. Since the weather did not improve, RV SONNE sailed to the northern summit and deployed 2 of 3 transponders in preparation of the following legs and the TECFLUX-II program in 2000.

Fig. 5: Cruise participants Leg SO134-1a (above) and Leg SO143-1b (below).

2.1.1 Leg SO143-1b: 11–13 July 1999, Astoria - Astoria
E. Suess

In the morning of 14 July a significant part of the world's deep sea research fleet was assembled in the port of Astoria. As part of the TECFLUX '99 field work, the RV ATLANTIS with DSV ALVIN aboard was moored alongside the research vessel FS SONNE for an exchange of scientists and equipment. The RV THOMSEN with the Canadian remotely operated vehicle ROPOS on board happened to have tied up during the previous night to load equipment for work on the Juan de Fuca Ridge. Hence, a bustling activity filled the otherwise sleepy port before FS SONNE departed at 1600 hrs. under overcast skies to start the second part of Leg SO143-1.

The short transit to the study area and the extensive data sets and maps obtained during the previous cruises allowed station work to commence early the next day. An OFOS track was run over the southern peak of Hydrate Ridge, (Fig. 4G) where vigorous methane escape had been detected by DSV ALVIN two weeks earlier (Beaver Mounds). In the afternoon two TV-grabs collected interlayered sediments and gas hydrate specimens. The enormously high porosity (styrofoam fabric) of near-surface hydrate layers and more solidly cemented sediment layers below attracted the attention. In addition very thin hydrate carbonate crusts, only a few millimeters thick, directly below the sediment surface indicated extensive biogeochemical turnover of hydrate methane.

Later, on 17 July and after adapting a TV-guided system to the multi-corer (TV-MUC), more surface layers with bacterial mats, vent faunas, but also with gas hydrates from near surface sediments could be selectively sampled. In that way, high-resolution pore water profiles were obtained along a profile spanning sites of considerably varying vent activities.

The remarkable spatial variability of the vent fields, the peculiar morphology of dune-like elevations (Beaver Mounds) as well as flat and nearly circular depressions stood out as characteristic features of the southern summit region. The morphology and also the indication of a variability in gas and fluid emissions, possibly depending on tides, had been observed by DSV ALVIN as well. Stationary methane plumes, detectable by the ship's 18 kHz and 20 kHz systems on the northern summit (Fig. 4D), were mapped to look at the time-dependent modulation of the fluid flow. The intensity of the methane plumes appear to correlate with the variability of the tidal current. On 19 July the hydroacoustic measurements on the plume distribution were supplemented by CTD-casts (every 4 hours) and deployments with the ZAPS system using a new methane sensor. The preliminary interpretations gave an impressve idea of the dynamics of the gas and fluid emissions at Hydrate Ridge. At the end of the first week (21 July), a second combined operation („methane-circus") involving hydroacoustics, CTD- and ZAPS-deployment was successfully concluded.

During the following days acoustic anomalies (white spots) on side-scan-sonar images from the survey in early June (RV NEW HORIZON; 1-11 June, Table 2); were inspected with the OFOS system and sampled by TV-MUCs and gravity coring (SLs). In all six locations of white spots (one at Hydrate Ridge and five in the Eastern basin) were examined in detail, but without finding clear indications for the origin of the

anomalous surface reflections. Also gravity coring, which yielded two cores, 550 and 140 cm long, did not provide conclusive information.

Next on the working schedule was the structure with a distinct morphology and a side-scan-sonar characteristics at the eastern flank of Hydrate Ridge in 900m of water (Fig. 4E; Mud Mound). Three OFOS-profiles were completed, which extended a previous profile taken during the first half of the cruise. Impressive images of giant sponges, a field of current ripples, bacterial mats, and clam colonies at the highest point of Mud Mound were found. The Mud Mound sediment was of dark coloration, had a blocky structure, and contained less carbonate mineral formations than its surrounding environment. Two deployments by the TV-grab yielded dozens of living vent clams as well as various highly lithified rocks like stratified dolomites, calcites, conglomerates, mud stones and over-compacted sediment from which only drops the pore water could be extracted. These characteristics are in agreement with the existence of a mud volcano or the exposure of over-compacted sediment from greater depths caused by diapirism.

Further operations by the TV-grab at the northern summit of Hydrate Ridge (Fig. 4D), where presently six instruments are deployed by the various groups of the TECFLUX project, showed again clearly the wide-spread carbonate deposits and the resulting difficulties in obtaining active fluid and gas seeps. The deployment yielded vent organisms and carbonates of various classifications as well as sufficient sediment for pore water extraction.

On 22 July FS SONNE started work in the northern region of the area (BSR-outcrop; Figs. 4A, B) to look for fluid escape structures as well as bacterial mats, both detected during the first cruise. These features are possibly connected to a BSR-outcrop projected from the sub-surface. The outcrop is situated closely to other type of pock marks observed in the side-scan-sonar records, which also suggest active fluid venting.

Among the unexpected results were the variety of hydrate carbonates. Carbonate crusts, chimney segments of various sizes and shapes were dredged (Fig. 4B; monster doughnuts) from the seaward flanks of two low ridges at 450 and 550 meters depths (Fig. 4A; seismic line L 100; 23 July). In most cases these fragments with diameter up to 1 meter are extinct and overturned chimneys. Typical were horizontal changes in thickness and incorporation of stratified sediment, indicating that they formed under sediment cover rather than standing above the sea floor.

Another form of syngenetic formation of carbonates are oddly-shaped concretions (bone-bed carbonates) found at the summit of Mud Mound central (Fig. 4F); east off the central saddle of Hydrate Ridge on 25 July. Other lithologies were carbonate-cemented coarse-grained sandstones from a large vent field at the summit north of Hydrate Ridge (Fig. 4C; NW-knoll, 26 July). This vent field, which was unknown up to now, is of considerable extension but shows no evidence for gas hydrates, instead seems characterized by free-flowing vent fluids. Several slabs of cemented rock, colonized by bacteria and channellized by flowing water -in horizontal direction- could be recovered by the TV-grab

During the following days (25-26 July) the work focussed on recording OFOS profiles along existing seismic lines with „white spots" in areas east of Hydrate Ridge and on

completing the central profile across the ridge westward (Fig. 3; 4H). Sampling the western basins was completed by deploying gravity cores and MUCs. A gravity core from the southern summit (Fig. 4G) provided one of the most important results of the entire cruise: Interlayering of hydrate and sediment with salt exclusion from in situ hydrate formation. This was possible by separating the hydrates from the sediment-pore water system before they decomposed. A flexible plastic tube, instead of the usual liner, were used for this purpose.

During the final operation with the TV-grab (27 July) at the southern summit, more than 100 kg of hydrate could be extracted from the sediments of a vent field. Specimens of the hydrates were conserved in liquid air. These hydrates did not show the bubble-fabric, like the specimens obtained at the beginning of the cruise, but were of more solid material.

The ZAPS methane sensor was used successfully for several hours on 27 July in mapping a methane plume over the southern summit which was detected by a large acoustic anomaly registered by the 20 kHz system. Water samples, which were taken at the same time from above the sea floor, again were supersaturated by more than 1.000 times their value relative to air. It remains unclear whether this supersaturation originates from dissolved gas or includes finely dispersed methane bubbles in water.

At low tide on 27 July at 7 a.m. local a 20-kHz survey was started at the northern summit which later was supplemented by ZAPS- and CTD-deployments. The survey ended after 16 hours on 28 July at 1400 hours with the ZAPS- and 20-kHz systems recording only moderate gas signals, the methane analysis of discrete water samples taken simultaneously showed values of more than 200.000 nl/L. The last topic on the agenda were two OFOS profiles in the saddle between Hydrate Ridge and the NW-knoll (Figs. 4C and D; 28 July). The highlight of this survey was a small pogonophora colony among the ridge structures at a depth of 1.200m indicating for the the first time that these organisms exist in the area of the second accretionary ridge.

Due to the organisational and logistical problems caused by a last minute port change to Astoria instead of to Newport, work was terminated at 22:30 hours on 28 July. The pilot came aboard at 08:00 hours on 29 July and FS FONNE tied up at 1100 hours. On 29-30 July the equipment, which had been assembled at the Marine Science Center in Newport, arrived in Astoria and was loaded aboard for the second Leg SO143-2. The calm weather throughout facilitated the work at sea immensely.

2.2   Multibeam swathmapping

J. Bohnert and watchkeepers

Equipment

Bathymetric data were recorded on board RV SONNE with the swathmapping system HYDROSWEEP (HYDROgraphic SWEEPing survey echosounder; ATLAS Elektronik GmbH, Bremen). The instrument is fixed to the hull of the ship and consists of 59 acoustic beams. The beam fan has an opening angle of 90°, therefore the surveyed swath is about twice the water depth. According to the maximum range of beams of 10.000 m the maximum registration water depth is about 7000m. Precision is very high (about 1%) when rolling and pitch is less then +/-5°. Data are continuously written to magnetic tape and consists of location, time, pitch, roll, heaving and acoustic travel time of the acoustic signals. In order to achieve good data quality SOG (speed over ground) ranged between 6 and 8 kts.

Processing

After acquisition, raw data were transferred to the onboard computer network and then copied to the hard disc of the UNIX workstation (SUN-sparc), simultaneously data were stored to DAT-tape. For processing we used the multibeam sonar processing software package MBSYSTEM. Processing consists of eliminating and editing bad navigation data from recorded data sets. Then acoustic traveltimes were converted to waterdepth by applying water sound velocity function. Water sound velocity values were generated from a CTD (Conductivity Temperature Depth) gauge. Last processing step was cleaning every single swath from erroneous depth values. Finally data were grided and visualized by using the GMT software package (General Mapping Tool).
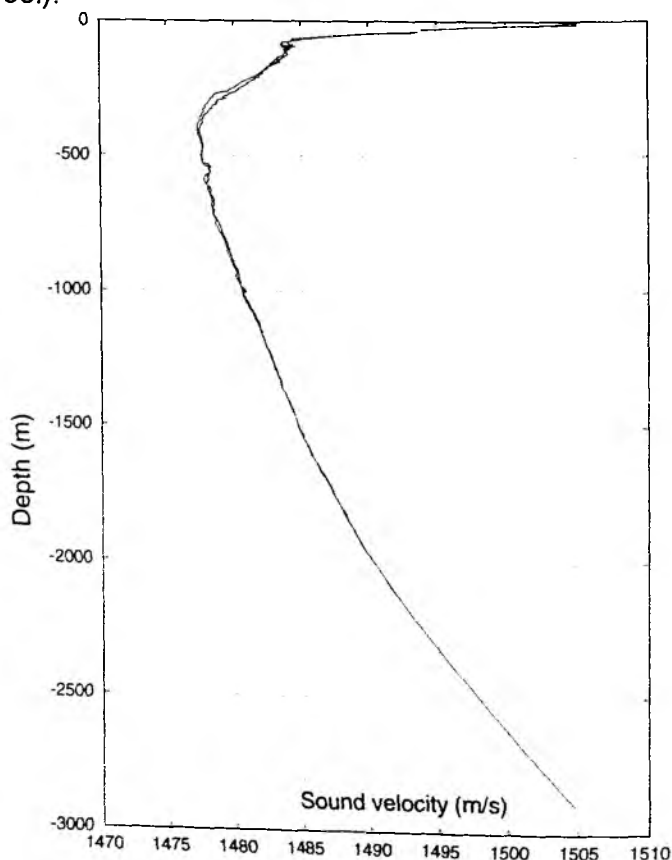
Fig. 6: Water sound velocity measuered during SO143-1.

Water sound velocity

CTD cast was used to evaluate water sound profile. It was run in deep water (2900m) west of the deformation front at 44°40.25 N, 125°22.12 W (Fig. 6). In shallow depth water sound velocity decreased very fast until it reached a local minimum of 1484 m/s in a depth of 80 m. The velocity then slightly decreased to the absolute minimum of 1477 m/s in a depth of 490 m. In greater depth water the velocity increased exponentially and reached at the ocean bottom a value of 1505 m/s.
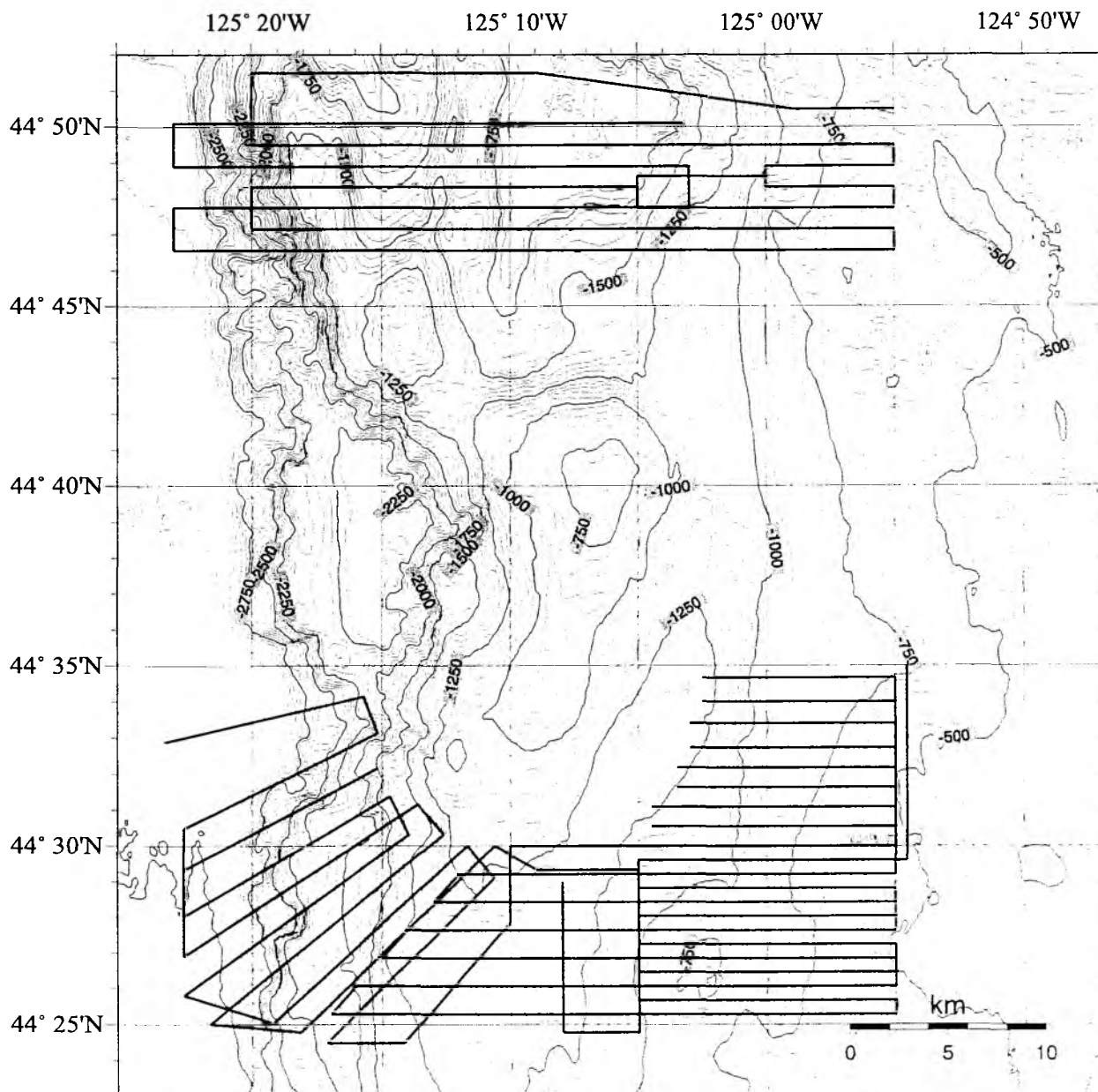
Fig. 7: Hydrosweep tracks measured during SO143-1.

Hydrosweep tracks

On cruise SONNE 105 and 110 bathymetric data of Hydrate Ridge were collected. During SO143-1 adjacent areas of hydrate ridge were surveyed to complete these tracks. The latitude of the southern region was between 44°25.00 N – 44°34.50 N, the northern pattern ranged from 44°46.50 N to 44°51.00 N (Fig. 7). Longitude of both surveyed regions was between 125°22.00 W and 124°55.00 W. Hydrosweep tracks were run by night, acompanied by fishing ships forcing RV SONNE to deviate the calculated tracks from time to time.

Data quality

Weather conditions were moderate at some nights. During some tracks of SO143-1 roll and pitch exceeded the limits guaranteeing good data quality. By eliminating the erroneous data from every single swath, data quality could be improved enormously. This is a very time-consuming processing step but lack of manpower prevented the optimal processing for all data during SO143-1 cruise.

2.3   Methane in the water column and surface waters, ZAPS and 18kHz surveys

G. Rehder, G. Klinkhammer, K. Heeschen, M. Whiticar, K. Brooksforce, J. Prins, L. Barrazoul, B. Cumberland

Introduction

The Cascadia Margin is an extremely active site for the turnover of carbon at and near the seafloor. Considering the large accumulations of methane-derived authigenic carbonates that we have mapped, together with the vast, yet unknown volumes of methane gas hydrates in the surface sediments, there are clear indications of high rates and amounts of carbon flux. The active collisional tectonic setting of this region is constantly readjusting the positions and movements of the carbon deposits in the sediments at this accretionary margin. In particular, gas hydrate deposits are continually being exhumed and eroded due to the uplifting of sediment packages along the accretionary prism. Furthermore, this tectonic rearrangement leads to channels, such as fractures in the sediment fabric that enhance vertical fluid and gas flow. We have repeatedly observed the release of methane gas from the ocean floor into the water column. These methane plumes have considerable areal extent and can be tracked by hydrographic studies.

Some of this gas release across the sediment-water interface may be attributed to the destabilisation and dissociation of gas hydrates deposits. Althought the uplifted sediments experience a change in pressure and temperature, they remain within the P,T stability field of gas hydrates. This phase change from methane clathrate to methane gas and water is primarily the result of hydrates coming in contact with gas undersaturated ocean bottom water.
Additionally, outflux and ebullition of methane from the sediments, in part via vents, contributes to the methane inventory in the deeper water column. Once in the water column, the methane undergoes dispersion and bacterial oxidation. However, the relative magnitudes of the various fluxes and removal process remains unclear.
Our CTD experiments during and in conjunction with the RV SONNE Leg SO143-1b address a series of questions, including:

*   How extensive is the distribution of active gas venting sites in the study region,
*   What is the magnitude of the gas released (plumes) into the water column,
*   What is the physical and temporal dispersal of the methane plumes,
*   What are the physical, sedimentary and biogeochemical controls on the rates of gas release from the hydrates and sediments into the water column,
*   What is the relationship between the acoustic signatures of gas plumes (18 and 20 kHz) and the measured concentrations,
*   How do the methane concentrations in the CTD casts correspond to the towed Zero Angle Photometer Syste (ZAPS) information,
*   Do the CTD and ZAPS methane sensors have sufficient response,
*   What are the processes that remove methane from the water column,

- How far does the methane gas released rise into the water column and does methane released from the sediment and/or hydrates ultimately flux out across the air-sea interface into the troposphere.

To answer these questions, a total of 15 CTD casts were made during the two-week cruise. In addition, water samples from bottles on 5 ZAPS tows were taken. Both the CTD and ZAPS carried a methane sensor Shipboard, the CTD and ZAPS waters were degassed and the methane concentrations determined. Samples of gas were collected for shorebased stable isotope measurements. This analytical information is interpreted in conjunction with the

- T,S and methane senor data from the CTD and ZAPS,
- The backscatter from the ZAPS,
- The ship's 18 and 20 kHz acoustic records,
- Visual ocean bottom information obtained by towed photo sled (OFOS), TV-Multicorer (MUC) and the large TV-hydraulic grabber (TV-G),
- Direct sediment, carbonate, interstitial fluid and gas samples obtained by gravity coring (SL), MUC and TV-G.

CTD deployment

Water column sampling was performed using the ship CTD/rosette system equipped with sensors for temperature, conductivity, pressure, and oxygen (Seabird 911 plus, SBE 13 oxygen sensor, SBE 32 caroussel with 24 x 10l Niskin bottles). Additionally, a membrane/chemical CH_4 sensor provided by Bob Collier (METS sensor) was attached to the CTD.

Y = M0 + M1*X	
M0	0.16799
M1	0.97327
R	0.99746
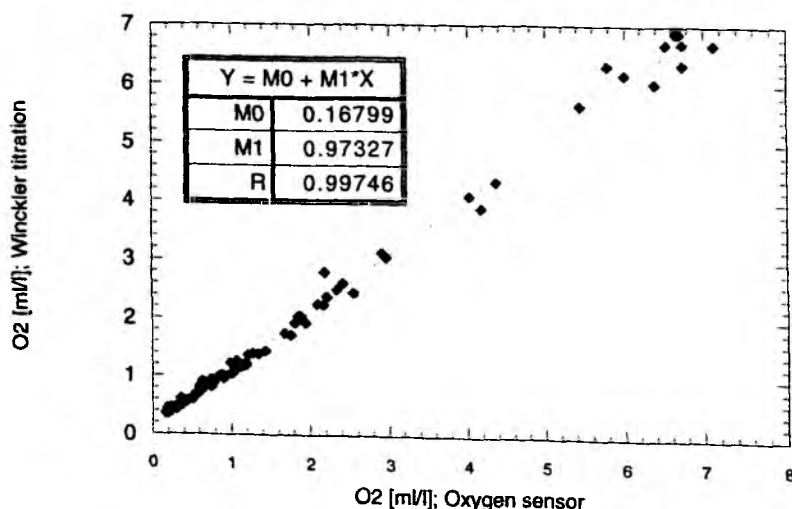
Fig 8: Oxygen concentration measured by Winckler titration versus oxygen concentration determined by the SBE13 oxygen sensor.

The sensors and rosette worked without problems throughout the cruise. The CH₄ sensor showed a slow reaction to enhanced CH_4 in the water column during only one deployment. The output indicated that the sensor has a large time constant. This explains the continual drift to lower values (voltages) during the cast the downcast and upcast. The surface values are elevated due, in part, to the time required for the surface air influence to be removed from the sensor.
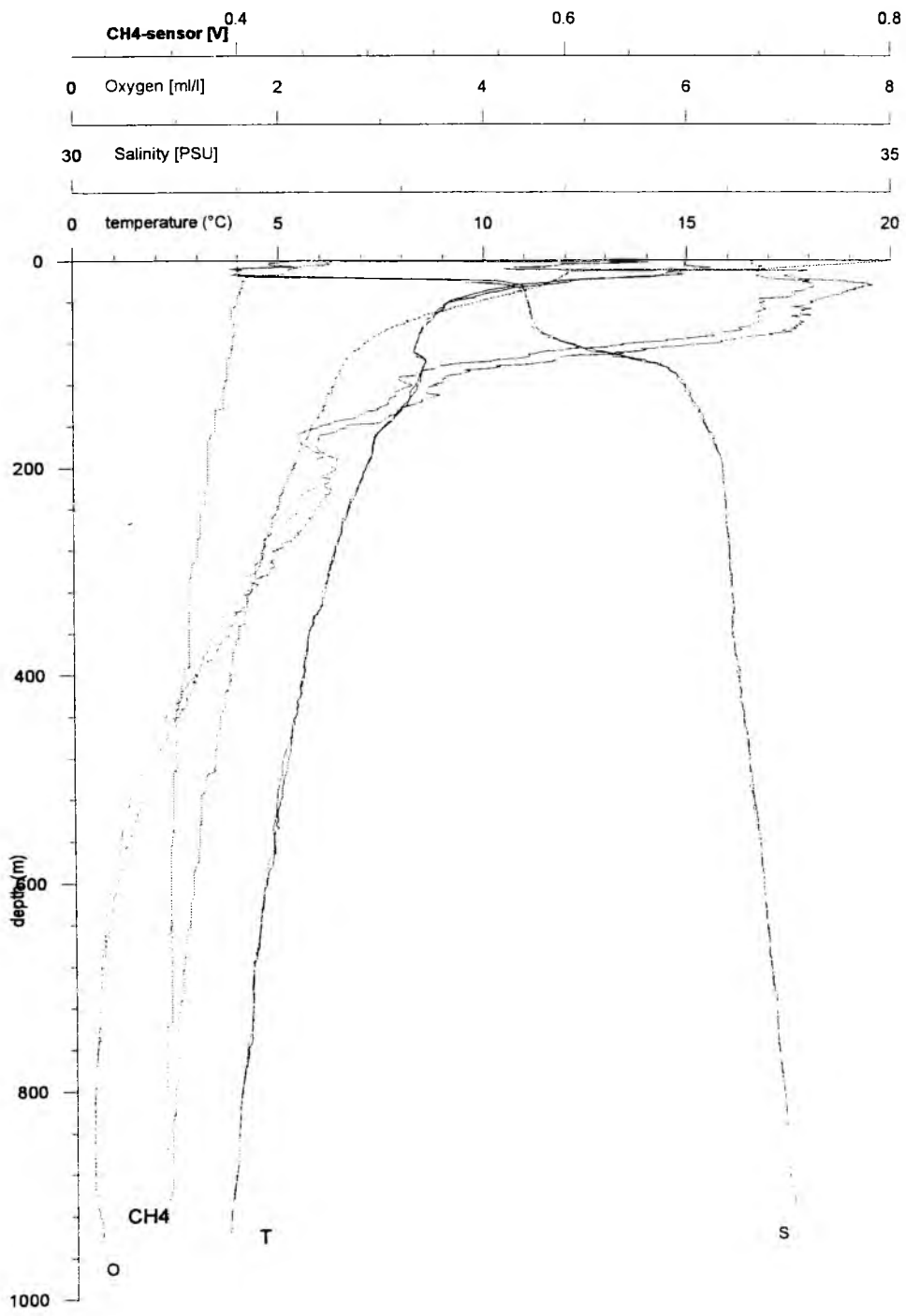
Fig. 9: Typical shape of temperature, salinity, and oxygen in the working area (here: Station 67-2). Also shown is the uncalibrated output of the METS CH₄-sensor. Note the irreproducability of the CH₄-sensor output during upcast and downcast.

The sensor seemed to be less sensitive than the CH_4 sensor (same type) used on the ZAPS package. The oxygen sensor worked remarkably well and was calibrated against the results from Winkler titration based on 88 samples (Fig. 8). The water column on all stations was characterized by a thin (6-10m) lens of warm, low salinity (31 PSU or less) water. The low salinity likely reflects the influence of freshwater input from the shelf. Temperature and salinity properties in the water column were similar at all stations. A typical profile (Station 67-2) is shown in Fig 9. The oxygen content near the bottom is about 0.3-0.4 ml, remarkably low if compared with samples in the open Northeast Pacific from similar depths. Although this might result from the high input of organic matter in the highly productive TECFLUX area, it is noteworthy that the oxidation of CH_4 in the water column should result in an additional demand of dissolved oxygen. The enhanced AOU would not correspond to a commensurate increase in nutrients.

Methane measurements

During cruise _RV Sonne_ Leg 143b, methane in the water column was measured on discrete samples collected directly from the CTD/rosette and ZAPS packages,. Furthermore CH_4 and CO2 in the surface waters was continuously surveyed along the entire cruise track using a gas equilibration system (Rehder, 1996). For CH_4 analysis on the discrete CTD and ZAPS samples, a modified vacuum degassing method was used as described by Lammers and Suess (1994). The proceedure involves sampling 400 ml of seawater directly from the water bottles using a large glass syringe. The water sample was immediately injected and sealed into pre-evacuated 600 ml glass bottles. The air and water phases in the sample bottles were equilibrated by shaking for at least 30 min. The gas phase was subsequently recompressed to atmospheric pressure in a preparation line. The CH_4 mole fraction of the extracted gas was determined by gas chromatography using flame ionization detection. The total gas content of the sample was calculated from the measured dissolved oxygen concentration and assuming that N_2 and Ar were 100% saturated relative to their atmospheric partial pressures (Weiss, 1970). The dissolved oxygen concentration was derived from the oxygen sensor of the CTD package, calibrated against Winkler titrations (see CTD chapter). The dissolved methane concentration was calculated as the product of the mole fraction in the extracted gas phase and the amount of total gas (STP) in the sample. For the FID calibration, bottled mixtures of 9.91ppm ± 2% and 904 ± 2% methane in synthetic air were used.

The atmospheric mole fraction of CO_2 and CH_4 in marine air and surface water pCO_2 and pCH_4, was measured using a fully automated, semi-continuous system based on gas equilibration/gas chromatography (Weiss, 1981) (Bange, 1994). A sample of either (1) calibration gas, (2) marine air continuously pumped from the ships bow, or (3) air equilibrated with a continuous flow of seawater, is sequentially deviated to a thermostated 10-Port valve via a flowmeter and Sicapent^{TM} drying agent. About 80 ml of gas sample pushed through 2 sample loops before the sample valve is rotated. For methane, N_2 is used as carrier gas and methane is detected using an FID. For CO_2 determinations, H_2 is used as carrier gas, and the CO_2 is detected after conversion to CH_4 by a Ni-catalyst (380°C) using a second FID.

The sequence used for the analysis of the different gases was CG1-E-A-EW-CG2-E-A-EW, where CG1 and CG2 are the calibration gases, E the air equilibrated with surface seawater and A the atmospheric air sample. The time for a single measurement was 10 min., resulting in atmospheric values every 40 min. and values for the equilibrated air every 20 min. The reproducability for CO_2 and CH_4 is 0.6 ppm and 0.01 ppm, respectively. The determination of CH_4 and pCO_2 in surface seawater is based on the equilibration of a recirculating gas phase with a counter-current flow of continuously renewed seawater. A detailed description of the system is given in Rehder, 1999. During the first 2 days of the cruise (Leg SO143-1b), the ship's clean seawater system was used. Afterwards, water was sampled with our seawater system, using a submersible pump deployed in the water of the ship's moonpool. Based on our results, it appears that the contamination levels of the ship's clean seawater system are low for both CH_4 and CO_2. Unfortunately due to the long run from the intake port to the lab, the temperature shift between the *in situ* surface water temperature and temperature of the seawater at the outlet is substantial, ca. 1.5 °C.

During a high resolution survey of the methane distribution in surface waters (Station survey 47, track 1-5), the system was run manually. A 1 ml sample of equilibrated air was taken from the equilibrated gas phase with a gas tight syringe every 4 min. through a septum port and injected into the GC.

Results

Surface water survey
The methane surface distribution in the TECFLUX area shows a strong gradient with increasing concentrations towards north-northeast (Fig. 10). The entire area is oversaturated with respect to the atmospheric mole fraction of methane and hence is a source for atmospheric CH_4. During the survey (Station 47), the degree of oversaturation of the water wrt the air varied from less than 10% in the southwestern part of the survey (44°34.7' N, 125° 18.0' W) to about 150% oversaturation in the northeast (44°40.5'N, 124° 40' W). This distribution can explained by upwelling of cold, CH_4-rich waters and is not caused by the input of low salinity waters from riverine input (Fig. 10 b, c, d).

The entire area was strongly undersaturated for pCO_2, with surface partial pressures sometimes lower than 230 µatm. This appears to be caused by a high primary productivity in this region, driven by the input of nutrients from the shelf and upwelling. This interpretation of CO_2 drawdown by high productivity is supported by the deep green colour of the surface water. The automated system was run during the entire cruise, permitting an combined evaluation of the local, short-term variations of pCH_4 and pCO_2 in surface with the data from the ships DVS system.

Methane in the water column
The distribution of methane in the water column in the TECFLUX area is highly variable, particularly at the bottom near 150m. Some features of the upper water column are worth discussing. The surface water concentration and thus, the input of

Methane concentration [nmol/l]

Surface Temperature [°C]

Surface Salinity [‰]
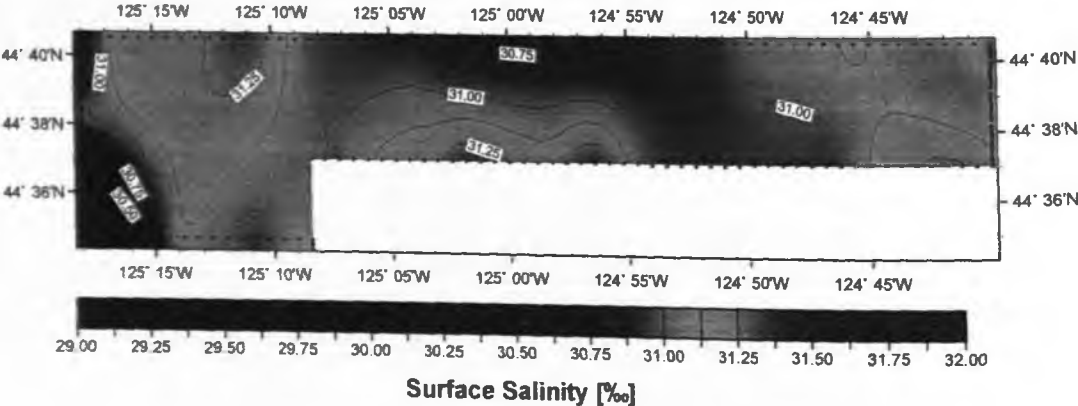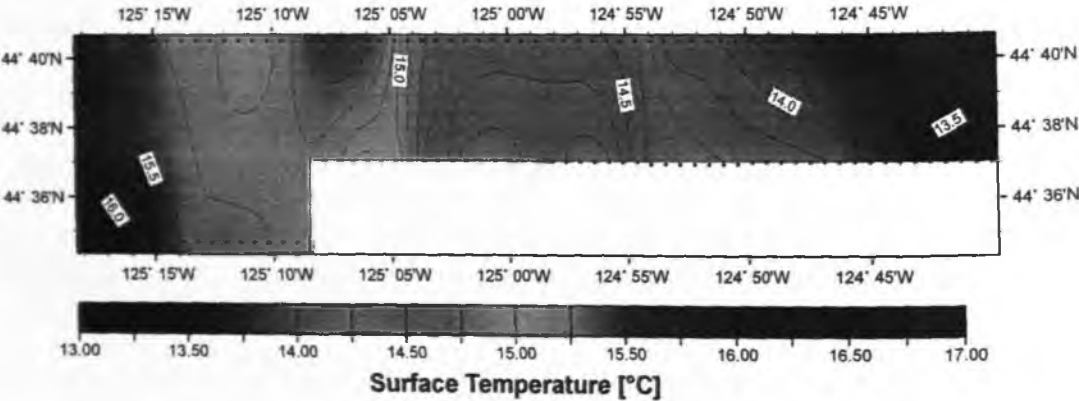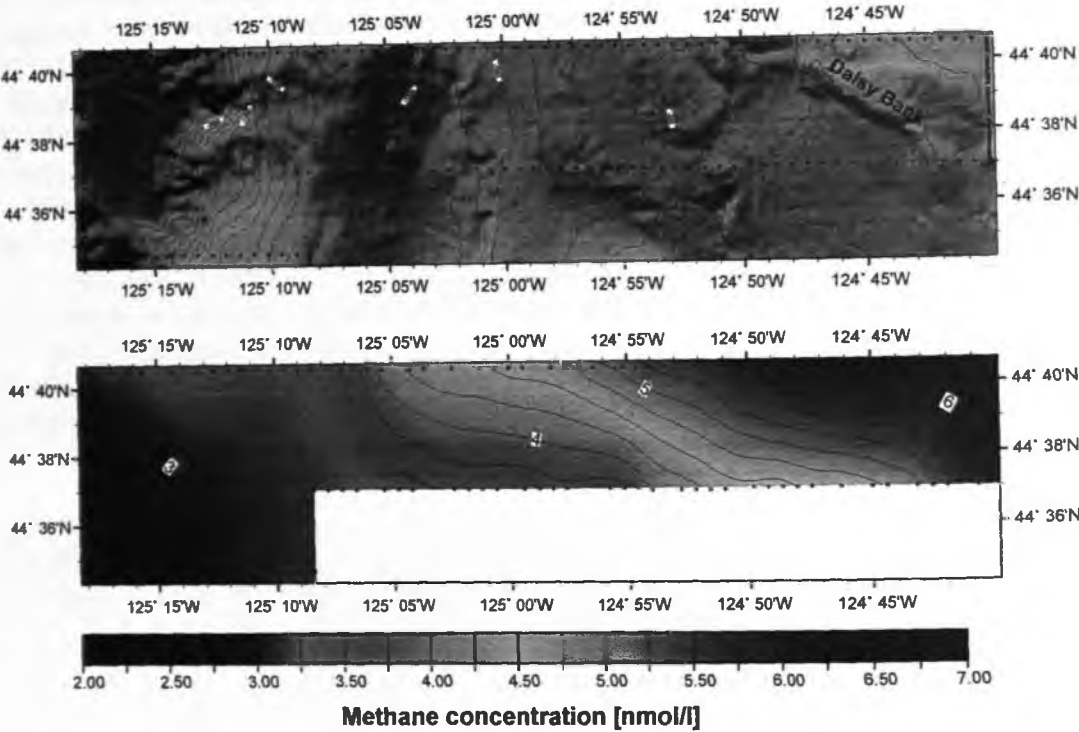
CH_4 to the atmosphere, is determined by the CH_4 content of a shallow (~10m) layer of low saline, warm water which varies from 10 - 130 % oversaturation (see surface survey). Between 150 and 350m, particle-rich layers were detected by the backscatter and reflectance sensor of ZAPS at all locations where ZAPS and CTD were deployed. This well-known phenomenon is caused by the introduction of particle-rich water from the shelf into the mid-water column according to its density properties (INL). From our observations, it appears that the backscatter/reflectance anomaly corresponds with enhanced methane contents (Fig. 11ab). Hence, in this area, i.e., around Hydrate Ridge the enhanced methane concentrations in this mid-depth range are clearly not caused by the seepage/advection of deep-water or sediment gas. The CH_4 profile at Station 67-2 on the NW knoll (Fig. 11a) indicates that the natural CH_4 background below 500 m depth is in the range of 10 nl/l or lower, in in agreement with the general pattern of the CH_4 distribution in the open Pacific Ocean. These low background concentrations provide an important baseline for the interpretation of the CH_4 profiles on the active degassing sites at Hydrate Ridge. The increasing CH_4 concentrations at Station 67-2 towards the bottom (up to 130 nl/l) indicate active fluid flow at this site (NW knoll) in the northwest. Enhanced concentrations in the depth range between 50 and 200 m are absent. Hence, there is no indication for gas bubble release at this site. This is consistent with other findings in this area. No gas bubbles were detected by the 18 kHz survey (65-1); no response of the methane sensor was observed during ZAPS station 67-2, the OFOS tracks (66-1, 2) showed large fields of active vent organisms, susbstantiated by the large number of living vent biota recovered with TV grab Station 68-2.

During the expeditions of RV New Horizon and RV Atlantis, some indications were found that the release of gas from the active sites at Hydrate Ridge is, perhaps in part, influenced by tidal forcing. This leading to lower gas release rates during high tides (increasing hydrostatic loading) and higher gas flow during low tides (decreasing hydrostatic loading). To test this hypothesis, a sequence of 4 CTD casts and 1 ZAPS survey in a time frame of about 16 hours were run at Station 36, 43, and 74. This covered a large part of the tidal cycle. The station positions were selected based on the results of the 18kHz surveys. The results of the CTD sampling and an overview of the tidal cycle, amplitude, and the time of water sampling for stations 36 and 43 is given in Figs. 12a, b and 13a, b.

Fig 10: Results from a surface survey from July 24, 1999. a: bathymetry ; b: surface methane concentration; c: surface seawater temperature; d: surface seawater salinity. The decreasing temperatures towards the coast resulted from coastal upwelling and decreased down to less then 9°C further onshore. Note the NW-SE-direction of the isolines west of a bathymetric high, the Daisy Bank, parallel to the isolines. The surface methane concentration increases from near equilibrium with the atmosphere (SW) to more than 250% saturation in the northeastern part of the survey area. The surface salinity shows no connection to the observed CH_4-pattern. Hence, it can be ruled out that the enhanced methane concentrations result from the influence of methane rich freshwater release from the Columbia River. In contrast, the correlation with surface temperature suggests that the high CH_4 concentrations are connected to the upwelling of CH_4 rich waters.

Fig. 11: a: CH₄-concentration on station 67-2 and b: backscatter and reflectance from a ZAPS-survey at the same location. The peak of the CH₄ profile slighly above 200 m water depth corresponds to enhanced responses of both optical sensors.

TIDAL EXPERIMENT STATION 36
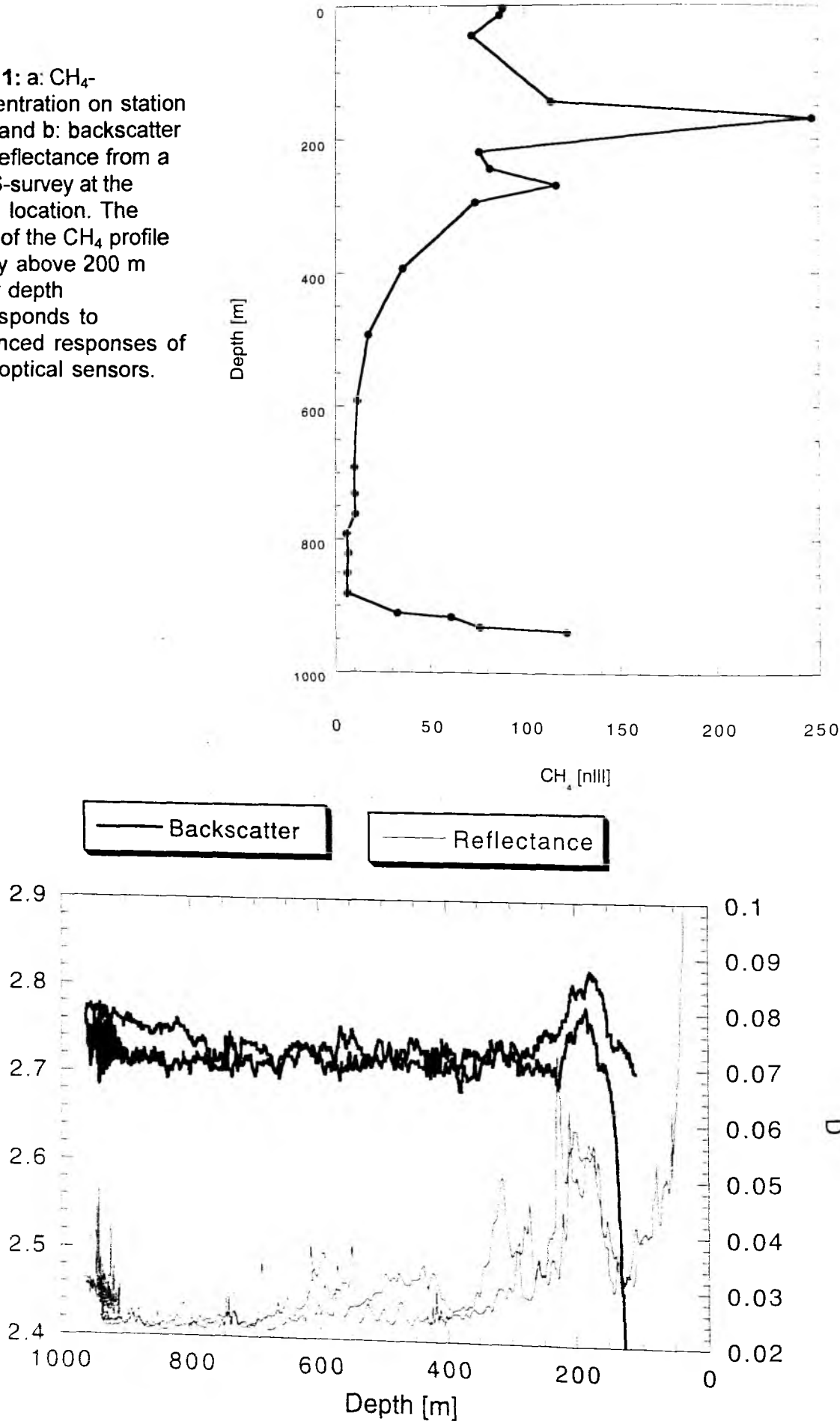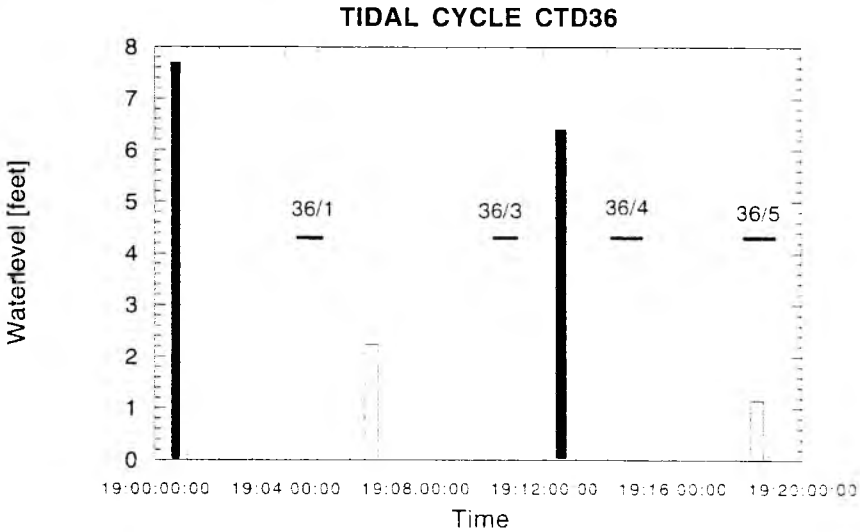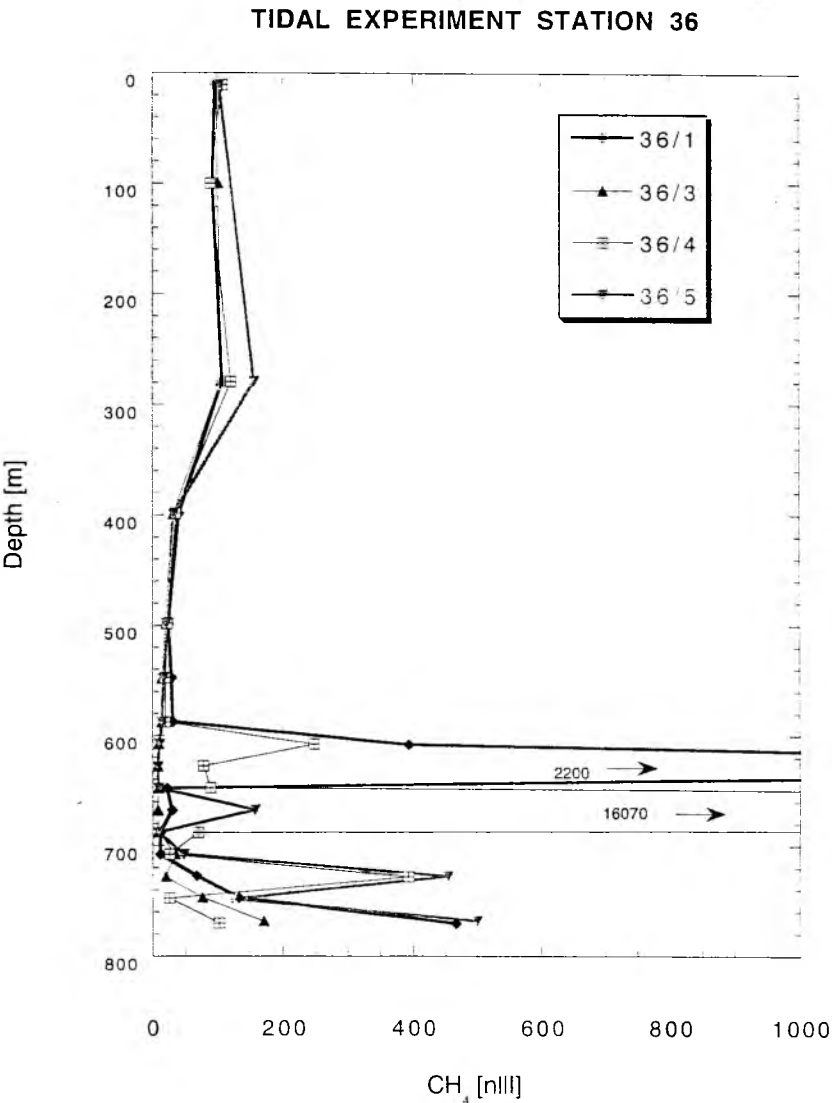
TIDAL CYCLE CTD36

Fig. 12: a: CH$_4$ concentrations and b: Time of CTD-sampling in regard to the tidal cycle on 4 hydrocasts at the same location on the southern sumnit (Station 36).

TIDAL EXPERIMENT STATION 43
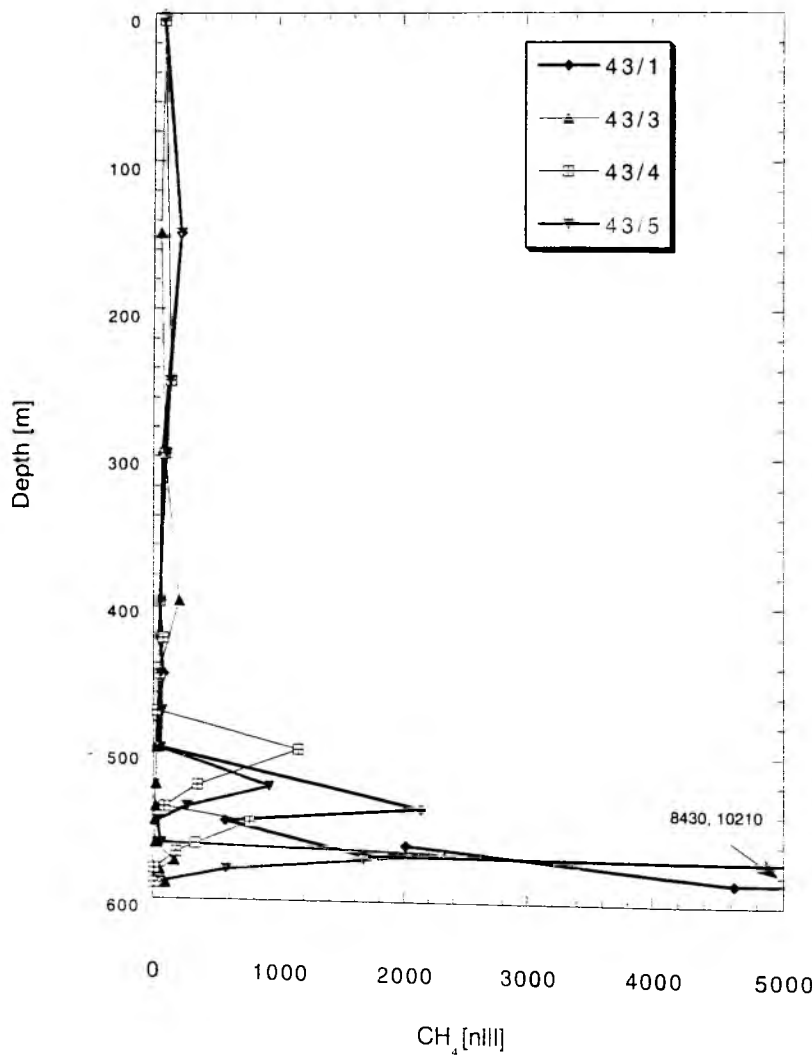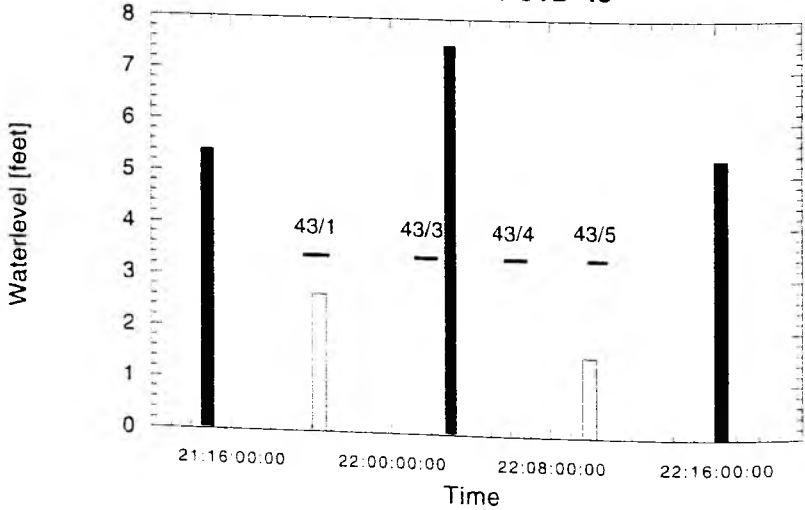
Fig. 13: a: CH₄ concentrations and b: Time of CTD-sampling in regard to the tidal cycle on 4 hydrocasts at the same location on the northern sumnit (Station 43).

Station 36 on the southern summit was sampled 4 times at same depths. The amplitude between low and high tide was relatively small, mainly because the sea level at low tides were higher than usual. CTD 36-1 and 36/4 were sampled between high and low tide, while 36-3 was sampled about 1.5 hours before high tide. CTD 36/5 was sampled immediately after low tide. By far the lowest CH_4 inventory in the lower 200 m of the hydrocast was found in CTD cast 36-3, i.e, before high tide. The highest concentration (170 nl/l) was encountered only near the base of the water column. Elevated concentrations were only detected in the lower 70 m of the water column. The other casts showed enhanced concentrations up to 200 m (36-1, 4) or 150 m (36-5), respectively, with very high maxima (2200 nl/l, cast 1; 16070 nl/l, cast 4) at single sample depths. The results suggest that the highest inventory of CH_4 occurs during periods of decreasing hydrostatic pressure. Although currently unclear, it may appear that during periods of increasing hydrostatic pressure some hours before high tide, the activity of the gas seeps on Hydrate Ridge is lowest.

A similar experiment was performed on Station 43 on the Northern Summit. Here, Casts 1 and 5 were sampled close to low tide; Cast 3 about an hour before high tide, and Cast 4 between low and high tide. The CH_4 concentrations are generally higher than on the Southern Summit, with concentrations as high as 10200 nl/l on Cast 1. Similar to the result at Station 36, the inventory of methane in the water column at Cast 3, just before high tide, is much lower than on the other casts.

Although our findings do not disprove the hypothesis of a tidal triggering of the gas venting rates at Hydrate Ridge, this method of CTD sampling of the lower water column is not ideally suited to assess the inventory of CH_4 has several restrictions. The plumes of high concentrations seem to be very small in footprint. Having a sample of several 1000 nl/l without deviations from the background in the samples below and above makes it impossible to estimate the size of the feature (see for example Cast 36-4). Furthermore, the relatively small scale of the CH_4 anomlies makes it difficult for ship positioning and the plume dispersion is subject to the direction of bottom currents. Knowledge about the current direction is also essential to judge whether or not the observed low CH_4 inventory during flood is caused by lower gas flow rates or by deviating the plume in a direction not covered by the hydrocast.

18 kHz surveys

To detect areas of free gas and its variable occurence in water column 18 kHz surveys were conducted on the northern summit of Hydrate Ridge. For a high frequency survey neccessary to detect this feature the ship Parasound system was used running at only 18 kHz (Narrow Beam Survey NBS-mode). For overlapping between the tracks an aperture angle of 20° was chosen resulting in a swath of about 200m width at a water depth of 600m. Unfortunately, the system supplies only analogue data (paper printout) in the NBS-mode. Digital data storage is currently not possible.

In addition to the short surveys supporting the CTD deployments, we conducted 3 long-term surveys of up to 16 hours in the area of northern Hydrate Ridge to investigate the amount and variablity of gas venting. The grid choosen for these surveys is shown in Fig. 14 with about 170 m between the tracks.
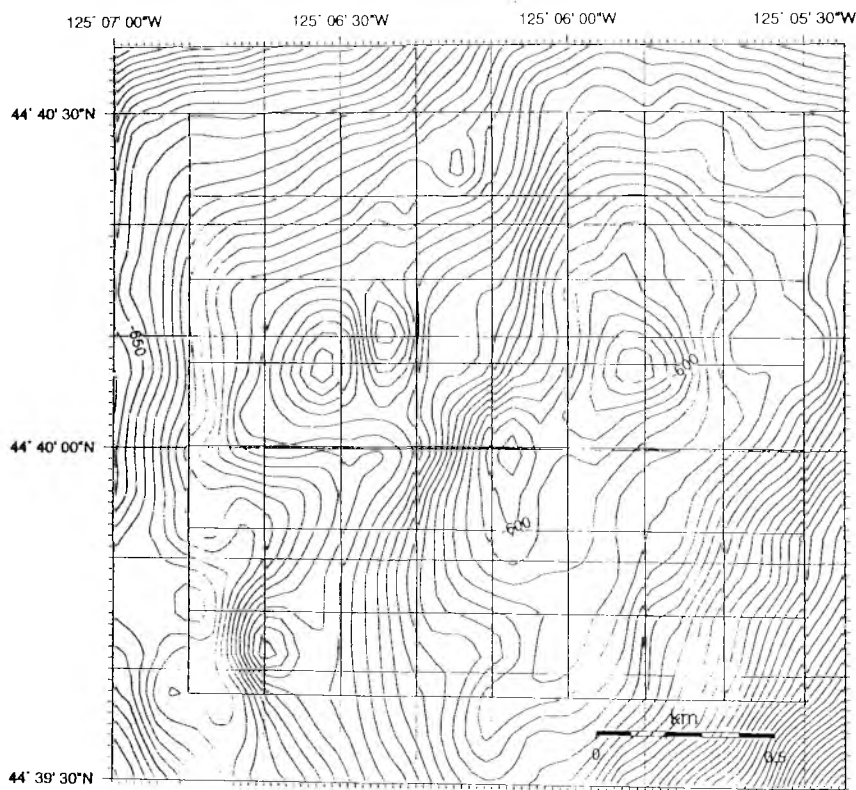
Fig. 14: Map showing the grid of the 18 kHz survey (Station 44). The distance of the grid lines is about 170m, which allowed a complete coverage ofthe area (20° aperture angle).
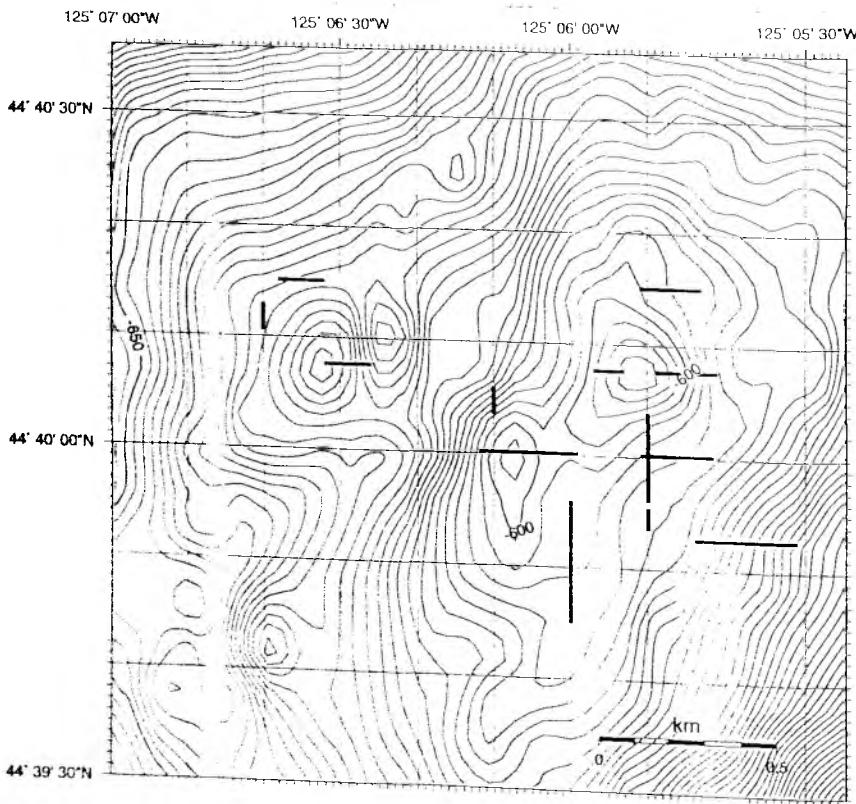
Fig. 15: Grid of the 18 kHz survey shown in Fig 14. Areas where free gas in the water column was detected are indicated by the fat lines.

The entire area was covered 8 times during the first 18 kHz survey (Station 22), with alternating series of 9 south-north and 8 east-west tracks.

The 18kHz survey shows a clear response to free gas in the water column. The occurrence of gas bubbles was observed up to 200m above seafloor on well-defined spots of the survey area (see Fig. 15). However, only very few of these locations proved to be active every time the survey passed through. Others seemed to show free gas in the water column only sporadically, and both signal intensity and maximal heigth were highly variable. The station location for the repeat hydrocasts on the Northern Summit (Station 43 and 74) was chosen according to the results of survey at Station 22. The signals were always observed in association with topographic highs in the area. A relation of signal intensity to the tidal cycle was not established. Additionally, the spatial location of the bubble plumes could not be determined with great precison due to the 20 degree aperture angle of the NBS-mode. Hence, the free gas detected on the lines shown in Figure 8 could be located only to within 90 m on both sides of the tracks. Subsequent attempts to repeat the 18 kHz survey were comprimised by miscalibration of the instrument.

Zaps deployments

The ZAPS instrument package on SONNE 143-1b consisted of the following pieces of equipment.

SeaBird 911 plus CTD
The CTD provided temperature, depth, and the conductivity data used to calculate salinity. Precision from this unit was ±0.002°C, ±1dbar, and ±0.003ppt as determined by calibration at SeaBird Electronics in Seattle, WA. This unit was also fit with a Beckman dissolved oxygen sensor.
This CTD and DO sensor was the same equipment as operated by the RV SONNE which allowed for direct comparison which was favorable in most cases. The O2 sensor on the CTD/rosette was calibrated against Winkler titration and showed that this sensor was providing exceptionally accurate oxygen concentrations. The DO sensor output from the package provided similar results in the top 300 meters (although somewhat more noisy) but diverged from the accepted values at depth until there was an offset between the two data sets of about 0.2 ml/L at 600 m. We attribute this difference to a problem with the calibration of the sensor on the package. Still this is remarkable agreement for this sensor.
CTD data indicated the presence of several distinct water masses in the TECFLUX area. A freshwater lens from the Columbia River that caps the seasonal thermocline dominates surface waters in the summer. Thermocline waters that are influenced by exchange with the shelf (see OBS section) and bottom waters that flow NE-SW with instantaneous currents that can exceed 10cm/sec (preliminary results from New Horizon cruise).

SeaTech Optical Backscatter (OBS) device
This turbidity meter was adjusted for improved sensitivity at the factory. This adaptation makes the device somewhat noisier than other instruments of this type but

also makes it possible to detect features that are normally only seen with more expensive devises. Fig.16 shows OBS data from the SeaTech for operation 45-1. There are three water column features in the TECFLUX area that have OBS anomalies: (i) surface water that is strongly influenced during the summer months by input from the Columbia River plume in the top 20m (ii) a turbidity maximum associated with main thermocline water (iii) a benthic boundary layer. All three of these features have potential impact on the flux of CH_4 associated with the TECFLUX area. The surface mixed layer will ultimately control any exchange with the atmosphere and certainly influenced the results of the surface water CH_4 survey.
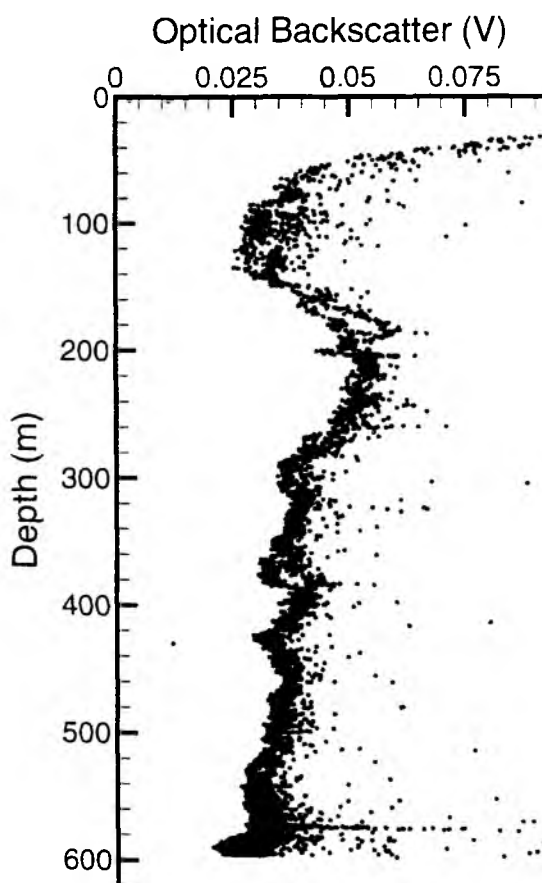
Fig. 16: Vertical profile of the response of the optical backscatter sensor on station 45-1.

The thermocline maximum is thought to reflect offshore exchange from shelf areas. There is a CH_4 anomaly associated with this feature (see table) indicating that this turbidity may originate at cold seep sites. There is variability in the depth and extent of this feature across the TECFLUX area indicating that this water originates fairly close to the study area. Since the presence of this feature influences the flux of CH_4 through the water column it deserves further study.

The benthic bottom layer was not prominent at station 45 but shows up as a strong feature of other stations. Of the three OBS features the benthic boundary layer is obviously most important in controlling the distribution of CH_4 in the water column. It was clear from the ALVIN dives that strong bottom currents in the area affect the rise of bubbles from the TECFLUX sites and undoubtedly influences the distribution of

dissolved CH_4 as well. This latter point was driven home by METS sensor data that often showed CH_4 maxima near the seafloor, including the highest concentrations found during the cruise. This was the case even though the acoustic plume showed gas bubbles that seemed to be collecting 50-150m off the bottom. Perhaps the best example was the last ZAPS operation (74-3).

Chelsea nephelometer
This instrument is calibrated in ftu (fluorazine turbidity units) and gives us a more quantitative measure of suspended particle matter (SPM) levels. Results from the Chelsea look similar to the OBS profiles except that this instrument is sensitive to a wider size range of particles including small and more translucent ones. Output from the Chelsea showed much more texture than OBS profiles. Because these optical turbidity devices are sensitive to different particle types it is often informative to ratio their outputs. This analysis will be done during post-cruise processing.

SIMRAD altimeter
This device has a range of 300m and becomes extremely accurate (±0.5m) at short distances (<20m). We use this device to position the package near the bottom. The SIMRAD in combination with the favorable sea-state that we experienced during this leg, allowed us to routinely position the package 5m or less from the bottom.

SeaBird rosette and 1.7L bottles
Our goal in the TECFLUX project is to determine the flux of CH_4 through the water column and the influence of this flux on the chemistry of the overlying water. This work requires the development of a reliable CH_4 detection system (see METS sensor section below). In order to be able to develop such a system and in order to develop an inventory of CH_4 in the water column requires the measurement of CH_4 in water samples. Our ability to reliably collect water samples with the ZAPS package is an integral part of this process. Although we had communication problems on the conducting cable we were able to attain this goal with the exception of the first operation (see table).

ZAPS fiber optic spectrometer
ZAPS is a fixed-filter instrument designed and constructed at Oregon State University that couples a photomultiplier tube and xenon flash lamp through a short (18cm) bifurcated bundle of fused silica fibers potted in stainless steel tubes. The fiber assembly is external to a pressure case that holds interference filters, xenon lamp, flash power supply, PMT detector with focusing lens, and signal processing board. A microprocessor on the ZAPS signal board relays digital commands and sends data to a specially designed "power bottle" that contains the system's power supply, data packaging circuits, and modem. The circuits in this bottle package data from ZAPS, the CTD, and the other sensors. The modem transmits the packets to the ship through the conducting cable to a specially constructed deck unit that disseminates data to three locations: real-time display, primary storage, and backup archiving. The deck unit supplies the instrument package with 500W of power and encodes digital commands downloaded to the ZAPS instrument.

Unlike most commercial instruments, ZAPS' operating parameters can be changed at any time. These variables include PMT bias voltage (300-1100V), flash lamp intensity (600-1200V), and flash rate (1-50Hz). During this leg we operated one ZAPS instrument with a flash rate of 3Hz, flash intensity of 900V, and PMT bias of 400V. We set up the lens and filter configuration to measure reflectance with the hope that this measurement would make it possible to detect bubble of methane in the water column. This information would complement the dissolved CH_4 results from the METS sensor and the bubble swarms imaged with the acoustic devices on the ship.

The only operation where we were able to position the package in an intense acoustic plume was 143-74-1 over the Hydrate Ridge South. We saw no strong reflectors in the water column during this operation as we would have hoped, although small anomalies were present. We did use output from this device to take CH_4 samples in earlier operations (36-2 and 45-2) with some success (see table).

We feel that the reflectance technique has promise but needs to be refined. As we used it during this cruise the background was fairly high. We feel that we improve our signal/noise ratio considerably by further development in a calibration tank. We plan to undertake this work later this summer and re-deploy ZAPS as a reflectometer on the TECFLUX cruise that will take place on the RV WECOMA later this year.

METS methane sensor
(summary after CTD deployments on RV ATLANTIS)

It is clear that the METS sensor works on some level. The greatest success of the cruise was CTD 3 where the sensor went off at the same depth of the acoustic anomaly when being lowered at 5 m/min. During CTD 5 the sensor read the lowest near the bottom of ant station during the cruise and indeed the CH_4 concentrations turned out to be the lowest as well. Again during CTD 6 the sensor showed large anomalies when being brought up (nothing going down) and this cast produced high concentrations at approximately the same depths. However the sensor also produced enigmatic results as exemplified by the last cast, CTD 7. There was a small but distinct CH_4 anomaly at the bottom of this station but the sensor showed nothing going up or down. Also the severe memory effect of the sensor was also evident. When a large anomaly occurred it took at least 30 minutes for the signal to flush from the sensor head (apparently). This and the slow response time of the sensor make it virtually impossible to use the METS sensor as an exploration tool. For when an anomaly occurs it is never exactly clear where the parcel of water is that caused it to go off. We tried flushing the surface of the membrane by pumping water over the sensor head. At first this seemed to work and the sensor "equilibrated" faster on the way down. But this effect did not seem to be consistent or reproducible. There is no doubt that the sensor is capable of detecting CH_4 on some occasions, but overall its output is unreliable and hard to interpret. On this leg we started to address some of the problems with the sensor identified during the NEW HORIZON and ATLANTIC cruises. We realized that the sensor seemed to be fairly sensitive but failed to recover from signals in a timely fashion making it difficult to use for directing sampling. We overcame this problem by looking at the slope of the response with time (dV/dt) instead of voltage output.

We could see that when we compared dV/dt to CH_4 concentration as shown in Fig. 17 that there was a correlation. These results also highlighted the fleeting nature of

these plumes as several bottles closed on the same dV/dt peak often had a wide range of CH_4 concentrations.

SONNE 143-45-2
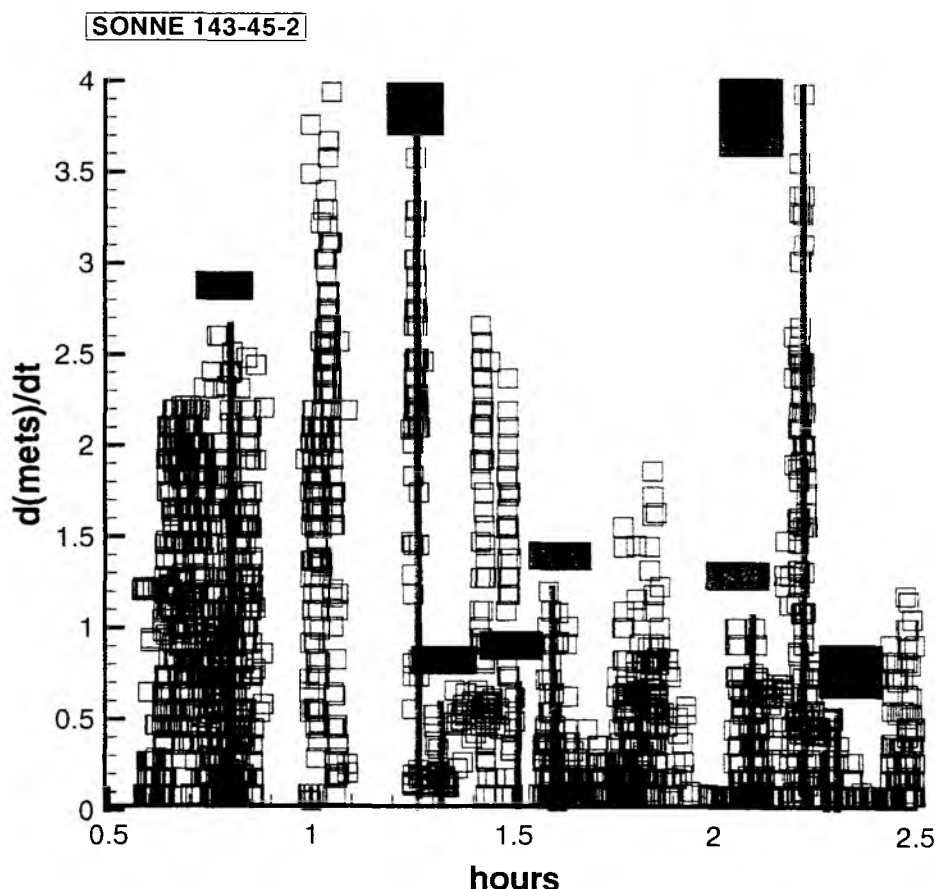
Fig. 17: Plot of the derivative of the CH_4-sensor output vs time. Also shown is the result of CH_4 measurements of discrete samples from the ZAPS rosette and the the time when the Niskin bottles for these measurements were closed.

Initially we could only look at voltage output from the sensor in real time. Midway through the cruise we were able to modify our software to plot the derivative during the operation. We attribute the high concentrations that we were able to sample to this improvement (see Table 3). Fig.18 and Fig. 19 are profiles of dV/dt data. The first operation where this parameter was available (67-1) produced a very flat profile with no anomalies. This station was carried out over a sandstone ridge in the NW corner of our study area. Water samples collected with the package and CTD/rosette verified that CH_4 at this site was at background levels. This result contrasts sharply with the

CH$_4$ plumes detected at HRS and HRN during the last two operations, as shown in the figures.
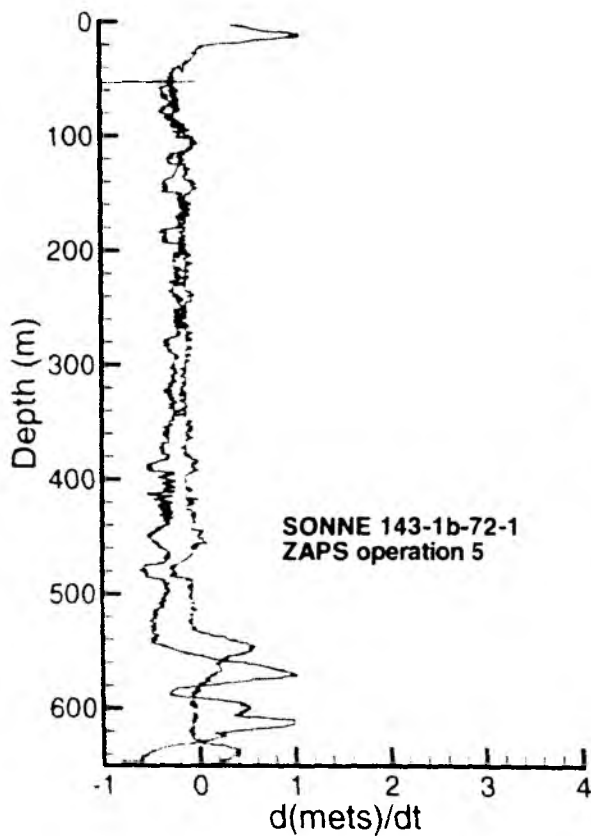
Fig. 18: CH$_4$ derivative vs time on stations 72-1 , where CH$_4$ anomalies was seen from the sensor's response. The finding is supported by discrete CH$_4$ measurements from the discrete measurements of water samples from the ZAPS rosette (see Table 3)
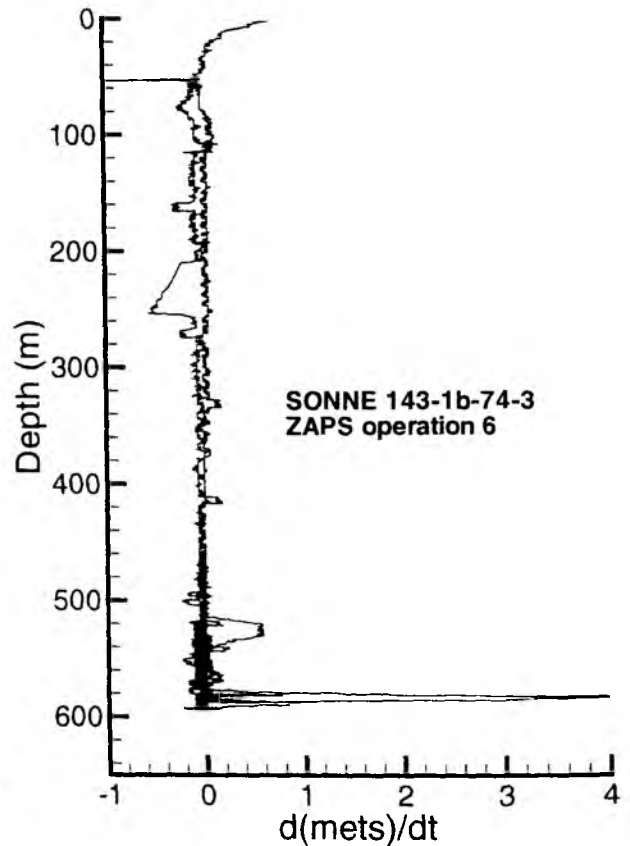
Fig. 19: CH$_4$ derivative vs time on stations 74-3.

In summary, we now feel that using this new parameter we can get at least a semi-quantitative view of CH$_4$ concentrations in the water column. We need to work on finding ways to further quantify these levels, correlate the acoustic plumes with

bubbles in the water column, and explore other methods to image the methane flux, loptical techniques.

Operation summeries

SONNE 143-1b-25-1
ZAPS operation 1
16 July 1999
short tow over summit of Hydrate Ridge North

SONNE 143-1b-36-2
ZAPS operation 2
18 July 1999
profile at site of acoustic plume on Hydrate Ridge South

SONNE 143-1b-45-2
ZAPS operation 3
21 July 1999
second profile and drift and Hydrate Ridge North summit, part of first temporal study at HRN

SONNE 143-1b-67-1
ZAPS operation 4
26 July 1999
drift across NW ridge where sandstone slabs were later recovered with the TV grab

SONNE 143-1b-72-1
ZAPS operation 5
27 July 1999
dip of opportunity over hydrate site at Hydrate Ridge South -very intense acoustic plume in bottom 150 meters imaged when positioning for TV grab

SONNE 143-1b-74-3
ZAPS operation 6
28 July 1999
part of second temporal study at Hydrate Ridge North summit

Table 3: Methane concentrations (ppm) in ZAPS bottles.

	36-2	45-2	67-1	72-1	74-3
1	12.94	272	—	128/127	22.4
2	18.14	130/155	3.77	10.72	4.91
3	4.95	?	6.03	220	162
4	14.19	7.27	—	6.84	2060
5	44.9	19.7	4.30	—	258
6	4.36	58.4	—	389	11 0
7	47.3	43.5	5.48	1045	4.70
8	6.84	112	—	954	61.8
9	117	39.3	—	128	7.07
10	<2	4 76	—	881	7.21
11	2.36	6 26	—	—	—
12	2.95	6.28	—	474	—

2.4   Ocean Floor Observation System (OFOS)

C. Jung, B. Teichert, S. Bollwerk, N. Aberle, H. Florianova, T. Eisenhauer, M.J. Whiticar

2.4.1   Introduction and equipment

During RV SONNE Cruise 143-1a and 1b seventeen OFOS (Tab. 4) surveys were performed. The objective of the OFOS-program was to establish a detailed geological map to study morphological and biological aspects and to support future investigations at the Hydrate Ridge. Further objectives were to identify new vents and gashydrate areas in order to verify previous results.

Table 4: Summary of the data of the OFOS tracks.

SO 143-1a/b OFOS-tracks								
Date	Start No.	Time (UTC) at bottom	Time (UTC) off bottom	Start Lat (NS) at bottom	Long. (EW)	End Lat (NS) off bottom	Long. (EW)	Working area	Observations
	143-1a								
8.7.99	4-1	13:41	21:16	44° 50,24'	125° 53,67'	44° 50, 15'	125° 01,32'	BSR Outcrop, SL 100, Northeast of Hydrate Ridge	at 900 m water depth patches of bacterial mats, sediment cover
9.7.99	7-1	13:44	18:38	44° 26,99'	125° 02,44'	44° 27,01'	124° 53,98'	Southeastern of Hydrate Ridge, SE-knoll	carbonate crust, small carbonate chemoherm
10.7.99	10-1	13:32	22:41	44° 36,88'	125° 00,24'	44° 36,86'	125° 10,21'	Hydrate Ridge, saddle between Northern and Southern summit	saddle structure with carbonate pavement
11.7.99	13-1	13:28	16:32	44° 44,68'	125° 06,99'	44° 40,67'	125° 02,73'	Hydrate Ridge, continental side of Northern summit	some carbonate boulders and small clam fields, field of big sponges
11.7.99	14-1	18:25	22:51	44° 35,14'	124° 56,49'	44° 35,13'	125° 02,15'	Eastern basin, acoustic white spots	patches of bacterial mats, sediment cover
	143-1b								
15.7.99	20-1	13:24	16:51	44° 34,14'	125° 08,48'	44° 34,19'	125° 08,35'	Southern summit of Hydrate Ridge, Beaver mounds	orange and white bacterial mats, clam fields, carbonates, active venting
17.7.99	27-1	14:27	16:58	44° 34,69'	124° 58,48'	44° 34,69'	125° 01,13'	Eastern basin, acoustic white spots	patches of bacterial mats, sediment cover
17.7.99	28-1	18:31	21:21	44° 33,89'	125° 08,50'	44° 34,64'	125° 11,18'	Southern summit of Hydrate Ridge	carbonate boulders, living clam fields, bacterial mats
18.7.99	33-1	18:28	22:30	44° 35,95'	125° 57,33'	44° 35,46'	125° 01,81'	Eastern basin, acoustic white spots	sediment cover, some current ripples, small patches of bacterial mats
19.7.99	37-(1-3)	20:45	4:05	44° 35,97'	124° 57,30'	44° 40,59'	125° 02,49'	Northern summit of Hydrate Ridge	carbonate outcrops, carbonate slabs and boulders, sceletal carbonates, sediment and current ripples,
22.7.99	44-1	13:08	20:37	44° 50,10'	124° 47,94'	44° 50,20'	124° 59,71'	BSR Outcrop, SL 100, Northeast of Hydrate Ridge	carbonate boulders, big doughnuts, chimneys, soft sediment, less patches of bacterial mats
23.7.99	53-1	3:58	5:02	44° 33,90'	125° 08,83'	44° 34,75'	125° 08,74'	Southern summit of Hydrate Ridge, south-north extension	carbonate pinnacles, clam fields and bacterial mats
25.7.99	57-1	4:23	6:46	44° 36,90'	125° 09,95'	44° 36,97'	125° 12,86'	Saddle of Hydrate Ridge, track 10-1 continue to the west	pogonophorans, soft sediment, rocky slope
25.7.99	58-1	8:37	10:22	44° 37,56'	125° 06,00'	44° 37,60'	125° 03,88'	Eastern slope of Northern summit of Hydrate Rigde	carbonate pavement, carbonate outcrops, sceletal carbonates and chimney structure
25.7.99	59-1	11:53	18:18	44° 44,00'	125° 01,85'	44° 44,02'	125° 52,88'	Western of Hydrate Ridge, Seismic Line 8a	plain soft sediment, some patches of bacterial mats, carbonate boulders
26.7.99	66-(1-2)	14:40	19:46	44° 43,13'	125° 14,58'	44° 44,05'	125° 14,33'	Northern of Hydrate Ridge, NW-knoll	big living clam fields and bacterial mats at the top, carbonate outcrops
28.7.99	75-(1-2)	3:17	4:30	44° 43,64'	125° 13,10'	44°40,49'	125°07,29'	Northern of Hydrate Ridge, NW-knoll and Northern summit	carbonate outcrops, some clam fields and patches of bacterial mats,
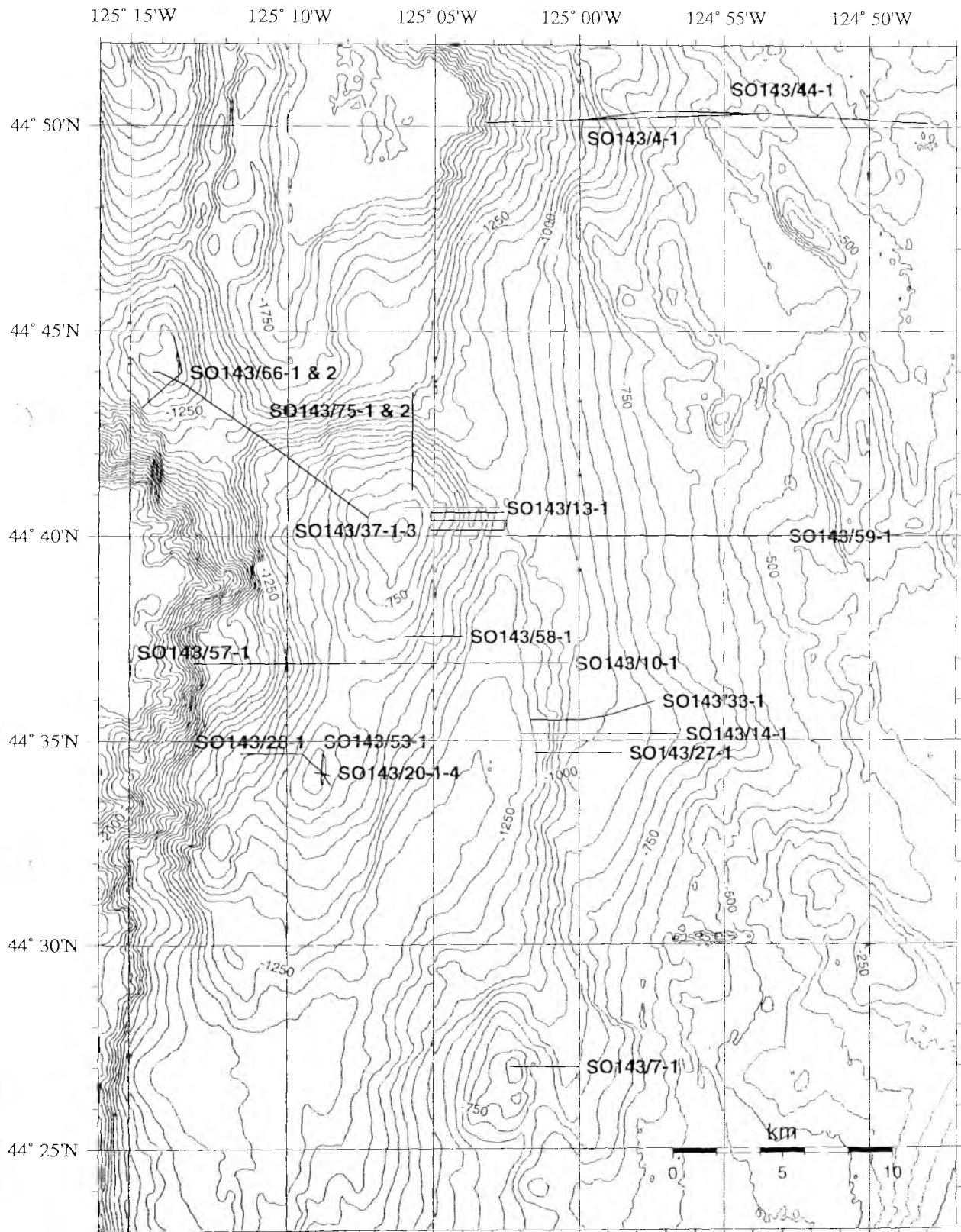
Fig. 20: Location of OFOS-tracks.

OFOS is a video-controlled deep-towed device with SIMRAD SSBL (Super Short Base Line System) responder system for online navigation. The conception of the OFOS is to send video signals and data signals simultanously.

There are also two video cameras installed, the color video camera (DEEP SEA POWER AND LIGHT)) and the black and white video camera (SIMRAD OSPREY). The stereophotosystem (PHOTOSEA) allows to take 800 color slides with each camera. Two xenon lights and two halogene lights (DEEP SEA POWER AND LIGHT) are installed.The OFOS is equipped with a compass, an altimeter (BENTHOS) and a temperature sensor (RTB). The attached CTD (SEABIRD) allows simultanous online data aquisition of conductivity, temperature and depth. The fibre optic controls data transfer and the coaxial cable controls the electric power supply. Data and slide managment can be controlled manually by the operator.

2.4.2   Survey areas and results

Northern summit

Two OFOS-tracks were performed at the northern summit, SO143-13-1 and SO143-37-(1-3) and another one extending to the east. The purpose of SO143-59-1 was to investigate new unknown area in order to complete the general map. The Track 37-(1-3) consisted out of three parallel track lines. The first track (Station 13-1) was performed to verify the morphology of the east slope of the Hydrat Ridge. The target was to search for indications of active venting or fossil vent sites. It was expected to find carbonate outcrops, living clam fields or bacterial mats. The track extended from west to east and started at a water depth of 645 m. Deepest water depth reached 1067m. At the beginning ocean floor was dominated by soft sediments with traces of bioturbation. Living fauna was present e.g. sea urchins and star fishes. Following the track carbonate fragments and further on carbonate outcrops dominated. In between the carbonate few clam fields were visible. Before reaching the end of the track a field of living silicate sponges appeared. Single sponges are about 50 cm high and were placed on the west side of a small hill, east of the Northern summit.

Of particular interest was to investigate the mud mound east (Stations 37-1, and -3) which was previously detected by multibeam seafloor investigation. Another target was to find a spongefield discovered during track 13-1. It was of interest wether or not these sponges are influenced by venting activity. The track started in the south and headed eastward. Later on it turned back to the west and finally again to the east. At the beginning of the track a small area of soft sediment cover beyond a hard crust of presumably carbonate dominated. Reaching the mud mound east some living clam field and alsosmall bacterial mats appeared. Carbonate pavement outcropped steps are coming out and talus gets more. Going down the slope of the Northern summit oceanfloor seems to consist of sediment covered carbonate pavement.

At the End of OFOS 37-3 we again reached the extended sponge field, already seen on Track 13-1. However, there were no indications of a vent influenced area. Presumably, sponges are supplied with nutrition by the prevailing current system.
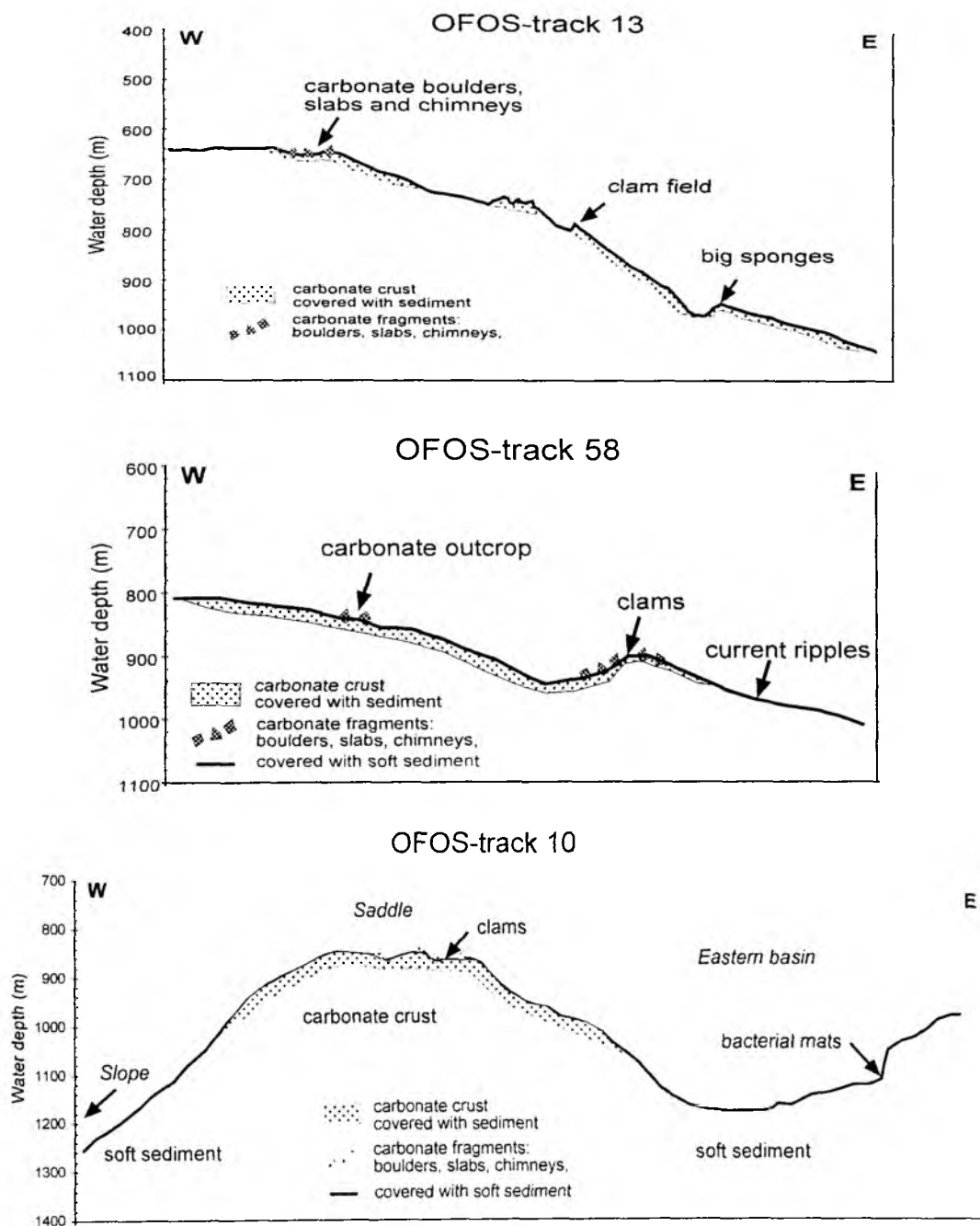
Fig. 21: OFOS tracks 13-1, 58 and 10. The data of the water depth are from CTD.

Southern summit

For the southern summit three tracks were performed. OFOS track 20-(1-4), track 28-1 and Track 53-1 in south-north direction. All tracks were expected to be very interesting because the southern summit appeared to be the most active area. OFOS 20-(1-4) was a very short survey (with 4 seperate tracks) starting in a water depth of

798 m and ended in a depth of 828 m.The anticipated target was to find bacterial mats, living clam fields and typical vent carbonate precipitations for focussing the exact location.There were four seperate tracks but the third one hit the extended bacterial mats and extensive living clam fields around the mats. The color of the mats appeared to be white and orange, respectively with the third track the bacterial mats and clam fields were reached once again. The track crossed large erected pinnacles in between the bacterial mats. These pinnacles seemed to be overgrown by bacteria and appear to be still active. The OFOS-track also crossed a flowmeter, Alvin traces and the marker No.7 placed by a ALVIN-dive.

The track 28-1 also crossed the top of the southern summit coming from south-east and changed the direction to west. At the beginning the water depth was 816 m and ended with a water depth of 1167 m. The track once again found bacterial mats and living clam fields. Vent carbonates were also present. Going down the eastern slope of the summit only soft sediment with some carbonate talus and some brittle star fields were noticed.

The OFOS Track 53-1 was performed at the south-northern most position, starting in a water depth of 797 m and stopped at a water depth of 830 m. The target of this investigation was to find the carbonate pinnacles again and furthermore to discover new active vent sites. Bacterial mats and clam fields appeared, however, no more active venting indications were found further down. The sediment cover increased with increasing water depth. The relocation of extended bacterial fields and the erected pinnacles failed because of difficulties with transponder navigation and bad weather condition.

Saddle and mud mound

On this site were three OFOS-tracks performed. All tracks extended from east to west. Track 10-1 reached a waterdepth of 1001 m at the beginning and at the end a water depth of 1332 m. Track SO143-57-1 continued track 10-1 reaching a water depth of 1847 m. Track SO143-58-1 was performed to start at the west end with a water depth of 814 m and ended at a water depth of 1050 m. The saddle area of the hydrate ridge consisted of a carbonate pavement covered by sediments. The carbonate crust is flat with a rough surface covered with more or less sediments. More sediment accumulated in the east basin of the saddle of hydrate ridge. Some carbonate slabs and carbonate outcrops characterised the carbonate crust area. The track 57-1 continued the last one, but no objects of interest were detected. However, two massive and steep hardrock edges appeared at the slope.
The track 58-1 showed the same carbonate pavement like the southern track (10-1). Reaching the little summit carbonate outcrops and fragments were visible. Following the track sediment covered carbonates outcropped followed by current ripple.

Acoustic white spots

Three OFOS-tracks were located in this basin area, OFOS 14-1, 27-1 and 33-1. Acoustic white spots were detected by side scan sonar survey. Three OFOS-tracks were performed at the basin west of hydrate ridge. The OFOS investigations were performed to investigate this white patches. However, although there were clear acustic anomalies no visible changes of usual morphology could be detected with the OFOS system. The sediment cover increased with increasing depth. Few small

patches of bacterial mats appeared. The sediment showed traces of bioturbation. There also exists some living fauna, e.g. star fishes, snails and crabs.

BSR-outcrop
The OFOS-tracks 4-1 and 44-1 were performed near the seismic line 100, in the northern part of our working area. Both tracks were about 8 nm long. The water dephts reached 1600 m in the west and 600 m in the east. Former investigations expected a BSR-outcrop and mud vulcanos. However the survey detected only soft sediments, clam patches and small bacterial mats. A field of big and presumably fossil carbonate chimneys or doughnuts existed in the east part of the track. Later on doughnuts were recovered with the TV-G.

NW-knoll
For this new working area two OFOS 66-1-2 and 6-1, and -2 were performed. The two tops of this summit showed two area of activ venting indicated by living clam fields and bacterial mats.The slopes were covered with sediment and sometimes carbonate fragments appeared.
The Track 75-1, -2 connected the NE-knoll with the northern summit of hydrate ridge. The target was to investigate the morphological and geological on the slopes. The first track started in north-east and heated to south-west. The track crossed two extended carbonate outcrops indicating probably inclined carbonate layer The second track started at the northern summit and headed northward.No further carbonate outcrops could be found.

SE-knoll
The OFOS 7-1 was performed in the south of the working area. There was a little summit and water depth reached 689 m at the top. Deepest water depth reached 885 m. This track was dominated by sediment cover alternating with talus. There were no indications for activ venting sites.

2.5   Vent sampling and flux measurements

P. Linke, F. Appel, B. Bannert , A. Petersen

2.5.1   Introduction

Hydrogeologic processes can exert a fundamental control on the stress state, dynamics, and the thermal, and geochemical processes along continental margins. Hydrogeologic processes impact (1) the physical and chemical evolution of sediments and the oceanic basement during subduction, (2) the state of stress and seismic properties of major plate boundary fault zones, (3) earthquake dynamics, and (4) global chemical cycles of green house gases and other chemicals. It has also been recently recognized that in some regions ground water seepage may be volumetrically significant enough to effect the chemistry of the coastal ocean waters (Moore, 1996).

Although direct evidence for the chemistry and volume of fluids migrating towards the sediment surface is relatively sparse, especially in zones of diffusive flow, there is strong evidence for locally significant focused advection of fluids carrying reduced sulfur and/or reduced carbon compounds (e.g., methane) from the presence of dense chemoautotrophic giant clams (*Calyptogena*) and/or tube worm communities at cold seeps (Kulm et al., 1986; Boulegue et al., 1987; Suess et al., 1985). Other evidence for past and present fluid expulsion is the occurrence of carbonate pavements and chimneys (e.g. Kulm et al., 1986). Once seeps began to be identified based on this visible evidence, it was found that they were a common feature all along the continental margins in a variety of tectonic settings. Focused discharge rates can be large. Determinations made at seeps off Oregon suggest that, where seepage is marked by obvious biologic communities, H_2O and CH_4 flux rates can be as high as 100-1065 m/y (average Darcy flow) and 120 mmol m^{-2} day^{-1} respectively (Linke et al., 1994).

Focused discharge at theses seeps, may, however, be only part of a larger hydrogeologic puzzle. It quickly becomes apparent that fluid migration and discharge is strongly heterogeneous with regions of focused and diffuse flow (Moore and Vrolijk, 1992; Brown et al., 1994). The diffusive flow component could be of sufficient magnitude to promote the regional build up of significant gas hydrate bodies along continental margins (Hyndman and Davis, 1992). Structure, lithologic, and diagenetic patterns contribute to heterogeneity in flow and expulsion pattern through their effect on the permeability distribution at depth. Heterogeneity occurs at a variety of scales. Linke et al. (1994), for example, report they encountered at seeps off oregon an „enormous variability in the rates of fluid expulsion within the same accretionary prism". Seeps, however, typically represent much less than 0.01% of the surface area of most active tectonic systems. There is also strong evidence for irregularly but widespread diagenetic hard grounds all around the Oregon seeps, suggesting that widespread elevated rates of diffusive flow may be occurring over a region of many 10's km^2 (Carson et al., 1994). Even though it occurs at generally lower rates, the diffuse component flow can be as important as focused flow in terms of the total mass balance of fluids because of the greater area involved. For a variety of reasons,

however, direct quantification of this diffusive component has been difficult, with the exacerbating factor that it is also likely to be spatially heterogeneous.

These factors have fundamentally limited our past ability to constrain the complete hydrologic system in many environments. Ultimately, in large offshore hydrogeologic systems, the statistical relevance of mass flux and hydrogeologic determinations can only be proven through a large number of surface flux measurements that allow us to build accurate maps of heterogeneous fluid and chemical expulsion patterns. The basic problem associated with accurately quantifying heterogeneous fluxes applies to almost any type of studies our work relates to, whether we are interested in the relationship between aqueous (and gaseous) discharge patterns and (1) structure/statigraphy, (2) gas hydrates, (3) other chemical fluxes, and (4) benthic biological seep communities and nutrient fluxes.

2.5.2 Material and methods

Our basic concept to sample fluids and to measure the fluid and gas flow is the channeling of the effluent from the sea floor into a semi-enclosed benthic chamber with a large opening at the bottom and a small exhaust port at the top (Linke et al., 1994). After deployment of the chamber the internal volume is initially flooded with ambient seawater and is then slowly replaced by vented fluids. Sequentially timed water samples are collected inside the chamber. Changes in the concentration of dissolved components within this time series are used to calculate flux rates (Carson et al., 1990). Parallel to this, a thermistor flowmeter is mounted in the exhaust port of the chamber to record the *in situ* fluid flow rate.

During cruise SO130 we used two video-guided devices for the deployment of a benthic chamber from a conventional research vessel on a cold seep at the seafloor (VEnt SamPler - VESP). The ship's cable (either coaxial or a hybridic with fiber optic and coaxial fibres) is used for bidirectional transmission of the video images, commands, data, and power supply of the underwater units (ADITEC/SCHOLZ). The instrument is towed in view of the seafloor approx. 2 – 3 m above the sediment and is deployed when signs of seepage become visible (e.g. clam clusters, bacterial mats). During deployment the given slack of the cable is kept away from the moored instrument by floatation attached to the cable (FLOATATION TECHNOLOGY). On modern research vessels like the RV SONNE, the positioning of the ship in respect to the deployed instrument is obtained with a computer-controlled differential positioning system (DGPS/Multifix) and SSBL-(Super Short Base Line) navigation (SIMRAD) with a cable-mounted transponder close to the instrument on the seafloor.

In the first device, the barrel is attached to the central piston of a modified multicorer frame which operates on a water hydraulic basis and assures gentle deployment of the barrel once the frame settles on the sea floor (Linke et al., 1994). VESP I is equipped with five 5 L water bottles (HYDRO-BIOS) and a programmable data logger (TATTETALE) mounted within the barrel which is activated from the surface telemetry unit to start the water-sampling cycle. Furthermore, a storage CTD probe (Sealogger SBE25) is mounted on the frame to continuously record conductivity, temperature, and

pressure. In the case of very small flow rates silicon tubings were connected to the pump (SBE 5T) of the Sealogger to provide a better convection within the barrel. Another storage probe (Seacat SBE16) was customized with 3 thermistors in a stainless steel sting to record sediment temperature during deployment of VESP. By using a BENTHOS camera and flash still photographs can be obtained during the towed survey for a suitable spot and the deployment of the barrel. The benthic barrel is a commercially available 55-gallon polyethylene barrel with a large opening at the bottom and a small exhaust port at the top. The exhaust port at the top of the chamber carries a thermistor flowmeter which directly records the flow rate from the chamber in the data logger. A small plexiglass tube with a simple rubber valve on top and a core catcher on the bottom was attached to the chamber to retrieve a sediment core from the deployment site.

Since this VESP system requires a permanent cable connection to the ship for bidirectional power, video signal and data transmission which limits the deployment time (up to 2 hours) we developed a concept to deploy a lander system with a launcher and disconnect it from the ship's cable after it's video-guided deployment on a suspected seep site (Cremer, 1995). The lander (VESP II) is equipped with an improved chamber to obtain both direct water flow and samples expelled from active sites and is designed as an instrument carrier for a variety of different measurements which could be integrated within this system. The lander is designed to stay on the seafloor for several days recording the different parameters (e.g. temperature, oxygen, methane, fluid flow, microseismicity), could take photographs and would take samples prior to the recovery of the instrument by acoustic release of the additional weight.

In the configuration used during cruise SO130 the launcher carried two b/w video cameras (OSPREY 1392 & 1358), a survey camera on the front and a backward oriented camera showing the chamber during deployment. Both cameras and floodlights can be switched with a PC-controlled telemetry surface unit (ADITEC/SCHOLZ). Two laser pointers are used to obtain a scale for the video images of the seafloor. Additionally, the lander is designed to carry a scanning sonar (SIMRAD, 675 kHz) with on-line data transmission to the surface to scan a broader field for acoustic objects (like precipitates, clams fields) than obtained by the video cameras. The attached lander can be disconnected from the launcher by a mechanic release (NICHIYU GIKEN KOGYO). It carries a floatation unit with upto 16 BENTHOS floats and instrument housings which can be easily exchanged with a floatation unit containing synthatic foam instead. Pieces of train tracks are used as weights and are dropped by paired acoustic transponder releasers (MORS RT 661 B1S & RT 361 BS). Beneath the floation unit the lander has a wide open space for carrying various instruments like i.e. benthic chambers. The chamber used on the SO130 cruise is a pyramidial stump made of titanium with a height of 30 cm. The bottom (surface) area covers $1m^2$ and the exchangable top area (40 x 40 cm) was equipped with ports for the thermistor flowmeter and a methane sensor, provided by GKSS. In the present configuration, the chamber is suspended within the lander frame during deployment by strong rubber bands and lowered on the seafloor by its own weight. To faciliate water exchange during deployment and recovery valves are opened by rubber bands and kept close through spring action when the chamber is placed on the seafloor. A

motor-driven syringe sampler with 8 x 100 ml glas syringes will be attached to the chamber to take water samples in a time series during deployment. To obtain a larger sample at the end of the deployment a single 1.7 L water bottle is mounted within and another as a bottom water reference sample outside the chamber respectively. Both are tripped simultaneously at the end of the deployment when the acoustic releasers are activated and provide water samples for the analysis of dissolved seep fluid species. For spotting and recovery the lander is equipped with a radio beacon and strobe light (NOVATECH) and flag.

2.5.3   Results

During cruise SO130 ten VESP I casts with 8 successful deployments on visible targets (bacterial mats and clusters of *Calyptogena* sp.) and 2 successful test deployments with VESPII were performed. The obtained water samples were splitted for the analysis of oxygen, methane, H_2S, microbial numbers and activity. Sediment cores were analysed for microbial species (like *Beggiatoa* and *Thioploca*). CTD- and flowmeter data will be processed and analysed at GEOMAR. The scanning sonar was deployed for the first time successfully on the OFOS and proved to be a promising tool for the survey of the sea floor. For a detailed interpretation of the obtained scans it became visible that further developments like a correction for the ship's movements (pitch and roll) and digital recording are needed.

2.6   Sediment sampling and carbonate sedimentology

T. Naehr, K. Heeschen, A. Eisenhauer, B. Teichert, S. Bollwerk

2.6.1   Sampling and equipment

During RV SONNE Cruise SO143-1b, sediments, vent fauna, authigenic carbonates, and gas hydrates were recovered using a gravity corer (Schwerelot, SL), a TV-guided multicoring system (TV-MUC) and a TV-guided grab (TV-G). Details on sampling with the different systems, as well as station numbers, locations, and sample type are given in Tables 5-8.

The gravity corer was deployed with a weight of 1.5 t and a core barrel of 10 cm in diameter with variable length ranging from 6 to 12 m. Operation of the gravity coring system usually resulted in poor core recovery, due to a combination of indurated or partly cemented sediments and technical problems with the coring system (faulty ball valve). Recovery varied from 122 to 555 cm. Both PVC and thin plastic tubing and were used, the latter allowing very fast access to the sediments, which proved to be a great advantage for sampling sediment cores containing gas hydrates.

Table 5: Multicorer station.

Station SO143-3/	Date [UTC]	Lat./Long.	Depth [m]	Cores [cm]	Analyses	Recovered samples
24–1	16. Jul	44°34.229°N 125°08.806°W	788	A - 27	pw., oxygen	
				B - 23	biol.	vent fauna
				D - 26	pp., meth.	sediments, carbonates
				C	biol.	vent fauna
24–2	17. Jul	44°34.222°N 125°08.801°W	787,4	A - 25	pp., oxygen	sediments, carbonates
				B - 25	biol.	vent fauna
				C - 24	biol.	vent fauna
				D - 28	pw.	
24–3	17. Jul	44°34.229°N 125°08.809°W	787	A - 28	pp.	sediments, carbonates
				B - 28	biol.	vent fauna
				C - 28	pw., oxygen	
				D - 29	biol.	vent fauna
63–1	26. Jul	44°37.010°N 125°03.010°W	1201	A - 48	biol., oxygen	non vent fauna
				B - 47	-	archiv (full core)
				C - 43	pw.	
				D - 49	pp., meth.	sediments?
				E - 50	biol.	non vent fauna
				F - 51	biol.	non vent fauna
				G - 47	biol.	non vent fauna
70–2	27. Jul	44°38.500°N 125°14.500°W	2307	A - 40	biol.	non vent fauna
				B - 39	biol.	non vent fauna
				C - 35	biol.	non vent fauna
				D - 40	-	archiv
				E - 40	biol., oxygen	non vent fauna
				F - 41	pw.	
				G - 40	pp., meth.	

Abbreviations: biol.= biology, meth.= methane, pp.= physical properties, pw.= porewater

Table 6: TV-multicorer stations.

Station SO143-3/	Date [UTC]	Lat./Long.	Depth [m]	Cores [cm]	Analyses	Recovered samples
29–1	17. Jul	44°34.264°N 125°08.811°W	776	A	biol.	vent fauna
				B	biol.	vent fauna
				C	biol.	vent fauna
				E	biol.	vent fauna
				F	biol.	vent fauna
29–2	18. Jul	44°34.264°N 125°08.827°W	773	A -20	pw.?	vent fauna
				B - 19	meth.	
				C - 22	pp., biol.	vent fauna
				D - 11	biol., oxygen	vent fauna
29–3	18. Jul	44°34.260°N 125°08.834°W	789,1	A - 24	pp., meth.	
				B - 28	oxygen	
				C - 44	pw., oxygen	vent fauna
29–4	18. Jul	44°34.220°N 125°08.820°W	786,9	A - 31	pp., meth.	
				B - 27	biol., oxygen	vent fauna
				C - 31	pw.	vent fauna
				D - 34	biol.	vent fauna
31–1	18. Jul	44°34.732°N 125°59.330°W	886	A - 39	pp., meth.	
				B - 29	oxygen	
				C - 36	pw., meth. (in pw.)	
				D - 36	biol.	non vent fauna
34–1	18. Jul	44°35.600°N 125°59.100°W	923,3	A - 41	pp.	sediments
				C - 36	pw.	
				D - 37	oxygen, biol.	non vent fauna
				E - 37	biol.	non vent fauna
				G - 42	biol.	non vent fauna
				H - 41	meth. (in pw.)	
45–1	22. Jul	44°50.290°N 124°59.370°W	993,5	A - 31	pp., meth.	sediments
				B - 31	-	archiv (full core)
				C - 31	biol., oxygen	non vent fauna
				D - 31	biol.	non vent fauna
				E - 31	biol.	non vent fauna
				F - 31	biol.	non vent fauna
				G - 31	pw.	
				H - 30	biol.	non vent fauna
45–2	22. Jul	not dropped				
45–3	23. Jul	not dropped				
46–1	23. Jul	44°50.323°N 124°58.466°W	840	A - 35	biol.	sediments
				B - 40	-	archiv (full core)
				C - 32	biol.	non vent fauna
				D - 35	pw.	
				E - 33	biol.	non vent fauna
				F - 37	pw., oxygen	
				G - 37	pp.	
				H - 35	biol.	non vent fauna
55–1	24. Jul	44°34.201°N 125°08.854°W	785,9	A - 23	pw.	vent fauna
				B - 31	pp., meth., meth. (in pw.)	
				C - 32	biol.	vent fauna
				D - 28	pw., oxygen	vent fauna
55–2	24. Jul	44°34.230°N 125°08.840°W	788,1	A - 21	pw.	vent fauna
				B - 9	biol.	vent fauna
				C - 34	pw.	vent fauna
				D - 15	pp., biol., oxygen, meth.	vent fauna
55–3	24. Jul	44°34.250°N 125°08.880°W	791,5	A - 26	pw., meth. (in pw.)	vent fauna
				B - 24	pp., meth.	
				C - 27	pw., oxygen	vent fauna

Abbreviations: biol.= biology, meth.= methane, pp.= physical properties, pw.= porewater

Table 7: TV-grab sampler stations.

Station SO143/	Date [UTC]	Lat./Long.	Depth [m]	Subcores	Analyses	Recovered samples
21–1	15. Jul	44°34.213'N 125°08.806'W	786	C – 40 cm	meth., pp., core descr.	carbonates, sediments,
				D – 40 cm	pw.	gas hydrates, clams
21–2	15. Jul	44°34.2115'N 125°08.8103'W	788	A' – 24 cm	pw.	carbonates, gas hydrates, clams
				A" – 33 cm	pw.	
				D – 20 cm	core descr.	
40–1	20. Jul	44°40.150'N 125°03.287'W	945,7	–	–	carbonates?, clams
40–2	20. Jul	44°40.141'N 125°03.322'W	908	A –	pw.	carbonates, gas hydrates, clams
				C –	pw.	
				D – 47 cm	meth., pp., core descr.	
41–1	20. Jul	44°39.977'N 125°06.099'W	609,5	B – 45cm	pp.	carbonates, clams,
				C – 41cm	pw.	C: +5 cm surface sample
41–2	21. Jul	–	–	–	–	–
49–1	23. Jul	44°50.1869'N 124°50.1623'W	344	–	–	carbonate chimney, many non–seep organisms
49–2	23. Jul	44°50.177'N 124°50.204'W	340	–	–	carbonate chimney
50–1	23. Jul	44°50.335'N 124°52.650'W	429	–	–	carbonates, few non–seep organisms
50–2	23. Jul	44°50.305'N 124°52.698'W	490	–	–	carbonates
56–1	24. Jul	44°34.220'N 125°08.798'W	787,1	–	–	carbonate crusts, clams
56–2	25. Jul	–	–	–	–	–
60–1	25. Jul	44°37.541'N 125°04.661'W	922,2	–	–	'bone bed' carbonates
61–1	25. Jul	–	–	–	–	carbonates
68–1	27. Jul	–	–	–	–	–
68–2	27. Jul	44°43.891'N 125°13.868'W		–	pw.	sandstones/carbonates
71–1	27. Jul	44°34.216'N 125°08.841'W	786,3	–		gas hydrates (7 samples frozen in N2, clams)
71–2	27. Jul	–	–	–	–	–

Abbreviations: core descr.= core description, meth.= methane, pp.= physical properties, pw.= porewater

Table 8: Gravity corer stations.

Station SO143-3/	Date [UTC]	Lat./Long.	Depth [m]	Recovery [m]	Analyses	Recovered samples
32-1	18. Jul	44°34.720'N 124°59.340'W	905	-	-	-
32-2	18. Jul	44°34.730'N 124°59.340'W	905,2	5,55	core descr.	archiv (half core)
35-1	19. Jul	44°35.590'N 124°59.090'W	921	1.40	core descr.	archiv (half core)
39-1	20. Jul	44°37.800'N 125°03.000'W	1200	0,83	-	archiv (full core)
48-1	23. Jul	44°50.320'N 124°58.370'W	827,8	1,85	core descr.	archiv (half core)
48-2	23. Jul	44°50.330'N 124°58.380'W	830	?	-	archiv (full core)
55-4	24. Jul	44°34.250'N 125°08.880'W	791,8	0,55	core descr.	no archiv core
55-5	24. Jul	44°34.210'N 125°08.809'W	787,1	1.05	core descr.	-
62-1	26. Jul	44°37.010'N 125°03.010'W	1201	1.10	-	archiv (half core)
70-1	27. Jul	44°38.500'N 125°14.500'W	2307	2.40	core descr.	pw., pp., archiv (1 m half core)

Abbreviations: core descr.= core description, pp.= physical properties, pw.= porewater

In general, deployment of the TV-guided multicorer was very successful and resulted in cores of up to 51 cm length. The system consists of 4-8 polycarbonate tubes with 10 cm inner diameter and 50 cm length, a video camera, two lights, and a telemetry unit.

The TV-guided grab contains an OSPREY video camera, two lights, and a telemetry unit to allow a survey of the target area prior to sampling. We successfully sampled sediments, gas hydrates, authigenic carbonates, and vent biota using this system. The main advantage of the TV-G lies in the large sample volume (up to 0.7 m^3). Thus, decomposition of gas hydrates during recovery was slowed down considerably and we were able to sample substantial amounts of gas hydrate and gas hydrate bearing sediments. However, sampling with the TV-G usually disturbs the sediment and never preserves the original sediment surface.

2.6.2   Preliminary sedimentological results

Based on stratigraphic investigations on DSDP Site 174, the sedimentary sequence on the Juan de Fuca plate consists of pelagic carbonate-rich oozes and terrigenous mudstone overlain by turbidite sequences with intercalated mud layers (Kulm and von Huene, 1973). On top of this sequence follow sandy turbidites and the Pleistocene terrigenous sediments of the Astoria and Nitinat fans and Cascadia and Astoria channels.

Preliminary petrographic examination based on macroscopic core description and smear-slide analysis indicates that the dominant sediment type in the study area is terrigenous, dark greenish gray mud. The sediment is almost barren of microfossils and consists predominately of clay minerals and very fine-grained quartz and feldspar. Framboidal pyrite is common and indicates reducing conditions in near-surface sediments. H_2S concentrations in the sediment were usually very high (see pore water chemistry chapter).

In the north-western part of the study area, we observed dark sandy layers, up to 40 cm in thickness, consisting of volcanic glass and sand-sized quartz. These layers most likely represent turbidites, which redistributed volcanic material originating from the Cascadia volcanism. In the NW-knoll area (Station SO143-68-2), seepage of methane-rich fluids leads to the cementation of these sandy sediments.

The release of water during gas hydrate decomposition in some of the sediment cores (e.g., Core SO143-62-1) resulted in a fluidization of the sediment and destruction of the original sedimentary texture. In seepage areas, small (2-10 mm), irregular shaped authigenic carbonate nodules and crusts were observed in the sediments (e.g., Cores SO143-21-1, 40-2, 55-4, 55-5).

2.6.3   Gas hydrates

In order to sample gas hydrates for physical, geochemical, and textural studies, the TV-guided grab was used both on the northern and southern summit of Hydrate Ridge (Table 7, Stations SO143-21-1, 21-2, 40-2, and 71-1) and successfully recovered large volumes of gas hydrates. However, smaller volumes of gas hydrates
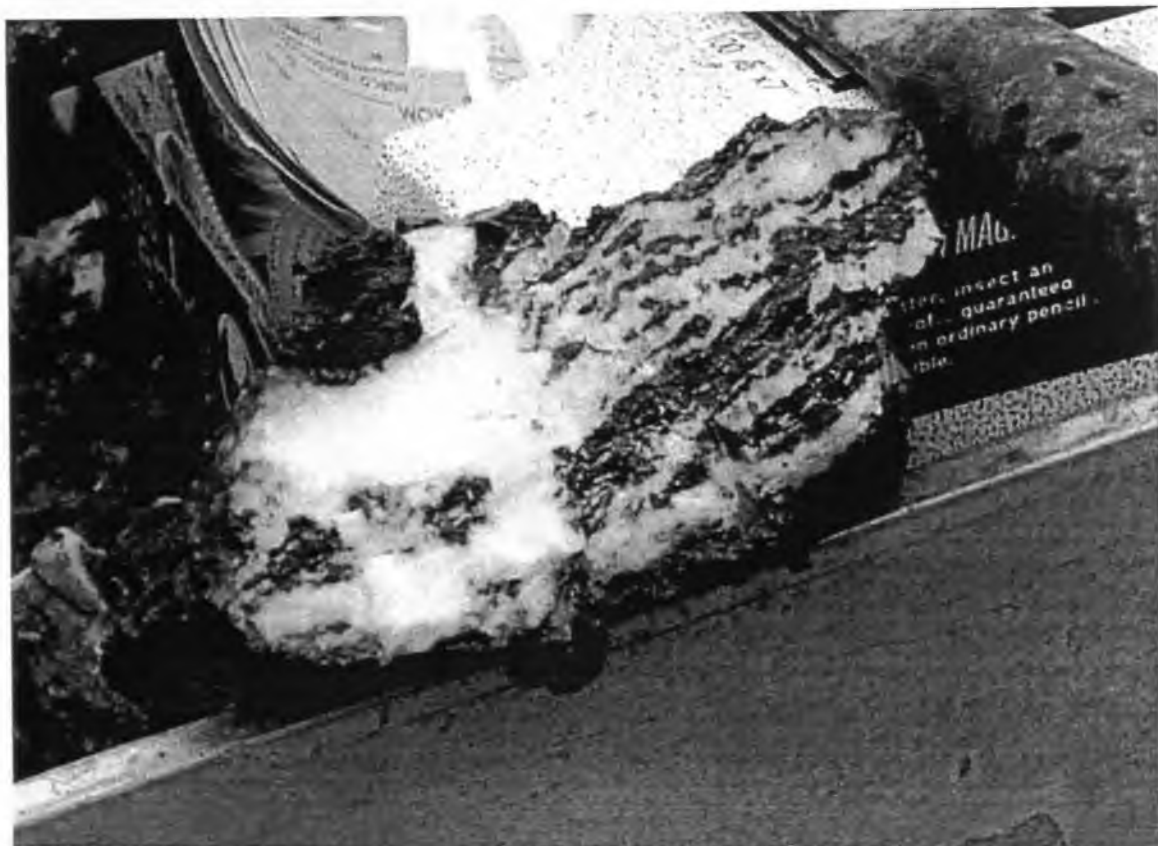
Fig. 22: Gas hydrate specimen of Station 71-1.
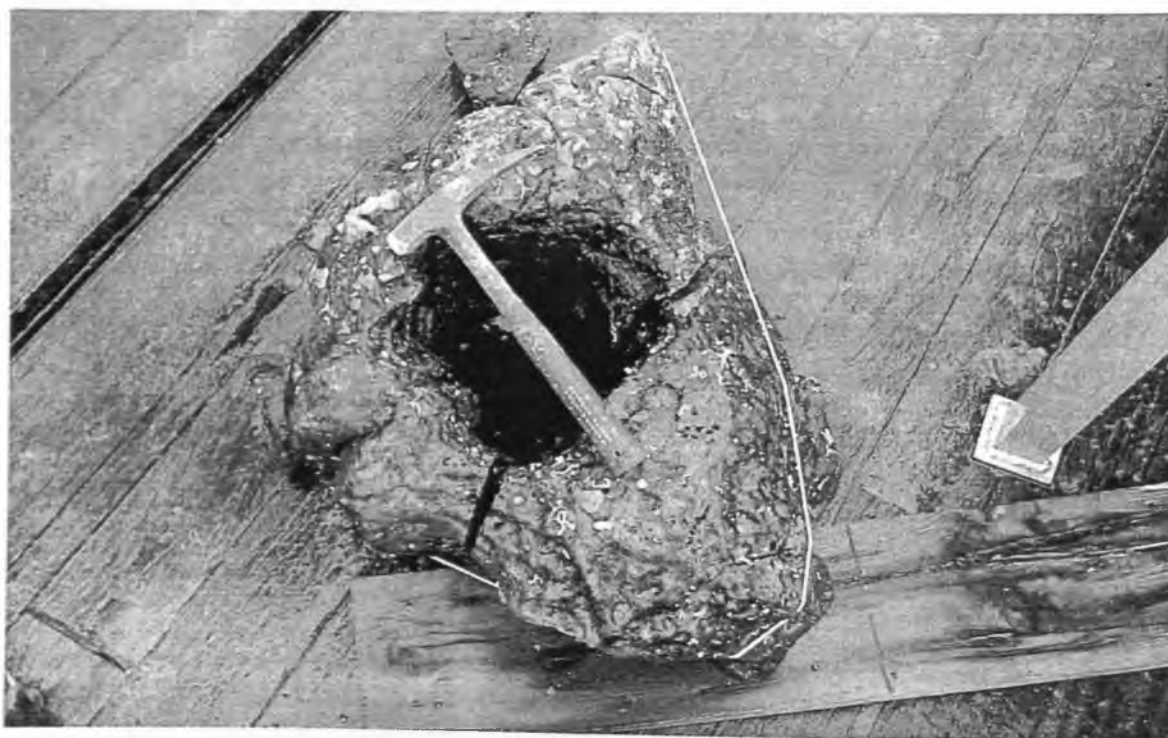
Fig. 23: Segment of carbonate chimney; TV-G 49-1.

were also recovered with the gravity corer and TV-guided multicoring system (Stations SO143/21-1, 21-2, 55-5). Upon retrieval, gas hydrates were immediately sampled for geochemical analysis (methane, stable isotopes), physical properties (specific gravity), and textural analysis. The samples were either degassed and both water and gas collected, frozen in liquid nitrogen, or stored in stainless steel pressure containers for shorebased degassing and analysis.

Preliminary textural analysis of recovered gas hydrates and gas hydrate bearing sediments indicates two main textural distinct types of gas hydrate: (1) relatively dense layers and veins of hydrate, which seem to brecciate the surrounding sediment (Fig. 22), and (2) highly porous, thick layers of hydrate with a pore volume of up to 80%. Shipboard investigations of the specific gravity of the gas hydrates (Table 5) indicate an average specific gravity of 0.89 ± 0.04 g·cm^{-3} (Fig. 24 and Table 9).

Table 9: Specific gravity of gas hydrates from SO143-71-1.

Sample No.	Volume (ml)	Weight (g)	Specific gravity (g·cm^3)
1	288	200	0.69
2	384	310	0.81
3	208	210	1.01
4	336	345	1.03
5	368	325	0.88
6	352	320	0.91
7	208	190	0.91
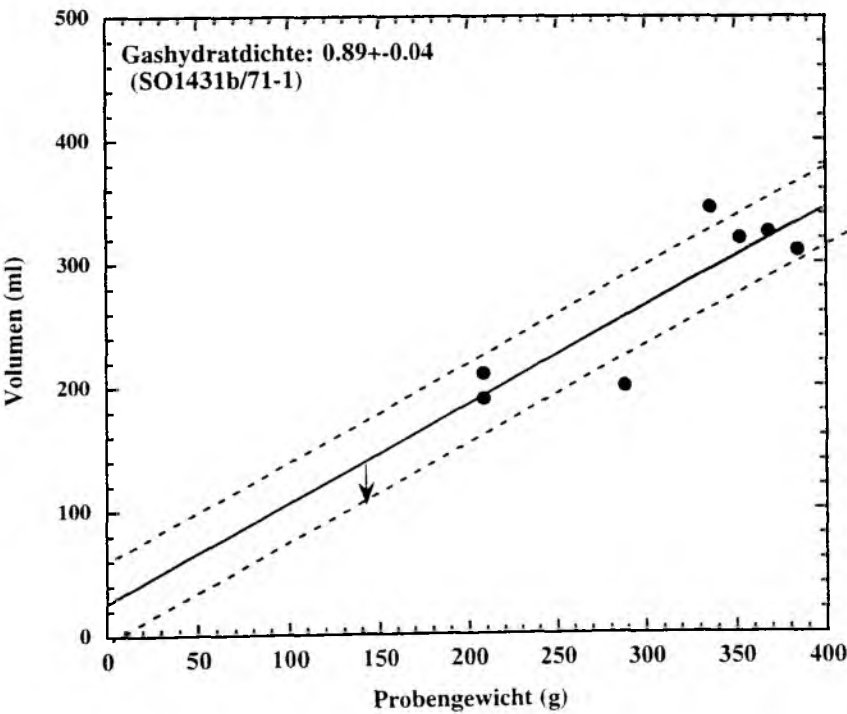
Fig. 24: Specific gravity of gas hydrate samples.

This low specific gravity and the resulting high buoyancy in seawater became evident during station SO143-71-1, when a piece of gas hydrate detached from the seafloor or the TV-grab during recovery and floated to the sea surface, where it decomposed.

Shorebased further analysis of the hydrates will provide new insight in the physical and geochemical properties of these ephemeral masses.

2.6.4 Methane

To further understand the methane cycle throughout both the water column and sediment, as well as their interrelationship, sediment samples were taken (water samples see Chapter 2.3) to determine the methane concentration and the carbon isotopic composition of CH_4. Due to fluid venting and gas hydrate occurrence as well as bioirrigation, methane profiles can differ from porewater profiles usually found on continental margins. The area of Hydrate Ridge is famous for all three of them.

For sediment sampling two different methods were used. About 150 g of sediment were taken and put into Zip – lock bags for on shore degassing, which are stored in liquid nitrogen until measurement. After measuring methane concentration the gas left over from the degassing procedure will be stored in gas-tight vials for isotopic measurements using a gas chromatography-Combustion-Isotope Ratio Mass Spectrometry (GC-IR-MS).

For immediate methane measurement 3 ml of sediment were taken in open syringes with the needle-ends cut off. The sediment is then extruded into 20-ml vials, and mixed with 5 ml of 1 M KOH to form slurry and avoid biological activity. The vials were sealed with black rubber stoppers and cramped tightly immediately (headspace analysis). For better and faster equilibrium between the slurry and the gas phase the vials were shaken for 24 – 48 hours. 100 μl subsamples of the gas phase were taken off the vials by gas tight syringes and detected with a gas chromatograph (Shimadzu), which is equiped with a flame ionization detector (FID). Samples for physical properties were taken and will be measured on shore giving us the possibility to recalculate the data from μl/ml sediment into μl/g or μmol/g sediment.

Samples were taken as soon as possible to minimize the degassing of the core, which of course was significant when gas hydrates were abundant. Mostly samples for both the headspace analysis and the degassing were taken. For details see sampling list. For some of the MUC bottom water samples were taken and analyzed. For method see the chapter about methane in water samples.

Preliminary results

Methane profiles show a lot of different shapes in the area of Hydrate Ridge and the surrounding (Fig. 24). The MUC of Eastern Basin 63-1 can be referred to as a background core. No more than 0.02 μl CH_4/ml sediment occur. Very low values were also found in 34-1MUC at East Patch (south) and 48-1SL at the BSR Outcrop suggesting low methane production and little diffusion (not shown).

South Hydrate Ridge; contained gas hydrats
55_1MUC

SE Patch; area of high reflectivity without seep fauna
31-1MUC

Eastern Basin; no vent fauna, no high reflectivity
63_1MUC

depth [cm bsf]

CH_4 [µl/mlsediment]

bacterial mats/55_2MUC

bacterial mats/29_3MUC

clam site/55_3MUC

clam site/29_4MUC

clam site/55_1MUC

depth [cm bsf]

CH_4 [µl/ml sediment]
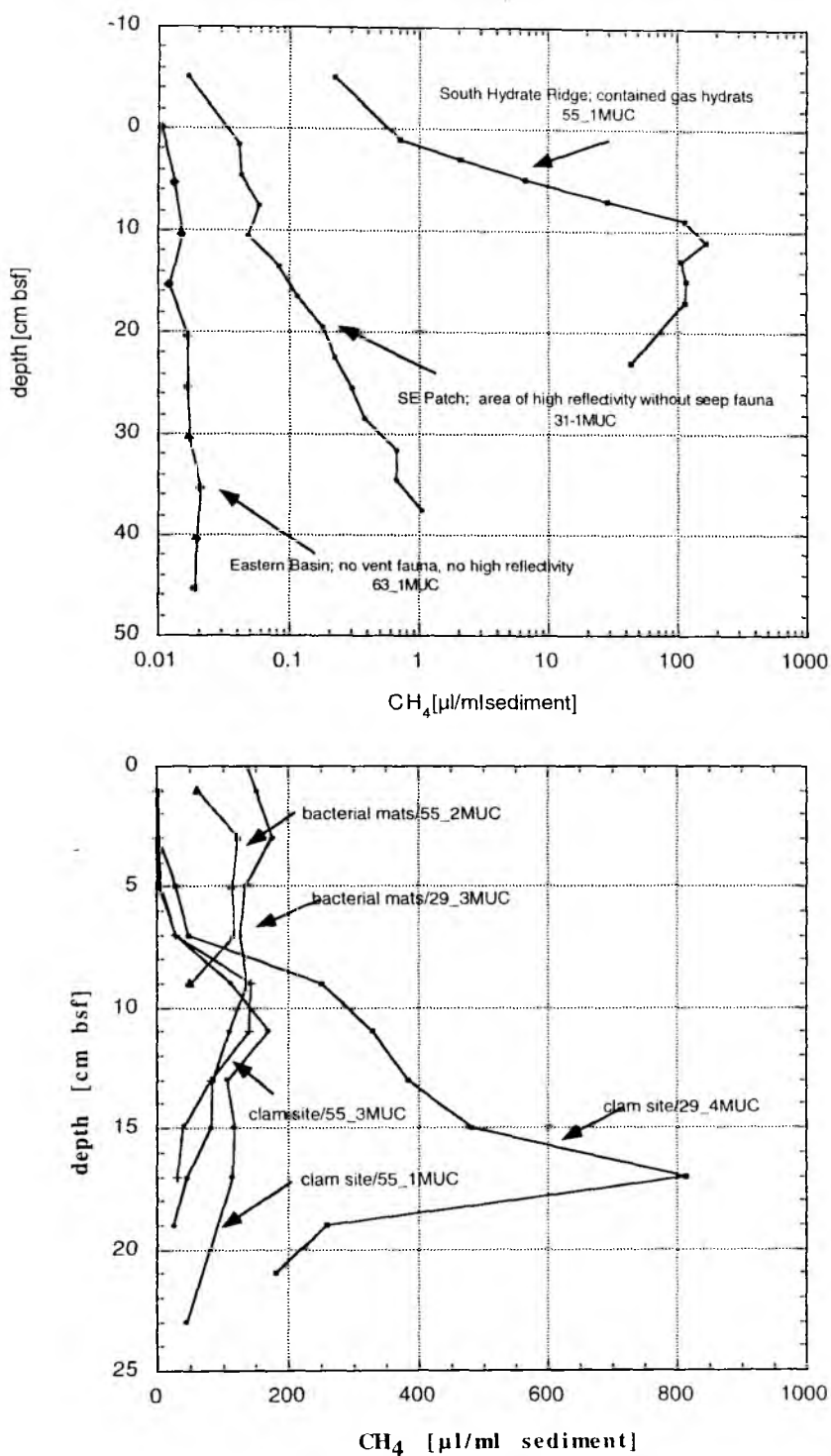
Fig. 25: Methane concentrations in sediment cores.

A profile dominated by methane production in greater depth where methane is transported upwards and oxidized within the sulfate reduction zone is represented in the profile of MUC 31-1 from the SE patch (north), which is shown in Fig. 25. The concave profile and the occurence of H_2S below 30 cm indicates oxidation of methane and reduction of sulfate. Isotope values will also give more information about the dominant processes taking place. Profiles of MUC 24-1 and 45-1 are very much alike the one of MUC 31-1.

Multicorers from station 29 and 55 were taken at the southern summit of Hydrate Ridge (SHR). They contained gas hydrate. Also fluid flow is meant to have a big influence on the porewater composition on SHR. Due to the gas hydrates the cores were degassing strongly while recovering and sampling procedure. The methane concentrations measured can only be a rough estimation as they are also dependent on how much gas hydrate the sample had. Profiles from MUC 29-3 and 4 and 55-1 and 2 and 3 are displayed in Fig. 25. The shape of the profiles gives hints on the processes taking place. Highly enriched concentrations of methane were measured in all cores from SHR with highest concentrations in core 29-4 due to the most gas hydrate with a maximum in about 17 cm depth. The maximum methane content in the cores of MUC 55 was found around 11-cm depth. Beneath the maximum the methane concentrations decreases, indicating lower gas hydrate abundance.

Due to the fauna on top of the core two different profiles were discovered in these methane-enriched cores. Whereas, cores with bacterial mats reveal highest methane concentrations up to the sediment surface the cores with living clams exhibit much lower concentrations in the upper 7 centimeters. Other than bacterial mat clams changes their environment due to bioirrigation. Next to their movements within the sediment they pump bottom water into the sediment to increase the oxygen and decrease the hydrogen sulfide content.

The profiles of TV-G 21-1 and 40-2 show high values with TV-G 40-2 (with *Calyptogena* on top) having lower methane values in the upper 6 cm while TV-G 21-1 (bacterial mat community) has strong enrichments up to the top of the core (not shown).

2.6.5   Authigenic carbonates

Authigenic carbonates are widely distributed at the sediment surface along the Cascadia continental slope and shelf (Kulm and Suess, 1990). These carbonate structures are prominent features associated with fluid venting, which is well known to occur in this area (Kulm et al., 1996). Recent studies have discovered a great variety of authigenic carbonates along the Cascadia Margin (Greinert, 1999) and have documented the large influence of gas hydrates on the formation of carbonates (Suess et al. 1999). Based on their mineralogical composition, structure and isotopic composition, a close connection between gas hydrates and the formation of carbonates (so-called „gas hydrate carbonates") has been established (Bohrmann et al.1998).

During R/V Sonne cruise 143-1b, authigenic carbonates were recovered from several areas using the TV-guided grab. Other samples were found in multicorer cores and include a great variety of carbonate buildups, crusts, concretions, slabs, and irregular edifices. The samples will be investigated with regard to their microtexture, as well as their mineralogical, geochemical and isotopic composition at GEOMAR and MBARI within the framework of the TECFLUX program. Station numbers and sample locations are given in Tables 5-8.

The most prominent types of authigenic carbonates in the study area were slab-like and irregular carbonate deposits. However, the seepage-derived mineral deposits, which were recovered during SO143-1b, range from large dolomite chimneys to tube-

like concretions (Fig. 23), to carbonate-cemented sandstones and fragile aragonite crusts. This wide variety of forms and carbonate mineralogies of the recovered samples attests the enormous variability of the processes related to fluid venting and carbonate deposition in the study area.

2.6.6 Characterization of the authigenic carbonates by X-ray diffraction

In order to get a first overview of the variation and distribution of different authigenic carbonate minerals in the study area, 17 sediment and carbonate samples were investigated by X-ray diffraction analysis (XRD) using the shipboard Philips PW 1840 X-ray diffractometer on R/V Sonne. Samples were crushed with an agate mortar and pestle, mixed with an internal standard (alpha-Al_2O_3), and prepared as randomly oriented powder slides. Scans were run from 4° to 60° 2θ at a scanning speed of 0.01° 2θ/s, using monochromatic Cuk$_\alpha$ radiation. The different carbonate minerals were characterized on the basis of the (104) peak positions of calcite, Mg-calcite and dolomite, and the (111) peak position of aragonite. In addition, the position of the (104) calcite peak was used to determine Mg content of carbonate minerals (Goldsmith et al., 1961; Lumsden, 1979). Calcite with less than 5 mole% $MgCO_3$ is considered low-Mg-calcite (LMC), and all other calcite compositions are referred to as high-Mg-calcite (HMC) after Burton and Walter (1987).

Preliminary XRD results (Table 10) show a wide variation of carbonate mineralogies ranging from low-Mg calcite over high-Mg calcite to protodolomite and dolomite. High-Mg calcite seems to be the dominant authigenic mineral deposit of the recent fluid venting in the study area as indicated by fluid-induced HMC cements in sample SO143/68-2, a lithified turbidite sequence of presumably young age.

Table 10: Summary of XRD results.

Sample	d-value of (104) or (111) peak	Carbonate mineralogy	Mole% Mg in Mg-Cc / Dolom.
29-2A	?*	-	-
40-2A	3.006	HMC	10
40-2B	2.897	dolomite	47
40-2C	2.868	dolomite	50
40-2 clast	3.027	LMC	3
40-2 cement	2.990	HMC	17
41-1 TVG	2.995	HMC	14
41-1 chimney	2.907	protodolom.	45
50-1 tube	3.001	HMC	12
56-1 TVG	?*	-	-
55-5 80-82	2.9903	HMC	15
56-1 black sand	-	volcanic glass	-
68-1 yellow crust	3.003	HMC	10
68-2 cem. sandst.	2.999	HMC	13

* pattern was not recognized during shipboard analysis.

Different carbonate mineralogies were also recognized within individual samples, such as in Sample 40-2, a cemented mudstone conglomerate, in which the clasts show a micritic cement with low-Mg calcite composition, whereas the intraclast cement is a high-Mg calcite. This indicates a change in the geochemical conditions during the formation of these two cement types. Dolomite cements were always

associated with more intensively weathered, presumably older authigenic carbonate structures, such as the large chimneys from the northern Hydrate Ridge area (Station 49-1 and -2). More detailed petrographic analysis will show whether these cements are secondary dolomites, which might have formed during burial of the sedimentary sequence. Alternatively, these structures might have formed deeper in the sediment, in the zone of methanogenesis (Greinert, 1999).

2.7   Pore water chemistry

D. Rickert, A. Heuser, B. Domeyer, B. Heitmann

2.7.1   Introduction
Pore waters were sampled from cores taken on the Northern and Southern summits of Hydrate Ridge in order to assess the effect of hydrate formation and decomposition of sediment diagenetic processes. Venting of methane-enriched fluids was first reported on the first ridge of the Oregon accretionary margin by Kulm et al. (1986) followed by observations of active methane ebullitions on the second accretionary ridge, now known as Hydrate Ridge (Linke et al., 1994).
Distinctive colonies of clams as well as precipitates of authigenic carbonates resulting from biogeochemical turnover, interaction between fluids and ambient bottom water are found at cold venting sites (e.g. Suess et al., 1985; Suess and Whiticar, 1989; Henry et al., 1992; Torres et al., 1996; Suess and Bohrmann, 1997). Bacterial mats have also been identified and are indicative of subsurface gas hydrate pavement (Bohrmann et al., 1998).
The most dramatic differences in pore water chemistry, solid phase composition and the occurrence of different seep biota are important issues reported from the pore water studies during this cruise.

2.7.2   Samples
The relatively large sediment packet recovered by the TV-guided grab was mixed with rocks and either several carbonate precipitates or gas hydrates and covered by vent organisms or bacterial mats. These sediments were subcored where the surface appeared least deformed. Surface sediments with almost undisturbed surfaces were taken with a video-guided multicorer. Sediments from gravity cores were sampled by inserting syringes into the core. Pore waters were separated

Table. 11: Techniques used for pore water analysis. For modifications see text.

Constituent	Method	Reference
Alkalinity	Titration	Ivanenkov and Lyakhin (1978)
pH	2-point titration	Dickson (1993)
Ammonium	spectrophotometry	Grasshoff et al. (1983)
Calcium	EDTA titration	Gieskes et al. (1991)
Magnesium	EGTA titration	Gieskes et al. (1991)
Phosphate	autoanalyser	Grasshoff et al. (1983)
Silicate	spectrophotometer	Grasshoff et al. (1983)
Nitrate	autoanalyser	Grasshoff et al. (1983)
Chloride	Mohr (AgNO$_3$)titration	Gieskes et al (1991)
Hydrogen sulphide	spectrophotometry	Grasshoff et al. (1983)

from the sediments by squeezing them in the ship's cold room at 4 °C and 3 atm using argon gas. The types of analyses performed on the pore waters of the different cores are listed in Table 1.

2.7.3   Analytical methods
The analytical techniques used on board to determine the various dissolved constituents are listed in Table 11. Modifications of pore water analyses were

necessary for samples with a high sulphide content. Different procedures were evaluated prior to analysis, which are briefly summarized in the subsequent section.

Spectrophotometric methods

Concentrations of dissolved nitrate, nitrite, phosphate and ammonia were determined using an autoanalyser employing standard photometric procedures (Grasshoff et al., 1997). In order to remove the H_2S in samples containing high concentrations of sulphide, a certain volume (1-5 ml) was acidified with 65% suprapure HCl (10 µl/ml sample) then left uncapped for 48 hours in the cold room. An alternative method of sulphide removal involves bubbling nitrogen gas through an acidified aliquot of the sample. Although the latter method is more efficient and immediate, the former produces reliable and reproducible results and thus was used. Silicate was measured after the elimination of sulphides using the standard manual molybdum blue method (Grasshoff et al., 1983).

The method for sulphide determination described by Grasshoff et al. (1983) has been adapted for pore water concentrations with sulphide concentrations in millimolar amounts. For reliable and reproducible results, a pore water sample was diluted with appropriate amounts of oxygen-free artificial seawater (35 g NaCl/1 litre MilliQ) and a zinc acetate solution, which fixed the sulphide. After dilution, the sulphide concentration should be lower than 50 µM. For example, 8.9 ml of oxygen-free artificial seawater and 1 ml of zinc acetate gelatin solution were added to a 100 µl sample to produce a total dilution of 1:1000.

Titration of Ca, Mg, Cl

Ca and Mg titrations are almost unaffected by high sulphide concentrations and can be applied as described in Gieskes et al. (1991) and standardized against IAPSO seawater. Chloride titrations are largely affected by H_2S concentrations >> 1 mM through Ag_2S precipitation that enhances the amount of total silver nitrate added. Additionally, the reliable detection of the titration endpoint is more difficult to achieve with the black Ag_2S precipitate. Samples should be pretreated with a 1:1 dilution of 0.01 N suprapure HNO_3 rather than HCl and degassed overnight in the cold room in open vials. Again, bubbling nitrogen through the acidified sample shortens the procedure length.

The subsequent titration with silver nitrate is standardized against IAPSO seawater or a 1:1 dilution of IAPSO seawater for samples containing sulphide.

pH/Total Alkalinity (TA)

pH electrodes were used for the determination of pH in the sediment at 4°C in the cold room and were calibrated using a buffer prepared in artificial seawater (Dickson, 1993). BIS and 2-Aminopyridine were used as buffers in the neutral pH range (pH 7 to 9). Samples of the sediment pore water for total alkalinity measurements were analyzed by the direct titration of 1 ml of pore water with 0.02 N HCl in an open cell (Ivanenkov and Lyakhin, 1978). The acid was standardized using a IAPSO seawater solution.

Table 12: Number of samples taken from each core and types of analyses performed.

ANALYSIS STATION	PO$_4$ [μM]	NO$_2$ [μM]	NO$_3$ [μM]	NH$_4$ [μM]	H$_2$S [mM]	Cl [mM]	TA [mM]	SiO$_2$ [mM]	Ca [mM]	Mg [mM]	pH	Depth [cm]	No. samp.
I. Hydrate Ridge													
Northern summit													
41-1B TV-G	x			x	x	x	x	x			x	46	12
Mud mound east													
40-2A TV-G				x	x	x	x	x	x	x	x	48	18
40-2C TV-G				x	x	x	x	x	x	x	x	47	18
Southern summit													
21-1D TV-G	x			x	x	x	x	x			x	40	20
21-2AI +AII TV-Gs	x	x	x	x	x	x	x	x			x	24/33	10/16
24-1A MUC	x	x	x	x	x	x	x	x			x	25,5	18
24-2D MUC			x	x	x	x	x	x			x	28,5	13
24-3C MUC	x	x	x	x	x	x	x	x			x	28,5	17
29-2A TV-MUC	x			x	x	x	x	x			x	16	12
29-3C TV-MUC	x			x	x	x	x	x			x	40	20
29-4C TV-MUC	x			x	x	x	x	x			x	30	17
55-1A+D TV-MUCs	x	x	x	x	x	x	x	x			x	16/27	12/16
55-2A+C TV-MUCs	x			x	x	x	x	x			x	13/25	11/15
55-3A+C TV-MUCs	x	x	x	x	x	x	x	x			x	21/25	14/15
55-4 SL	x	x	x	x	x	x	x	x			x	57	7
55-5 SL	x			x	x	x	x	x	x			104	12
71-1 TV-G					x	x						?	2
II. Reference sites:i) BSR-outcrop													
45-1G TV-MUC	x	x	x	x		x	x	x			x	30	17
46-1D+F TV-MUC	x	x	x	x		x	x	x			x	34/35	19/18
48-1 SL	x	x	x	x	x	x	x	x			x	~180	15
ii) Acoustic white spots -side scan sonar													
SE-patch													
31-1C MUC	x	x	x	x	x	x	x	x			x	37,5	19
32-2 SL	x	x	x	x	x	x	x	x			x	532	19
E-patch (south)													
34-1C MUC	x	x	x	x	x	x	x	x			x	35,5	20
35-1 SL	x			x	x	x	x	x			x	135	8
iii) Eastern basin													
63-1C MUC	x	x	x	x		x	x	x			x	40	20
iv) Western basin													
70-1 SL	x	x	x	x		x	x	x			x	229	11
70-2F MUC	x	x	x	x		x	x	x			x	39	20
NW-knoll													
68-2 TV-G				x	x	x	x				x	?	2
					total of samples	483							

for all MUCs oxygen of bottom water was measured (titration)

TA, Cl, Ca, Mg = titration; PO$_4$, NO$_2$, NO$_3$, NH$_4$ = autoanalyser; H$_2$S, SiO$_2$ = spectrophotometer

This method is especially suited for samples containing H_2S and those with TA values largely exceeding 2.3 mM as the CO_2 and H_2S is removed during the titration by a continuous stream of pure argon through the samples and standards. A mixture of methylene blue and methyl red was used as an indicator and the titration was completed when the yellow-green colour of the solution turned to a continuous light pink (pH at the end point is 5.4-5.5).

Shore-based laboratory analyses

Acidified subsamples (10 _l/ml sample) were prepared for ICP analyses of major cations (Na, K, Li, Mg, Ca, Sr and Mn). Sulphate DIC and $\delta^{13}C$ of CO_2 will be determined on selected samples in the shore-based laboratory.

2.7.4 Results and discussion

Eight TV-grabs (TV-G), 19 multicores (TV-MUC) and 6 gravity cores (SL) were recovered and analyzed for their pore water constituents. A summary of cores, numbers and distribution of samples as well as geochemical analyses performed on board is given in Table 12.

Here we focus on a single deployment and show important features of the pore water profiles and related solid phase composition or seep biota. Pore water analyses of all cores from Hydrate Ridge and cores from reference sites are listed in Appendix XX. Selected depth profiles of chemical constituents of the pore waters are illustrated in Figures 1-4 and described in the following section.

Pore water at on-vent and off-vent sites

The pore water profiles of both a subcore taken in a dense clam field of Calyptogena sp. (55-1D TV-MUC) and a reference core (46-1D TV-MUC) taken at the BSR outcrop are plotted in Figure 1 and are defined as on-vent site (for location see Table 2). The reference core shows a nitrite and nitrate penetration depth of 17.5 cm.

The phosphate concentration has a maximum concentration of ~13 μM at 2.5 cm and decreases down to a concentration of 5 μM and again increases slightly below the nitrate penetration depth. Ammonia shows a general increase throughout the bulk of the core.

Total alkalinity values are approximately equal to or slightly elevated relative to IAPSO seawater. Chloride concentrations of ~550 mM are characteristic values observed for non-venting sites in this area.

Sulphide is not detectable in the pore waters. This deficit in the reference core indicates a suboxic environment probably typical for most locations in the vicinity of Hydrate Ridge, which are not affected by fluid venting. In contrast, extremely high sulphide and ammonia concentrations were observed in sediments inhabited by vent fauna or overlain by bacterial mats. The maximum concentration of the metabolites occurs at various depths below the sea floor. This maximum relates to the type of sediment and therefore the faunal communities (for further discussion see below), e.g., 15-20 cm in the vent core 46-1D TV-MUC (Fig. 26). These abnormally high metabolite concentrations in all on-vent sites indicate an enormous intensity of microbially mediated material turnover. Based on the H_2S concentration of ~20 mM,

SO_4 appears to be almost completely exhausted. Shore-based SO_4 analyses should soon confirm this important information.

Almost identical to the H_2S distribution varies the depth concentration pattern of total alkalinity TA (mM) and PO_4 (µM). All cores show a general increase in dissolved silica concentration Si (µM). The maximum concentration throughout all cores is between 300-600 µM but give no clear indication of non-local mixing in the form of the dissolved silica profiles (e.g. Wallmann et al., 1997). The high level of reduced inorganic compounds in cores taken on the Southern summit of Hydrate Ridge indicate that the pore waters are composed of fluids that are transported to the vent site from an anoxic environment within the accretionary prism or via hydrate decomposition underlying the sediments and strongly supports methane oxidation as the dominant early diagenetic reaction.

For this preliminary evaluation, it suffices to note the high TA content from which supersaturation with respect to calcite and/or aragonite can be assumed. The high supersaturation and presumed concurrent Ca-deficit was proven by the determination of Ca and Mg performed on TV-grabs 40-2C TV-G and on subcores from 40-2A TV-G and 40-2C TV-G (Fig. 27) from east of the mud mound area (for location, see Fig. 4).

A Ca-and Mg-deficit of >10 mM is probably the result of authigenic calcium carbonate formations in these vent cores. Concretions of various shapes and sizes were observed during core processing and are described elsewhere (see Section 2.6). Again, high H_2S and ammonia concentrations indicate the increasing intensity of microbially mediated material turnover.

Vent biota influence of pore water profiles
The most significant indicator for active venting is the occurrence of seep biota. The fauna sampled from the surface sediments on the Southern summit of Hydrate Ridge was dominated by _Calyptogena_ sp. and _Acharax_ sp. communities as well as bacterial mats. A more detailed description of the biological observations and related descriptions of the overlaying seep fauna is given in Chapter 2.8. For the initial interpretation of the pore water data, the H_2S profiles of six cores (Fig. 28; for location see Appendix) were examplarily chosen from which two were dominated by _Calyptogena_ sp. with an absence of H_2S up to 2.5 cmbsf (29-4C TV-MUC) or 4 cmbsf (55-3C-TVMUC) and an increase to 20-25 mM H_2S at depth. Another two cores were chosen which were dominated by _Acharax_ sp., which show a nitrate penetration depth of almost 15 cmbsf (24-1A MUC; 24-3C MUC) and completely exhausted in H_2S that increases slightly below that suboxic zone.

In sediments overlain by bacterial mats (29-2A TV-MUC; 55-2C TV-MUC) H_2S concentration rises immediately from the surface. The different patterns, depending on vent biota clearly demonstrate the role of vent organisms whose pumping activity and motion, a process termed bioirrigation, affect the transport and distribution of dissolved species in surface sediment (Aller, 1980). This process associated with vent organisms is well described by Wallmann et al. (1997).
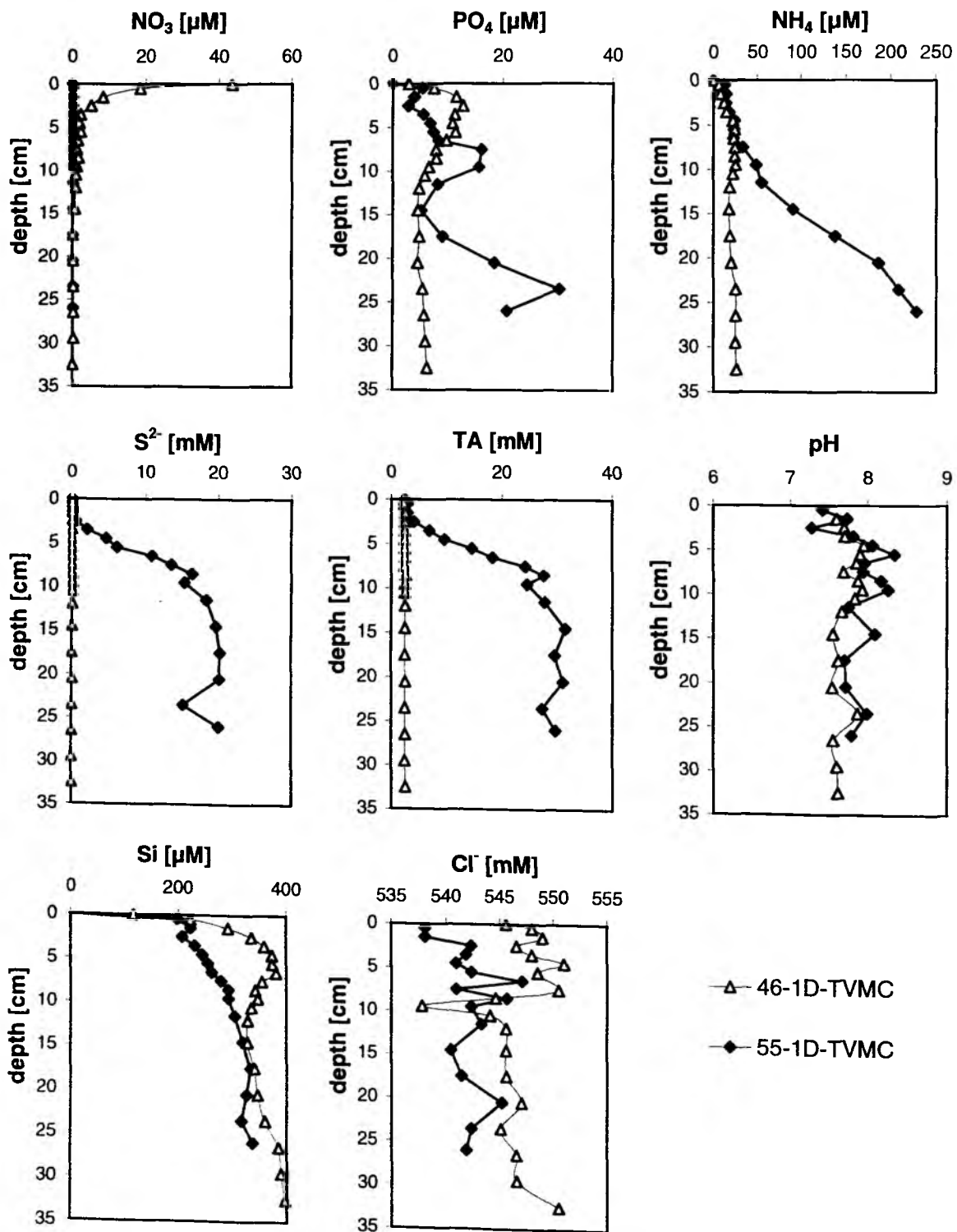
Fig. 26: Pore water composition of 46-D TV-MUC (reference site) and 55-1D TV-MUC (on-vent site).
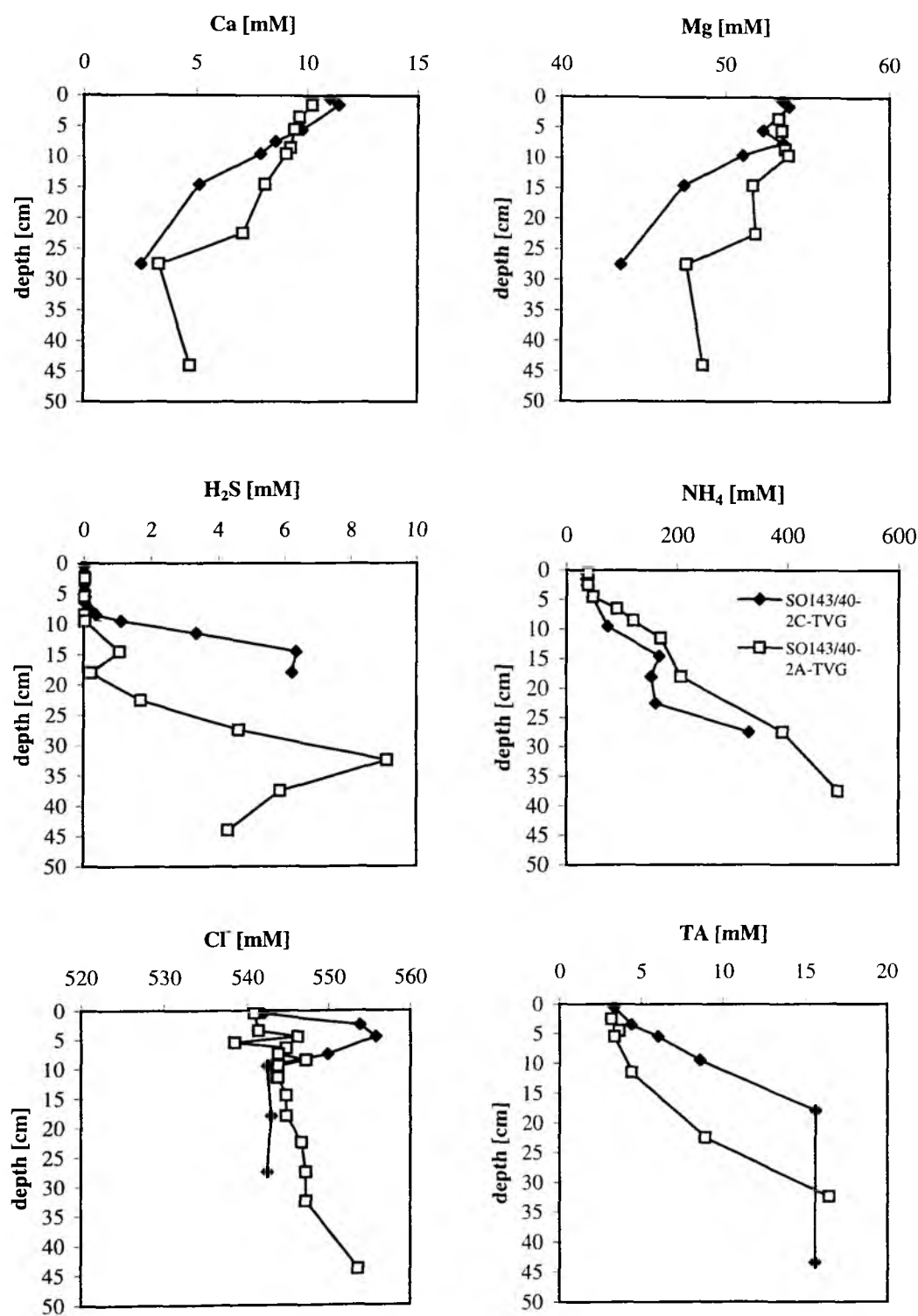
Fig. 27: Pore water chemistry of 40-2A TV-G and 40-2F TV-G. Calcium and Magnesium decrease significantly with depth, a probable result of carbonate formation.
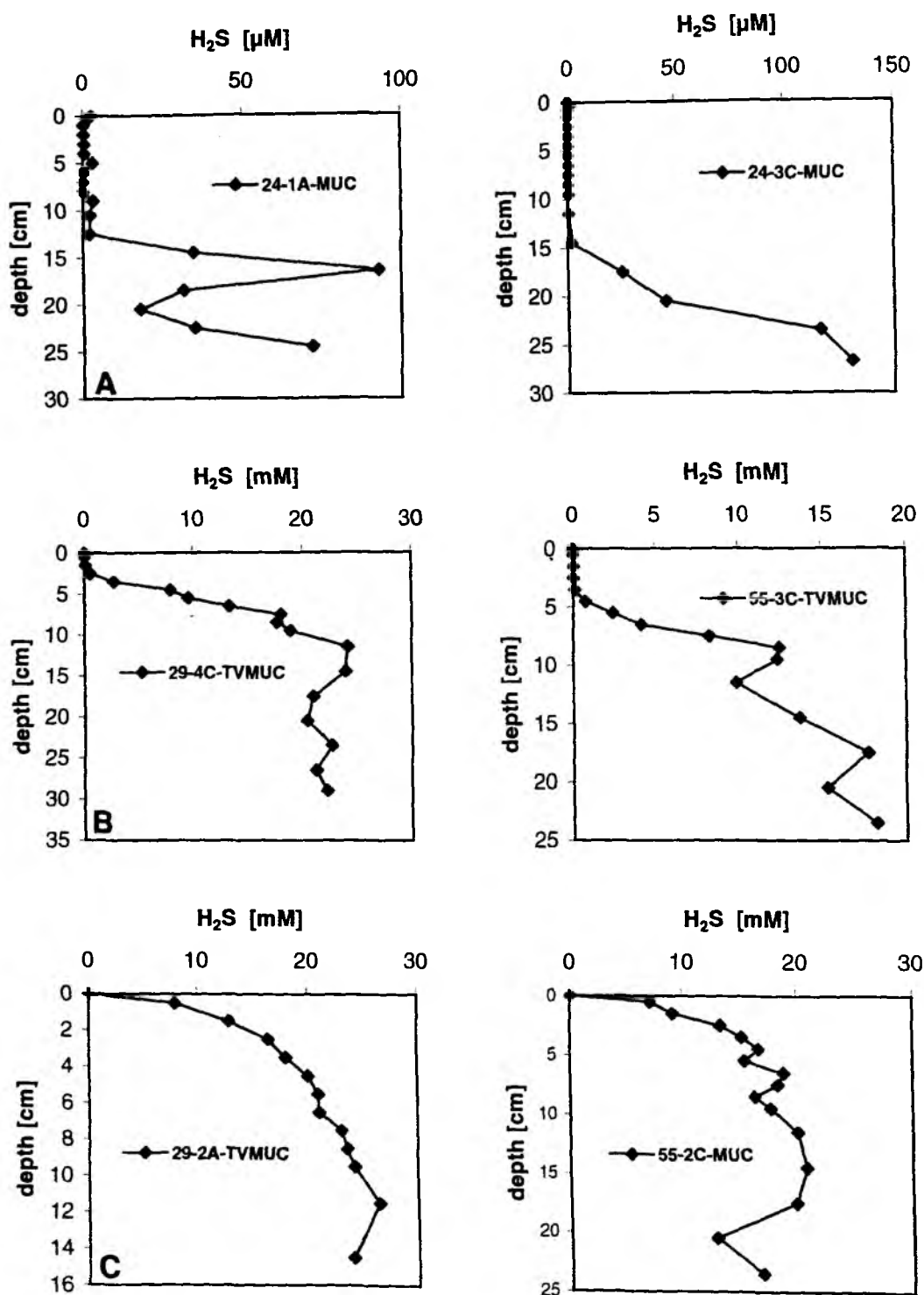
Fig. 28: Depth penetration of H_2S, as a result of overlying *Acharax* sp. (A, B), *Calyptogena* sp. communities (C, D) and bacterial mats (A, B) from selected cores. Note the different penetration depth of H_2S as well as different concentration units.
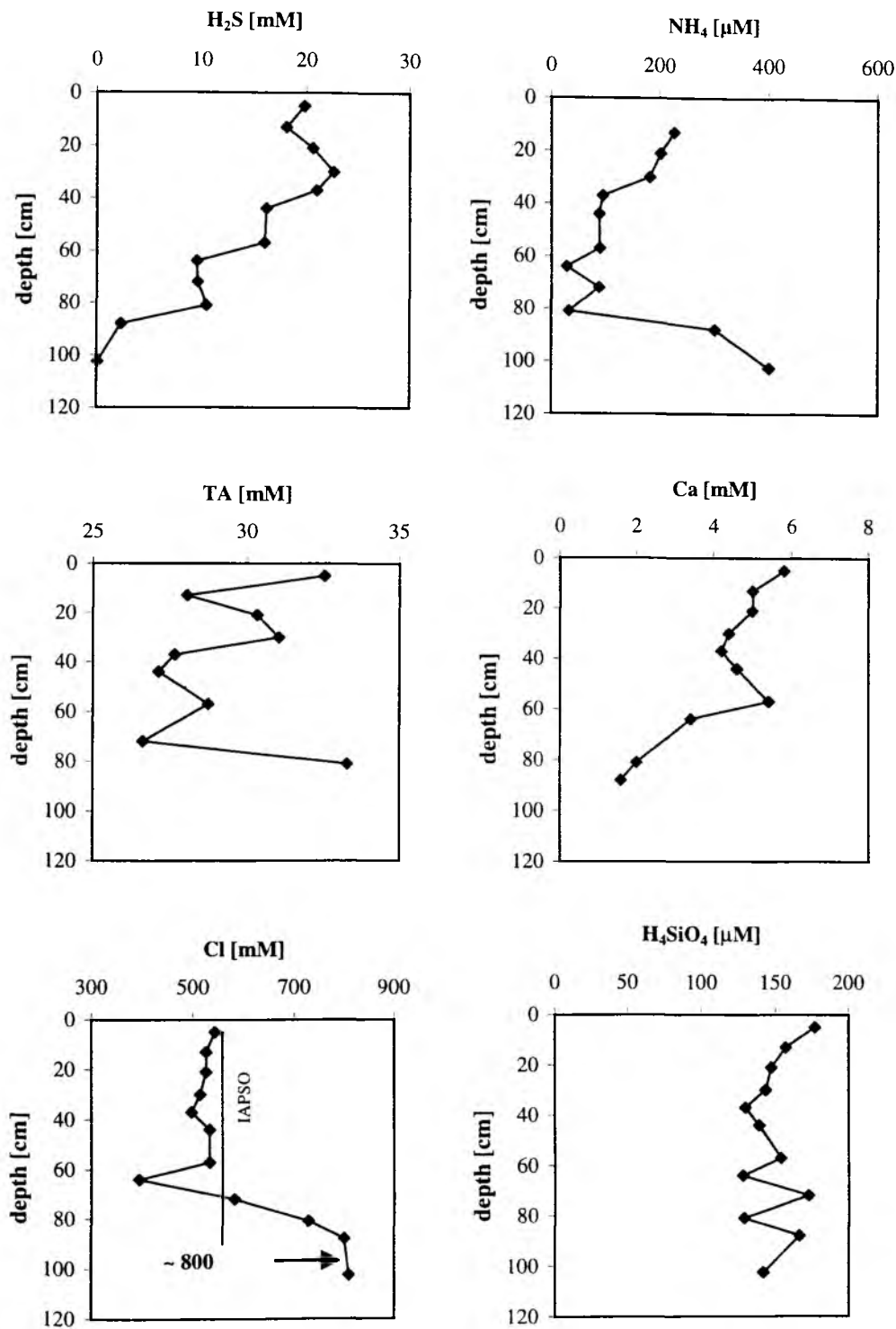
Fig. 29: Pore water composition of 55-5-Sl. Note chloride concentration at depths clearly demonstrate salt exclusion through gas hydrate formation below the deepest section of the core.

"Salt exclusion" through gas hydrate formation

In gravity core of Station 55-5 deployed on the southern summit of Hydrate Ridge, three layers of gas hydrates were recovered. The core description further yields important information about these gas hydrate layers. In this core, the outstanding feature in the pore waters is the concentrations of chloride with a sharp gradient from 60 cmbsf to the end of the core at 103 cmbsf. At the bottom of the core extremely dry sediment surrounds almost undecomposed from gas hydrate so that dilution of the pore waters is minimized. This provides important information about the process of gas hydrate formation through extraction of fresh water from the pore waters resulting in massively enriched chloride concentrations (~ 800 mM), almost 50 % enrichment compared to mean seawater concentrations (Fig. 28). A possible limitation of gas hydrate formation through the water content of the surrounding sediments is suggested.

2.8   Benthic biology of seep fauna

H. Sahling, N. Aberle

The occurrence of cold seep characteristic organisms in the subduction zone off Oregon is well known, however, there is a lack of a complete inventory of seep related species so far. Therefore the collection of animals by TV-G and TV-MUC and adequate preservation is one of the mayor goals during the Leg SO143-1b. Isotopic and electron microscopy investigations as well as enzyme assays will show the degree of dependence of the species on fluid seepage.

The extension of the area influenced by venting and new areas of fluid expulsion will be identified with the help of the towed TV-sled OFOS. The collection and determination of organisms will give the possibility to identify the species on the videos and pictures. Quantitative sampling of vent organisms simultaneous to the analysis of geochemical parameters can be used to identify different fluid flow provinces. After identifying vent communities typical for measured or derived fluid flux it may be possible to estimate the fluid flow on a larger scale by extrapolating the single point measurements based on the biological communities observed.

Because of the unusual physiological pathways of the chemoautotrophic symbiosis bigger amounts of tissues will be analysed for natural substances.Symbiont containing and host tissue will be collected for genetic studies. The genetic investigation may help in understanding the role of the Oregon Subduction Zone in comparison to other know vent sites.

Samples have been taken by the TV-guided grab (TV-G) or TV-guided multiple corer (TV-MUC), four times the MUC was used without the TV-equipment. The MUC is equipped with up to 8 cores (Core diameter: 10 cm, core area: 78,54 cm^2). Macrofauna was extracted from the TV-G by select specimens from the surface or sieving qualitatively parts of the sediment trough 0.5 mm net. Sediment samples from the MUC have been divided into the upper 0-5 cm and lower portion, and sieved through 0.5 mm. Macrofauna was selected from the sediment quantitatively by hand and preserved adequately. Organisms from the core which has been squeezed have been removed during the process of slicing.

Organisms have been preserved adequately in ethanol or formaldehyde for taxonomic studies, in formaldehyde for biomass estimations, in glutaraldehyde/seawater for electron microscopy and frozen (-20°C) for enzymatic and stable isotopic investigations. Samples for biochemical screening to search for natural substances have been stored frozen, too. The Vesicomyid and Solemyid bivalves were dissected into symbiont containing gill tissue and other tissues without bacteria, frozen, and the shells length measured before drying at 60°C overnight.

2.8.1   Distribution of chemoautotrophic fauna

The observations with the TV-sled OFOS confirmed and defined the occurrence and extension of vent-characteristic fauna on the hydrate ridge. However, more vent indications have been found on the NW-Knoll (OFOS 66 & 75-1), at the BSR-outcrop (OFOS 4-1 & 44-1) and between the NW-Knoll and the Hydrate Ridge (OFOS 75-1).

Detailed studied on the southern Hydrate Ridge could confirm the occurrence of so called "beaver mounds", an area with mounds (up to 1 m height, some m width) which are covered with two different types of bacterial mats. A white, filamentous bacteria is most widespread while an orange and more thick looking mat is less frequently found. This mounts are typically surrounded by colonies of Vesicomyid clams with a high percentage of living clams, in contrast to the clamfields around the beaver mound area, were the portion of clam-shells is much higher.
Around the BSR outcrop area, along seismic line 100, very few clamclusters of a few individuals and scattered shells were observed at different depth during the OFOS-deployments. No samples were taken in this area.

The NW-Knoll, a continuation of the second ridge with a small displacement to the west does not show any indication for gashydrates. The top is with about 950 m water depth well within the stability zone of gashydrates, therefore no influence of gashydrates can be expected and a pure tectonically driven fluid flow postulated. The observed Vesicomyid clam colonies appeared to be dominated by the larger Calyptogena sp. 3, and comparable few shells of this species have been found, most clams looked alive. This would indicate a more recent but continuos supply of this communities with fluids.

Most surprisingly and unexpected on the last OFOS Profile 75-1 a small clam cluster and one single bunch of pogonophora, most likely Lamellibrachia barhamii, was found between the NW-Knoll and Hydrate Ridge at water depth around 1350 m.

2.8.2   Chemoautotrophic organisms recovered

A total number of at least 5 different bivalves with endosymbiontic sulphur oxidising bacteria have been recovered. Not one pogonophora, characteristic at seeps and vents, has been recovered. Other vent characteristic organisms without symbionts, or species not investigated so far, like Provannid gastropods and limpets have been sampled, but are not listed.

The two known species of the genus Calyptogena (Vesicomyidae, Bivalvia) are named sp. 1 and 3, are likely to be the species kilmerii and pacifica, respectively, but final identification need to confirm this. Both species occur within a vent field. *Calyptogena* sp. 1 is generally smaller and dominant in number.

Another Vesicomyid bivalve, Vesicomya sp., was found only in very few numbers. The shell is much smaller with a length of about 2 cm. The species is new to science. All Vesicomyids rely almost completely on their chemautotrophic sulphur oxidising endosymbiontic bacteria.Two species of protobranch bivalve, *Acharax* sp. (syn. *Solemya* sp.; Solemyidae) and a unnamed and preliminary titled *Protobranch* sp. occur at the seeps. Acharax sp. lives buried in the sediment, so that only few of the shells can be seen when laying on the sediment surface, which give only an indirect hint on the occurrence.

The other Protobranch species is small, the shell length does not exceed 1.5 cm and lives on the sediment surface. While *Acharax* sp. is well known from seeps, vents, and other extremely sulphidic habitats all around the world and in all water depth, about the occurrence of the *Protobranch* sp. is not much known. Many species of this

group occur in normal sediment at the oxic/anoxic boundary, using, with the help of endosymbiontic bacteria, chemosynthese as a supplementary food source but do filter feed too.

Soft tissues for biochemical analysis have been collected in sufficient amounts from *Calyptogena* sp. 1 & 2 and *Acharax* sp.

2.8.3   Classification of observed and sampled communities and porewater characteristics

A classification into three different community types within the zone of venting may be undertaken based on visual observations and measured porewater composition. Beside this three communities at least one more can be postulated to exist, the Calyptogena sp. 3 community which was observed but not sampled and analysed for porewater composition. A summary of the biological observations is given in the table.

Bacterial mat community:
White filamentous bacteria on sediment surface, clearly visible on TV-guided tools. Sometimes some orange bacterial (?) mats have been observed, but not sampled so far.Within the area with bacterial mats Vesicomya sp. and the Protobranch bivalve occur, both are very likely new to science. Both clams rely on sulphur oxidising bacteria in their gills as indicated by stable isotope and electron microscopy investigations on material collected during Cruise SO110. Both are very small, with a maximum shell length of up to 2 cm. The bivalves occur only in sediments with very high sulphide concentrations close to the sediment surface. An influence on the porewater chemistry can only be expected in the very first few cmbsf (cf. *Vesicomya* sp.: TV-MUC 55-1D). Always the same species of polychaets, limpets and provannid Gastropods are associated with the bacterial mats.

Acharax sp. community:
Acharax sp. (syn. *Solemya* sp., Solemyidae, Protobranchia, Bivalvia) lives buried in the sediment with normally two openings of the burrows at the sediment surface. Sulphide and ammonia are consumed by the bivalve therefore the influence on the porewater profile can be quite deep (20-25 cm) depending on the size of the specimens. Uptake of inorganic carbon and oxygen takes place from the water in the burrow. The burrow is maybe not highly bioirrigated and geochemically best described by non-local mixing. Only very few bottom water is transported through the burrow as can be deduced by the Si-Profiles. In contrast to *Calyptogena* sp. the uptake of ammonia by Acharax sp. can be significant.

The extension of the Acharax sp. communities are difficult to evaluate as the bivalve burrows can not identified without doubt. However, in all three MUC-stations 24 near, but not at the beaver mound area on south Hydrate Ridge, the *Acharax* sp. community has been sampled, pointing to a much broader occurrence.

The fauna on the sediment surface is not specific for the area of seepage as there is no influence of the toxic hydrogen sulphide and too less sulphide near the sediment/water interface to sustain other chemoautotrophic species.

Calyptogena sp. community:

The genus Calyptogena is represented by two different species preliminary titled sp.1 and sp.3. Both species live on the sediment/water interface, buried up to the length of the shell into the sediment. They both take up sulphide through the foot. The way of nitrogen uptake is not known. Bioirrigation is significant and important for the clams as the tissue other then the foot is very sensitive to sulphide. The bottom water inflow can be seen in the Si-Profiles. Shell length and with it sediment penetration depth varies in between the clam species depending on the age, but on average the length of the shells of Calyptogena sp. 1 and sp. 3 are 3-4 and 7-9 cm, respectively.

The tolerances and demands of the two clams concerning the sulphide concentrations are known to differ significantly. Most cores recovered so far have been inhabited only by *Calyptogena* sp. 1, however, in TV-MUC 55-3A one living specimen of *Calyptogena* sp. 3 occurred together with 2 living *Calyptogena* sp. 1, due to the larger shell-size, the influence on the sediment geochemistry is deeper.

2.8.4   Discussion and future perspectives

Venting in the subduction zone off Oregon is much more wide spread, the fauna consist of many more species known so far, the small scale heterogeneity is much higher then described and the geochemical setting of individual biological communities can be predicted by looking at the characteristic species.

With the help of a most complete map of the vent fields which needs to be done by observations with OFOS, an estimation of fluid flow within an area of venting, e.g. on the scale of the beaver mounds, or even on a ridge scale may be possible. For this estimations more OFOS tracks are needed. The *Calyptogena* sp. 3 community needs to be geochemically characterised.

Taxonomic, isotopic, and enzymatic studies will give many more information's about the influence of venting on the species. In combination with the taxonomy, genetic studies will give strong indications about the frequency of venting along the active and passive continental margins by comparing similarities to known venting sites.

Table 13: Biological observation of TV-G and (TV-)MUC deployments.

Station	Area Description at drop	Biological Observations
TVG 21-1	**Gashydrates at HR-South** On a beaver mound with white/orange (?) bacterial mats	At present typical **bacterial mat community** with a dominance of living *Vesicomya* sp. (5), no Protobranch, few Gastropod sp. 3 (3). Influence of fauna only on the very few uppermost mm of sediment. Area with alternating but continuos vent activity in the past indicated by dead *Calyptogena* sp. 3-community (shells of C. sp. 3 (~100), *Acharax* sp. (~16) and bacterial mat community (Protobranch-shells (~100), Gastropod sp.3 (~100)).

Table13: _Continued._

Station	Area	Biological Observations
TVG 21-2	**Gashydrate at HR-South** On beaver mound with white/orange (?) bacterial mats	**Bacterial mat community** but only indicated by few Gastropod sp. 3 (4). Influence of fauna only on the very few uppermost mm of sediment. Area with vent activity in the past with a mixed _Calyptogena_ sp. 3 community (shells of _Calyptogena_ sp.3 (~30), _Acharax_ sp. (~10)) and _Calyptogena_ sp. 1-community (C. sp. 1 shells (many, maybe some 100, not extracted from sediment).
MUC 24-1	**Gashydrate-Area at HR-South** No TV-guidance	_**Acharax**_**-community**. 1 living _Acharax_ sp. in Core A (PW) in 9.5-13.5 cm, 1 more _Acharax_ sp. alive, few shells of molluscs indicate only a bit of venting in the past. Some Polychaets (6). _Acharax_ sp. may influence porewater by non-local mixing and accounts for the relative minimum in between the H_2S-maximum. 2 Ind/4Cores = ca. 60 Ind/m^2!
MUC 24-2	**Gashydrate-Area at HR-South** No TV-guidance	_**Acharax**_**-community**. Few polychaets. 2 _Acharax_ sp./4 cores = 60 Ind/m^2. Venting in the past as indicated by molluscs shells, all community-types.
MUC 24-3	**Gashydrate-Area at HR-South** No TV-guidance	_**Acharax**_**-community**. Few polychaets. 4 _Acharax_ sp./4 cores = 120 Ind/m^2. Very few indications of venting in the past by mollusc-shells.
TV-MUC 29-1	**Gashydrates at HR-South,** bacterial mats on beaver mound.	**Bacterial mat community.** No porewater squeezed.
TV-MUC 29-2	**Gashydrates at HR-South,** bacterial mats on a beaver mound.	**Bacterial mat community.** Free gas in core.
TV-MUC 29-3	**Gashydrates at HR-South,** bacterial mats on a beaver mound	**Bacterial mat community.** Free gas in core.
TV-MUC 29-4	**Gashydrate at HR-South,** in between beaver mounds, where dense aggregations of clams visible	_**Calyptogena**_ **sp.1 community.** Sediment taken from in between clams and squeezed for porewater, very good sample strategy! In PW-core: 8 C. sp. 1 Ind / core (= 1020 Ind/m2!) Average: 15 Ind./ 4 cores = 470 Ind/m^2.
TV-MUC 31-1	**SE-Patch,** Area of high reflectivity E of HR, surface for SL 32, OFOS 27 surveyed the area before	**No seep fauna** with tiny bivalves (5), giant foraminifers and polychaets
TV-MUC 34-1	**E-Patch,** Area of high reflectivity E of HR, sediment surface for SL 35, based on OFOS 33	**No seep fauna** with abundant and diverse polychaets.

Table 13: *Continued.*

Station	Area	Biological Observations
TVG 40-1	**Mud mound east**	*Calyptogena* sp. 3 community. No porewater. Mainly *Calyptogena* sp. 3 (12) alive.
TVG 40-2	**Mud mound east** Sediment surface with lots of taluses, maybe bacterial mats and single clams	***Acharax* and *Calyptogena* community in one grab.** ***Acharax* community:** geochemical habitat of the very big *Acharax* sp. (14) may be described by porewater profile A. ***Calyptogena* sp. 3 community** represented by 2 specimens alive and maybe profile C.
TVG 41-1	**Northern HR** Carbonate taluses, in between clams	***Calyptogena* sp. 1 community.** Many *Calyptogena* sp. 1 (73) alive, many carbonates and non-cold-seep organisms.
TV-MUC 45-1	**BSR-outcrop** Soft sediment, no vent indication	**No seep fauna.**
TV-MUC 46-1	**BSR-outcrop** Soft sediment with a small patch of slight whitish appearance	**No seep fauna.** Some polychaets with a very distinctive smell.
TVG 49-1	**BSR-outcrop** Grabbing chimney-like carbonate in relative shallow water	**No seep fauna.** No porewater. Many ophiuroids.
TVG 50-1	**BSR-outcrop** Dropped on chimney-like carbonates	**No seep fauna.** No porewater. Some polychaets, polyplacophora, ophiuroids
TV-MUC 55-1	**South-HR** At the base of a beaver mound, with dense aggregation of clams	**Core A: *Calyptogena* sp. 1 community.** 10 *Calyptogena* sp. 1 in core (= 1200 Ind./m^2!). **Core D: Bacterial mat community.** 3 *Vesicomya* sp. alive on top of this core
TV-MUC 55-2	**South-HR** At the very top of a beaver mound, in bacterial mat	**Bacterial mat community** on both cores.
TV-MUC 55-3	**South-HR** At base of a beaver mound in clamfield	**Core A: *Calyptogena* sp. 1 community** with one single *Calyptogena* sp. 3 occurring together with 2 living *Calyptogena* sp. 1. **Core C: *Calyptogena* sp. 1 community** with 3 living *Calyptogena* sp. 1.
TVG 60-1	**Mud mound saddle** Grabbing "bone-shape-like" carbonates.	Only one *Acharax* sp., no porewater, no smell of sulphide, surprisingly **few epilithic or non-vent organisms**.
MUC 63-1	**Eastern Basin** Surface for SL 62	**No vent fauna.** Mollusca and polychaeta.
TVG 68-2	**NW-Knoll** Small cluster of *Calyptogena* sp. 3, many more in the surrounding.	***Calyptogena* sp. 1 community.** Many living and relatively large *Calyptogena* sp. 1 (64) and *Calyptogena* sp. 2 (~20) and very few empty shells may indicate that venting has started very recently but continuously. No porewater.
MUC 70-2	**Western Basin** Surface for SL 70-1	**No vent fauna.** Polychaets.

3.1   Cruise narrative SO143-2
O. Pfannkuche

During the course of Saturday 31 July the scientific equipment for Leg SO143-2 was taken on by the vessel. After securing the heavy equipment on the working deck, RV SONNE left Astoria at 17:00h and headed back to the TECFLUX area. The first station on the northern summit of Hydrate Ridge was reached on Sunday morning of 1 August. Station works started with continuing the running number system SO143-76 with the recovery of a VESP-lander which had been deployed during Leg 143-1a followed by some CTD/rosette deployments for hydrographic studies and methane measurements in the water column.

In the afternoon the ship steamed to the southern summit of Hydrate Ridge to deploy the second VESP-lander. This station was followed by a TV-grab deployment. During the night of 1/2 August two OFOS-tracks were conducted on the western slope of the northern summit. The next morning was dedicated to sediment sampling with the TV-MUC in the western basin to gain samples for porewater chemistry and biochemical sediment analyses. After the recovery of a transponder of the transponder navigation net on the northern summit the ship headed south again for an 18 kHz-sonar track to trace gas plumes at the southern summit.

The CTD/rosette samples positioned after the survey yielded the highest methane concentrations measured so far during the TECFLUX campaign. The night of 2/3 August was dedicated again to an OFOS survey in the vicinity of the NW-knoll. In the morning of 3 August RV SONNE returned to the southern summit to deploy another video-guided lander. The VESP-lander was placed on a bacterial mat followed by another 18 kHz-sonar survey.

At mid day the ship headed back to the western basin to deploy a video-guided BC-lander and to sample sediments with the TV-MUC and GKG (macrofauna). The night 3/4 August was spent with an OFOS survey in the vicinity of the NW-knoll. In the morning of 4 August another GKG sample was retrieved from the western basin followed by an 18 kHz sonar survey and a CTD/rosette cast at the southern summit. The BC-lander was successfully retrieved from the western basin in the early evening. After another CTD/rosette cast at the southern summit the ship proceeded to the southeastern part of the TECFLUX area to complete Hydrosweep and Parasound profiles started during Leg SO143-1b.

The next days until 7 August saw activities in a triangle between the northern summit, western basin and southern summit with the southern summit as the focal area of activities. Several BC-lander and a DOS-lander were deployed and recovered along a gradient of varying biogeochemical activities indicated by specific organism communities (e.g. Calyptogena beds, bacterial mats). Sediment samples were taken with TV-MUC and GKG. CTD/rosette casts and 18kHz sonar surveys co-ordinated to the tidal rhythm were taken mainly around the northern summit. A beamtrawl was employed for sampling epibenthic organisms. The nights were mainly dedicated to OFOS- and Hydrosweep/ Parasound-surveys.

In the evening of 8 August the ship took course to the abyssal plain west of the first accretion prism. During the night we maintained all deep-sea wires and cables were paid out to their full length and were carefully hauled in after greasing.

After a short Hydrosweep/Parasound survey followed by sediment sampling with TV-MUC and GKG RV SONNE proceeded back to the southern summit stopping in between at the western basin for another TV-MUC. The period between 9-18 August was again filled with a sampling routine corresponding with the previous week. The southern summit was again the centre of activity. CTD/rosette casts concentrated around the northern summit. Sediment sampling was extended to the eastern basin and to the flanks south-east and north of the southern summit.

The VESP-landers and the DOS-lander were successfully retrieved and re-deployed on Calyptogena beds. Several BC-landers were employed along the biochemical gradient. More OFOS- and Hydrosweep/Parasound profiles were driven. From 16 August Hydrosweep/Parasound profiles were extended beyond the north-western limit of the permitted zone for TECFLUX activities, as a new research permit by the US government had extended the limits of our working area to the north and south (44° 25′N to 45° 45′N).

At 16 August RV SONNE had a rendezvous with the US RV ATLANTIS which visited the TECFLUX area for two days. After establishing VHF-contact with the chief scientist Dr. Lisa Levin we agreed that RV SONNE would keep clear from the northern summit for two DSR ALVIN dives. The american colleagues in return agreed to avoid the southern summit to prevent damage to our moored landers. RV ATLANTIS left the area in the afternoon of 17 August.

In the late night of 19 August RV SONNE steamed to Newport to disembark an OSU scientist on a small vessel. In return a scientist from SCRIPPS joined the scientific party. In the early afternoon we returned to the southern summit and continued our working programme. Benthic sampling again was focused on the southern part of the TECFLUX area that included a station on the slope 12 miles east of the Hydrate Ridge. In the late night of 22 August RV SONNE left the area of the Hydrate Ridge. Our last station was the mapping (Hydrosweep-Parasound) of a tectonic feature about 45 miles north of the Hydrate Ridge for investigations planned for the future TECFLUX activities.

Station works (running no. 210) ended at 23:00h on 23 August when the ship took course to Astoria. Astoria was reached on 28 August at 08:00h.

3.2   18 kHz Parasound survey

B. Collier, M. Eek, K. Heeschen, H. Schäfer

When set in NBS mode the parasound onboard RV SONNE can produce an echo from gas bubbles emanating from the seafloor. This feature of the parasound was utilized during SO143-2 as a tool in the planning of hydrocasts aiming to measure the concentration of methane at vent sites.

The first survey conducted during this leg was Station 90-1 covering the southern summit where, by using the 20° beamwidth, it was confirmed that the vents seen on the summit during the ALVIN dives were still active. Based on the information gathered during the survey a location was chosen for the following Station 96-1.

During Station 96-1 the Parasound was kept under close surveillance to confirm that the sampling took place at the place of gas venting. Since the footprint diameter of the 20 beam, at the depth of the station, was exceeding 250 m the beamwidth was changed to the narrower 4 beam. With this beamwidth the footprint diameter was limited to 54 m, increasing the likelihood that the CTD-rosette is close to the echo seen with the Parasound, and actually sampling water affected by the venting gas.

A clear bubble echo was observed with the parasund for the first 1.5 h the station was occupied after which the signal weakened and vanished within minutes. One possible reason for the signal to disappear would be that the bubbles were no longer there, i.e. the vents had closed. In an attempt to confirm this hypothesis the footprint of the Parasound beam was plotted to scale on a map and the location of the "positive" and the "negative" echo sightings were compared (Fig. 31). The map shows an overlap of the different footprints suggesting that the vents did indeed close. The analysis of the methane concentration also supports the hypothesis as the values were high during this cast while the following hydrocast (Station 99-1) at the same location 5 h later showed lower methane concentrations and no bubble echo. At the time this "closing" occurred the tidal cycle at Newport Bar was in a flooding tide 6 ft above the 0 tide mark for Station 96-1 and a ebbing tide also at 6 ft for Station 99-1. This may indicate a tidal influence on the regulation of the venting.

With the hope of increasing the resolution from an earlier parasound survey during SO143-1a small scale survey, using the 4 beamwidth, of the Northern Ridge was conducted. This survey (Station 146-1) failed to show any appreciable activity. However, it should be noted that this survey took place during high tide, 5-6 ft above the 0-tide mark.

3.3   Methane in the water column and surface waters

R. Collier, K. Heeschen, M. Eek, H. Schäfer, K. Nakamura

CTD deployment and oxygen demand

Water column sampling was performed using the ship CTD/rosette system equipped with sensors for temperature, conductivity, pressure, and oxygen (Seabird 911 plus, SBE 13 oxygen sensor, SBE 32 caroussel with 24 x 10l Niskin bottles). Also attached were a membrane/chemical CH_4 sensor (METS sensor) and a backscatter sensor, both provided by Gary Klinkhammer from Oregon State University. The METS sensor

was a newer version of the one used on SO143-1b and although calibration was not possible, it showed a much higher sensitivity to methane in the water column. Additionally, the time constant was somewhat smaller, making the METS helpful for qualitative observations and for taking water samples within areas of elevated methane concentrations. As on SO143-1b the oxygen sensor was very
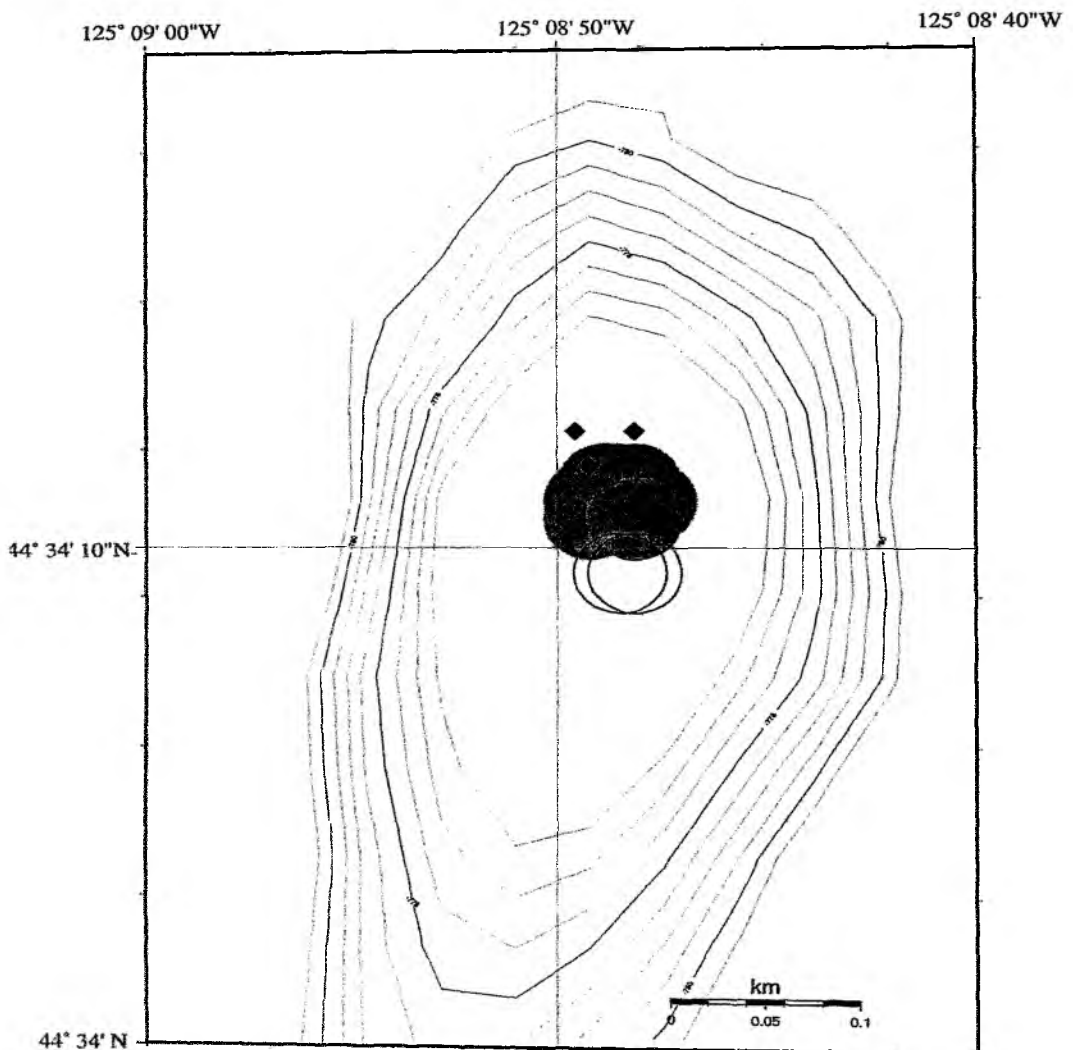
Fig. 30: Areas of bubble echos on southern Hydrate Ridge and site locations.

precise in its recordings (see SO143-1). The water column on all stations was characterized by a thin (6-10m) lens of warm, low salinity (31 PSU or less) water reflecting the influence of freshwater input from the shelf. Temperature and salinity properties in the water column were similar at all stations. For a typical profile see Leg SO143-1b. If compared with samples in the open Northeast Pacific from similar depths, a notably low oxygen content near the bottom of Hydrate Ridge (0.3-0.4 ml) was recorded on Legs SO143-1b and SO143-2.

During SO143-2 a total of 23 CTD casts were deployed. Shipboard, the CTD water samples were degassed and the methane concentrations determined. Gas samples were collected for shore-based stable isotope measurements.

Methane measurements

During Leg 143-2, water column methane was measured from discrete samples collected directly from the ship's CTD/rosette. Furthermore, CH_4 and CO_2 in the surface waters was continuously surveyed along the entire cruise track using a gas equilibration system (Rehder, 1996). For CH_4 analysis on the discrete CTD samples, a modified vacuum degassing method was used as described by Lammers and Suess (1994). See Chapter 2.3 for descriptions of both methods. During tracks towards both the coast of Newport and Astoria two high resolution surveys were performed. The standard routine was changed to measure the double amout of water samples.

Results

Surface water survey

The entire investigated area is oversaturated with respect to the atmospheric mole fraction of methane and hence is a source for atmospheric CH_4. pCO_2 was strongly undersaturated. The automated system was run during the entire cruise thus permitting a combined evaluation of the local and short-term variations of surface water pCH_4 and pCO_2 when compared with the ship's DVS system data.

Methane in the water column

Particularly within about 150 m of the seafloor, the methane concentration is highly variable within small depth ranges in the water column on Hydrate Ridge. Indications of a tidal forcing found on former cruises (New Horizon, Atlantis and SONNE Leg 143-1b) could still neither be proved nor disproved but former results were supported. Another "tidal experiment" (Station 130; Fig. 31) on the southern summit of Hydrate Ridge (SHR) revealed low methane concentrations during periods of rising hydrostatic pressure. The highest values retrieved occurred at any other time, including directly after high tide (1395 nmol CH_4/l; 2 m above Zero). By running the 18 kHz Parasound system during the whole experiment to trace the gas bubble signal, measurements of concentration variation due to current changes depending on the tide system were avoided. The amplitude of the tidal cycle was the highest within the cruise time-period (-0.4 m - 2 m).

Station 86 (CTD 17 & 18) and Stations 97 & 99 (CTD 19 & 20) confirmed these results. No higher values could be measured at rising hydrostatic pressure, but evaluated concentrations of up to 150 % of the methane background inventory were found at high tide (2.2 m). Two Niskin bottles, closed at 700 m depth within 15 minutes time difference (CTD 19), obtained methane concentrations differing by an order of magnitude. The changes could also qualitatively be seen on the methane sensor. The methane sensor (METS) also supported two CTDs towed across (137, CTD 27) and around the summit of northern Hydrate Ridge (NHR) (159-1 CTD 21). On both tows, discrete water samples and METS data both revealed higher methane concentrations in the SW of the summit of NHR at a water depth of about 600 m, attributed to a SW current, which matches current data from former cruises. Confirming the variability of the Hydrate Ridge system, samples taken from the same location at the end (22-24) and the beginning (1–3) of the CTD 31 tow, showed clearly distinguished methane concentrations.
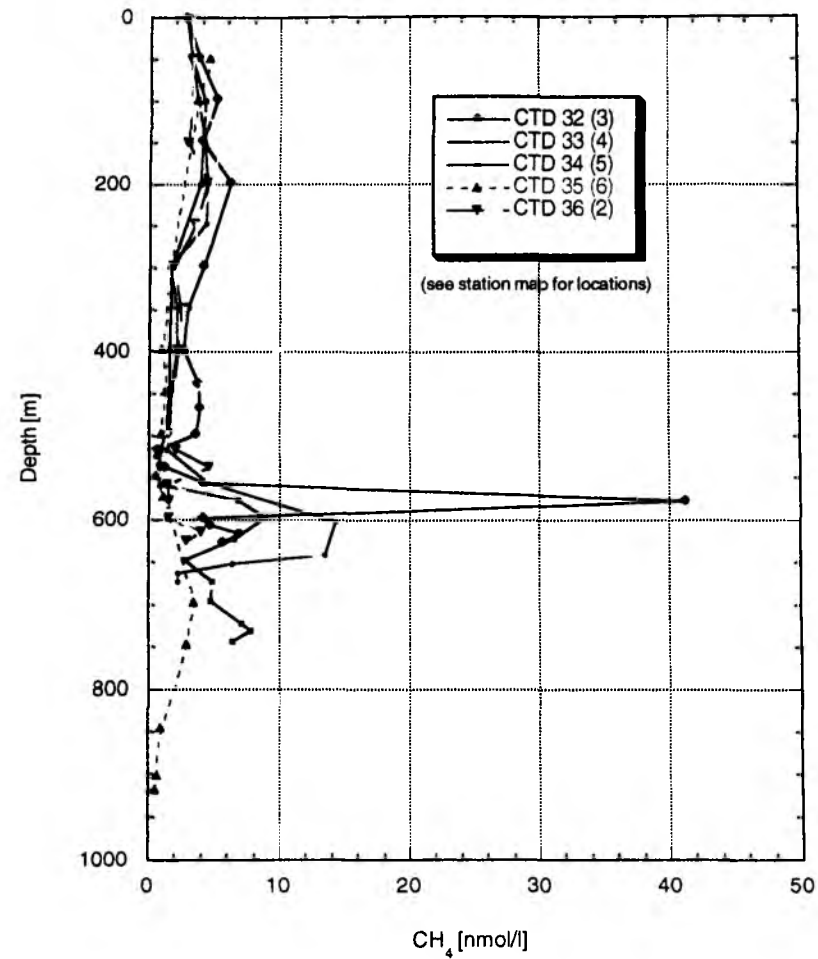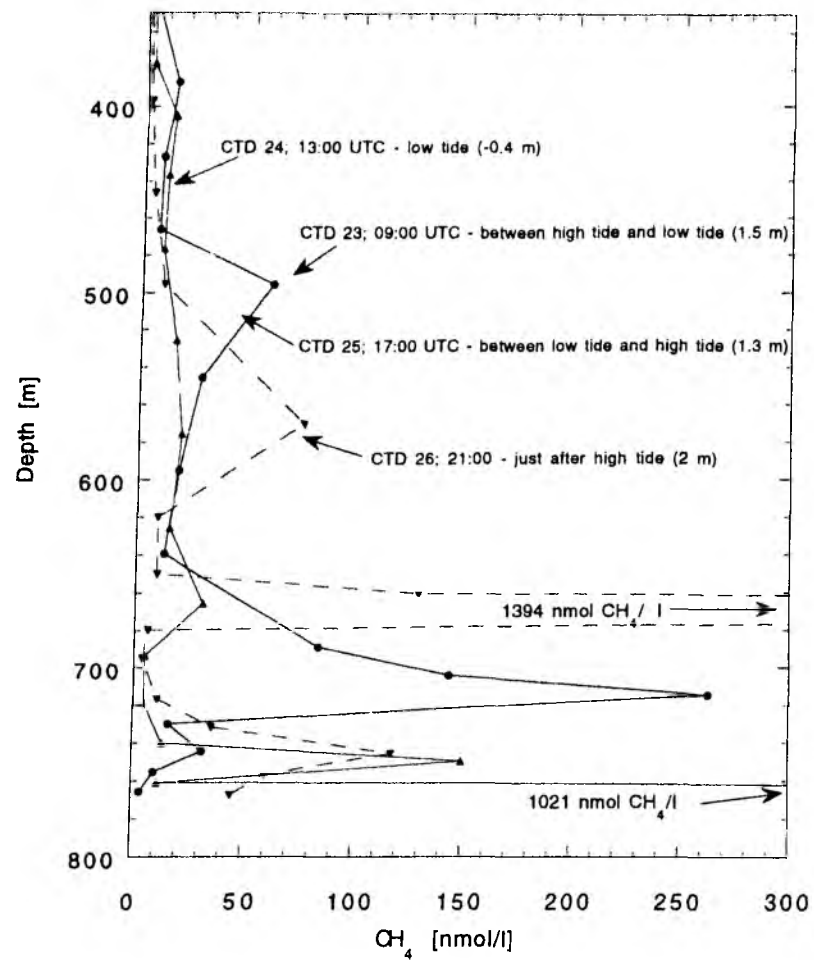
Fig. 31: CH₄-profiles from southern (left) and northern (right) Hydrate Ridge.

Based on the data from the towed CTDs, an ENE – WSW transect (CTD 32-38) was undertaken alongside the area of highest methane values found in the tows (Fig. 31). With current data and CTD transects from former cruises, calculations of flow rates should be possible. As the tidal cycle might have an influence on the methane released from the seafloor, CTDs were always taken at the same time within a tide cycle.

Next to the investigations at the Hydrate Ridge summits, hydrocasts were deployed at a pockmark in the eastern basin (145-1 CTD 28), the BSR-outcrop (120-1 CTD 21), a western summit of NHR (147-1 CTD 29), a station north of NHR (148-2 CTD 30), and in the western basin (77-1 CTD 16; 124-1 CTD 22; 197-1 CTD 37). CTD 21 and 28 showed enhanced methane concentrations within the deeper water column (450 m), probably sourced from NHR and the SW current. In comparison, slightly higher values at 800 m depth are related to local fluid expulsion, as sources on NHR are within a depth range of 600 - 650 m. Unlike the eastern basin pockmark and most sites on Hydrate Ridge, the BSR-outcrop showed elevated values just above the seafloor, that might be related to fluid flow rather than gas expulsion. Fields of active vent organisms were seen with the video sled OFOS at the CTD location.

Methane concentrations as low as those of background stations 77 (CTD 16) and 124 (CTD 22) in the Western Basin, were obtained only 3.5 km north of the methane sources on top of NHR (CTD 30). To maintain water samples for measuring stable isotopes of CH_4 in water masses with the lowest methane concentrations CTD 16 and 37 were deployed at Western Basin (for Nick Grant, University of Victoria, Canada). Samples were taken from the intermediate water mass with the lowest oxygen values (840 m), also showing the lowest methane concentrations found on the TECFLUX investigation (0.16 nmol/l). Background values at lower depth are about 1 nmol/l and thus fit the background values found at the Hydrate Ridge Sites.

All water samples between 150 – 300 m revealed elevated methane concentrations whether or not they were taken at locations with CH_4 sources. This suggests sources other than the methane enriched fluid or gas expulsions from Hydrate Ridge. As the investigated area is very close to the continental shelf, the enhancement can be attributed to an intermediate nepheloid layer (INL) resulting from currents alongside the continental slope, freshwater supplies with high CH_4 content (Columbia River), known seepage on the shelf or to upwelling within this area (also see leg 143-1). Being accompanied by higher backscatter voltage between 150 – 300 m the INL seems to be the most reasonable explanation.

Methane sensor
Determining the concentration of methane dissolved in water is a pivotal analytical effort in the study of cold seeps and methane dynamics from a variety of environments, as methane determination by gas chromatography can only provide a limited dataset from a highly variable environment. Without in-situ detectors, conventional CTD-rosette sampling is essentially blind. For longer-term studies, the sensor was deployed on a Lander system (see Chapter 2.3).

The methane sensor, METS, was developed at GKSS-Forschungszentrum (Geesthacht, Germany) for long-term monitoring of dissolved methane in water.

Methane is exsolved from water across a membrane, diffuses into the sensor through a support frit. It is detected in the gas phase at the heated surface of an internal semiconductor, which changes its conductivity as a function of hydrocarbon adsorption. The current application depth is 1000 m, which is limited by the support frit. The METS sensor was interfaced with the CTD using three analog voltage channels.

Because of the long, diffusive path to the sensor, the response time is slow (several minutes) and the signal may never reach equilibrium in a heterogeneous environment. When deployed in a low concentration background, the system can easily detect changes of +10 nM. Once high concentrations of methane diffuse into the sensor cell, it takes a long time to return to low values. This irreversible response currently limits quantitative applications from CTDs although, throughout most of the cruise the sensor was a helpful tool (in combination to the 18 kHz system) for finding areas of higher methane concentrations and for closing the Niskin bottles at the correct depth.

3.4   Visual observations by TV-G and OFOS

H. Sahling

Introduction
During SO143-2 the observations which started during the previous legs were continued. The search for sites of venting and the mapping of fluid flow indication were the main objectives. The occurrence of seep organisms (chemoautotrophic bivalves, pogonophorans, bacterial mats) were mapped on a very small scale with the towed camera sled (OFOS), to analyse their distribution within a known vent field. OFOS transects through the seepage area were used to identify zones of vent influence based on changes in benthic community structures. OFOS profiles were also conducted to observe the seafloor at sites were the side-scan sonar mapping (C. Goldfinger) registered areas of high reflectivity, indicating strong density gradients e.g. caused by carbonates.

Results
An overview of OFOS and TV-G deployments is given in Table 14. The observations with OFOS were concentrated at four areas: Hydrate Ridge, the northern and southern summit, the NW-Knoll and the area around the BSR-outcrop.

Hydrate Ridge
With OFOS 81, 82, 94, and 133 the area at the southern summit was most extensively covered. The tracks could confirm, that fluid venting mainly occurs in the small area named "beaver mounts", small elevations of up to 1 m height, largely covered with bacterial mats and densely populated in the surrounding by vesicomyid clams. The mounts seem to indicate gas hydrate occurrence near the sediment surface, as could be confirmed by MUC and TV-G samples. The extension of carbonates at the southern summit area agrees well with the areas of high reflectivity on the side-scan sonar map. More indication of venting (clams, few bacterial mats, carbonates) were discovered at the western flank of the Hydrate Ridge.

At the base of the western flank (OFOS 111, 129) as well as at the NW base of Hydrate Ridge (OFOS 75, Leg 1b) colonies of the pogonophoran *Lamellibrachia* sp. were observed. This chemoautotrophic tube worms were also observed during OFOS 87 at the first ridge but could not be sampled with TV-G 106.

At the northern summit of Hydrate Ridge three OFOS tracks were conducted to confine the extension of active venting observed earlier by OFOS, ROPOS and ALVIN-dives. OFOS 112 covered the top of the northern summit, an area where boulders of carbonates dominate the surface and clam fields occur, and continued over the so-called SONNE and ALVIN Chemoherm. At the ALVIN Chemoherm a fishing rope was caught by the sled and the station was aborted. With OFOS 192-1 and −2 the area of the summit was covered in greater detail. Gas bubbles were observed on the southern summit of Hydrate Ridge confirming that free gas only escapes on the ridge tops. Vesicomyid clams and few patches of bacterial mats were observed all along the ridge crest of the northern summit, the E and W extension is now well defined. It is still unkown how far the vent areas continue to N and S is yet unknown. An attempt to grab clams and carbonates with TV-G 209 failed due rough weather conditions.

NW-knoll
Venting on the NW-Knoll was discovered during leg 1b, with two additional OFOS profiles (93 and 132) on leg 2. We now have a relatively complete picture of the distribution of clams and carbonates in relation to the geological structures. Extensive areas of Vesicomyid clams were observed near the ridge crests of the hill, most activity was found on the seaward flank.

BSR-outcrop
The area of the BSR-outcrop was observed during three OFOS deployments (121, 154, 167) and could confirm, that venting is a very widespread phenomenon. The distribution of carbonates was found to be in very good agreement with the side-scan sonar observations. Although most active venting seems to occur at ridges, few clamfields were observed in soft sediment without any obvious geological evidence for fluid venting. Samples taken by TV-G 167 can confirm, that in this area similar communities to Hydrate Ridge exist.

Discussion
Indications of venting (chemoautotrophic organisms, carbonates) can be found frequently in the Oregon Subduction Zone. While vesicomyid clams are the most widespread animals observed at NW-Knoll, the BSR-outcrop and Hydrate Ridge, below app. 1000 m mainly pogonophorans of the genus *Lamellibrachia* sp. indicate venting on the first ridge and the base of Hydrate Ridge. This finding may indicate a depth dependency of the species distribution. However, the distribution of the three different Vesicomyid species, *Acharax* sp. and the bacterial mats seem to be more controlled by the chemical composition of the fluids expelled. Taking into account, that bacterial mats were only found in combination with very high hydrogen sulphide concentrations, indicating also most vigorous venting, maximum venting activity appears on the southern summit of Hydrate Ridge. Only here massive gashydrates were observed. Gashydrate may act as reservoir for methane and help to supply the chemoautotrophic organisms continuously with reduced chemical compounds.

Table 14: OFOS and TV-G deployments during Leg SO143-2.

Station	Tool	Area	Description	Technical comments
80-1	TVG	HR-South	trying to grab gashydrates, only few pieces in grab	
81-1	OFOS	HR-South	SE-NW profile, similar to OFOS 28-1	no compass correction
82-1	OFOS	HR-South	small scale mapping of "beaver mounds"	no compass correction
87-1	OFOS	1st Ridge	search for vents, discovered *Lamellibrachia*-colonies	no compass correction
93-1	OFOS	NW-Knoll	x-shaped profile over W-flank	no compass correction
94-1	OFOS	HR-South	S-N profile	
106-1	TVG	1st Ridge	Trying to grab *Lamellibrachia*-colonies failed	
111-1	OFOS	HR-W-Flank	Incipient headwall, no active venting beside one *Lamellibrachia*-colony	
112-1	OFOS	HR-North	Active N-summit, Sonne and Alvin chemoherm	catched an old fishing rope at ALVIN chemoherm, station aborted
121-1	OFOS	BSR-outcrop	high vent activity at N-flank of ridge	
129-1	OFOS	HR-W-Flank	search for vents, discovered *Lamellibrachia*-colonies	
132-1	OFOS	NW-Knoll	W-E-N profile over hill	
133-1	OFOS	HR-South	E-W profile, more active venting at W-flank	
154-1	OFOS	BSR-outcrop	confirmed active vents at BSR-outcrop, and carbonate distribution	no CTD
155-1	OFOS	BSR-outcrop	confirmed carbonate distribution based on side scan sonar map	no CTD
167-1	TVG	BSR-outcrop	grabbing clams, carbonates, few sediment	
192-1	OFOS	HR-North	mapping small scale vent distribution N-summit	
192-2	OFOS	HR-North	mapping small scale vent distribution N-summit	
209-1	TVG	HR-North	trying to grab carbonates and clams failed	

3. 5   Vent sampling and flux measurements

P. Linke, O. Pfannkuche, F. Appel

A major focus of station work during leg 2 of Sonne cruise 143 was the video-guided deployment of landers and the VESP (**Ve**nt **s**ampler). Altogether, the two VESP-landers and the **DOS** – (**D**eep-sea **O**bservation **S**ystem) were moored twice on this leg (Figs. 34 and 35). The VESP was deployed 9 times on selected sites at the seafloor (Table 15).
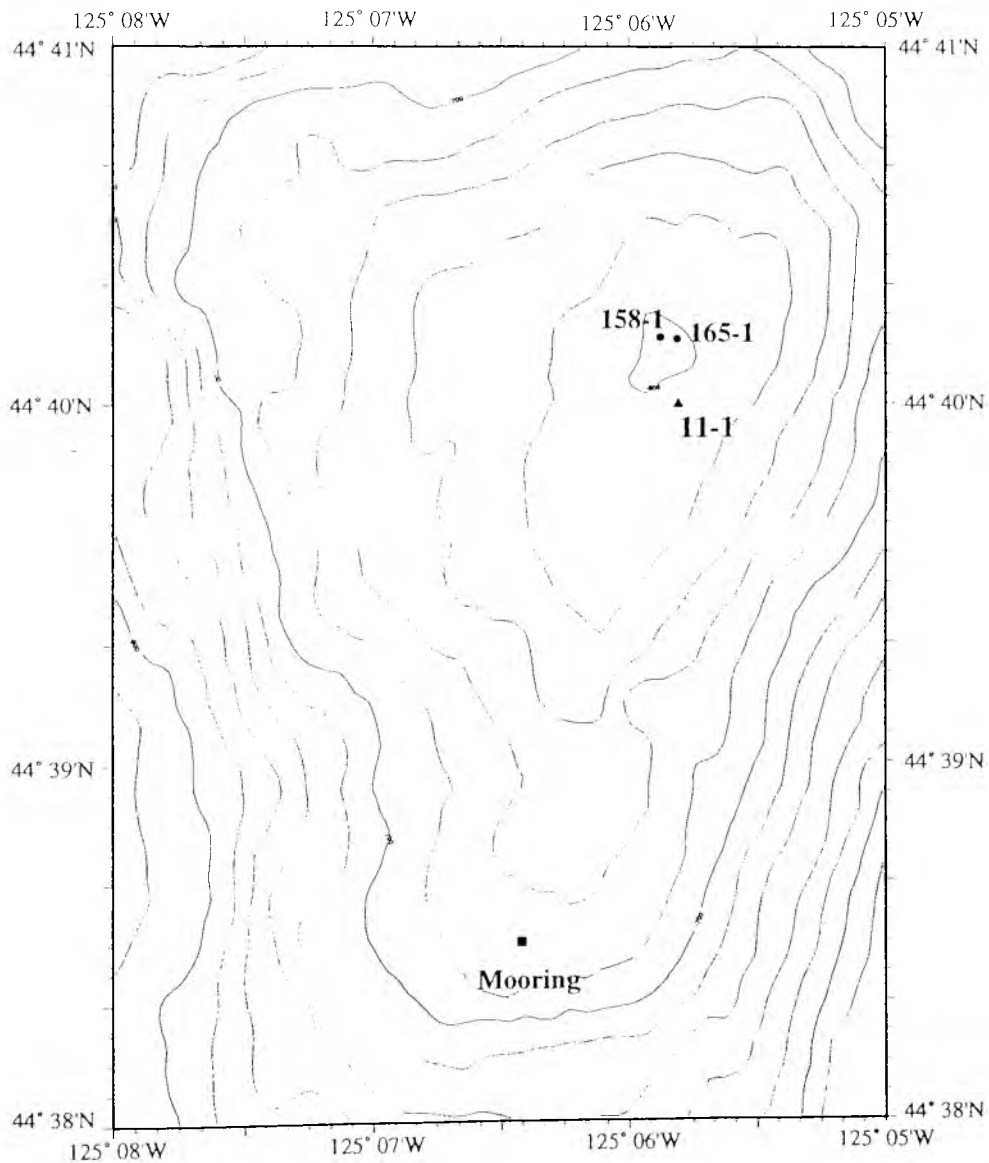
Fig. 32: Deployment positions of VESP-lander I (triangle) and VESP (circle) in respect to the OSU current meter mooring on the northern summit of Hydrate Ridge.

Table 15: Table of deployment times and sites of both VESP-landers, VESP and the DOS-lander on Hydrate Ridge.

Date	Station	Time UTC	VESP-Lander I	Site	Syringe sampling	Hours after deployment	Time UTC	VESP-Lander II	Site	Time UTC	VESP	Site	Time UTC	DOS-Lander	Site
10.7.99															
11.7.99	SO143/11-1	1:47	Deployment	Northern	12:10	10,55									
				Summit	18:10	16,55									
12.7.99				Bacterial Mat	6:10	28,55									
13.7.99															
14.7.99					6:10	76,55									
18.7.99					6:10	172,55									
23.7.99					6:10	292,55									
30.7.99					6:10	460,55									
31.7.99															
1.8.99	SO143/76-1	15:04	Recovery												
2.8.99	SO143/79-1	0:13					0:13	Deployment	Southern						
3.8.99	SO143/88-1	15:29	Deployment	Southern	19:23	4			Summit						
4.8.99				Summit	19:23	28			Clam Field						
5.8.99				Bacterial Mat	19:23	52									
6.8.99	SO143/109-1	22:33			19:23	76				22:33	Deployment Southern S.				
7.8.99	SO143/110-1	2:03			19:23	100							2:03	Deployment Southern	
8.8.99	SO143/118-1	0:14			19:23	124				0:14	Deployment Southern S.				Summit
9.8.99					19:23	148									Bacterial Mat near VESP-Lander II
10.8.99	SO143/128-1	2:35	Recovery												
11.8.99	SO143/131-3	2:25								2:25	Deployment Southern S.				
12.8.99															
13.8.99	SO143/142-1	0:15	Deployment	Southern											
	SO143/143-1	0:47		Summit			0:47	Recovery							
	SO143/150-1	18:40		Clam Field						18:40	Deployment Southern S.				
14.8.99	SO143/152-1	3:48											3:48	Recovery	
	SO143/156-1	19:32					19:32	Deployment	Southern						
15.8.99	SO143/158-1	1:34							Summit	1:34	Deployment Northern S.				
	SO143/162-1	20:36							Clam Field				20:36	Deployment Southern	
16.8.99	SO143/165-1	3:51								3:51	Deployment Northern S.				Summit
17.8.99															Clam Field
18.8.99	SO143/181-1	5:30								5:30	Deployment Southern S.				
19.8.99															
20.8.99	SO143/191-1	2:46								2:46	Deployment Southern S.				
21.8.99	SO143/196-1	1:18	Recovery							7:19	Deployment Southern S.				
	SO143/198-1	7:19													
	SO143/202-1	20:12					20:12	Recovery							
	SO143/203-1	20:39											20:39	Recovery	
22.8.99															
23.8.99															
24.8.99															

The VESP systems are described in detail in Chapter 2.5. The only change during this leg was that VESP-Lander I carried an additional pH-sensor (AMT) connected to the SBE 25 and the VESP was equipped with a new fluid sampler (Rimek, 1999). This fluid sampler obtains water out of the barrel through a 3-way valve into a pressure retaining sampling system which can be shut-off by a motor activated by the operator through the VESP telemetry (Fig. 34). The sampler is of modular design and obtains 2 pressurized water samples for methane and helium isotope analysis. Once, the design of this fluid sampler has proved its functional value several samplers can be mounted in a row to obtain a time series of pressurized water samples either mounted on a lander or a ROV-handled system.

The DOS-Lander (Fig. 35) carried a calibrated stereo still camera system with a single flash (BENTHOS) taking photographs of the deployment sites in 30 minute intervals. Furthermore, it carried 2 Sentinel ADCPs (Acoustic Doppler Current Profilers – RD Instruments) facing up and down from the landers outer frame. The uplooking ADCP (300 kHz) recorded the velocity profile with a 50cm cell resolution from 2.63 m up to 66 m above seafloor. The downlooking ADCP was a high-resolution (1.2 MHz) version measuring the bottom water current profile with a 5 cm cell resolution and a distance of 1.65 m from the transducers to the bottom.
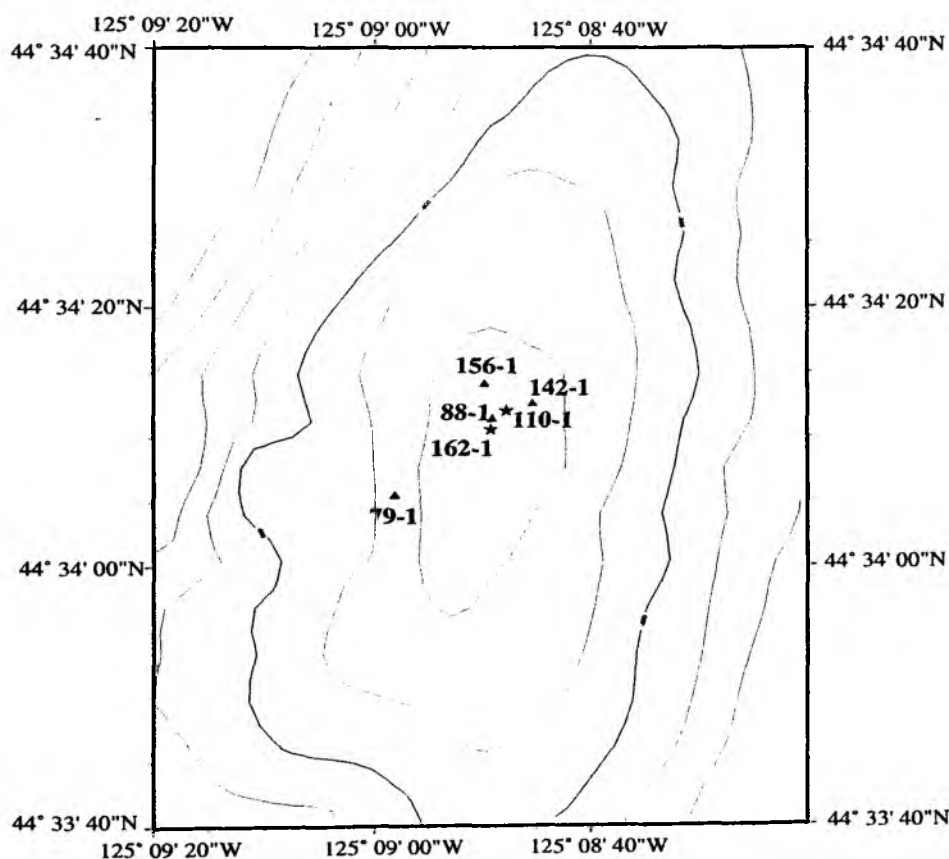
Fig. 33: Deployment positions of both VESP-landers and the DOS-lander at the southern summit of Hydrate Ridge.
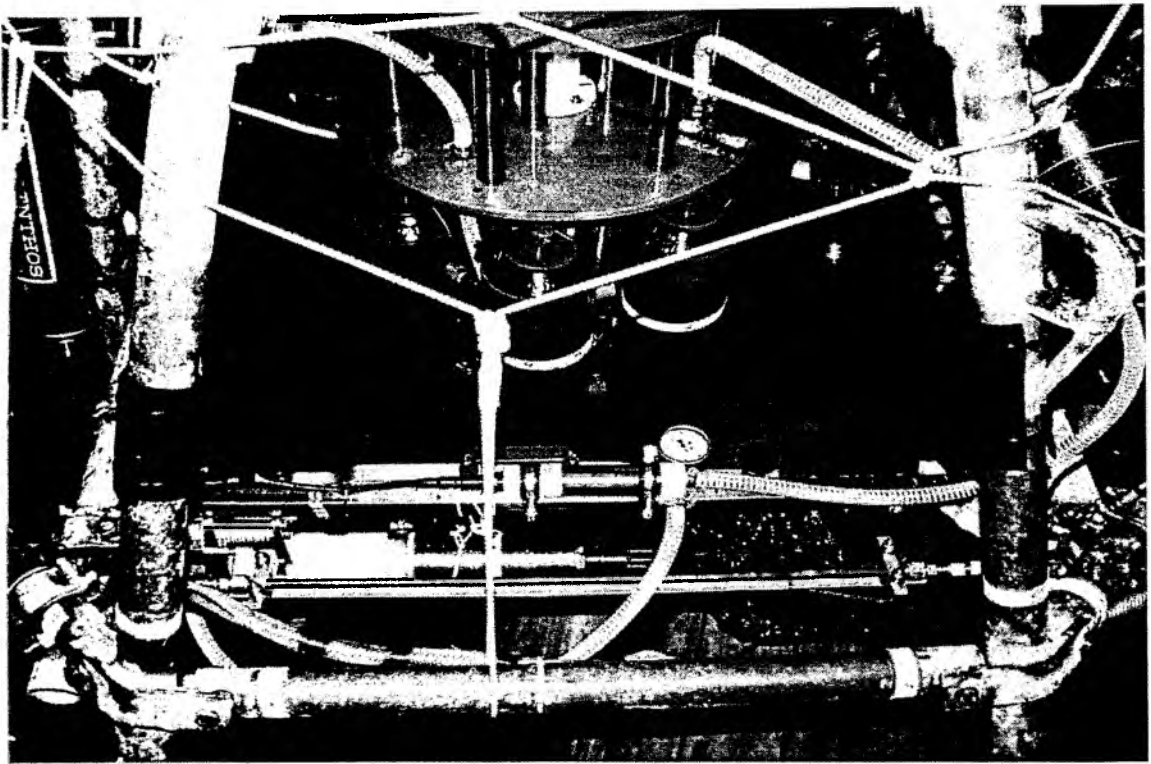
Fig. 34: Picture of the pressure retaining fluid sampler mounted on VESP.
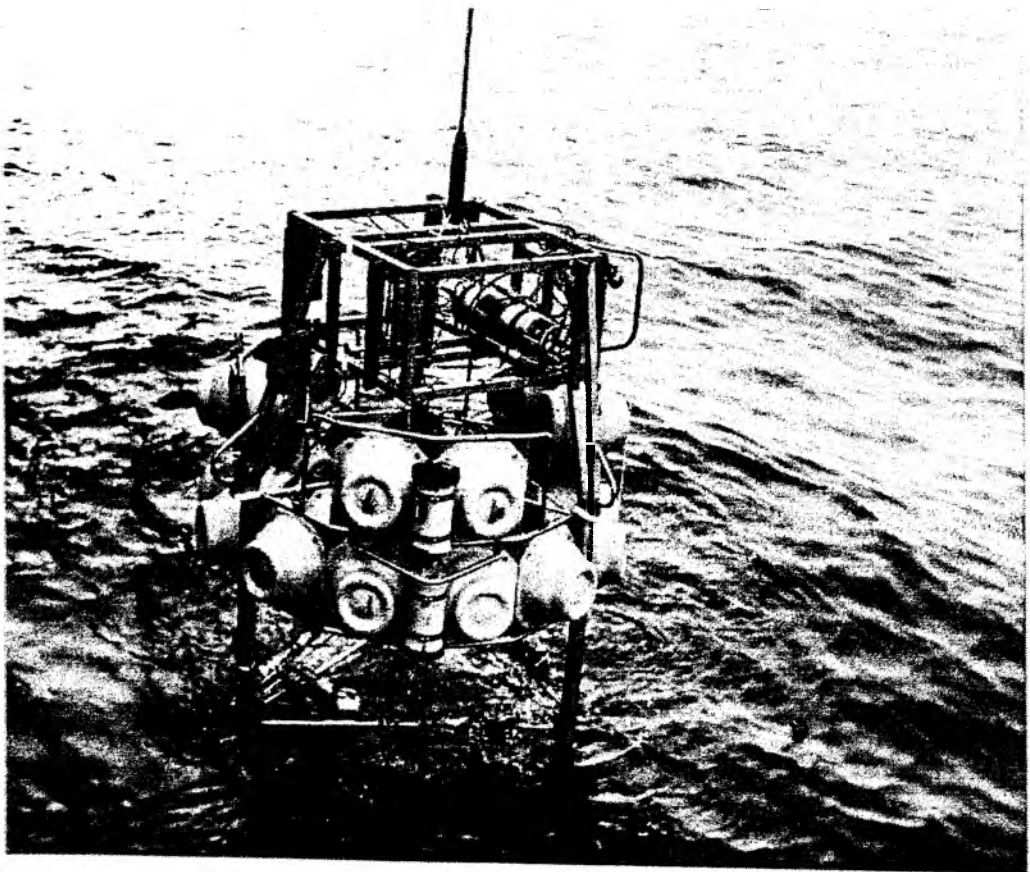
Fig. 35: Deployment of the DOS-lander. Visible are the up- and down-looking ADCPs mounted on the side of the lander.
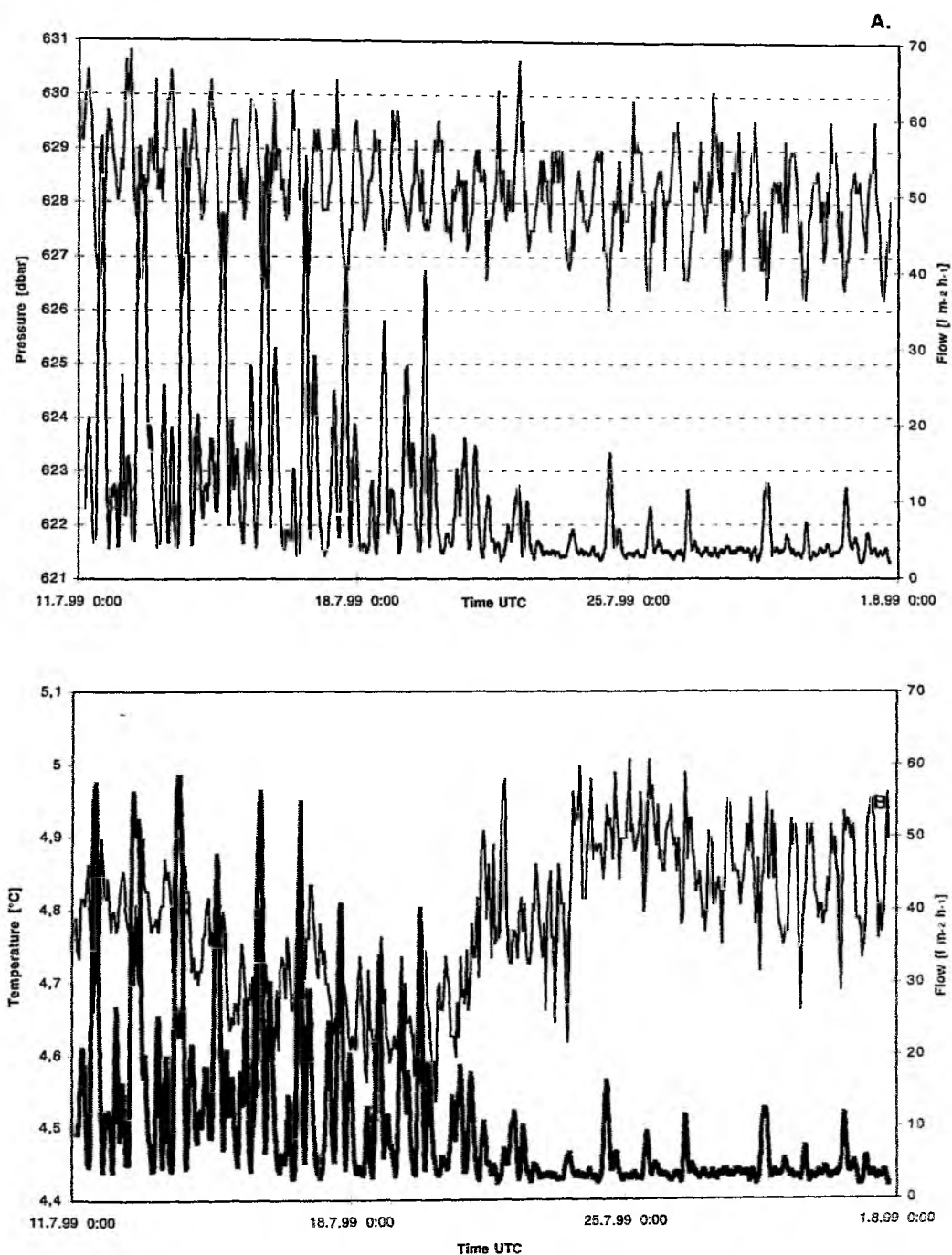
Fig. 36: A. Fluid flow data obtained during a 3 week deployment of VESP-lander I at the northern summit of Hydrate Ridge and pressure data obtained from the OSU mooring. Note the positive correlation between maxima in fluid flow and minima in pressure. B. Possible impact of temperature changes on flow rates.

Preliminary results

On August 1, the first station of Leg I2, the **VESP-lander I** was recovered after 3 weeks of deployment on a bacterial mat on the northern summit of Hydrate Ridge. The lander recorded CTD- and fluid flow data and obtained 7 water samples in 50ml syringes. A first view on the data revealed a tidal signal in fluid flow (Fig. 35), temperature and pressure. On July 16, the pressure amplitude diminshed by 1 bar and at the same time the flow magnitude dropped to much smaller values. Time-series analyses and comparison with tide gauge data from Newport Harbour and the OSU current meter mooring in the immediate vicinity of the deployment position are needed to varify this possible correlation (Fig. 36). VESP-lander I was deployed again for 1 week on a bacterial mat (Station 88-1) and for 8 days on a clam field (Station 142-1) at the southern summit of Hydrate Ridge. Data and samples will be processed at GEOMAR.

VESP-lander II was deployed for 11 (Station 79-1) and 8 days (Station 156-1) on a clam field at the southern summit of Hydrate Ridge (Fig. 33). Data from the CTD, flowmeter and methane sensors will be processed at GEOMAR. Unfortunately, during the second deployment the FSI-CTD did not store any data.

VESP was deployed 9 times for a period of 1 and up to 2 hours on several sites at the northern and southern summit of Hydrate Ridge. After the first unsuccessful deployment which was due to a problem in the power supply it proved to be a reliable instrument for short-term measurements and experimental setups like the use of the fluid sampler.

The **DOS-Lander** was deployed for 7 days on a bacterial mat (Station 110-1) approximately 2m next to one VESP-lander and for 6 days on the interface between a bacterial mat and a clam colony (Station 162-1) at the southern summit of Hydrate Ridge (Fig. 35). Both deployments gained pictures with the stereo camera and the ADCPs which will be analysed and processed at GEOMAR.

3.6   Radon measurements: samples from benthic landers and barrels

S. Colbert

Rn-222 was analyzed by alpha scintillation techniques. Aliquots of water were drawn from Niskin bottles on each of the three VESP landers (Lander 1, Lander 2, and benthic barrel). Each sample was injected into the RRES stripping system and transferred to counting cells.

Table 16: Results are presented in dpm/L and represent the concentration at the time of sampling.

Station	Sample #				
Barrels	**1**	**2**	**3**	**4**	**5**
118-1	0.61±0.20			1.00±0.20	
131-2	0.34±0.23	0.10±0.30	0.31±0.31	0.42±0.32	0.41±0.41
150-1	0.21±0.31	0.49±0.37	0.53±0.32	0.52±0.39	0.31±0.31
159-1	0.46±0.23	0.47±0.35	0.37±0.49	0.82±0.35	0.36±0.24
181-1		0.31±0.31		0.70±0.30	
191-1			0.49±0.29	0.91±0.34	1.08±0.27
198-1			0.74±0.25	1.42±0.33	0.97±0.32
Landers	**Outside**	**Inside**			
128-1	0.49±0.29	0.10±0.31			
142-1		0.34±0.23			

Benthic flux chambers

Aliquots of water were drawn for Rn analysis from the two Niskin bottles on the VESP landers. Unfortunately, any increase in Rn during the deployment was undetectable (Table 16). These results may be explained several different ways:

1) Rn is adsorbed by organic matter. If the surficial sediments are rich in organic matter, than it is possible that Rn is preferentially incorporated into this organic matter, reducing the flux to the overlying water column. This is unlikely, however, as Rn fluxes have been measured from similar environments during the RV ATLANTIS cruise AT9906 (TECFLUX '99).

2) Surficial sediments depleated in radium. If there is a thick bacterial mat or a high density of clams, then no Rn is being produced near the surface and the flux of Rn will be deminished. Coarse grained material with a high porosity would also have a low Rn emanation rate.

3) Advection into the sediments. A flow of water into the sediments would supress the diffusive transport of material into the chamber. The flow meter data will indicate if this is correct.

4) Leaky chamber. If the flux chamber did not have a good seal around its base, than it is possible that chamber was flushed out with bottom water.

5) Bottle malfunction. If the Niskin bottle on the inside of the chamber did not close immediately, than it could have been flushed out during the lander's ascent to the surface.

Comparisons with nutrient and oxygen measurements should be useful in determining if either Explanation 4 or 5 is valid. Explanation 2 is difficult to evaluate without sediment samples from the location of the lander. Sediment cores collected nearby will be analyzed in the laboratory for their solid phase Rn emanation rates.

Benthic barrels
Aliquots of water were drawn for Rn analysis from Niskin bottles in the VESP Benthic Barrels. For most deployments, Rn was within the range of average bottom water Rn (0.3 ± 0.2 dpm/L) and any increase in Rn was undetectable. This lack of increase alows an upper limit for flow to be calculated, based on the assumption that the Rn concentration in pore waters under the deployment sites is similar to that measured at depth in the whole core squeezer profiles (150 dpm/L). Some additional work must be done to evaluate the validity of this assumption. A change of 0.6 dpm/L during the course of the experiments should have been detectable. If we assume that the water in the barrel was well mixed, no more than 0.4% of the barrel water was replaced during the experiment. For a 73 cm high barrel, and the average length of time spanned by the samples was 1.5 hours, this constrains the upper limit for flow to be 2 mm/hr or 4.5 cm/day. While the assumption about good mixing and the concentration of Rn in pore water could be invalid, it should be interesting to compare this result to the flow velocity measured at the barrel exit.

Three deployments had Rn concentrations that were greater than bottom water and therefore must be explained individually. Two deployments (118-1, 198-1) resulted in Rn concentrations that were significantly above average bottom water concentrations. This is most likely caused by the barrel disrupting the sediments when it is deployed, releasing pore waters rich in Rn into the barrel. This was obviously the case for 118, where sediments were found in the Niskin bottles. However, for 198-1, there were no obvious indicators that the sediment had been disrupted. An advection of fluids through the sediments could produce an anomolous water mass that is enriched in Rn. Advection of fluids was not discernable in the Rn data at this station.

An increase in Rn was detected at Station 191-1. This corresponds to a flux of 817 ±121 atoms/m2-sec. This can then be used along with the same assumptions described above to calculate an upper limit for flow of 5.6 cm/day can be calculated.

3.7   Eh, temperature and potensiostat measurements
Ko-ichi Nakamura

Redox potential-, potensiostat-, and pressure-measurements were carried out with sensors attached to CTD/rosette sampler, OFOS, VESP, VESP-landers and DOS-landers during Leg SO143-2.

3.7.1 Eh measurement at CTD casts

Instruments
On each CTD cast, in-situ measurements of Eh (redox potential) were performed either through an on-line Eh measurement unit or by an independent (self-recording) Eh logger. In both cases, the electric potential of seawater was measured between an inert electrode (coiled 25 cm-long, 0.7 mm phi Pt wire) and a reference electrode (Ag/AgCl electrode sealed in KCl saturated solution by an oxidized zirconia electrode container, whose electronic connection was performed by a zirconia plug). The electrodes were located close to the other CTD sensors at the bottom of the CTD/rosette sampler. The on-line Eh measurement unit converts the electrodes' output voltage (+1 to -1 V) into +5 to 0 V, which is acceptable by an auxiliary channel of the SBE 911 plus CTD underwater unit. The self-recording Eh logger measured the electric potential of seawater at an interval of 2 seconds in 0.05 mV resolution.

Results
During the movement of the CTD/rosette in the water column, the measurement of electric potential using the regular electrodes never gives any equilibrated values. However, if a water-mass with anomalous composition exists in the water column, the electrodes will likely show the anomalies. Unlike to CTD casts in hydrothermal plumes, some signals appeared in the Eh records which were difficult to interpret.

In the hydrothermal fields, any small drops of Eh values, even if they are only several tenths of mV, appeared in the water depth from near bottom to several hundreds meters above the seafloor and can be correlated either with optical anomalies or with Mn and/or Fe anomalies. In the hydrothermal plumes, several kinds of short-lived metallic cations are concentrated and produce Eh anomalies. Whereas in the cold seeps, there are not so much cations or anions, which might produce Eh anomalies, other than the hydrogen-sulfide near the seeps. The other factor, which might mask the Eh anomalies, is the steep gradient of Eh against depth.

Because the surveyed area is located above the depth of the oxygen minimum zone, Eh values become low as depth increases as apparent in CTD Station 99-1. The maximum depth of this cast was about 770 m. In the deep cast of CTD Station 124-1 (ca. 2300 m), the Eh gradient in the deeper part of the cast became small and produced an "Eh minimum" in the records (Fig. 37). In the tow-yo casts, CTD stations 137-1 (Fig. 38) and 159-1, the Eh records are almost governed by depth. Above the four casts are some examples of the independent records of Eh measurement. A detailed analysis of the records using the on-line Eh measurement through the CTD underwater unit is necessary for further interpretations.

SONNE 143-2
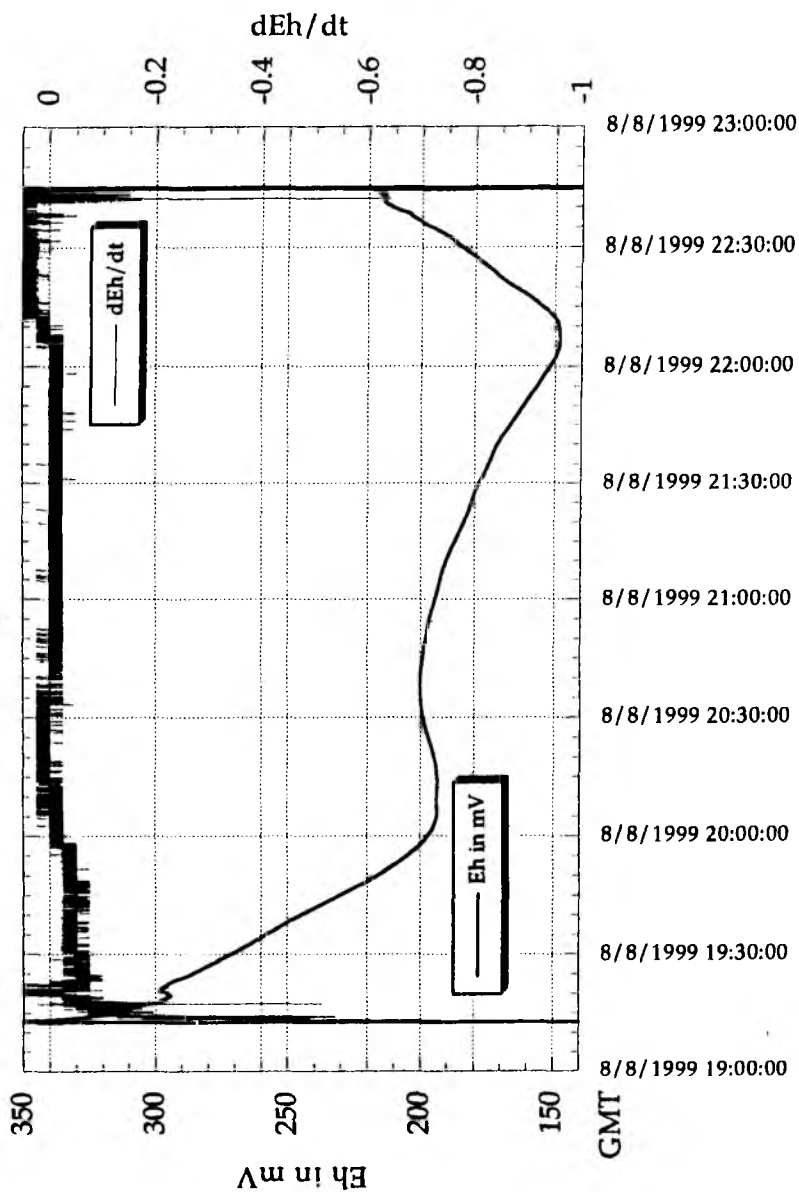
Fig. 37: Signal of the Eh-sensor during CTD Station 124-1 performing an Eh minimum.
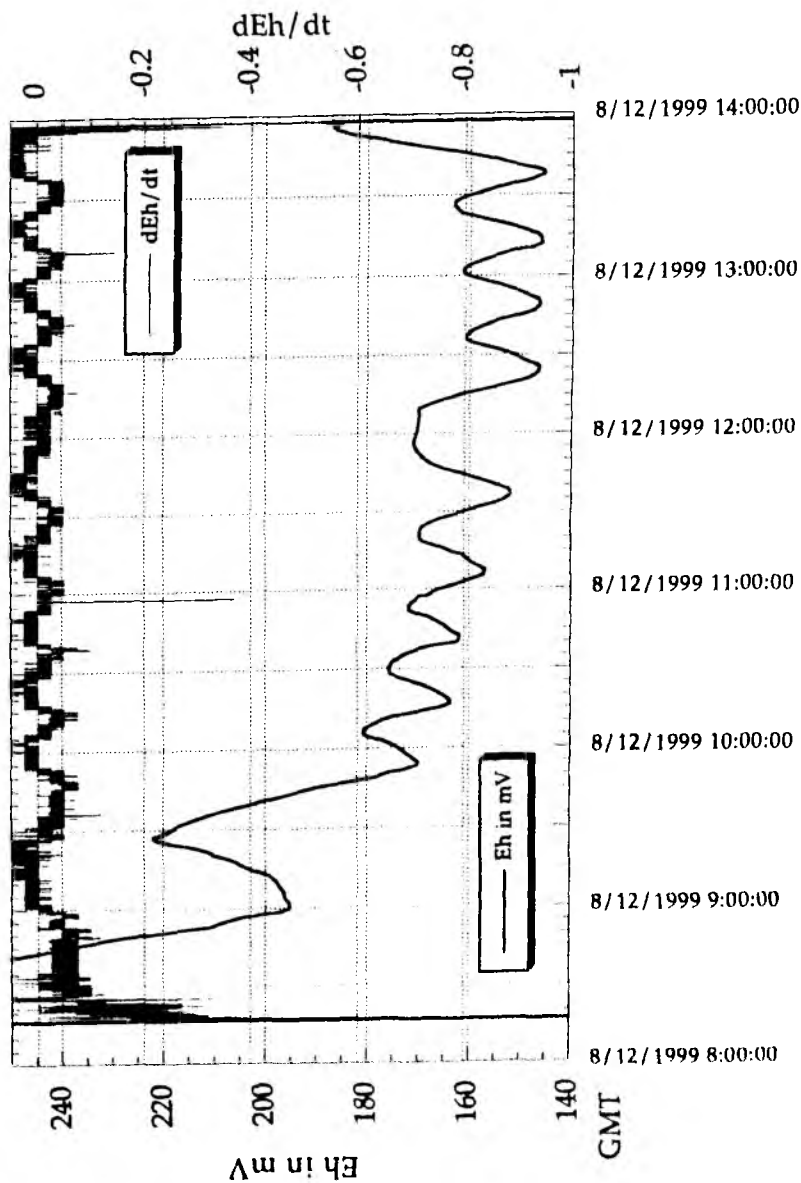
Fig. 38: Eh-record during CTD two-yo cast 137-1.

3.7.2 Eh and potensiostat measurements on OFOS

Instruments
On every OFOS station, a self-recording Eh logger was attached near the bow of the OFOS sledge. At the last OFOS stations (Stations 155-1, 192-1 and 192-2), a 3-channel pre-fixed voltage potensiostat was also attached on the port side of the OFOS to test the instrument application for the seafloor exploration. Each channel of the potensiostat keeps the electric potential between Pt and reference electrodes at a preset fixed voltage and measures the electric current between Pt and Au electrodes.

During the TECFLUX 99 cruise with RV NEW HORIZON in June, the system was attached to the CTD rosette and some negative potential setting measurement correlated with the oxygen profile. The basic idea of these tests was based on the assumption that some cold seeps, which might create local oxygen-depleted water on the seafloor, may produce some anomalous values of this measurement. The fixed given voltages for three channels were +420 mV, -200 mV and -400 mV.

Results
On a moving sled, like OFOS, the Eh measurement will never reach equilibrated values. However, some anomalous composition of seawater, for example, hydrogen-sulfide, may produce some anomalous values as the OFOS flying over the cold seeps. Although the detailed correlation with observed seafloor features have not yet performed during the cruise, some Eh drops appeared near the high point in the course, as are shown in the records of OFOS Stations 81-1, 82-1, 94-1, 112-1 (Fig. 39), 121-1 and 154-1 (no depth record) might be correlated with the locations of cold seeps.

3.7.3 Eh measurement at VESP deployment

Instruments
On every VESP station, self-recording Eh loggers were attached to the VESP, one inside of the barrel chamber and the other one outside of the barrel. The electrodes inside of the barrel were located 19 cm above the barrel brim plane (i.e., expected seafloor at the time of deployment), whereas the ones outside of the barrel were located 32 cm above the VESP paws (bottom).

Results
There were two sets of deployments with contrasting results (type A & B). On stations 118-1, 150-1, 181-1, 191-1 and 198-1 (Fig. 40) significant Eh drops were recorded inside of the barrel during the barrel deployment on the seafloor greater than the drops recorded outside of the barrel. Whereas, at deployments on stations 109-1, 131-3, 158-1 and 165-1 (Fig. 41), Eh drops in the barrel did not exceed those outside of the barrel. The Eh values inside the barrel during type A deployments were between -100 and -200 mV. Based on the sulfur pH-Eh diagram, these Eh values suggest that the redox potential in the barrel were mainly controlled by sulfate-sulfide reaction, if we assume not so extraordinary pH condition. Type B deployments might have been caused either by insufficient sealing at the bottom or by the different seep character, which did not produce much hydrogen-sulfide.
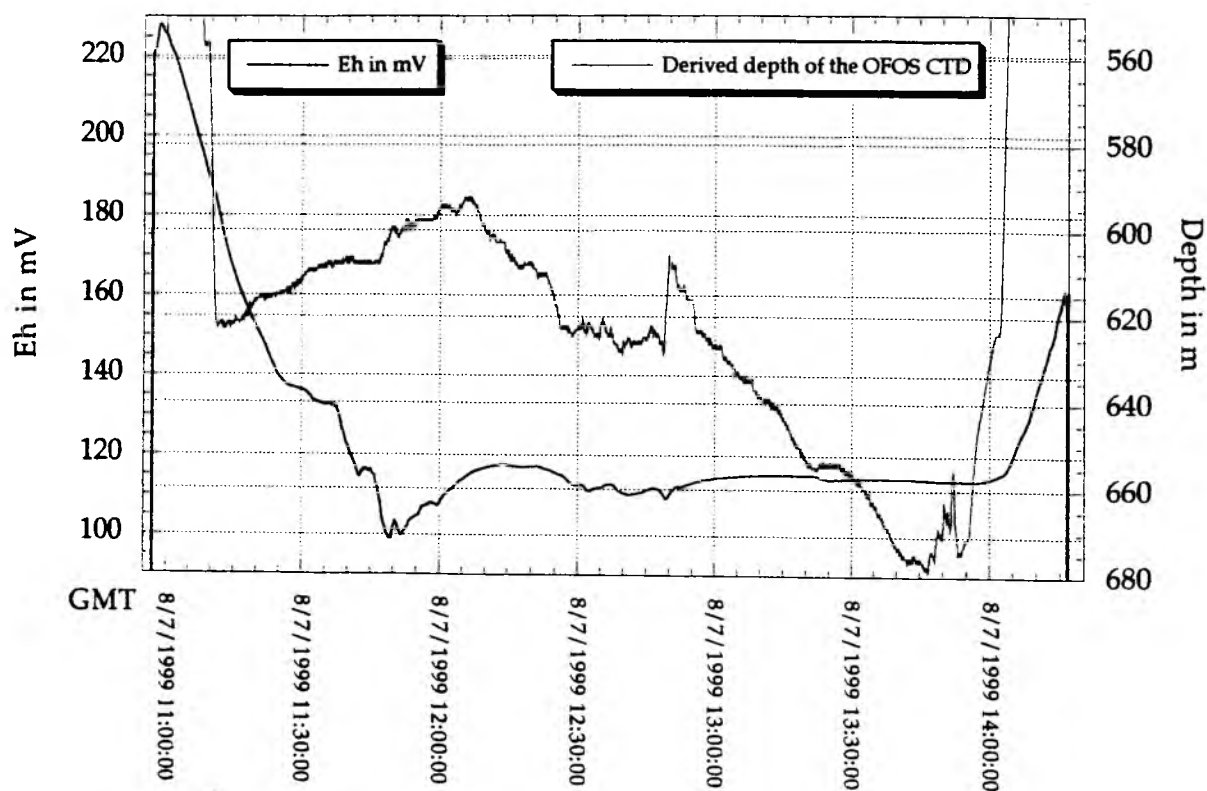
Fig. 39: Eh- and pressure record during OFOS Station 112-1.
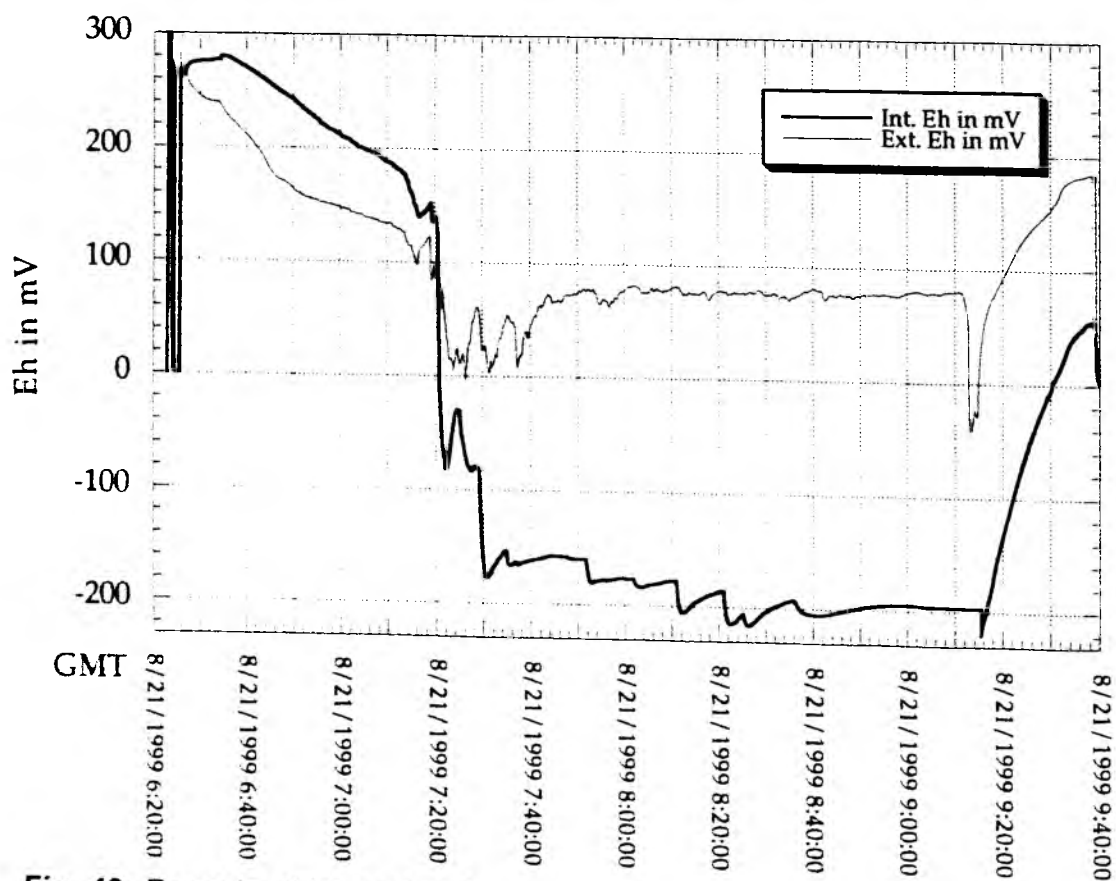
Fig. 40: Records of internal and external Eh-sensors during VESP deployment on Station 198-1. Significant Eh drops were recorded inside of the barrel during the barrel deployment greater than the drops recorded outside of the barrel (Type A).

Throughout all the records, the Eh values in the barrel were higher than those outside of the barrel before the deployment on the seafloor. This might have been caused by slow ventilation rate in the barrel through the small outlet. In the type A deployment, Eh values inside of the barrel took several minutes to twenty minutes to reach to the low stable value. These time-lag also might be caused by slow ventilation in the barrel. Further cross-check on the relation between the amount of time-lag and the recorded flow rate will be necessary.

The type B deployment might be subdivided into two subtypes. At stations 109-1 and 158-1, distinctive Eh drops were recorded at the landing and then a slow recovery of the Eh values continued for about 20 to 30 minutes (Type B-1 deployment). In contrast, at stations 131-3 and 165-1 there were no drops at the time of landing (Type B-2 deployment). Eh drops in type B-1 deployment might have been caused by sediment stirring at landing.

3.7.4 Eh, temperature and potensiostat measurement at VESP-lander stations

Instruments
During a VESP-lander I deployment (Station 142-1) Eh was measured both inside and outside of the chamber. The electrode tips were inserted from small holes located near the top of the chamber (ca. 35 cm above the chamber rim plane, i.e., expected seafloor at the time of deployment) for the measurement inside of the chamber, while the logger was located outside of the chamber. The external Eh measurement (outside of the chamber) was performed in the SBE/CTD frame, which was located at a corner of the lander. The external electrodes were located 27 cm above the lander paw near the CTD sensors.

During a VESP-Lander II deployment (Station 156-1) Eh was measured both inside and outside of the chamber. One self-recording Eh logger with a set of electrodes was attached to a Niskin bottle located inside of the chamber. Estimated height from the seafloor at the time of deployment was ca. 15 cm. Another Eh logger was attached to one leg, outside of the chamber. Its electrodes were located 29 cm above the lander paw. The other electrochemical instrument, which can measure temperature, Eh and fixed potensiometry (potensiostat channel) was attached to this VESP-Lander (outside of the chamber).

The potensiostat channel kept the electric potential between Pt and reference electrodes at -200 mV and measured the electric current between Pt and Au electrodes. The temperature sensor and the potensiostat electrodes were located 45 cm above the lander paw, whereas the Eh electrodes of this instrument was located 114 cm above the lander paw. In summary, three Eh measurements were performed during this lander deployment. One measurement was in the chamber (15 cm above the seafloor) and the other two were performed outside of the chamber in different height (29 cm and 114 cm) from the seafloor.

After the recovery of the landers, the reference electrodes were checked against standard electrodes in 0.1 mol/l KCl solution to confirm their stability during the deployment.
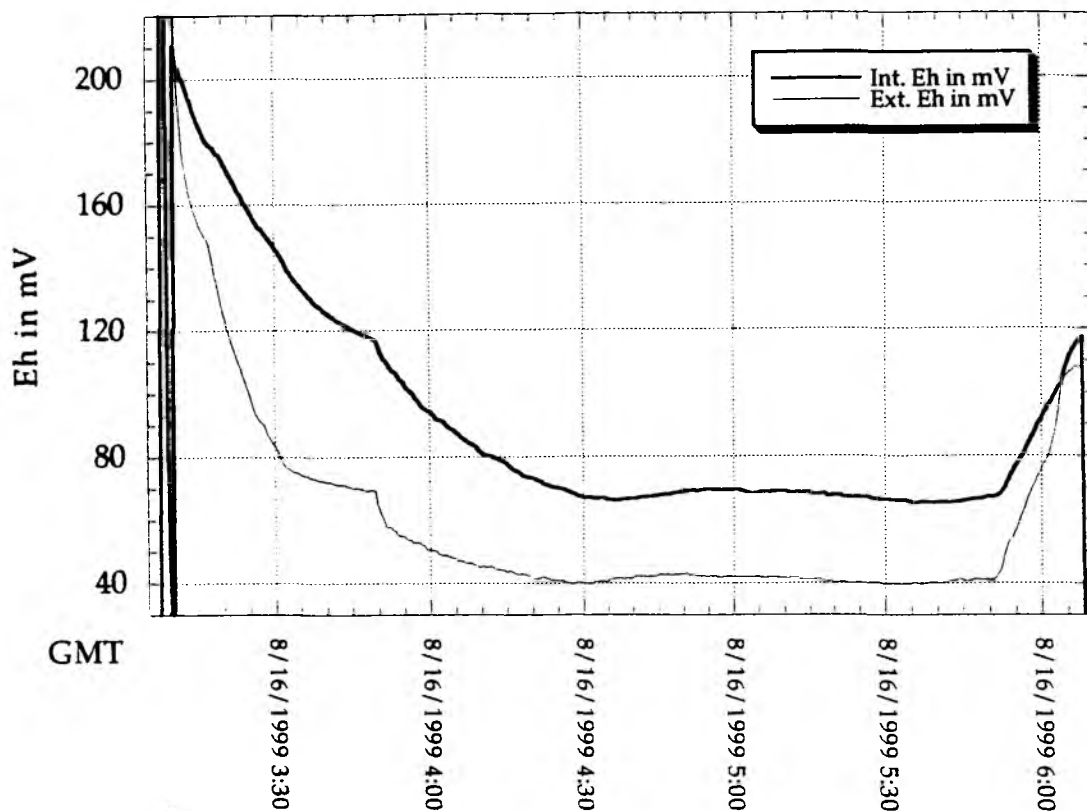
Fig. 41: Records of internal and external Eh-sensors during VESP Station 165-1 where Eh drops in the barrel did not exceed those outside of the barrel (Type B).
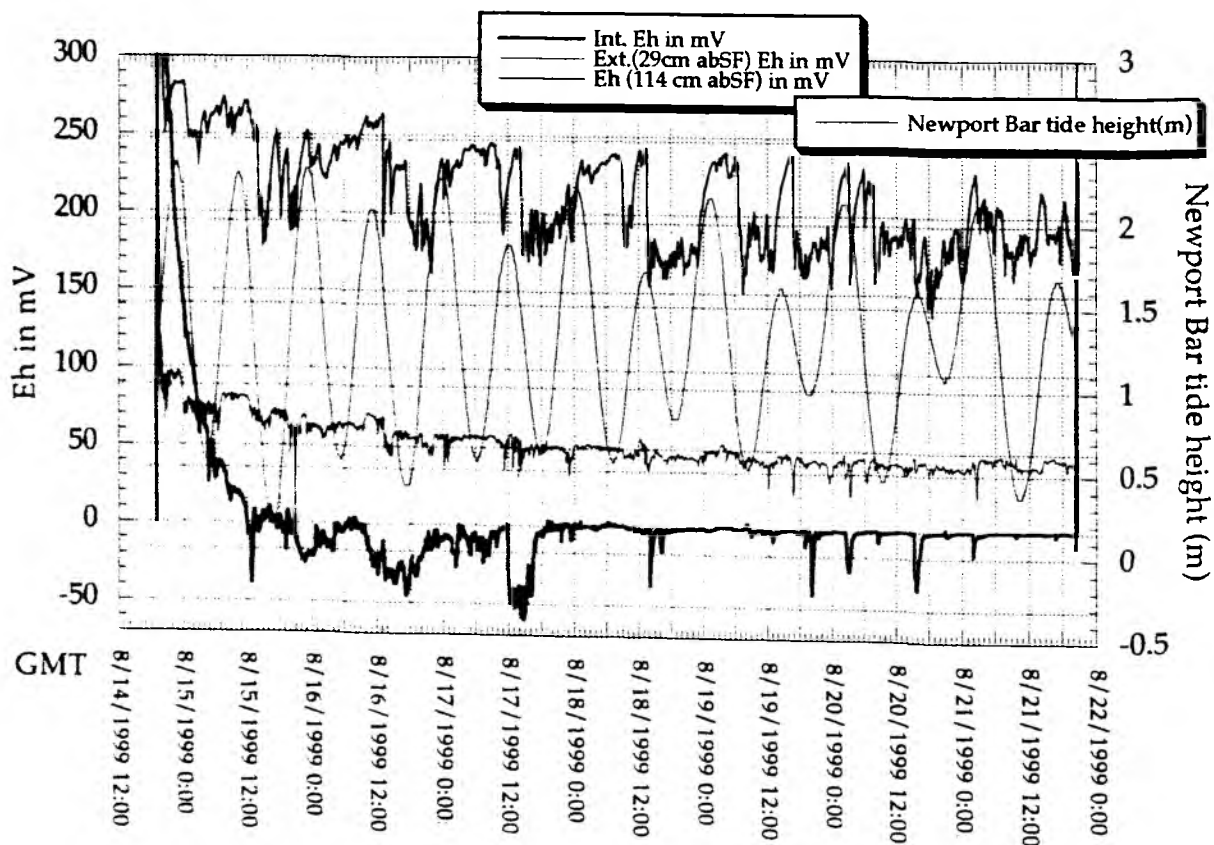
Fig. 42: Records of internal and 2 external Eh-sensors during VESP-lander station 156-1 in comparison with Newport Bar tide data.
Results

Eh records in the chambers of the VESP-landers at stations 142-1 and 156-1 showed different characteristics, although both records showed about for 1 day a gradual decrease of Eh values after landing.

At Station 142-1, after three days continuation of nearly stable Eh values, Eh gradually increased until the end of the deployment in contrast to the stable Eh condition outside of the chamber. This process could not be imagined from the VESP short-term deployment. One plausible idea to explain this process might be that the lander settlement changed the seep environment after four days of deployment and was going to another unknown equilibrated condition. Based on the gradual increase of Eh values, the other condition might be a rather oxygenated condition, which is also difficult to imagine.

At Station 156-1, both Eh measurements inside the chamber and outside the chamber near bottom (29 cm above the seafloor) were nearly stable in most of the period of the deployment (Fig. 42). In the former three days or so, Eh in the chamber show some undulation, whereas in the latter four days, it shows some episodic drops during the stable 0-mV condition. Eh measurement 114 cm above the seafloor and the temperature measurement outside of the chamber mostly showed tidal cycle.

Further studies combined with the data from other sensors on the landers are necessary to understand the process envolved inside of the chambers.

3.7.5 In-situ pressure measurement at DOS-lander stations
(In co-operation with H. Fujimoto)

A precise pressure sensor (Digiquartz, registered trademark of Paroscientific, Inc.) with self-recording logger, which was prepared and owned by the second author of this section, was installed on the two deployment of the DOS-Lander (Stations 108-1 and 162-1). The pressure sensor was located 120 cm above the lander paw. The in-situ pressure as well as temperature inside of the pressure sensor were measured at intervals of 1 minute.

Results
At the first glance of the data, pressure change at both stations have a good correlation in phase and in relative magnitude with the calculated Newport tide gauge data, which were provided by Dr. Robert Collier (Fig. 43).

3.7.6 Eh, temperature and potensiostat measurement at DOS-Lander stations

Instruments
At both DOS-landers deployments (Stations 108-1 and 162-1), an electrochemical instrument, which can measure temperature, Eh and fixed potensiometry (potensiostat channel) was attached to the DOS-lander. After the recovery of the landers, the reference electrodes were checked against standard electrodes in 0.1 mol/l KCl solution to confirm their stability during the deployment.
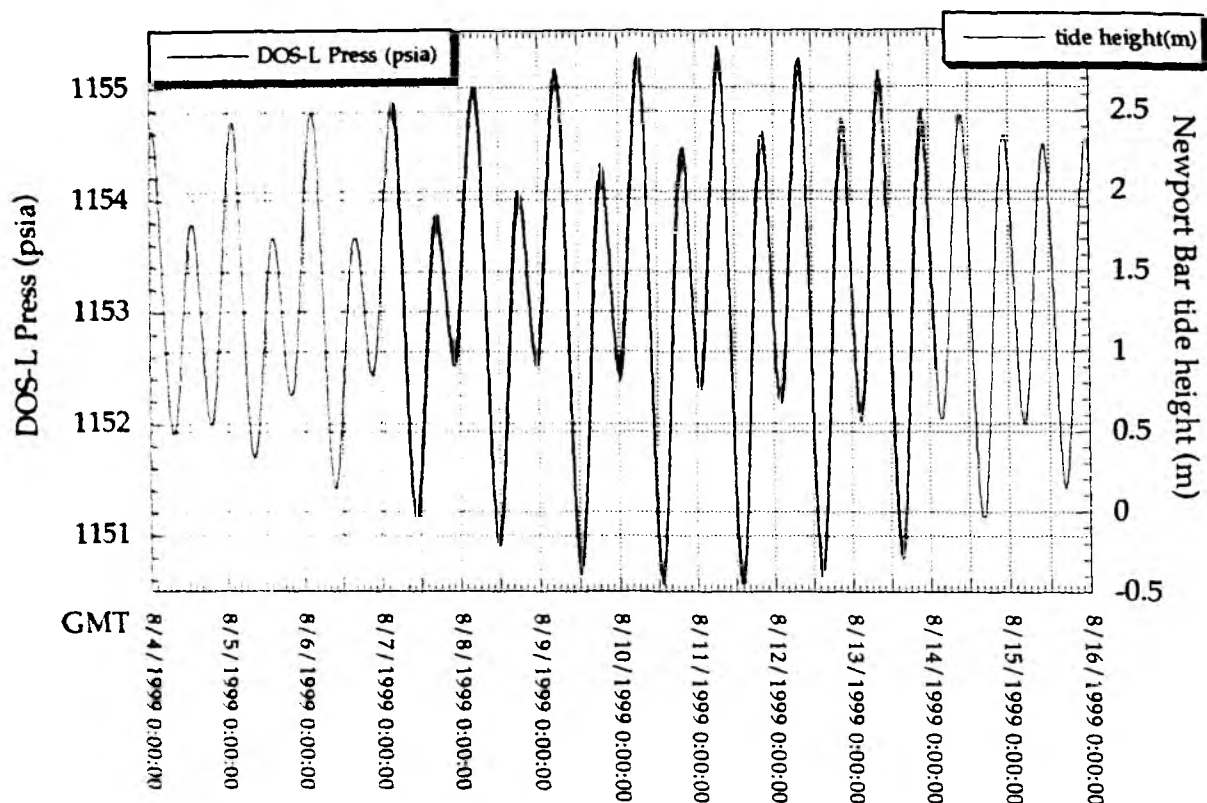
Fig. 43: Pressure data obtained at Station 108-1 during DOS-lander deployment. Note correlation in phase and in relative magnitude with the Newport tide gauge data.
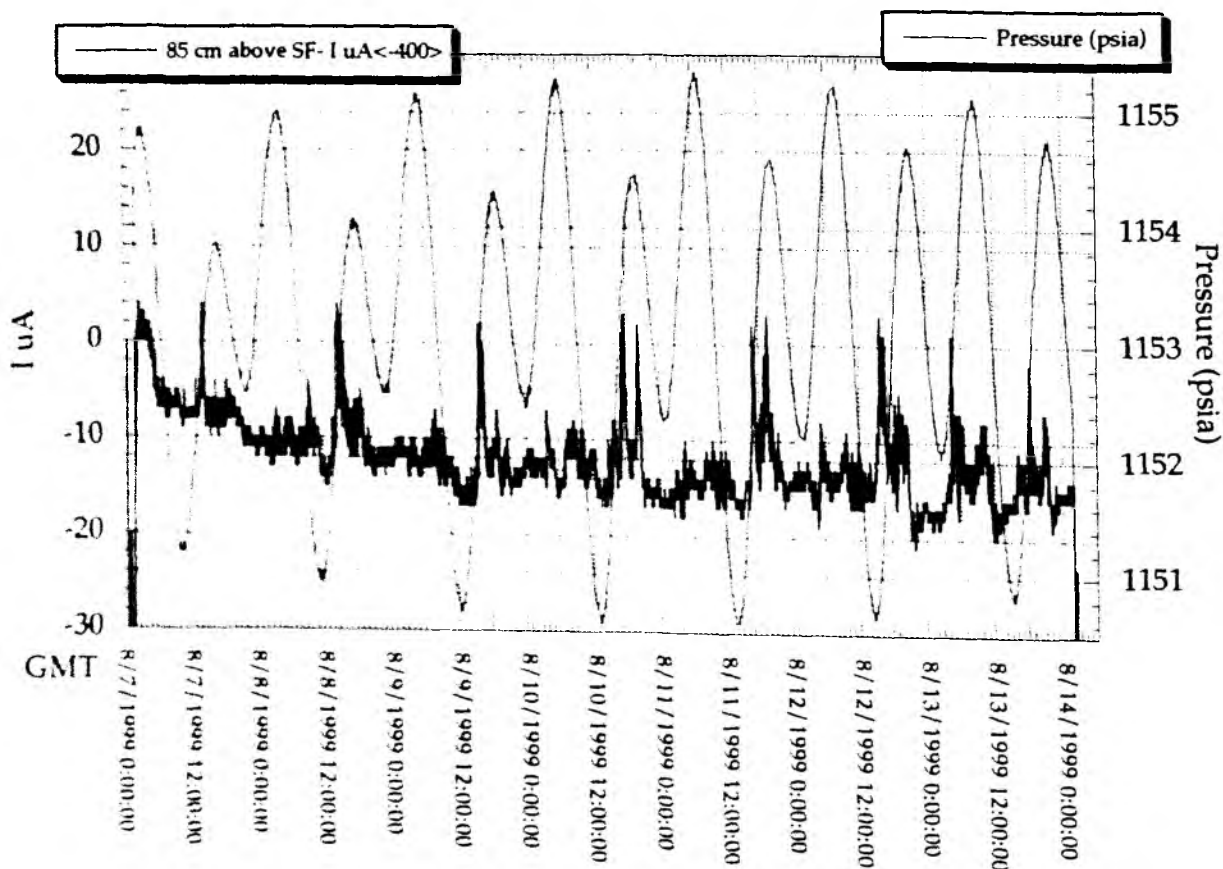
Fig. 44: Potensiostat electric current measurement at Station 108-1. Note the periodicity against the tide.

Results

Although temperature measurements by the electrochemical instruments need calibration, phase and relative magnitude of variation correlated well with those of the temperature measurements inside of the Digiquartz pressure sensor in both DOS-landers deployments.

Eh measurement at 145 cm above the seafloor at Station 108-1 and at 260 cm above the seafloor at Station 162-1 have to be examined after the re-calibration of the data logger and electrodes. In both measurements, the same sets of electrodes and the data logger were used.

Eh variation at 85 cm above the seafloor at Station 108-1 is likely governed by tide, although it is not clear whether Eh values were directly affected by the tide-generated cold seep emission or tidal bottom water currents. In the Eh records 85 cm above the seafloor at Station 162-1, short-period variation is dominant.

The potensiostat electric current measurement (at -400 mV) at station 108-1 shows a periodicity against the tide (Fig. 43). When the tide goes up, short events of current decrease to negative values were observed, which might indicate short events of oxygen depletion. The potensiostat electric current measurement (at -400 mV) at Station 162-1 seems to be mainly governed by tide. Again, whether these correlation with tide were created by direct effect of tide on cold seep source or by tidal currents remains to be analysed.

3.8 Benthic chamber lander work – *in situ* investigations of total oxygen consumption, solute dynamics and sulphate reduction

U. Witte, O. Pfannkuche, A. Cremer, S. Meyer, M. Poser

During Cruise SO143-2, a very comprehensive campaign of in situ measurements was carried out using the GEOMAR benthic chamber landers. Three of these modular lander systems were deployed, two carrying benthic chambers and one carrying a stereo camera system and two ADCP systems for long term observations (compare Chapter 3.5). The benthic chamber landers were equipped with two benthic chambers each. The chambers retrieve the sediment by closure of a shutter at the end of the incubation, and from each chamber, a series of 7 water samples is taken at pre-set intervals during the incubations. Main aim of the chamber measurements was to quantify the role of oxygen as electron acceptor along a gradient of stations from the H_2S dominated areas at near surface gas hydrates towards sediments not influenced by methane seepage. In addition to oxygen, water samples were analysed for H_2S, nutrient and methane dynamics. The sediments retrieved were sampled for measurements of the standing stock of small benthic size classes (compare Chapter 3.10) as well as for macrofauna. In addition, one lander was equipped with the injection module „Orpheus", developed at MPI.
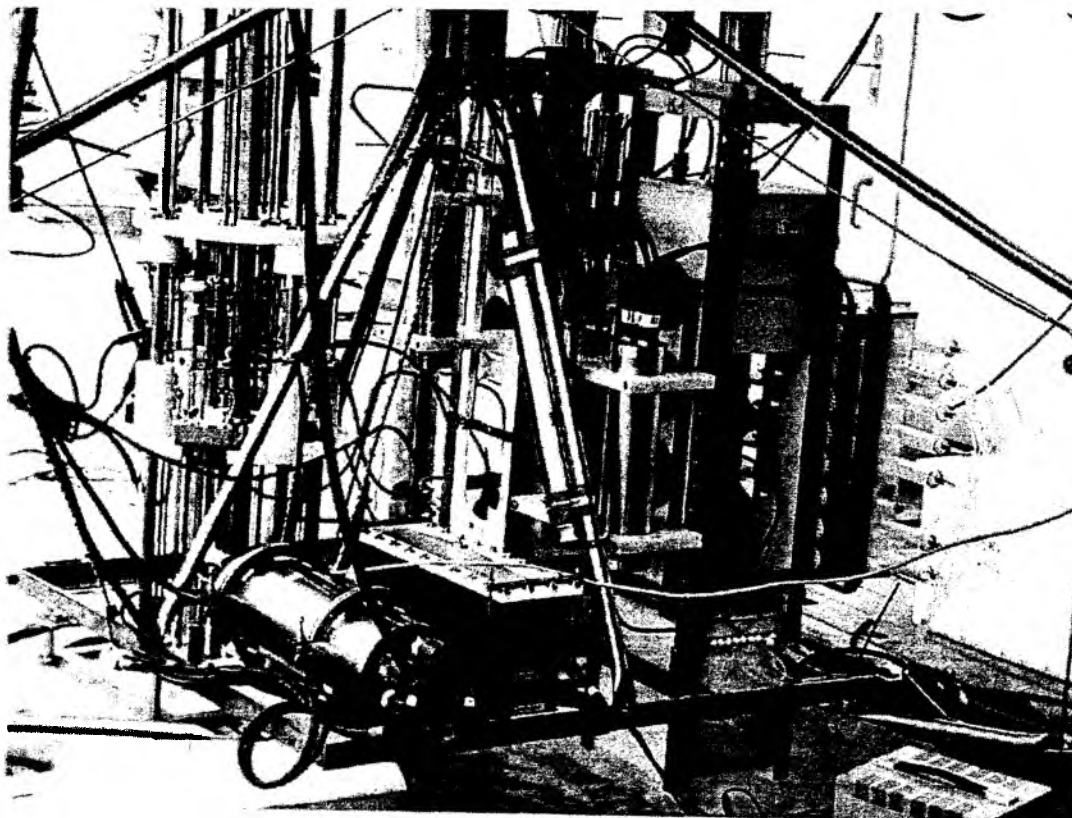
Fig. 45: Platform of the modular GEOMAR lander equipped with 2 benthic chambers and sulphate reduction module ORPHEUS.

ORPHEUS is designed for in situ measurement of sulphate reduction by injection of ^{35}S-labelled SO_4 into three parallel sediment cores. Its incorporation into the GEOMAR lander system allowed simultaneous measurements of oxygen consumption and sulphate reduction at the same spot. Parallel to the in situ incubations shipboard incubations for sulphate reduction measurements were carried out at both atmospheric as well as in situ pressure in order to investigate the importance of pressure for sulphate reduction rates.

Altogether, both chamber landers were deployed successfully ten times. In all cases the landers were deployed with a newly developed launcher system (Fig. 46) enabling us to place the instruments video-guided onto a desired spot of seafloor. Good weather conditions allowed for a very accurate positioning of the instruments directly at the sea floor. It was not – as originally planned – necessary to tow the instruments at low height above the sea floor and then release it and let it sink to the bottom. Besides a more accurate positioning this method also has the great advantage that it hardly disturbs the sediment surface. This was mirrored by almost undisturbed sediment surfaces in the benthic chambers after retrieval: even bacterial mats, that are very likely to be blown off ground by the bow wave produced by a sinking lander, were intact.

Preliminary results

An overview of the different benthic habitats sampled with the benthic chamber landers (BCL) is given in Table 17.

Table 17: Chamber lander deployments during SO143-2.

Site	Water depth	gear no	no of successful measurements
Western basin	2300 m	BCL 1, 5	4
Southern summit Reference	850 m	BCL 2	2
Bacterial mat	790 m	BCL 3, 7, 8, 10	6
Calyptogena field	790 m	BCL 3, 4, 7, 9	5
Acharax comm.	790 m	BCL 6	2

Initial oxygen concentrations at the beginning of the incubations were very low, ranging between 0-80 µmol O_2/l. Nevertheless, total oxygen consumption in the benthic chambers was high. Lowest uptake rates of 1 – 5mmol O_2 m^{-2} d^{-1} were encountered at 2300-m water depth in the western basin. At our main working area, the bacterial mats and clam fields of the southern summit, oxygen consumption was up to 20 times higher. The highest rates were measured in an incubation of a very dense Calyptogena-field (ca. 2500 Ind. m^{-2}, see Fig. 47)

The greatest variability of oxygen consumption was measured over the white-yellowish bacterial mats. In all cases gas hydrates were found in the sediment beneath bacterial mats and the degassing of hydrates in one case was so strong as to destroy the shutter mechanism of one chamber, resulting in a loss of the sediment sample.
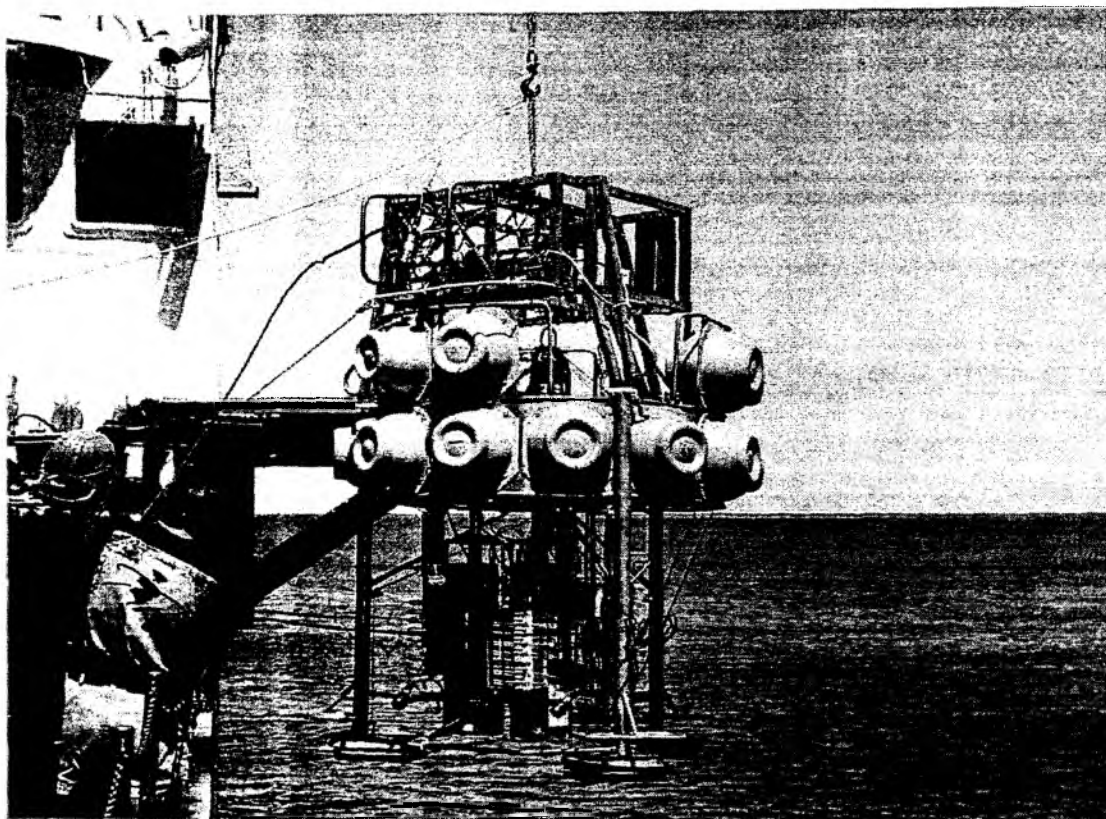
Fig. 46: Deployment of benthic chamber lander. The launcher is
mounted on top of the flotation package.

Fig. 47: Calyptogena field inside benthic after retrieval of gear
(BCL 3, chamber 2).

The variation of total oxygen consumption (TOU) can be related to strong fluctuations of the oxygen content of the bottom water at the beginning of the in situ incubations, which varied from $0 - 30 \mu mol$ O_2 l^{-1}. Fluctuations of oxygen content were also encountered at sites colonised by Calyptogena, but the variation was far less pronounced and never resulted in oxygen-free bottom water as it was found above a bacterial mat in one incubation (BCL 10; chamber 2), Whether these fluctuations are a result of a very high oxygen consumption in combination with tidal variations of bottom current velocities, needs to be investigated. Observations of bottom currents during video-guided lander deployments indicate strong fluctuations between periods of very high bottom currents and almost stagnant periods, where the resuspension cloud created by the bottom contact of the ground weight was not transported away by the currents even within several minutes of observation.

Main aim of the measurements of suffocate reduction at the deep western basin station was to investigate the influence of pressure and decompression during sample retrieval on sulphate reduction rates. Samples from the in situ as well as the laboratory incubations will be analysed at MPI in Bremen.
First results indicate that even for the relatively shallow area on the southern summit in situ measurements seem to be of utmost importance especially where the sediments contain gas hydrates as the degassing of hydrates during core retrieval greatly influences sediment structure and gradients of pore water solutes.

3.9   Microbial ecology

A. Boetius

Aim of this study was the investigation of microbial activity at vented and non-vented sites at the Hydrate Ridge, the central working area of the TECFLUX program, and its surrounding basins.

Table 18: Station list, list of parameters investigated.

Station	Gear No.	Date	Depth (m)	Parameters	Sample Charact.
143/83	MC83-1	2.8.99	2300	EEA; Bac. Production; Bac. Numbers	W-Basin (deep)
143/91	MC91-1	3.8.99	850	EEA; Bac. Production; Bac. Numbers	SE-Basin
143/105	MC105-1	5.8.99	780	EEA; Bac. Production; Bac. Numbers;	Hydrate Ridge (bacteria mats)
143/105	MC105-2	5.8.99	780	Bac. Taxonomy	Hydrate Ridge (bacteria mats)
143/114	MC114-1	7.8.99	760	EEA; Bac. Production; Bac. Numbers; Bac. Taxonomy	Hydrate Ridge (bacteria mats and Calyptogena)
143/126	MC126-2	9.8.99	2890	EEA; Bac. Production; Bac. Numbers	W-Basin (deep)
143/127	MC127-1	9.8.99	2300	SRR; S-Isotopes	W-Basin (deep)
143/131	MC131-1	10.8.99	780	EEA; Bac. Production; Bac. Numbers	Hydrate Ridge (Calyptogena)
143/135	MC135-2	11.08.99	785	Bac. Taxonomy	Hydrate Ridge (Calyptogena)
143/139	MC139-1	12.8.99	830	EEA; Bac. Production; Bac. Numbers; Bac. Taxonomy; SRR	SE-Basin
143/151	MC151-2	13.8.99	1280	EEA; Bac. Production; Bac. Numbers	E-Basin (deep)
143/157	BCL157-1	14.8.99	785	SRR (ex situ)	Hydrate Ridge (bacteria mats and Calyptogena)
143/173	MC173-1	16.08.99	785	SRR; S-Isotopes Bac. Numbers; Bac. Taxonomy	Hydrate Ridge (bacteria mats and Calyptogena)
143/179	MC179-3	17.08.99	785	EEA; Bac. Production; Bac. Numbers	Hydrate Ridge (Calyptogena)
143/185	MC185-1	18.08.99	785	SRR; S-Isotopes Bac. Numbers; Bac Taxonomy	Hydrate Ridge (Calyptogena)
143/187	MC187-1/4	18.8.99	785	EEA; Bac. Production; Bac. Numbers	Hydrate Ridge (bacteria mats)
143/190	MC190-1	19.8.99	825	EEA; Bac. Production; Bac. Numbers	Hydrate Ridge
143/193	MC193-1	20.8.99	685	EEA; Bac. Production; Bac. Numbers	SE-Basin

For the analysis of bacterial abundance, activity, and taxonomic characterisation, samples were obtained from a total of 17 multiple corers hauls and one benthic chamber lander deployment (Tab. 18). The upper 30cm of the sediment cores were split into the same intervals as the samples for benthic biology and biogeochemistry, i.e. cm-wise in the 0-10cm layer and 3cm-wise below. Samples for bacterial numbers, extracellular enzyme activity (EEA) and bacterial production were taken

from the same sediment samples as for benthic biology, by pooling sediment from 3 cores per haul. Sub-samples for sulphate reduction rate (SRR) were taken by inserting small cores into the sediment for the use of the whole core injection technique. The SRR samples as well as the samples for bacterial production, which were incubated with ^{3}H-labeled thymidine at *in situ* pressure and temperature will be analysed in the home laboratory. EEA of the hydrolytic enzymes α-, β-glucosidase, chitobiase, lipase, sulphatase, phosphatase, butyrase and leucine peptidase were determined on board at *in-situ* temperature. Abundance as well as the taxonomic classification of the bacteria will be determined by epifluorescence microscopy (in situ hybridisation) in the home laboratory.

The most obvious indication of vented sites at the Hydrate Ridge was the presence of white and orange bacterial mats covering the seafloor. The patches of bacterial mats sized from a few centimetres up to a few meters, the largest mats occurring within or close to the fields of Calyptogena, a mussel well known for its symbiosis with sulfur-oxidizing bacteria. When samples of bacterial mats were recovered with the multiple corers, a strong degassing of methane was observed, in contrast to cores from the same haul, which were not covered by bacteria. Below the bacterial mats, which extended from a few millimetres above the sediment surface to 1-2 cm below the surface, sediments were black and smelled strongly sulfidic. Oxygen was low or at detection limit in the bottom water, but high concentrations of nitrate was measured in the porewater of the top sediment layer. Most likely, these chemoautotrophic bacteria are able to store and use nitrate to oxidise the sulfides, as it was observed for other large, mat forming bacteria in upwelling areas (e.g. *Thioploca*).
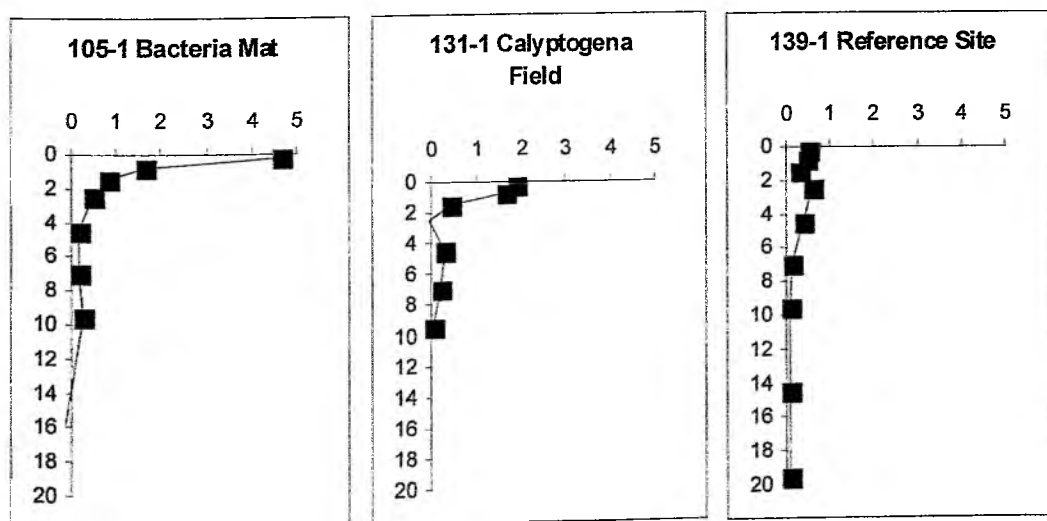
Fig. 48: Chitobiase activity ($\mu M\ h^{-1}$).

Since the formation of the mats at the Hydrate Ridge was so strongly linked to the occurrence of methane gas, a dependence of the mat forming bacteria on an yet unknown consortium of bacteria can be assumed, which oxidise methane with sulphate producing the large amounts of sulfide present in the vented areas of the Hydrate Ridge. Hence, we sampled these cores as well as the cores populated by Calyptogena in great detail, to analyse the relation between the distribution of nutrients, methane and sulfide and the distribution of bacteria. As reference sites, samples of non-vented parts of the Hydrate Ridge as well as of its surrounding basins were obtained. At all sites, microbial enzymatic hydrolysis, a measure of heterotrophic activity, was relatively high at all investigated stations from 680-2900 m water depth and comparable to upwelling areas in the Arabian Sea at similar water depths. The highest activities were always observed at sediment surface, in the samples of bacterial mats. Samples of Calyptogena Fields or the reference sites at the Hydrate Ridge were generally lower in activity (Fig. 48).

The analysis of the abundance and distribution of the sediment bacteria occurring below the mats will show whether this increased enzymatic activity at the vented sites is caused by the mat forming, chemoautotrophic bacteria or by other groups.

3.10   Coupling between benthic small-sized biota and methane gas seeps

O. Pfannkuche, S. Sommer, A. Kähler

Primary goal of the investigations was to identify a possible coupling between the small benthic size classes (Bacteria, Protozoa and Meiofauna) and seeping methane gas released from gas hydrates. This chemoautotrophic setting is compared with sites, which depend on ocean surface derived photoautotrophic produced carbon compounds.

Rationale

The presence of elevated concentrations of methane in marine sediments induces a series of different geochemical and bacterial processes. In surficial sediment horizons methane will be oxidised aerobically using oxygen as terminal electron acceptor. In deeper sediment layers, where no dissolved oxygen is available, methane will be oxidised anaerobically in consortia with sulphate reducing bacteria. As a final product of this process sulphide will accumulate in the porewater when the buffering capacity of the sediment is exceeded. This is the major process how sulphide is pumped into the sedimentary seep system. When sulphide diffuses along a concentration gradient to the surface of the sediment, it represents a source of electron donator for chemoautotrophic bacteria. The energy yielded by the oxidation of sulphide using either oxygen or nitrate as electron acceptor will be taken by the bacteria to sustain their metabolism and for the fixation of CO_2 in higher organic substrates. Thus organic loading of methane from beneath will create additional organic carbon sources in the sediment in excess to the organic matter which is received through the water column by sedimentation of particles. This organic carbon

source can be potentially used by benthic organisms and transferred through the benthic food web.

Approach

The investigations were concentrated to the southern summit of the Hydrate Ridge with water depth in the range of 750 - 900 m. Thus it is important to assess the signal of the primary productivity of the surface waters reaching the seafloor in contrast to the input of methane from beneath. Hence the concentrations of chlorophyll a (chl.a) and their vertical distribution in the sediment column, as well as pheopigment concentrations, which is a degradation product of chl.a, was measured.

Beside aerobic methane oxidation the input of methane induced organic carbon into the benthic food web is predominantly facilitated by chemoautotrophic processes. To estimate the relative proportion of these chemoautotrophic processes vertical distribution of CO_2 dark fixation in the sediment was measured using ^{14}C labelling. The exoenzymatic hydrolytic activity of bacteria, which represents a first step in organic matter degradation, was assessed using FDA analysis.

Biomass of the small benthic size classes was measured using total adenylates and DNA as representative bulk parameters. Size measurements of selected groups of the meiobenthos and their respective abundances will supplement the above biomass bulk parameters and allow to describe the effects of seeping methane gas on benthic communities at the level of higher taxonomic groups. A further high-resolution taxonomic analysis of the meiofaunal communities, particularly nematodes, enables the description of the input of methane on the distribution and diversity of functional groups.

Preliminary results

During Leg SO143-2 the southern Hydrate Ridge was sampled using a TV guided Multicorer (TV-MUC). This technique which was deployed for the first time allowed a precise sampling at the corresponding small-scale (dm-m scale) of the extremely heterogeneous investigation area.

The sampling stations were chosen in a way to obtain samples along a trophic gradient, which can be visually recognised by the epibenthic colonisation patterns of the sediments. Dense white bacterial mats are located at positions at which gas hydrates occur near the sediment surface layers. These mats are composed by thin, relative long tubular filaments, which might reach lengths of several millimetres. Striated appearance of these filaments is due to stacks of bacteria inside. A first macroscopical investigation showed that these mats are only poorly populated by meiofaunal organisms. This might be caused by the anoxic and highly sulphidic conditions in this environment and by the sediment texture. Another reason might lie in a shift in the food spectrum, induced by the chemoautotrophic bacteria, which cannot be exploited by the meiofaunal organisms.

Sediments next to the bacterial mats are characterised by dense populations of the bivalve *Calyptogena* sp. (densities of more than 1000 ind./m^2 were counted). More distal sediments did not show particular epibenthic colonisation patterns. However, preliminary results indicate that another bivalve *Acharax* sp., which harbours endosymbiotic, sulphide oxidising bacteria, is present in these sediments.

In order to compare this seep system to the natural background, further samples were taken in the western basin (TV-MUC 83-1 / 126-1), at the south-eastern slope of the Hydrate Ridge (TV-MUC 91-1 / 139 / 190-1), in the eastern basin (TV-MUC 151-2) and on the slope east of the Hydrate Ridge (TV-MUC 193-1).

The chl.a content in the uppermost 0-1cm layer of bacterial mats and sediments densely populated with clams is in contrast to the background depth gradient distinctively lower, Fig. 49. These relatively low chl.a concentrations in sediments affected by methane seepage might be due to two different processes. High-resolution vertical profiles of chl.a in bacterial mats showed an exponential decrease of the chl.a concentration in the uppermost 2-3 cm thick sediment layer, which indicates an active chl.a degradation. In contrast, vertical profiles of chl.a in sediments harbouring *Calyptogena sp.* and *Acharax sp.* indicate biological mixing of the upper 0-3cm layer of the sediment. In south-eastern slope sediments, further away from methane seepage, similar biological sediment mixing of the upper 0-3 cm of the sediment was found, which cannot be related to the presence of *Calyptogena sp.*. Since the chl.a inventories in the upper sediment horizons, colonised by *Calyptogena sp.*, are distinctively lower than in south-eastern slope sediments, further high chl.a degradation activity can be assumed in these sediments.

The plot shows: $y = 4{,}0782 - 1{,}0667e{-}3x$ $R^2 = 0{,}837$

y-axis: chlorophyll a [µg/ccm], x-axis: depth [m]

clam field / bacterial mat
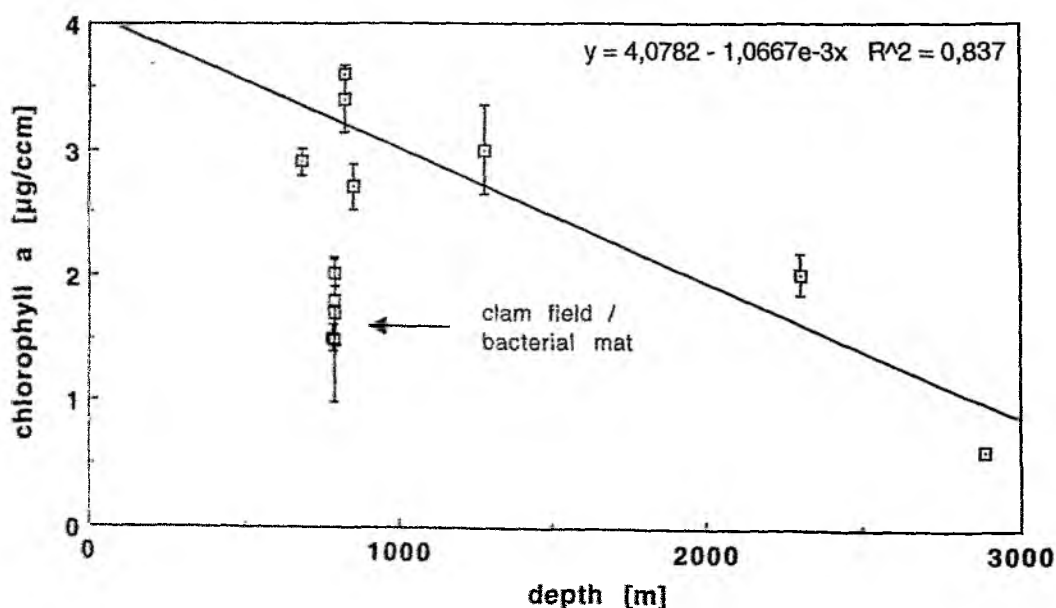
Fig 49: Depth gradient of chlorophyll a inventories integrated over the upper 0-1cm of the sediment. A cluster of chl.a inventories from clam fields and bacterial mat is indicated.

Hydrolytic activity (FDA analysis) of bacteria at the different sites showed high variability, but was lower at deeper sites in the western and eastern basins. With respect to the activity in the uppermost sediment horizon, no distinct differences were detected between southeastern slope sediments, clam fields and bacterial mats, despite increased activities were expected in bacterial mats. One explanation for

these relatively low activities in bacterial mats is based on the assumption, that chemoautotrophic bacteria exude less hydrolytic exoenzymes, which are needed for the degradation of longer chain organic carbons. Thus the relatively low hydrolytic activities in bacterial mats are suggested to be due to the relative dominance of chemoautotrophic processes in the direct seep environment, and will return to background level with increasing distance to the methane seepage.

In contrast to clam fields and south-eastern slope sediments the vertical distribution of hydrolytical enzyme activity in the sediment was very steep in bacterial mats, whereas highest activities were found in the upper 2cm of the bacterial mat sediments. This corresponds well with the vertical chl.a profiles from these environments. Highest hydrolytical activity was found in sediments densely populated with _Calyptogena sp._ where the vertical distribution of hydrolytical activity was less steep than in bacterial mats and higher activities were also found in deeper sediment horizons.

These first results indicate that methane released from gas hydrates induces alterations of transportation rates and degradation rates of organic matter by the benthic communities. The seep system appeared as a complex system with a vertical and horizontal shift in the relative dominance from chemoautotrophic to heterotrophic processes with increasing distance to the seep. For a more conclusive assessment of the spatial distribution and the magnitude of benthic exchange rates the analyses of the remaining parameters have to be awaited.

3.11   Macrofauna at Hydrate Ridge

H. Sahling

Introduction
The biological investigations started during Leg SO143-1b were continued (compare Chapter 2.8). During Leg SO143-2 emphasis was put on quantification of abundance and biomass of macrofauna in relation to gas hydrate occurrence and fluid seepage. The influence of seepage on the macrofauna distribution is thought to occur on different spatial scales. Within the area of fluid venting, chemical factors may influence faunal composition on a meter scale. In the surrounding areas without venting chemoautotrophically produced carbon may be exported and this enhanced food supply causes enhanced heterotrophic activity on a tens to hundreds meter scale. However, fluid venting at Hydrate Ridge may influence the macrofauna over the whole area of the second ridge. Quantitative samples were therefore taken within the area of seepage in combination with the porewater analysis, along a transect across the seep area on a hundred meter scale, and on a ridge scale by comparing the ridge fauna with the fauna at the adjacent basins.

Methods
Quantitativ samples were taken by boxcorer, multicorer and from the benthic chamber landers (BCL). Visual observations were collected with OFOS (compare Chapter 2.4). Three beam-trawls were deployed to collect specimens for taxonomic identification and re-identification on videos and photos. The trawl was towed with a speed around 1.5-2 knots for about 30-60 min on the seafloor.

Boxcorer and multicorer were equipped with video cameras to enable exact positioning on target areas. The entire sediment from the boxcorer (0.25 m^2) was sieved quantitatively through 0.5 mm sieves in the depth interval 0-2, 2-5, 5-10, 10-20 cm, a quarter of the box core was also sieved through 0.25 mm for meiofaunal studies. The residue was preserved in 10 % buffered formaldehyde. Less than the entire sediment content was sieved when sediment texture made sieving impracticable. Sediment from multicorer (10 cm diameter, 0.00785 m^2) were sliced in intervals 0-1, 1-2, 2-5, 5-10, 10-20 and sieved through 0.5 mm. Macrofauna was immediately extracted by hand and sorted. Sediment from the benthic chamber landers (0.04 m^2) was sieved through 0.5 mm as a whole. All animals were preserved adequately in 10 % buffered formaldehyd, 70 % Ethanol or by freezing at −20°C.

Results

Beam-trawl
All three beam trawls were successfully deployed. Trawl 103 was deployed in the western basin at around 2300 m water depth. Although the cod end was torn around the beam a representative set of specimens were collected. Trawl 116 was towed along the eastern flank of Hydrate Ridge, trawl 171 covered the western flank.

Interaction between macrofauna and porewater chemistry (TV-MUC 204 and 206)
With four multi corer deployments simultaneous estimates of macrofauna abundance and porewater characteristic were made to confirm observed distribution patterns. From selected cores sliced for macrofauna abundance subsamples for porewater analysis were taken out of the interval 1-2, 3-4, 9-10, and 19-20 cm. 1/2- 2/3 of the sediment horizon was needed for the squeezing procedure. The multi corer was equipped with only four cores to enable deepest sediment penetration.

TV-MUC 204-1 sampled with three cores an elongated bacterial mat, one core was empty and, as no gradient was visible between the cores no porewater was squeezed. TV-MUC 206-1 took samples only few tens of centimeters away from bacterial mats and contained 3 specimens of *Acharax* sp., this finding confirmed the occurrence of the *Acharax*-community (compare Chapter 2.8) in the direct vicinity of bacterial mats and Vesicomyid clams. Two cores were analysed for porewater. TV-MUC 206-2 was deployed on a small cluster with *Calyptogena* sp. (core H & F), 30 cm apart no vent indication was visible (core B & D). The cores without any chemoautotrophic organisms or any smell of sulphide were plugged by a clayish sediment in 15 cm depth. No porewater was analysed. TV-MUC 206-3 took samples close to a bacterial mat, in an area with Vesicomyid clams of different densities. All four cores were analysed for pore water.

Quantification of macrofaunal biomass in relation to fluid seepage
Samples for macrofauna species composition and biomass were taken along two profiles on different spatial scale. Within the area of fluid seepage TV-guided box corer (TV-GKG 140, 161) and benthic chamber landers (BCL 108, 119, 138, 157, 180) were taken and species composition and biomass will be estimated on shore. To compare the macrofauna standing stock box core samples were taken in a distance of 500, 800, and 1200 m (GKG 169, 170, 177) to the north of the main fluid venting area at the southern Hydrate Ridge and 500 and 800 m to the SE (GKG 113, 102). The same SE to N profiles were covered by OFOS profiles to estimate megafauna abundance. To compare the macrofauna on Hydrate Ridge background

samples of areas without any indication for fluid venting were taken at the continental slope at a similar water depth (GKG 193-2) and in the western basin at depths around 2300 m (GKG 92, 95).

TV-G at the BSR-outcrop

Beside Hydrate Ridge, NW-Knoll, and the first accretionary ridge many indications for fluid seepage were observed (compare Chapter 3.4) in the BSR-outcrop area. TV-G 167 was deployed recovering observed chemoautotrophic organisms to compare the faunal composition with studied venting sites. The seafloor in this area is covered by carbonates and is therefore only accessible with the TV-G. Many Vesicomyid clams were recovered together with bone-shaped carbonates. Two porewater and methane samples were taken in deeper sediment layers within the grab.

Discussion

It is obvious that fluid venting is a widespread phenomenon in the Oregon Subduction Zone. Indication for active venting was collected at the first accretionary ridge, the NW-knoll, the BSR-outcrop, and Hydrate Ridge. Chemoautotrophic organisms were not only found at areas with gas hydrate occurrence. The seepage of reduced chemical compounds lead to an enhanced standing stock of organisms based on chemoautotrophically fixed carbon.

3.12 Pore water and fluid chemistry of VESP, benthic chamber landers and CTD water samples

D. Rickert, A. Heuser, K. Getzlaff

3.12.1 Introduction

The objectives of the geochemistry program during Leg SO143-2 was to continue the investigations of the previous expeditions (ATLANTIS, SO143-1a and SO143-1b) and to combine pore water and biological investigations.

The data will provide more information about the mechanisms and consequences of hydrate formation and decomposition at actively venting sites and the complex interplay of biological activity and pore water chemistry.

Besides an extensive pore water chemistry program of sediment samples taken with TV-guided multicorers, samples of the overlying water column especially the fluid chemistry of the near bottom water were investigated with CTD/rosette sampler, vent sampler VESP (Linke et al., 1994; Chapter 3.5), and benthic chamber landers (BCL) (Chapter 3.8).The landers equipped with syringe water samplers were deployed for the measurement of respiration and pore water fluxes at the sediment-water interface. In order to obtain water samples and in situ flow rates from cold seeps the TV-controlled device for the deployment of a benthic barrel was developed in which sequentially water samples are collected by Niskin bottles mounted inside the chamber (VESP I; Linke et al., 1994; Chapter 3.5). VESP II was developed to overcome the permanent cable connection of VESP I which limits the deployment time (Cremer, 1995). VESP II is equipped with a syringe water sampler or/and two Niskin bottles inside and outside the chamber to gain long-term measurements of both direct water flow and samples expelled for active sites.

A more detailed description of deployment and preliminary results of VESP operations are given in Chapter 3.5 , those of benthic chamber landers are given in Chapter 3.8.

3.12.2 Samples and analytical methods

Pore water

Pore water was separated from the sediment by squeezing devices as described in Chapter 2.7. The pH, alkalinity and sulfide concentrations were determined almost immediately after collecting the pore water samples in order to avoid artificial results due to degassing of H_2S during long-time storage.

Table. 19: Techniques used for pore water analysis. For modifications see cruise report SO143-1b.

Constituent	Method	Reference
Alkalinity	Titration	Ivanenkov and Lyakhin (1978)
pH	2-point titration	Dickson (1993)
Ammonium	spectrophotometry	Grasshoff et al. (1983)
Calcium	EDTA titration	Gieskes et al. (1991)
Magnesium	EGTA titration	Gieskes et al. (1991)
Phosphate	autoanalyser	Grasshoff et al. (1983)
Silicate	spectrophotometer	Grasshoff et al. (1983)
Nitrate	autoanalyser	Grasshoff et al. (1983)
Chloride	Mohr ($AgNO_3$)titration	Gieskes et al (1991)
Hydrogen sulphide	spectrophotometry	Grasshoff et al. (1983)

Table 20a: Types of analyses performed on pore water.

ANALYSIS STATION	PO$_4$ [µM]	NO$_2$ [µM]	NO$_3$ [µM]	NH$_4$ [µM]	H$_2$S [mM]	Cl [mM]	TA [mM]	O$_2$ [µM]	pH pore-water	core depth [cm]	Numb. of sampl.
Hydrate Ridge											
Southern summit											
91-2A TV-MUC	x			x	x	x	x	x	x	27	17
105-2F+G TV-MUCs	x	x	x	x	x	x	x	x	x	22/20 ,5	15/15
114-1A TV-MUC	x	x	x	x	x	x	x	x	x	20,5	16
135-1B+F TV-MUCs			x	x	x	x	x	x	x	32,5/ 23,5	20/16
135-2B+F+H TV-MUCs	x	x	x	x	x	x	x	x	x	27/25 /25	18/17/1 6
173-1B+H TV-MUCs	x			x	x	x	x	x	x	21/23 ,5	16/17
185-1F TV-MUC	x			x	x	x	x	x	x	22	15
206-1B+F TV-MUCs	x			x	x	x	x	x	x	28/27	4/5
206-2B+D+F+H TV-MUCs	x	x	x	x	x	x	x	x	x	25/24 /28/2 5	4/4/4/4
Reference sites											
i) BSR-outcrop											
167-1 TVG	x	x	x	x	x	x	x	x	x	--	2
ii) Eastern basin											
151-2B MUC	x	x	x	x		x	x	x	x	44	22
iii) Western basin											
83-1F, 2A MUC	x	x	x	x		x	x	x	x	37	20
iv) Deep Sea											
126-2B TV-MUC	x	x	x	x	x	x	x	x	x	36,5	21
v) Continental Slope											
193-1E TV-MUC	x	x	x	x		x	x	x	x	50	23
									total of samples :		311

for most MUCs oxygen of bottomwater was measured (titration)
TA, Cl, = titration; PO$_4$, NO$_2$, NO$_3$, NH$_4$ = autoanalyser; H$_2$S, SiO$_2$ = photospectrometer

Table 20b: Types of analysis performed on CTD.

ANALYSIS STATION	PO$_4$ [µM]	NO$_2$ [µM]	NO$_3$ [µM]	NH$_4$ [µM]	H$_2$S [mM]	Cl [mM]	TA [mM]	SiO$_2$ [mM]	O$_2$ [µM]	water depth [m]	
I. Hydrate Ridge											
Southern summit											
97-1 & 99-1 CTDs	x	x	x	x	x	x	x	x	x	774	13
Northern summit											
86-1 CTD	x	x	x	x	x	x	x	x	x	602	11
II. Reference sites											
i) BSR-outcrop											
120-1 CTD	x	x	x	x	x	x	x	x	x	745	14
ii) Eastern basin											
145-1 CTD	x	x	x	x		x	x	x	x	904	18
iii) Western basin											
77-1 CTD	x	x	x	x		x	x	x	x	2650	10
									total of samples :		66

Table 20c: Types of analysis performed on VESP.

ANALYSIS STATION	PO$_4$ [µM]	NO$_2$ [µM]	NO$_3$ [µM]	NH$_4$ [µM]	H$_2$S [mM]	Cl [mM]	TA [mM]	SiO$_2$ [mM]	O$_2$ [µM]	water depth [m]	
I. Hydrate Ridge											
Southern summit											
118-1 VL-1	x	x	x	x		x	x	x	x	786	2
128-1 VL-2	x	x	x	x		x	x	x	x	785	1
131-3 VL-1	x	x	x	x		x	x	x	x	783	5
143-1 VL-2	x	x	x	x		x	x	x	x	787	1
150-1 VL-1	x	x	x	x		x	x	x	x	786	5
181-1 VL-1	x	x	x	x		x	x	x	x	788	2
191-1 VL-1	x	x	x	x		x	x	x	x	786	3
195-1 VL-2	x	x	x	x		x	x	x	x	?	7
198-1 VL-1	x	x	x	x		x	x	x	x	786	3
Northern summit											
76-1 VL-2	x	x	x	x		x	x	x	x	604	7
158-1 VL-1	x	x	x	x		x	x	x	x	605	5
										total of samples :	41

Table 20d: Types of analysis performed on benthic chambers (BC).

ANALYSIS STATION	PO$_4$ [µM]	NO$_2$ [µM]	NO$_3$ [µM]	NH$_4$ [µM]	H$_2$S [mM]	Cl [mM]	TA [mM]	SiO$_2$ [mM]	O$_2$ [µM]	water depth [m]	
I. Hydrate Ridge											
Southern summit											
101-1 BCL-2	x	x	x	x		x	x	x	x	858	12
117-1 BCL-3	x	x	x	x		x	x	x	x	796	12
122-1 BCL-4	x	x	x	x		x	x	x	x	787	9
144-1 BCL-6	x	x	x	x		x	x	x	x	787	10
164-1 BCL-7	x	x	x	x		x	x	x	x	784	14
178-1 BCL-8	x	x	x	x		x	x	x	x	790	12
184-1 BCL-9	x	x	x	x		x	x	x	x	795	9
196-1 BCL-10	x	x	x	x	x	x	x	x	x	786	14
II. Reference sites											
iii) Western basin											
98-2 BCL-1	x	x	x	x		x	x	x	x	2311	13
141-1 BCL-5	x	x	x	x		x	x	x	x	2307	14
										total of samples :	119

Subsequently, the pore waters were analyzed for silicate, phosphate, ammonia, nitrate, nitrite, and chloride. The analytical techniques used on board to determine the various dissolved constituents are listed in Table 19.

Acidified subsamples (10 µl HCl (30 %)/1 ml sample) were prepared for ICP analyses of major cations (Na, K, Li, Mg, Ca, Sr, and Mn). Sulphate, bromide, DIC and δ^{13}C will be determined on selected subsamples in the shore-based laboratory.

For further details concerning modifications of standard analytical methods due to high sulfide contents see Chapter 2.7.

A synopsis of cores, numbers of samples, subsampling, and geochemical analysis performed on board is listed in Table 2oa.

CTD, VESP and BCL samples
Water samples collected from CTD, VESP or BCL devices were partly filtered whenever sediment resuspension events visually contaminated the samples. Usually they were directly analyzed for nutrients, chloride and total alkalinity using standard analytical methods described above. A synopsis of water samples (CTD, VESP, BCL), numbers, subsampling, and geochemical analysis performed on board is listed in Tables 19b, 20c, and 20d.

3.12.3 Results and discussion
Here we concentrate on preliminary results and discussions of the distribution of nutrients, chloride and total alkalinity in the water column and the pore water. A more detailed description of VESP and BCL datas are given in Chapters 3.5 and 3.8 or can be requested from the authors. Results of all analyses performed on board are listed in the Appendix.

CTD water samples
A comparative diagram of nitrate, phosphate, silicate, chloride and total alkalinity of the CTD casts is given in Fig. 50a. In order to provide an overall, but sufficiently detailed characterization of the entire water column of an area of strong venting activity (southern and northern summit or CTD 97-1 and 99-1 and 86-1 respectively) in comparison to reference sites which showed no venting activity (BSR outcrop, Western and Eastern Basin or CTD 77-1, 120-1, and 145-1 respectively), the deepest part (100 m above seafloor) of the water column were sampled in high resolution whereas the remaining water samples were evenly distributed throughout the water column. For comparative reasons only water samples taken in the upper 1000 m water depth were considered for CTD-120-1, further results up to 2650 m are given in the Appendix.

Silicate shows low but measurable values of ~ 10 μM at the sea surface and increases to values of 110-120 μM in 700-800 m water depth. Nitrate and phosphate values represent an almost nutrient-free sea surface and increase to expected values for North Pacific bottom water (NO_3 ~ 43 μM, PO_4 ~ 3.1 μM). A comparison between nutrient values taken at on-vent or off-vent sites shows no significant deviation. This is not surprising since we did not measure methane anomalies in the water column during our CTD casts indicating that anomalies generated by gas and/or fluid flow from the summit sites are insignificant, restricted to a narrow zone or tidally induced. This is confirmed by comparison of chlorosity measurements between on-vent and off-vent sites which do not indicate venting activity during our deployments: chloride values between 600 and 800 m water depth determined at off-vent sites do not significantly range between 536 mM in western basin and 550 mM at the BSR outcrop location; on-vent sites both show values of ~ 543 mM (all measurements are standardized against IAPSO mean ocean sea water). Surface waters show reduced chlorosity values due to the influence of the Columbia river plume. It should be quite interesting to calculate the carbonate alkalinity since alkalinity values for Hydrate Ridge and BSR-outcrop location are surprisingly lower than for reference sites in the eastern and western basin.
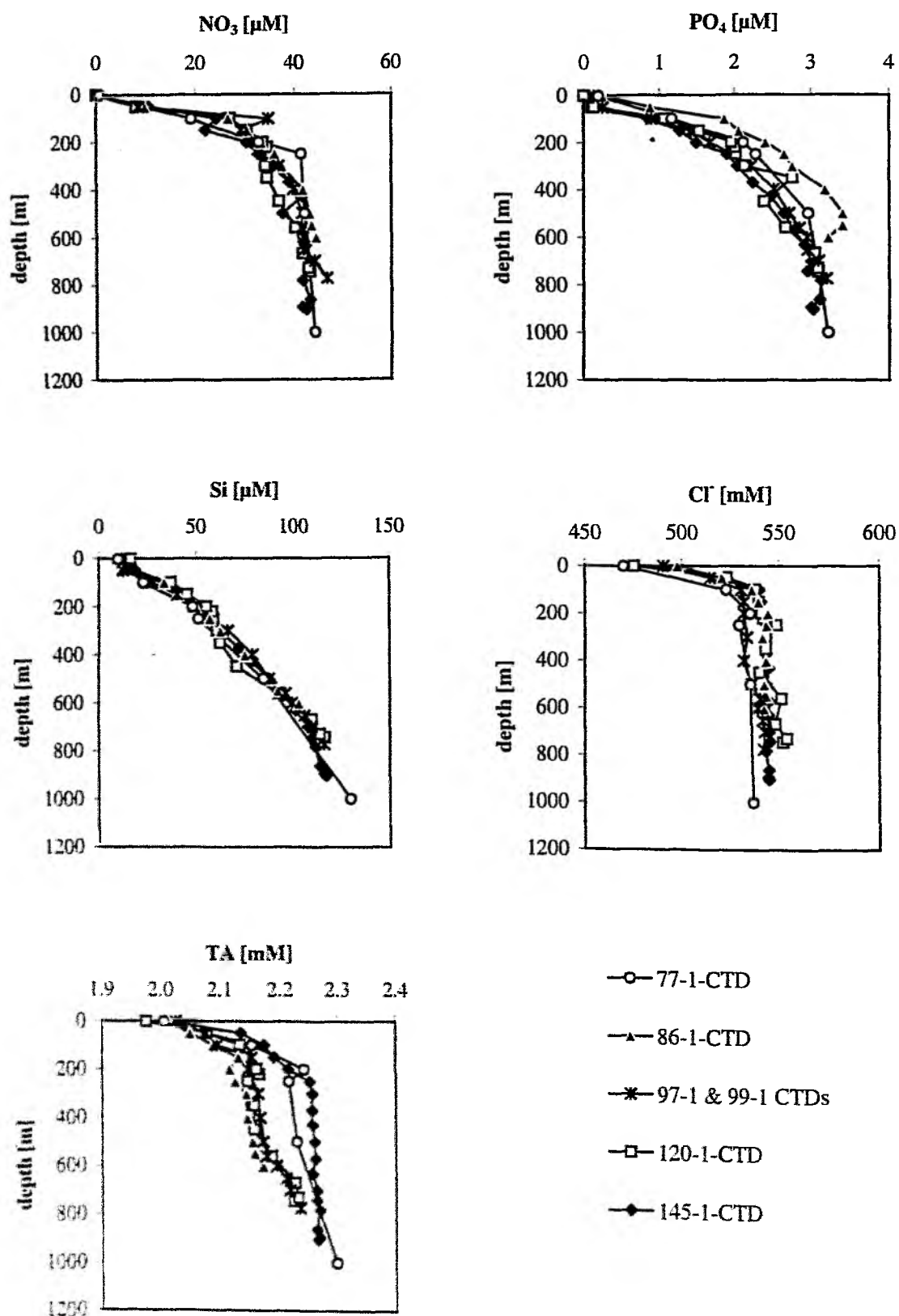
Fig. 50a: Nitrate, phosphate, silicate, chloride and total alkalinity of CTD Station 77-1, 86-1, 97-1 and 99-1, 120-1 and 145-1.
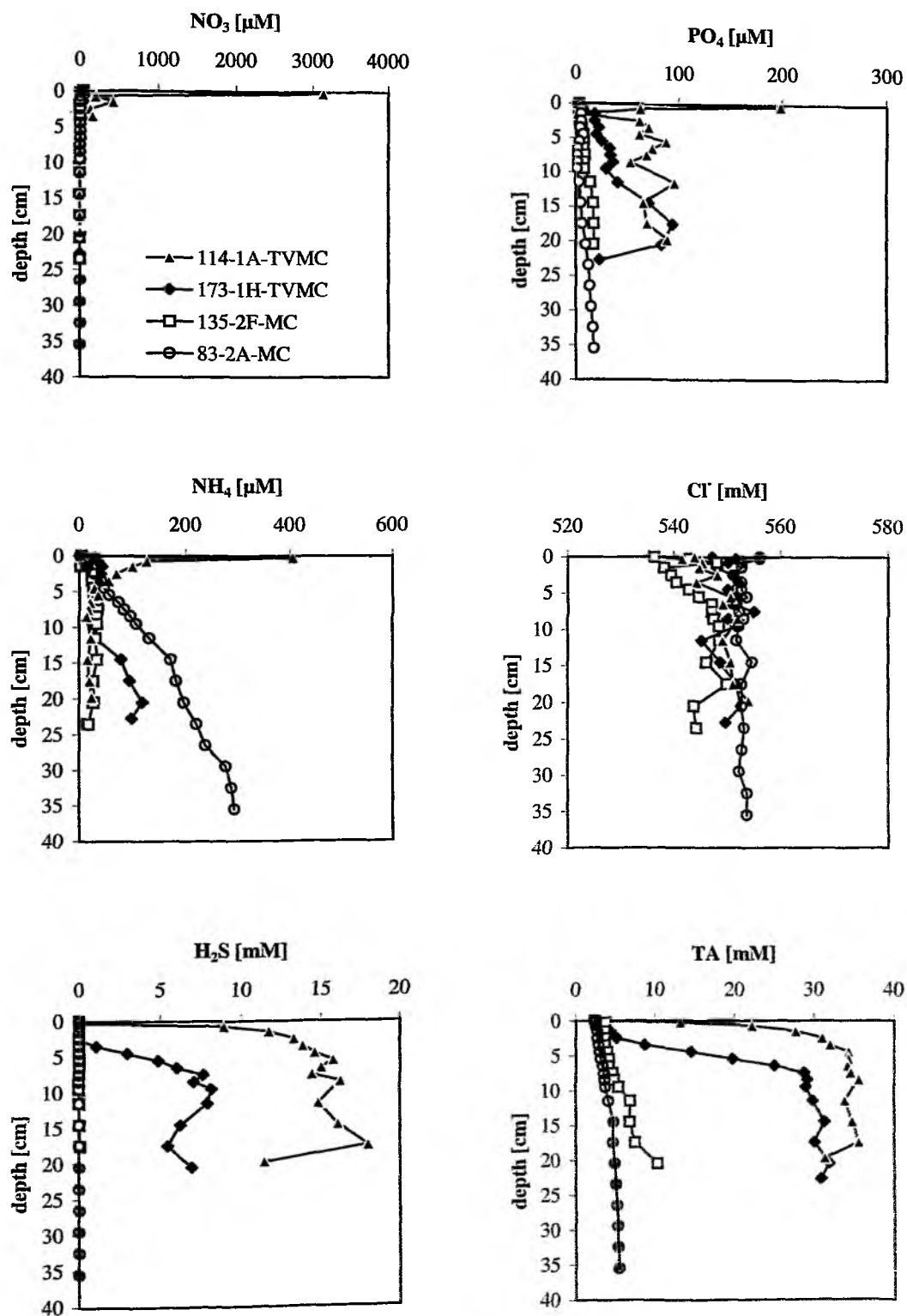
Fig. 50b: Pore water chemistry of 173-1H TV-MUC, 135-2F MUC and 114-1A TV-MUC.
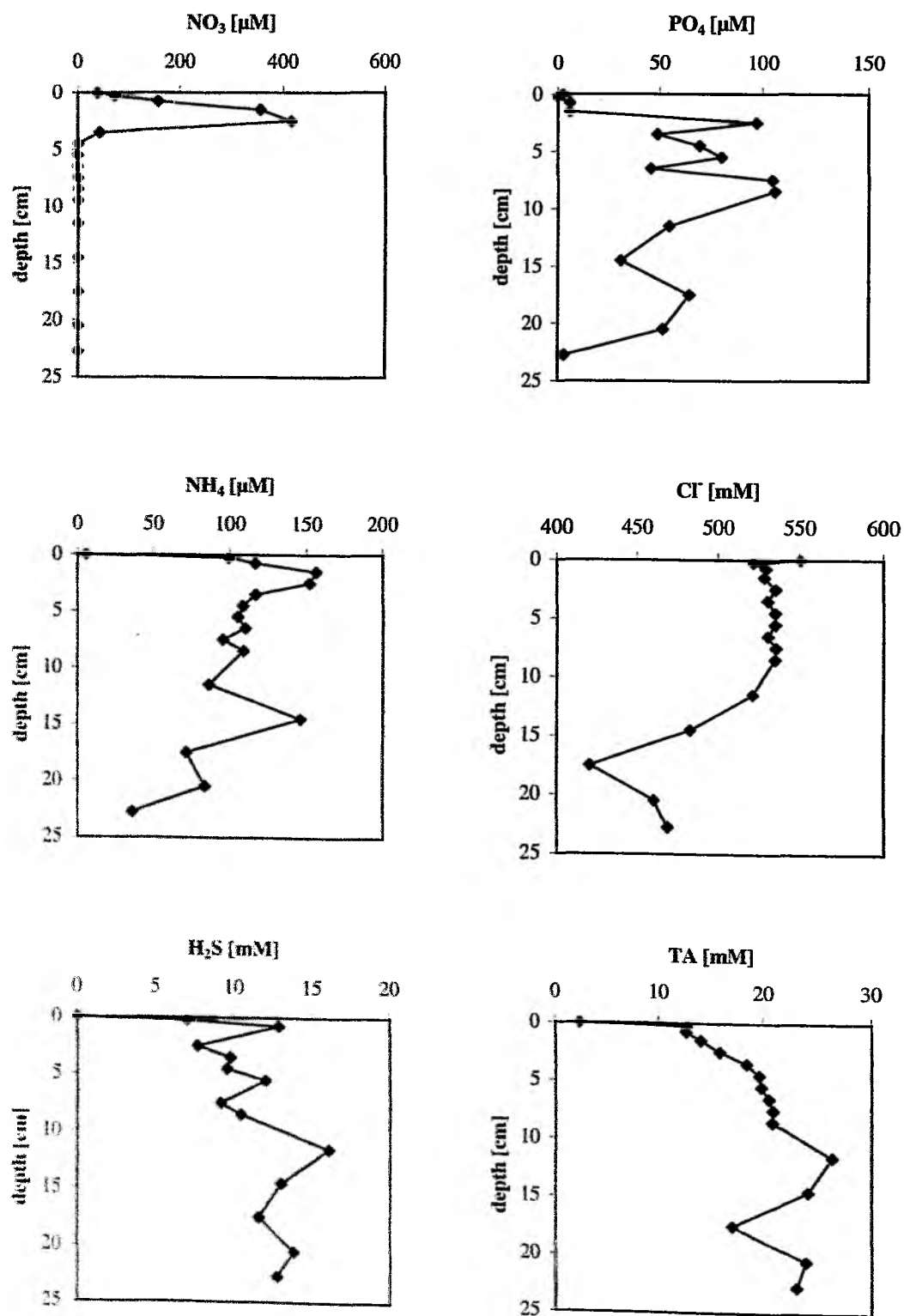
Fig. 50c: Pore water chemistry of 135-1F TV-MUC.

Pore water chemistry

Observation and sample collections with TV-guided multiple corers following the sampling strategy of the last cruise (SO143-1b) were used in order to monitor the pore water situation of an on-vent area with a full scale of biological phenomena which are associated with the occurence of pore water escape enriched in hydrogen sulphide and methane (for methane results see Chapter 3.12) in contrast to off-vent sites. In more detail pore water data were elevated which show striking differences depending on vent biota associated with the sampling site as reported for leg SO143-1b. Although fluid flow was not visually obvious and did not lead to anomalies in the overlying water column (see above) expression of sulfide-rich fluids was evident from authigenic precipitates (grayish white carbonate deposits), white and orange bacterial mats, clams (primarily *Calyptogena sp.* and *Accharax sp.*), and other seep-associated fauna (for a detailed biological characterization see Chapter 3.6). Four multiple cores recovered and analyzed for their pore water constituents were chosen to summarize the variability of pore water composition as a matter of different venting activity and/or associated vent biota (Fig. 50b).

As *already observed during the previous leg sulfide concentrations were low* (< 1 mM H_2S) within clam aggregations up to several centimetres (e.g. 3.5 cm in 173-1H-TVMC Figure 2), but considerably higher than in nearby sediments associated with *Acharax sp.* (135-2H-TVMC) where considerably smaller sulfide concentrations were detected below 15 cm depth or non-seep sediments from nearby reference sites (e.g. Western Basin 83-2A-MC), where sulfide was undetectable over the entire core length. In contrast, sediments with overlying bacterial mats start to become sulfidic almost from the top of the core (114-1A-TVMC) reaching values of 15-20 mM below 2.5 cm sediment depth. Consequently, TA shows the same principal pattern with especially high values (30-35 mM), where sediment depth exceed the penetration depth of overlain vent biota, i.e > 0.25 cm (bacterial mats), > 3-4 cm (*Calyptogena sp.*), >> 15 cm (*Acharax sp.*). Besides the geochemical characterization of the more or less vent-influenced pore waters this cruise was dominated by a detailed biological characterization of the pore waters (see Chapter 3.6) in order to better understand the relation between biological and chemical reactions associated with this venting area which is additionally influenced by the formation and decomposition of gas hydrates.

When samples with overlying bacterial mats were recovered, a strong degassing of methane from decomposing gas hydrates was observed creating stratigraphic disruptions and diluted pore waters through fresh hydrate water. Oxygen concentrations were low or at detection limit in the overlying water. Pore waters derived from squeezed sediments within the bacterial mats which extended from a few millimetres above the sediment surface to 1-2 cm below the surface gave anomalously high nitrate concentrations up to 3000-6000 µmol/l (e.g. 114-1A-TVMC in Fig. 50b). Phosphate and ammonia concentrations were also abnormally high especially in the first two sediment segments (0-1 cm) reflecting the bacterial density which is highest at the sediment-water interface. These bacteria are obviously able to store and use nitrate to oxidize the sulfide, as it was observed for other large, vent-forming bacteria (e.g. *Thioploca, Beggiatoa* or *Thiomargarita*) in upwelling areas (e.g. Gallardo, 1977; Jannasch et al., 1989; Jørgensen, 1977; Fossing et al., 1995; Schulz et al., 1999). The bacteria are able to commute between nitrate uptake from overlying seawater ($NO_3 \sim 40$ µM) and sulfide uptake within the sulfide reduction zone of the sediments resulting in a close coupling of the sulfur and nitrogen cycles.

In most of the upper centimetres (0-30 cm) of the sediments at on-vent sites pore waters were almost equal to CTD-chlorosity (~545-550 mM). However, 135-1F-TVMC (Fig. 50c) shows strikingly negative Cl-anomalies with a minimum of 420 mM at 17.5 cm. During recovery a strong degassing of methane was observed. Both of these effects could be explained by the presence and decomposition of gas hydrates which often underlay cores covered by bacterial mats. Again, the presence of bacteria is accompanied by nitrate anomalies within the first centimetres of the core, wheras H_2S values start to increase from the top of the core indicating highest sulfate reduction rates. H_2S reaches values between 10-15 mM with a sharp maximum at depth interval 10-13 cm. During gas hydrate formation salts are excluded and enriched in the surrounding pore water which was highlighted during the previous leg for pore water surrounded by almost undecomposed gas hydrates. During recovery of core 135-1F-TVMC this effect could be overcompensated by the decomposition of hydrates. Injection of hydrate water dilutes the pore water over the entire length of the core compared to CTD-chlorosity, especially at the intimate contact of hydrate and sediment at 17.5 cm. This dilution effect was measured in all kind of analyses performed on board.

3.13   Methane in sediment cores

K. Heeschen, H. Schäfer, M. Eek

Like during Leg SO143-1b methane concentrations were measured in several sediment cores giving us an even more detailed overview over sites at Southern Hydrate Ridge and its surroundings. While on SO143-1b sedimentological aspects and pore water measurements were the main goal, SO143-2 also provides a large set of biological parameters. This gives us the most interesting possibility to get an idea of how the biology influences methane distributions in areas of fluid venting and gas hydrate occurrence.

Method and sampling
Two different methods were used for measuring the methane content of sediment samples. For immediate methane measurements 3 ml of sediment were taken in syringes with the anterior ends cut off. The sediment was then extruded into 20-ml vials, and mixed with 5 ml of 1 M KOH to form a slurry and avoid biological activity. The vials were sealed with black rubber stoppers and immediately cramped tight (headspace analysis). In order to establish an equilibrium between the slurry and the gas phase the vials were shaken for 24 - 48 hours. 100 µl subsamples of the gas phase were taken off by gas tight syringes and detected with a gas chromatograph (Shimadzu), which was equipped with a flame ionization detector (FID). Recalculation from nl/ml sediment to nl/g or nmol/g sediment will be possible after the determination of physical properties on shore.

Another 150 g of sediment was taken and put into Zip-lock bags stored in liquid nitrogen for on shore degassing. Next to determine methane contents subsamples will be taken to measure the stable carbon isotopic ratio in CH_4 using a Gas Chromatography-Combustion-Isotope Ratio Mass Spectrometry (GC-IR-MS). Until measurement the gas is stored in gas-tight vials.

To minimise mixing within the liner only cores without visible degassing were used. The same criteria were applied for sampling the bottom water from the multicorer (MUC). The bottom water was sampled with the glass syringes which were also used for the water column sampling from the rosette sampler (for method see methane measurements on water samples). The water samples were taken before the cores were removed from the instrument to avoid mixing between sediment and water.

Table 21: Methane concentrations of sediments and bottom water were determined from the following multicorers.

Station no	Core no	Bottom water sample	Headspace analysis	Samples for isotopes
91-2	H	x	9	none
105-2	H	x	14	14
114-1	C	x	12	9
135-1	B		14	none
163-2	F	x	12	4
173-1	C	x	9	2
193-1	D	x	16	none

Preliminary results

With one exception all cores taken for methane measurements were recovered from the summit of Southern Hydrate Ridge, known for its abundance of gas hydrates, venting and biological communities of bacterial mats and the clam *Calyptogena* (see Chapter 3.11). Only one core (193-1) showed background concentrations with only a very small increase at greater depths (0.5 to 0.8 nmol CH_4/ml sediment).

Elevated values could be found in core 91-2 slightly SW of the summit of Southern Hydrate Ridge as well as in core 163-1 on top of Southern Hydrate Ridge. 91-2 had values of up to 18 nmol/ml with the strongest increase at 15 cm depth. No vent site communities were observed on top of the core. In core 163-1 the methane concentration reached up to 74 nmol/ml with strongest gradient at about 6 cm. The core showed a high degree of bioturbation, clams, and worms within the upper 4 cm. Compared to core 173-1, which was taken at about the same position the values are very low. Other than 163-1 core 173-1 was located within an area of bacterial mats and snails just nearby the clam site of 163-1 with abundant gas voids. Here methane concentrations were as high as 6000 nmol/ml in the upper centimetres. Within the core the CH_4 content decreased with depth. These cores show the highest variability for methane concentrations related to the biological community and gas hydrate occurrence even within very small distances. Other organisms than bacterial mats can reduce the concentration of H_2S and CH_4 by bioirrigation.

Cores 114-1 and 135-1 show similar profiles of methane distribution for the upper 10 cm. Both cores smelled strongly of H_2S and were highly populated by worms and the clam *Calyptogena*. The latter found as deep as 4 cm where the strongest increase in the methane concentration is observed. The similar profiles at 114-1 and 135-1 indicate the greater influence of the clams other than bacterial mats within core 114-1. Core 114-1 even has lower methane concentrations in the upper 10 cm compared to core 135-1.
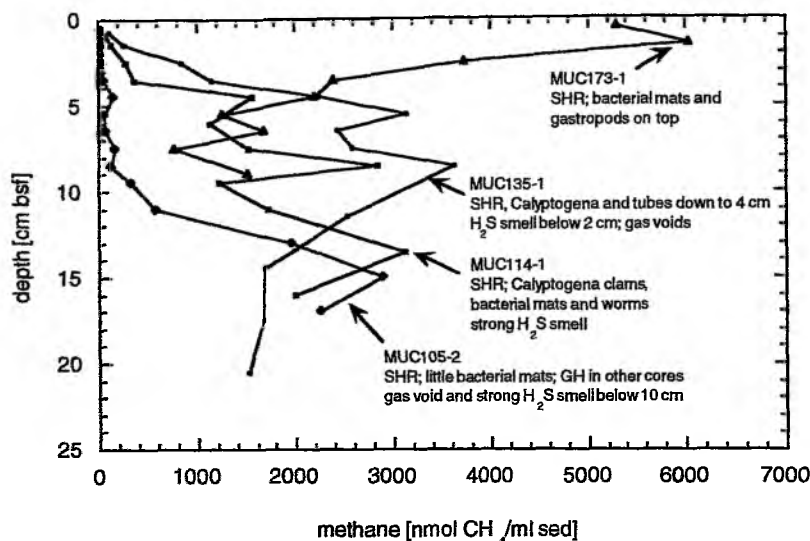
Fig. 51: Methane concentrations of several TV-MUC stations from southern summit of Hydrate Ridge.
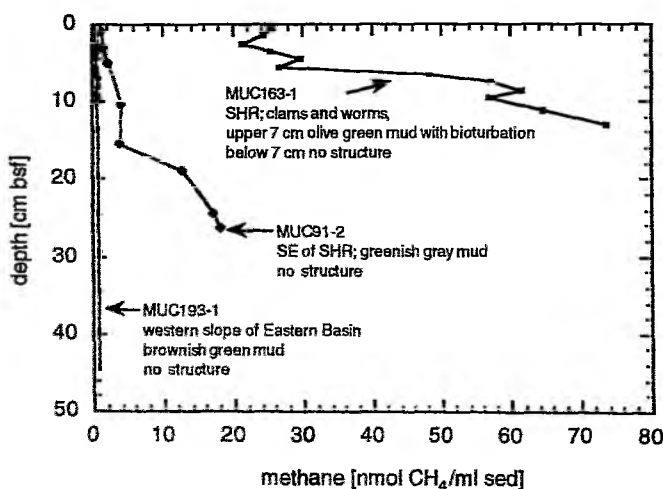
Fig. 52: Methane concentrations of several TV-MUC stations from northern summit of Hydrate Ridge.

Core 105-2 was taken in an area of bacterial mats on the south eastern summit of Southern Hydrate Ridge. Compared to other cores within comparable locations 105-2 shows clearly lower methane concentrations. Neither, the methane content nor H_2S increase strongly above 10 cm. They do rise below 10 cm where gas voids were abundant. Other cores from the same deployment contained gas hydrates between 10-14 cm. Comparisons with the isotopic ratios and with measured biological parameters might give an explanation for this unusual methane distribution.

Together with the water and sediment samples from SO 143-1b and SO 143-3 the data sets from SO143-2 provide a good basis to further understand the methane cycle throughout both the water column and the sediment, as well as their interrelationship.

4   Leg SO143-3: Astoria – San Diego (Aug. 26 – Sept. 6, 1999)

4.1   Cruise narrative

G. Bohrmann

RV SONNE departed the port of Astoria on 26 August and headed to the working area. SO134-3 was the last of four legs of the research vessel and the seventh of the TECFLUX cruises to the area of Hydrate Ridge off Oregon this year. The last TECFLUX cruise during 1999 was conducted by RV WECOMA during October. At the beginning of the cruise the scientists had to set up and/or to re-arrange the instrumentation. Before arriving at the area of investigation we analyzed an accretionary ridge, the so-called "R1 structure" (Trehu et al. 1999), where detailed research with the canadian ROV "ROPOS" is planned for next year. This accretionary ridge is very similar to Hydrate Ridge regarding the water depth and also other characteristics. The bathymetric mapping by Hydrosweep had already begun during the second cruise (SO143-2). We continued the survey on our leg and performed a first OFOS track crossing the structure from east to west. During the deployment we passed over the peak of "R1 structure" three times (Fig. 55). We obtained a very detailed visual observation profile of the sea floor. The western crest area consists of chemoherm carbonates; at the eastern flank the ridge is dominated by clam fields around active cold vents. As there were no peculiar bacteria fields at the sediment's surface we conducted no sampling.

The following days we accomplished sampling near the surface with the video-guided multicorer and TV-grab as well as sediment coring using the gravity corer in the area around the southern summit of Hydrate Ridge (Fig. 56). This was named the Beaver Mounds during RV ATLANTIS cruise 35b (Torres et al. 1999). All samples contained gas hydrates or traces of dissociated gas hydrates or their diagenetic products. Various gas hydrate structures could be analyzed and gas hydrate samples have been stored in liquid nitrogen. Detailed investigations in the laboratory will help to understand better the formation processes of gas hydrates.

The video-controlled multicorer sampling was impressive: selective branched, orange bacteria fields over massive gas hydrate deposits could be examined for biomarker analyses. The dissociation of the gas hydrates during the heaving in the water column shows the necessity of autoclave samplers. The autoclave piston corer was used on Sunday 29 August (Fig. 54). Due to a break of the piston rope at 5.7 tons of tensial we lost it unfortunately during this first operation. Afterwards, we again performed several OFOS investigations and Hydrosweep mapping.

During the second week of the cruise we continued with sampling at the southern Hydrate Ridge (Fig. 56). We were mostly interested in analyzing gas hydrates of the upper sediment layers to understand better their distribution, their association with carbonates and the geochemical signatures of their formation. The sampling of the upper 50 centimeters has been realized successfully with the video-grab (Fig. 58). During a grab operation the autoclave piston corer, which had gotten stuck in the sea floor, was found; the next day a salvage of the autoclave piston corer with a loop at the grab was not successful. After that we used the gravity corer more intensively. Due to the gas hydrate layers near the ocean bottom surface the gravity corer only penetrated up to 1.5 meters.
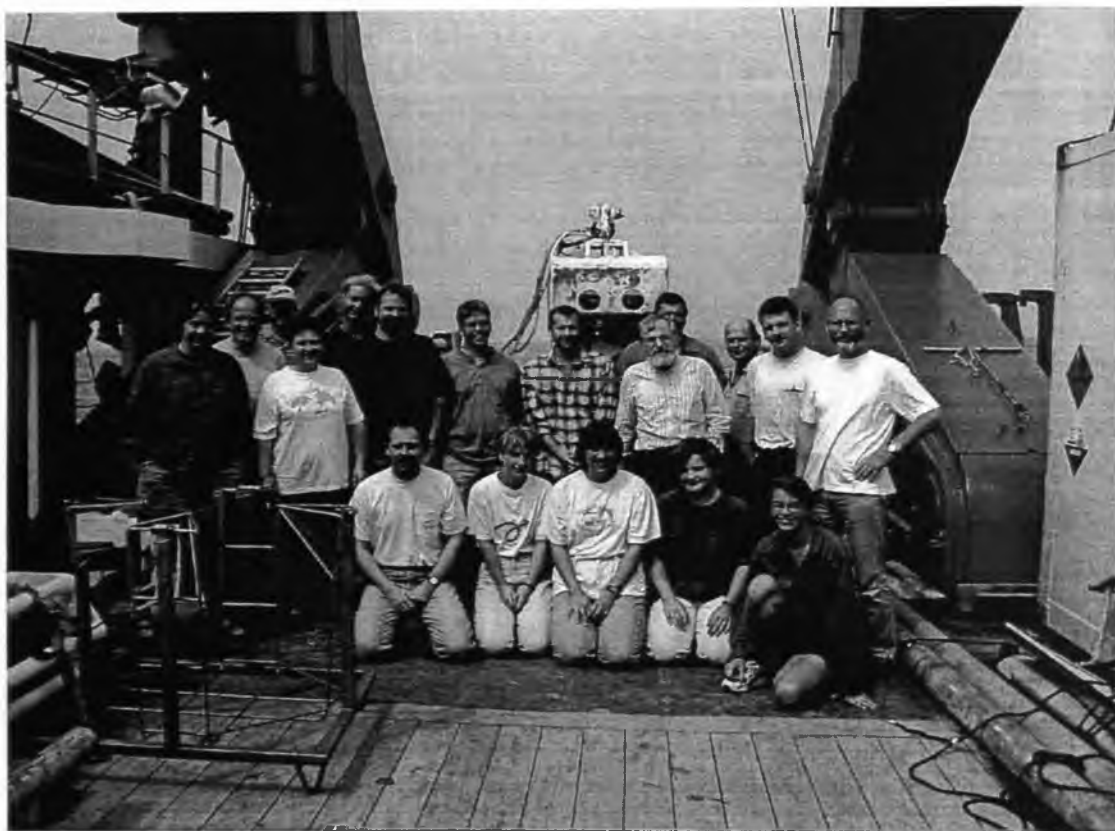
Fig. 53: Cruise participants during Leg SO143-3.
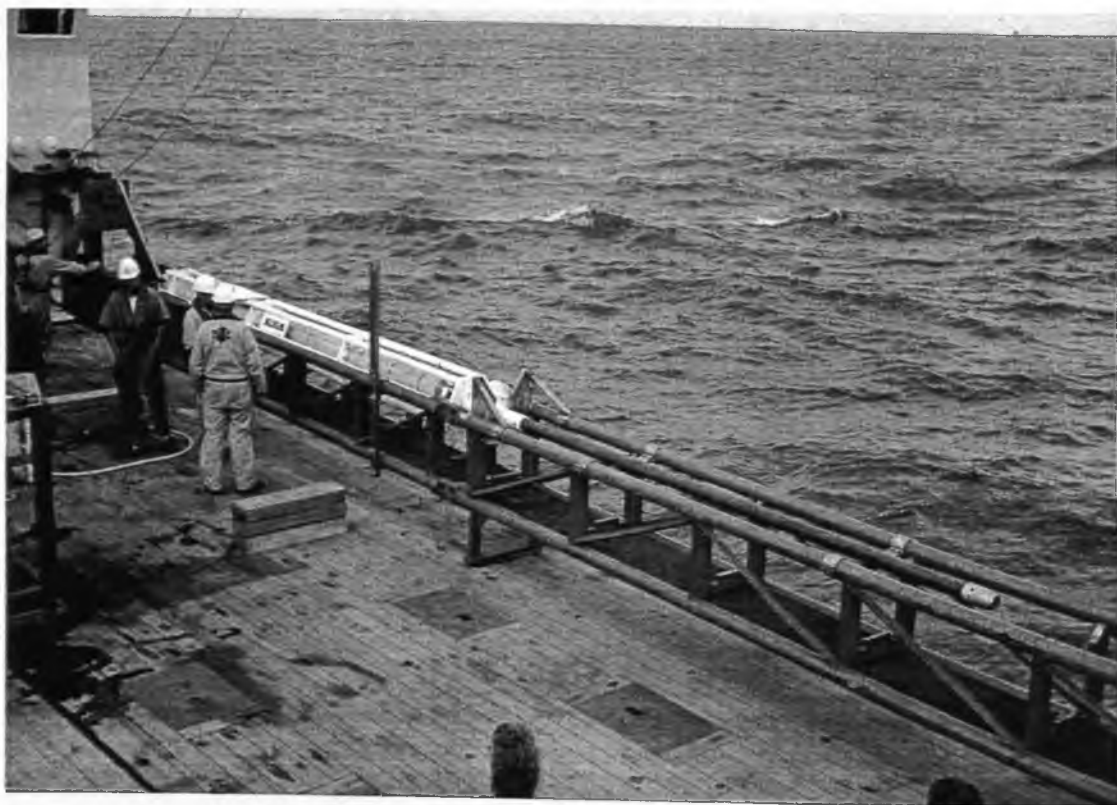
Fig. 54: The autoclave piston corer of BGR deployed during SO143-3.
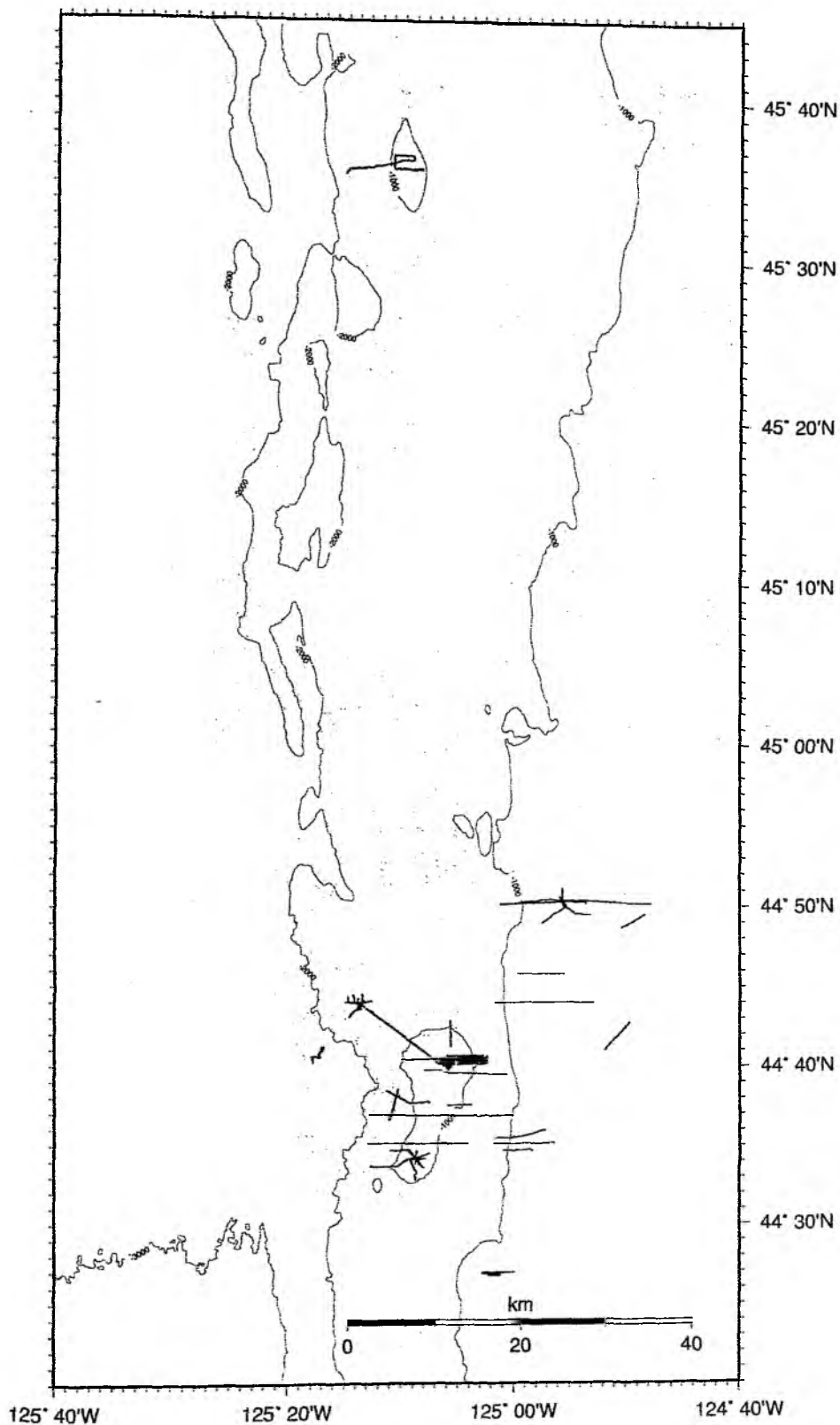
Fig. 55: Bathymetric map of the lower continental slope off Oregon. OFOS track in the north was conducted over the R1 structure. Navigation lines in the south show OFOS tracks in the area of Hydrate Ridge.
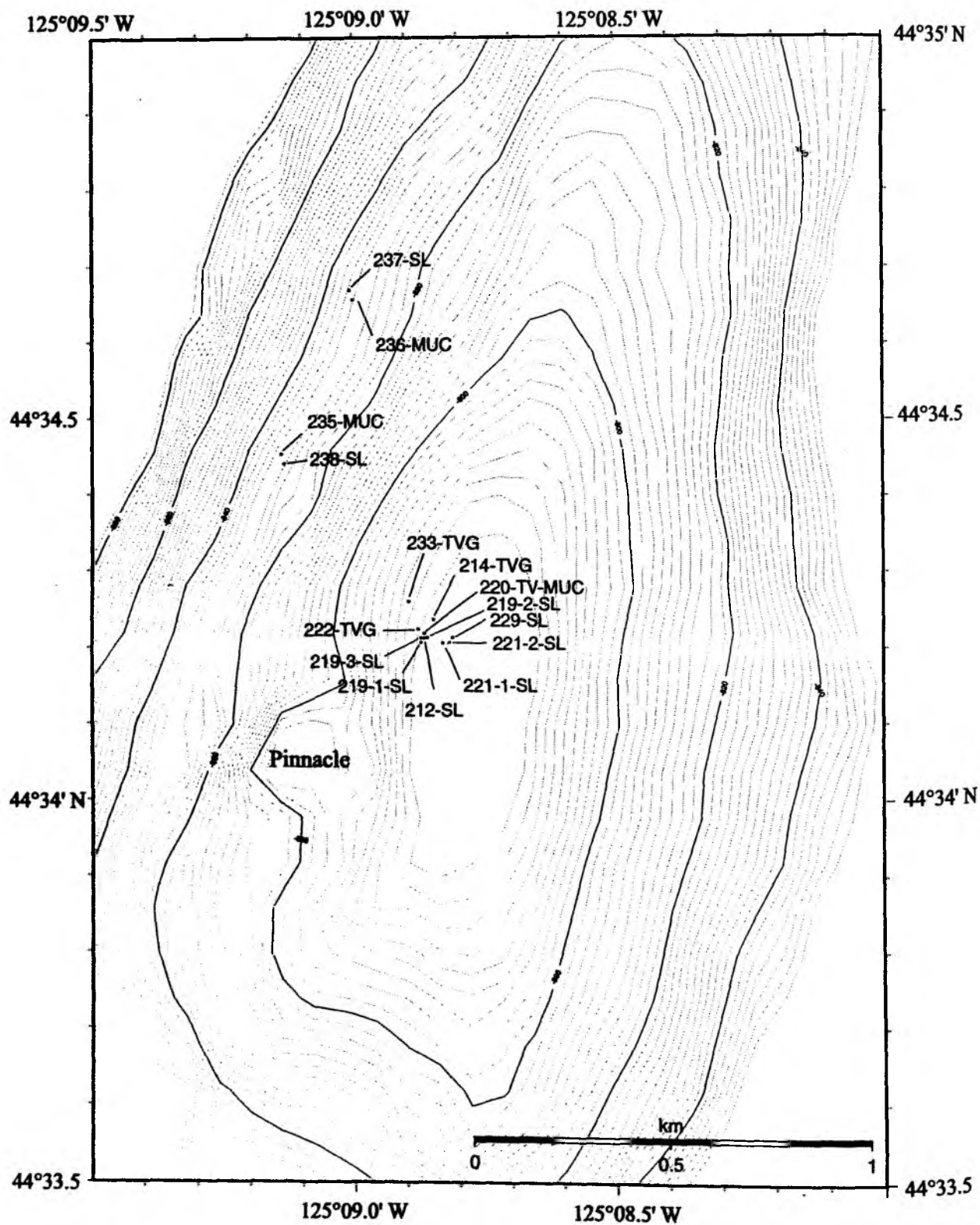
Fig. 56: Sample stations taken during SO143-3 at southern summit of Hydrate Ridge.

A core sequence of seven gravity cores at the southern Hydrate Ridge shows the high variety of the structures caused by the formation and decomposition of gas hydrates. In some of these cores we identified former gas hydrate layers with a very peculiar clastic structure.
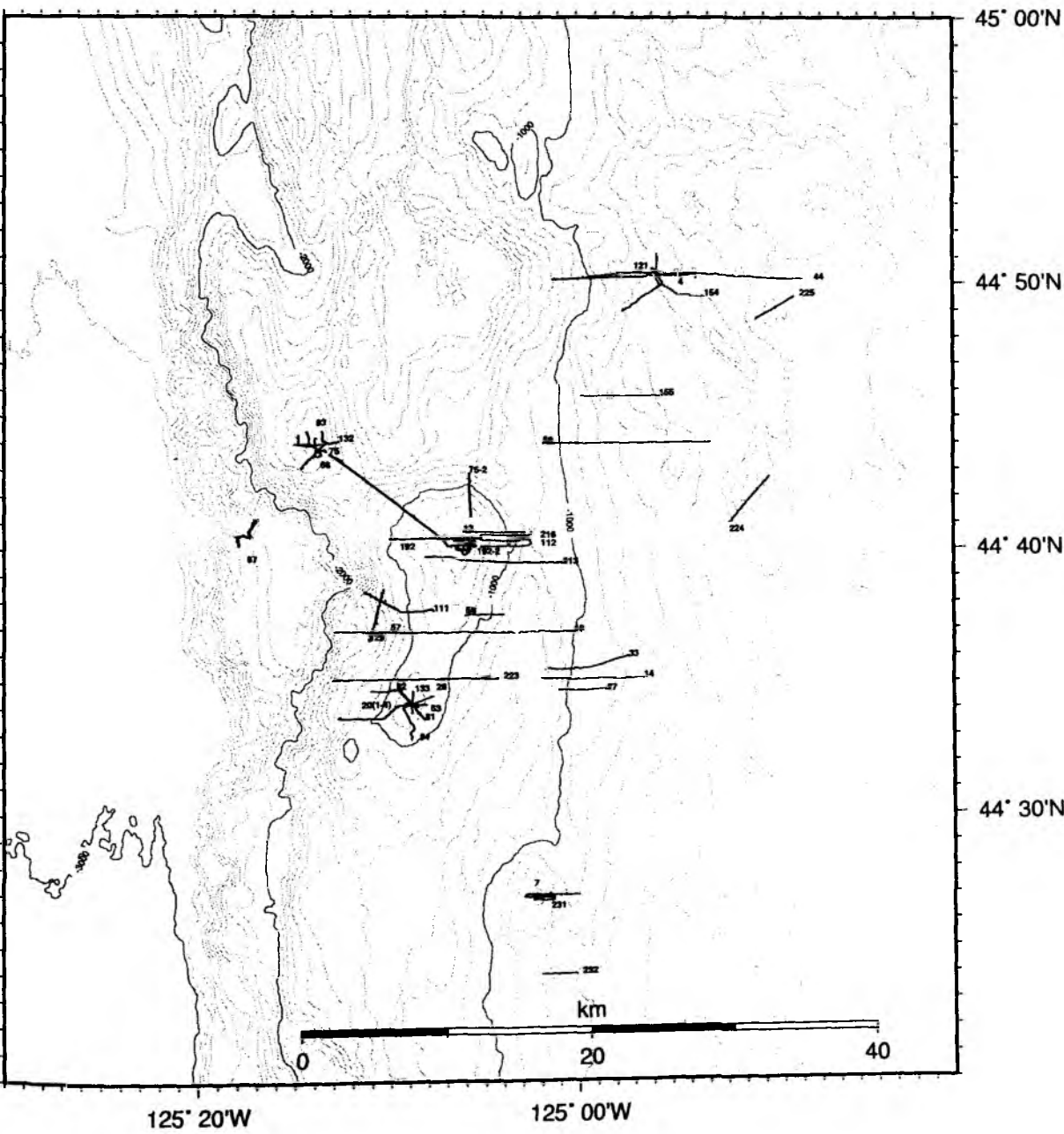
Fig. 57: OFOS tracks in the area of Hydrate Ridge recovered during SO143 legs.

Fig. 58: TV-grab deployment from A-frame on board of RV SONNE.

Fig. 59: "Flammable Ice" on board of RV SONNE. Flames are fed by methane which escaped from the decomposing gas hydrate.

Our work was also focussed on the mapping with Hydrosweep so that we now have a morphologically detailed map of the entire gas hydrate area at Hydrate Ridge. During this cruise the sediment echosounder "Parasound" worked on Parasound modus for detecting gas hydrates near the sea floor's surface. On previous TECFLUX expeditions the 18 kHz was mostly used for identifying escaping plumes of gas bubbles within the water column. Also the 4 kHz Parasound signal seems to identify gas bubbles in the water column, at least partially. This is shown in one of our profiles of the Daisy Bank's lateral fault, where particular reflexion patterns have been recorded in the water column above known vent locations at the sea floor.

Another important part of our work was the mapping of the seafloor using OFOS at selected cross sections. Along the seismic line 2, where three sites (Ocean Drilling Program) will be drilled during Ocean Drilling Program Leg 198 (01 August – 31 September, 2001), the detailed surface structures have been recorded (Fig. 57). Furthermore, sections at the seismic lines 7 and 9 have also been recorded with OFOS so that fluid expulsion sites, gas hydrates near the sediment's surface and the different carbonate types are registered and these will be compiled in a detailed map later on. This surface information will also be used for calibrating the backscatter image signal of the Side-Scan-Sonar survey in June this year, which will help to transfer the OFOS track informations to the area estimates.

Southeast of Hydrate Ridge, two OFOS profiles crossing over the so-called SE-knoll have surprisingly often documented massive chemoherm carbonates with some bacteria fields and marginal vent clams. This association at Hydrate Ridge always occurs together with gas hydrates in the sediment's surface, so that such gas hydrates are also expected at SE-knoll. Therefore this area is a potential investigation area for the ROPOS operations planned next year.

Expedition SO143 ended on 6 September in San Diego. We thank Captain Papenhagen and his crew for the very engaged and competent cooperation. During the whole cruise they were able to create best conditions for achieving our scientific successes.

4.2   Multibeam swathmapping

W. Weinrebe, C. Bartlett, and watchstanders

For continuous bathymetric profiling, the HYDROSWEEP multibeam system from STN ATLAS-ELEKTRONIK is available onboard the RV SONNE. Using a frequency of 15.5 kHz and 59 beams in a swath of 90°, it can map the seafloor with a scanline width up to twice the water depth. The range of the central beam is up to 10,000 m with an error of 1%, and for the outer beams is up to 7,000 m with a precision of about 1%. The precision requires that the roll is less than 10° and pitch less than 5°. Corrections for roll, pitch, and heave are automatically applied during data acquisition. Due to the fixed angle between beams, resolution is dependent upon the waterdepth, and varies from about 10 m in 200 m waterdepth to 200 m in depths of 5,000 m to 6,000 m.

Calculating depths from echo time delays requires using the velocity of sound in the different waterlayers. To determine an average water sound velocity profile HYDROSWEEP uses a second set of transducers and a calibration scheme with soundings along the track (Schreiber und Schencke, 1990). However, in certain areas this algorithm fails (Flueh and von Huene, 1994). Thus for better results, direct measurement of sound velocity at different depths using a CTD is required.

Postprocessing of HYDROSWEEP data comprises the merging of navigation data, the calculation of water depth and positions of the footprints of the beams, removing artifacts and erroneous datapoints, and generation of a digital terrain model (DGTM). The ATLAS HYDROMAP software, based on the CARIS software package, is available onboard for that purpose. However, for several reasons outlined in Flueh and von Huene (1994) and Weinrebe (1997), the academic software MB-System (Caress and Chayes, 1996) from Lamont-Doherty Earth Observatory were used onboard for HYDROSWEEP data processing.

A water sound velocity profile was measured with a CTD during Leg SO143-1 cruise at position 44°32.88' N and 125°23.41' W on July 8, 1999 (Fig. 6). Using this velocity function, raw HYDROSWEEP echo time data were converted to depth by complete ray tracing through the different water layers. Sweeps including all 59 beams were then displayed in profile on a screen and edited to eliminate erratic points. Edited sweeps were then assembled, gridded, and contoured with the GMT software (Wessel and Smith, 1991). No filters were applied to smooth the edited data for better resolution of the smaller tectonic features, but this allows more noise to be visible on the maps. However, the viewer can easily distinguish between small tectonic features and map artifacts in the unfiltered maps.

Several Hydrosweep profiles were planned and surveyed to supplement the bathymetric mappings of leg 1 and leg 2 of SO143 cruise (Fig. 60). Thus the area surveyed during SO109 (Herzig, 1996) and SO110 (Suess et al., 1996) was considerably extended. The profiles for leg 3 of SO143 were carefully planned to optimize the available time for mapping during the nights between station work. Water depths in the region vary between 200 m and more than 2,000 m, with the most

interesting areas located in water depths of 500 m to 700 m. In such depths the across-track spacing of adjacent beams of the Hydrosweep swath is around 20 m. The ping-rate of the Hydrosweep is also dependent on depth, therefore the speed of the ship during the surveys was kept to 8 knots allowing for similar (along-track) ping spacing.

We achieved a nearly complete Hydrosweep coverage of the Hydrate Ridge area between 44°24' N and 45°00' N, 125°25' W and 124°44' W (Fig. 61). Additionally, we mapped the „R1"-area between 45°28' N and 45°42' N, 125°20' W and 125°05' W (Fig. 63), which is named R1 as it is a future target for a ROPOS investigation. Due to favorable weather conditions, data quality was generally good. However, during several periods of leg 1 and leg 2, the gyro, required to correct for the ship's attitude (roll, pitch, and heave), failed to work properly. This resulted in many strong distortions oriented along-track of the digital terrain model (Figs. 61 and 62). The malfunctioning gyro was replaced during leg 2, diminishing the artifacts, however several tracks in the map are strongly affected nonetheless. As the offsets of roll, pitch, and heave values are not constant, these artifacts cannot be filtered out by postprocessing. We decided rather than disregard these recordings and prepare a map with a lot of white spots, but to produce a map with complete coverage, as the artifacts can easily identified as such in the maps and images.

R1 area

A detailed map of the northern R1 region highlights north-south trending ridges (Fig. 63). The highest of these ridges is a large football shaped hill along the eastern side of the map, which shallows to about 640 m below sea leavel. A perspective plot (Fig. 64) of these ridges shows the striking relief between the ridges and adjacent valleys and the slope heading west to the abyssal plain. Of note are incipient slumps and scars along the western edges of these ridges.

Hydrate Ridge

A detailed map for the Hydrate Ridge region comprising the combined Hydrosweep datasets of the SONNE cruises 109, 110, 143-1, 143-2, 143-3 is shown in Fig. 61. A perspective plot of the same area is given in Fig. 65. Though affected by several bad tracks due to the gyro failure, the general morphology of the area is clearly demonstrated. As the central part around the Hydrate Ridge has been presented in detail in Suess et al. (1996), this discussion is restricted to the northern and southern portions respectively.

Hydrate Ridge area, northern part

The area north of Hydrate Ridge is dominated by generally north-south trending ridges (Fig. 60). Differences in the morphology north and south of 44°52' N are obvious. To the north, a gentle sloping accretionary ridge is found, whereas in the south it has
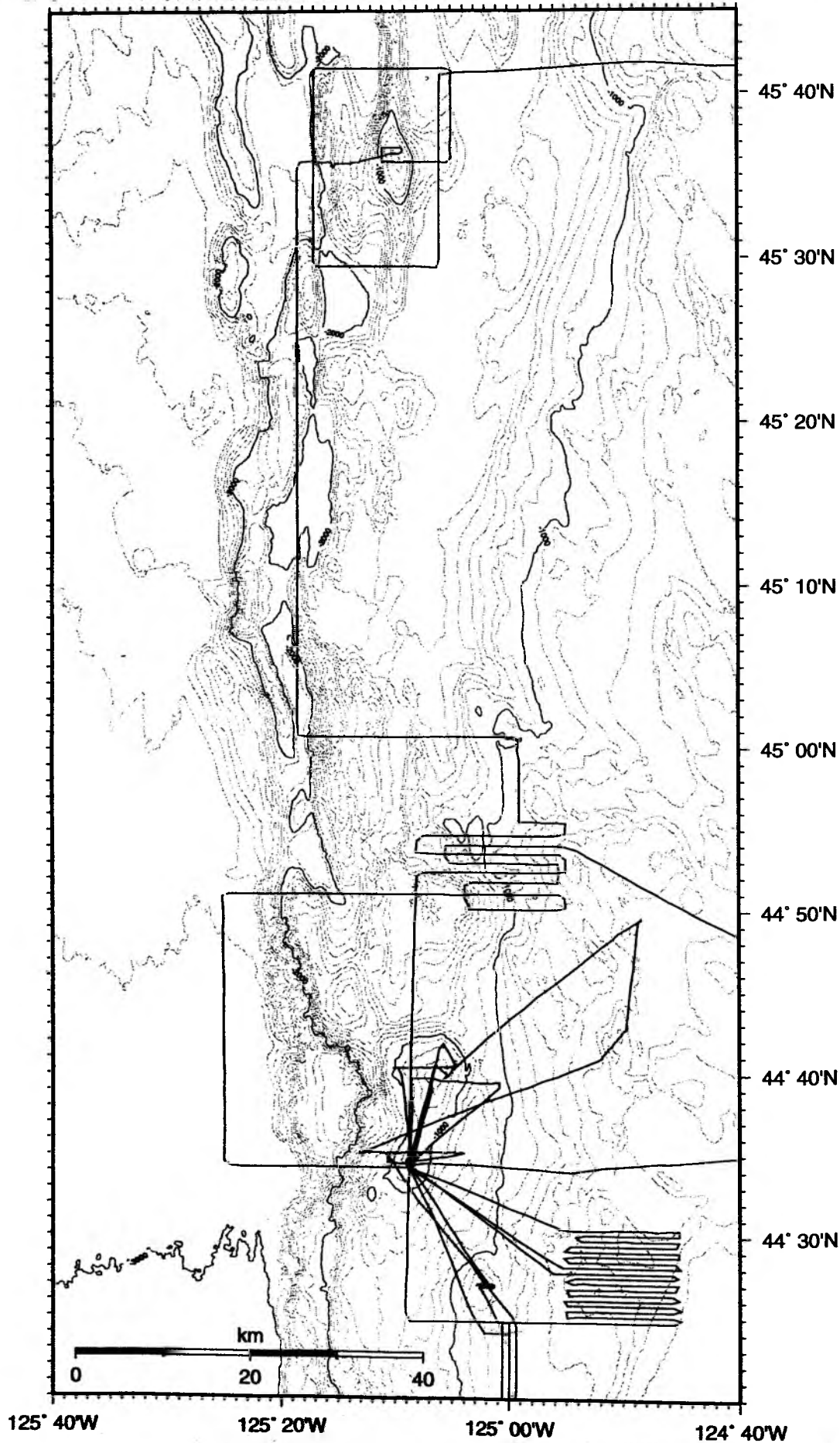
Fig. 60: Total cruise track of SO143 leg 3 with hydrosweep profiles (bold) and hydrosweep profiles of leg 1 and 2 (d   t d)
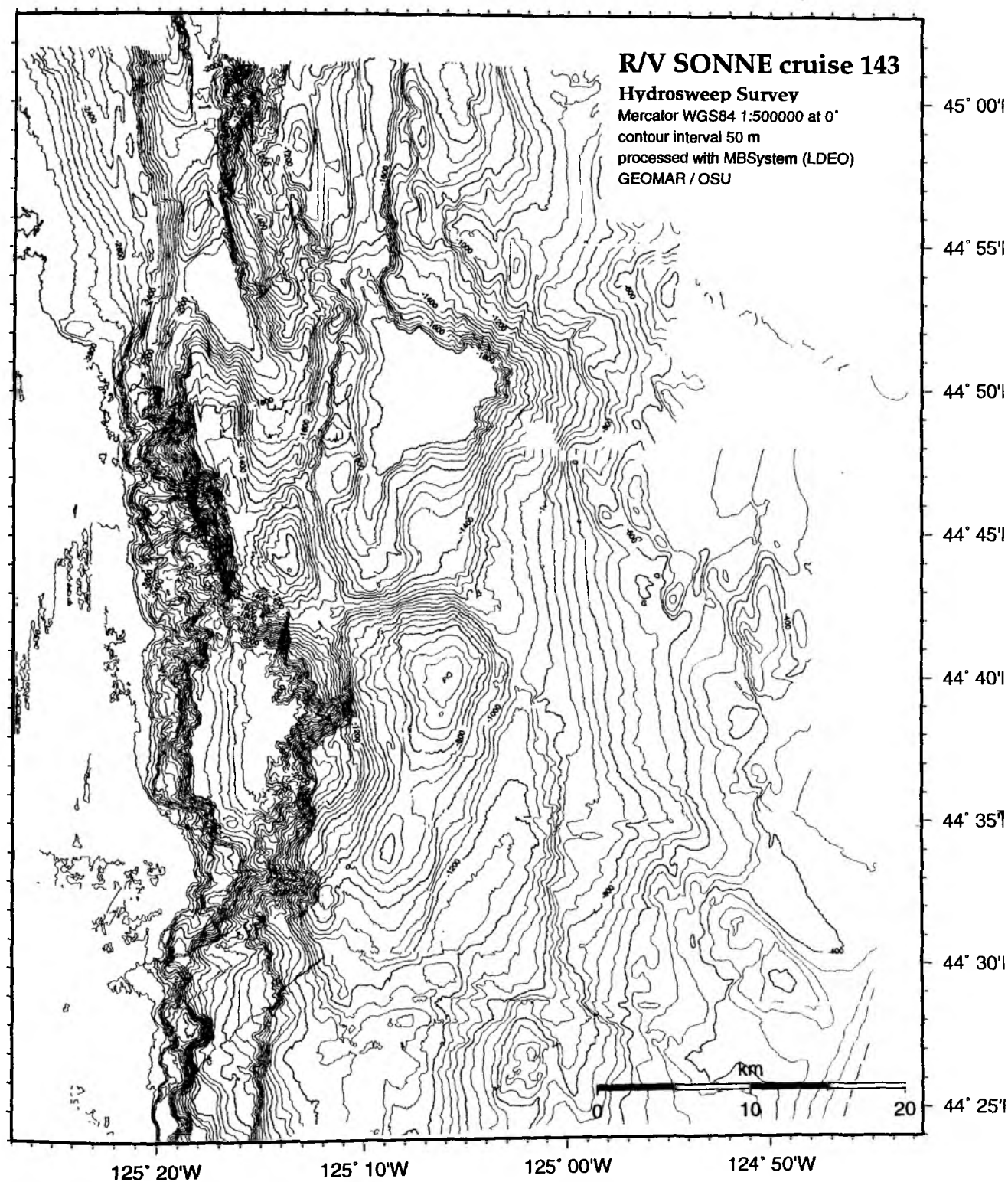
Fig. 61: Contour map of Hydrate Ridge area, based on SO109, SO110, and SO143 hydrosweep surveys.
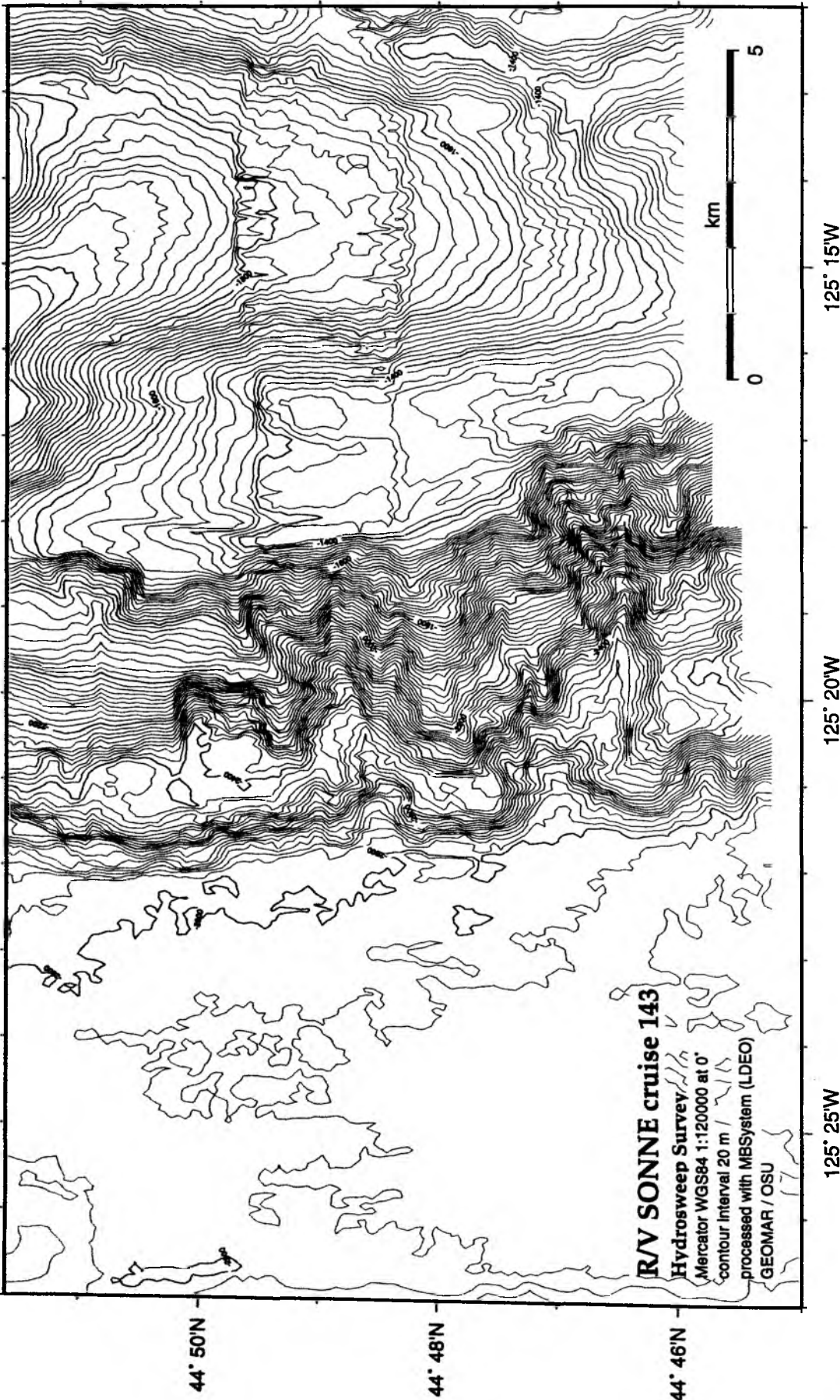
Fig. 62: Enlargement of an area of Fig. 61, showing strong distortions of the digital terrain model oriented along-track due to the gyro failure.

The map contains the following labels:

R/V SONNE cruise 143

Hydrosweep Survey
Mercator WGS84 1:200000 at 0
contour interval 20 m
processed with MBSystem (LDEO)
GEOMAR

km
0   2   4
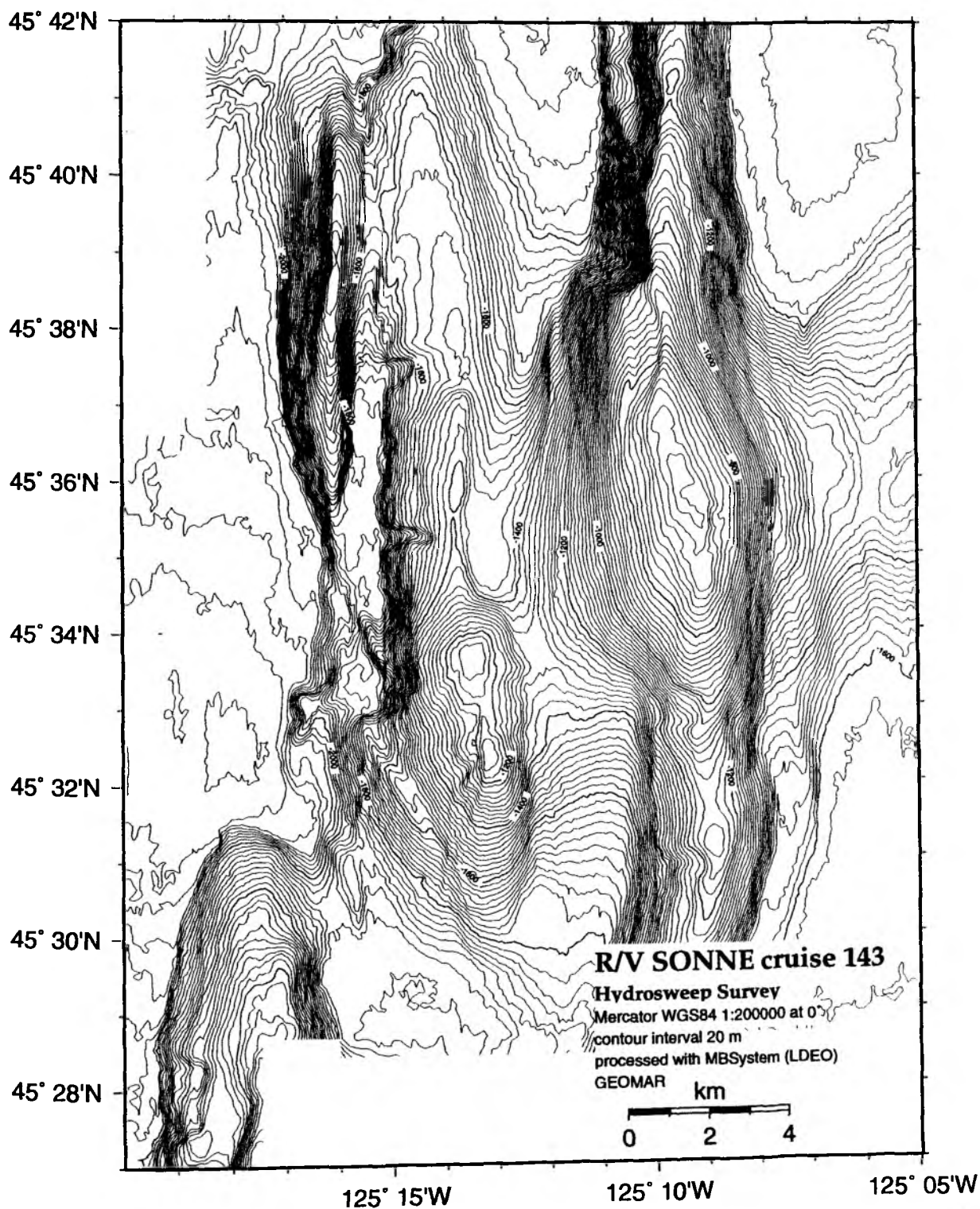
Fig. 63: Contour map of R1 area north of Hydrate Ridge, based on SO143 hydrosweep surveys.

Fig. 64: Perspective image of R1 area. View from southwest, illumination from the east.

Fig. 65: Perspective image of Hydrate Ridge area.
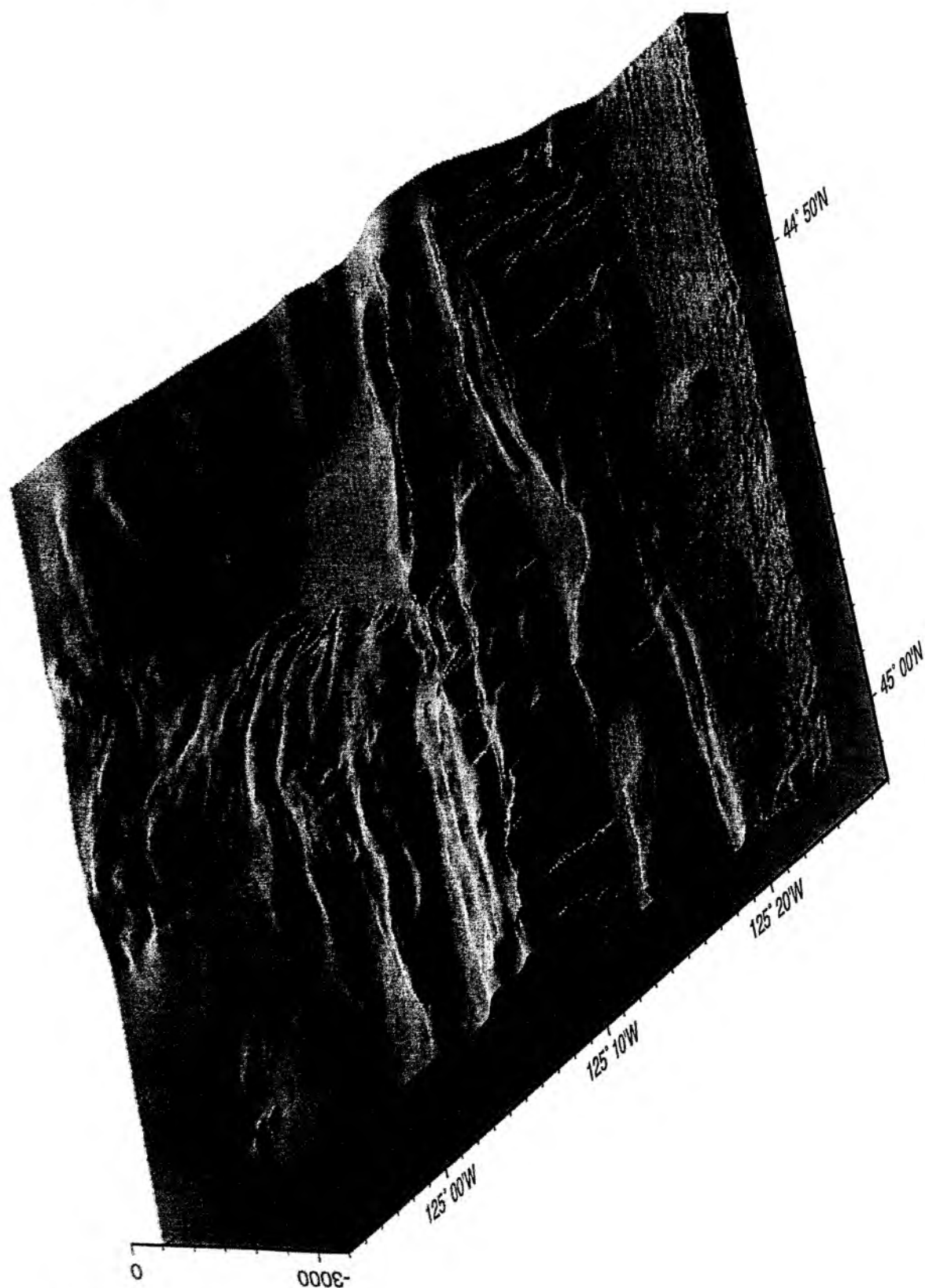
Fig. 66: Perspective image of northern Hydrate Ridge area. View from west, illumination from south.
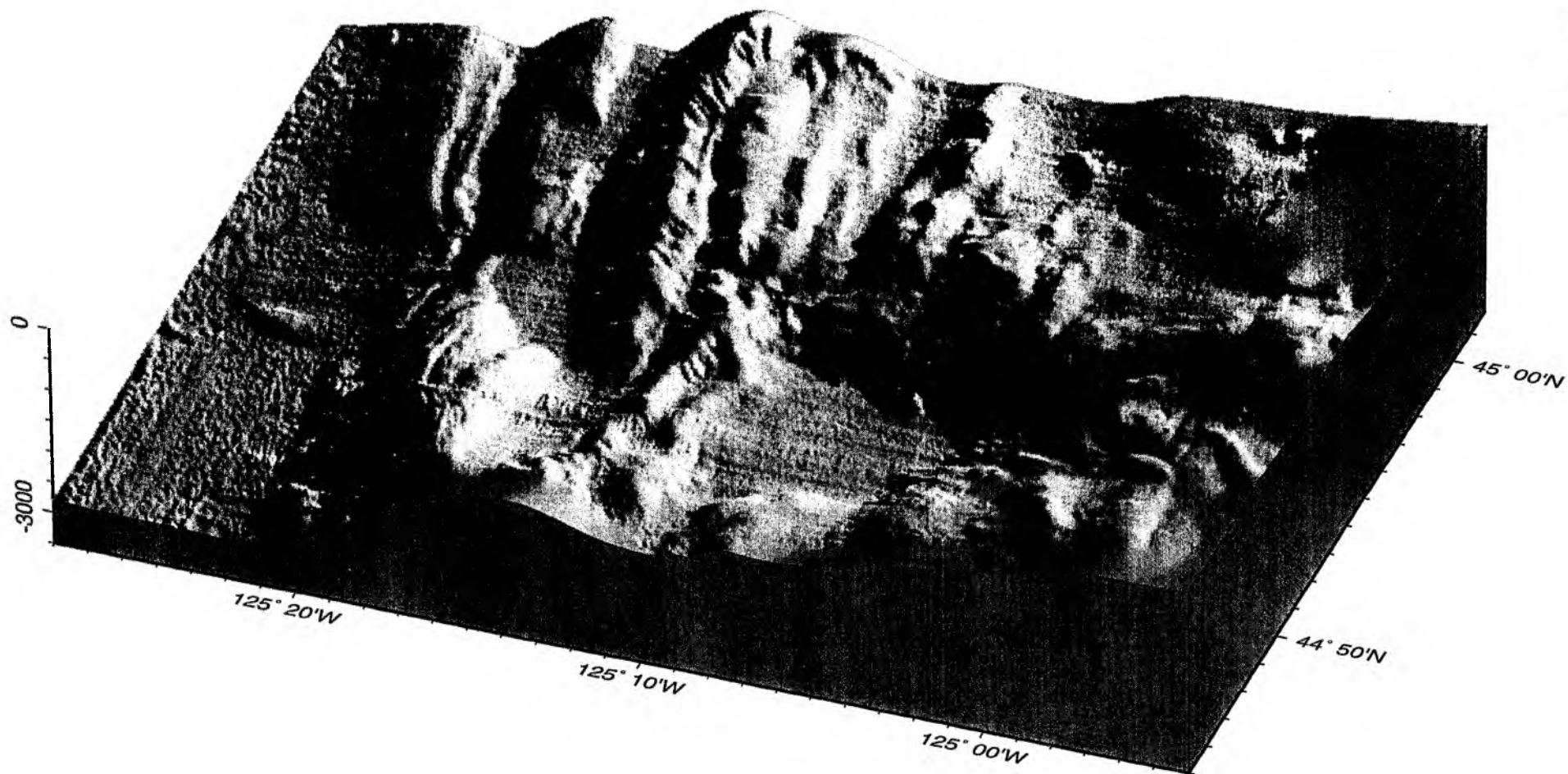
Fig. 67: Perspective image of northern Hydrate Ridge area. View from south, illumination from northeast.
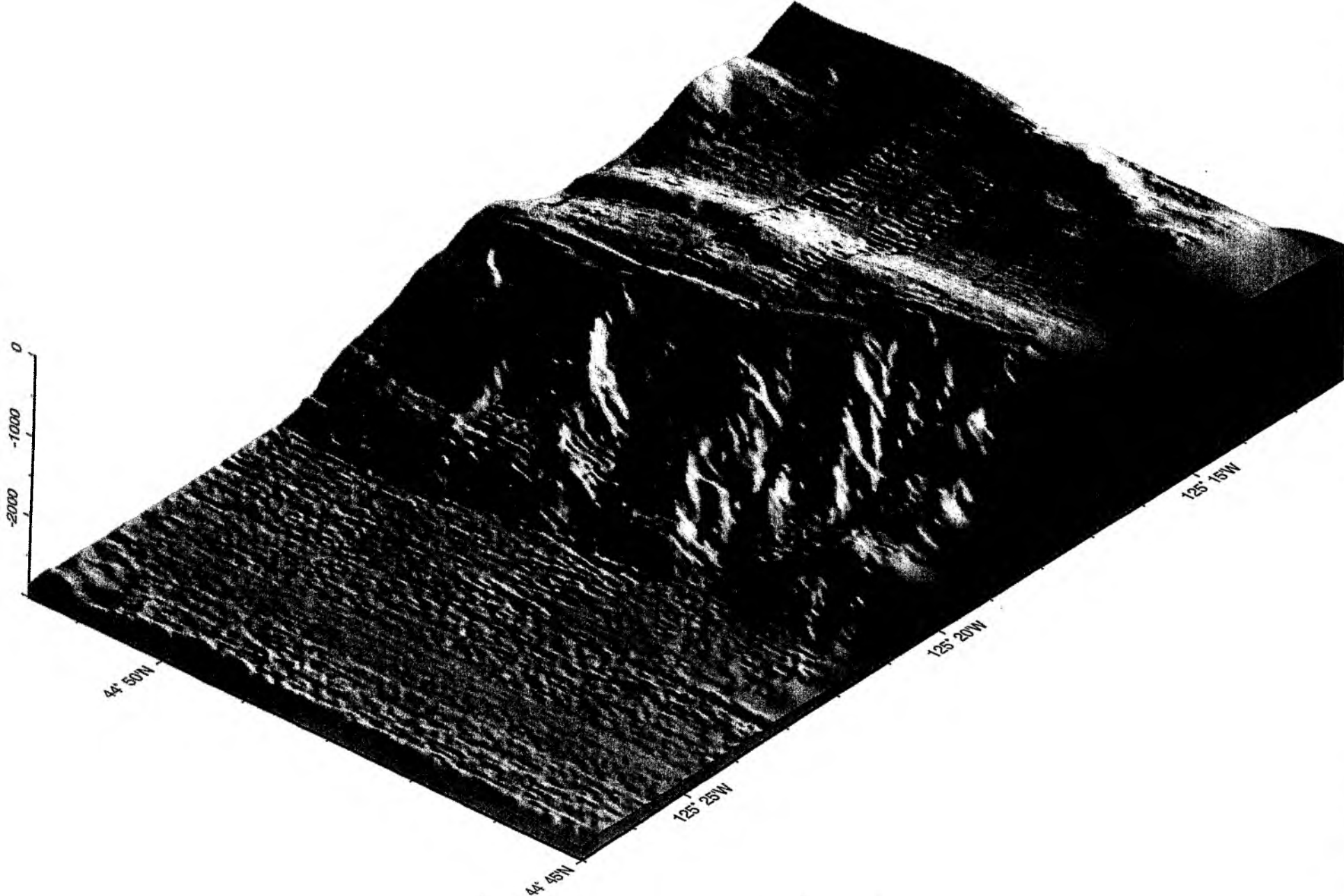
Fig. 68: Enlarged view on slump scars in the northern Hydrate Ridge area. View from southwest, illumination from southeast.

R/V SONNE cruise 143

Hydrosweep Survey
Mercator WGS84 1:200000 at 0°
processed with MBSystem (LDEO)
GEOMAR/OSU

km

0   2   4
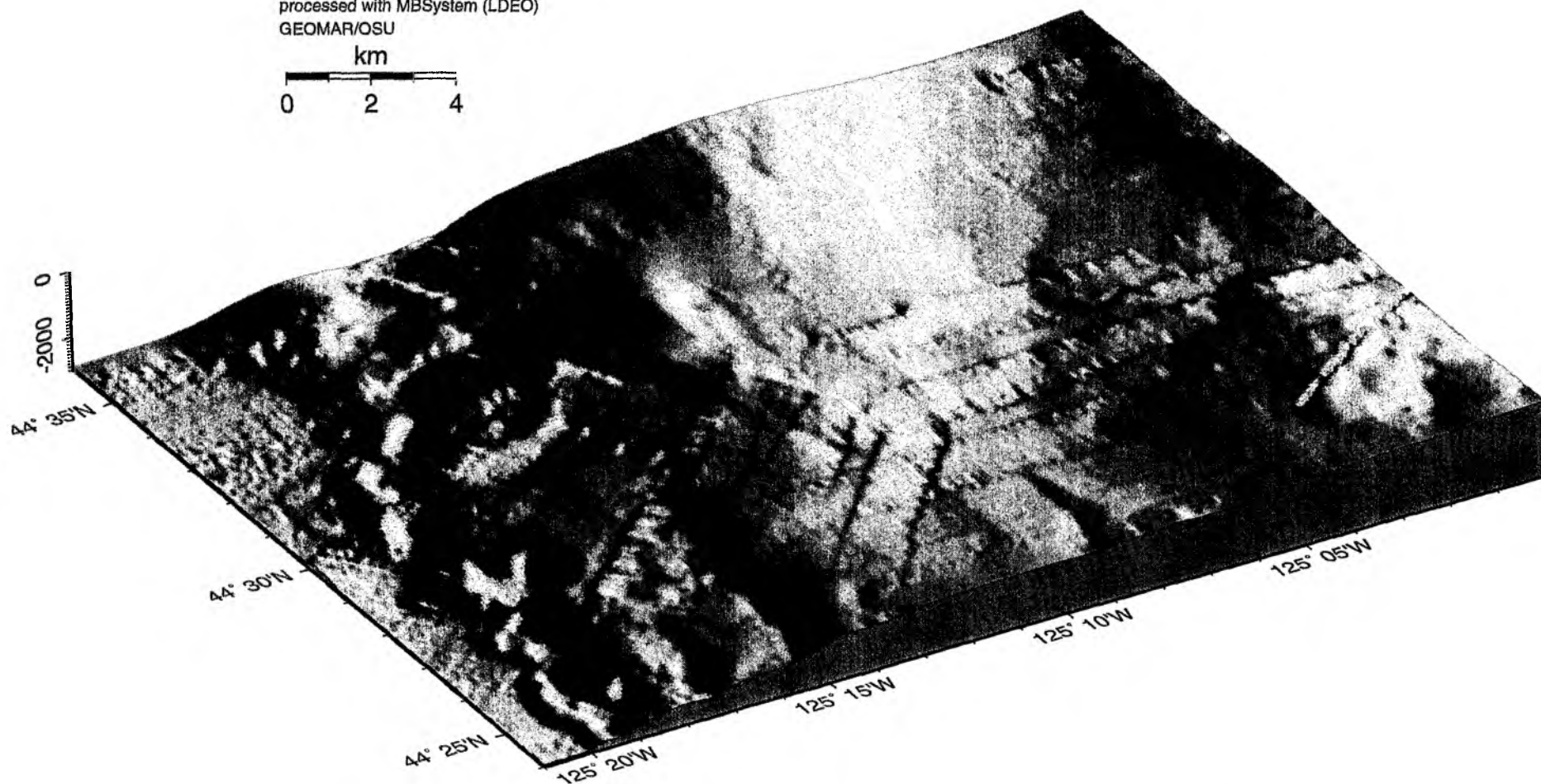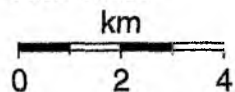
Fig. 69: Perspective image of southern Hydrate Ridge area. View from southwest, illumination from east. Note the strong distortions oriented along-track due to the gyro failure.

been shifted towards the east and appears more compressed. The front margin is marked by deep gulleys, likely due to slope failure and erosion from oversteepening and localized slumping. Eastward of the second ridge a large, 7 km x 7 km basin, can be seen. The top layer of sediment fill of this basin has a depth of 1,900 m, which decreases westward towards the second ridge (Fig. 67). A central valley along strike highlights the crest of the second ridge (Fig. 67), possibly the result of tight folding aand small scale slumping. These features illustrate the ongoing uplift of this area in response to east-west compression. Additionally, massive scars are frequent along the western flank of the ridges north and south of 44°52' indicating the overall instability along the margin.

Hydrate Ridge area, southern part

A perspective plot (Fig. 69) of the southwestern portion of the hydrosweep survey shows the north-south trending ridges and the relief heading west on to the abyssal plain. The relief is not as great in this southern portion as in the R1 area, and the perspective plot highlights well developed slump features along the western edges of the ridges towards the abyssal plain. The bathymetry to the east gradually rises towards the continental shelf.

4.3   Parasound

N. Kukowski, H. Kudraß and watchstanders

Instrument, operation, and data storage

By means of the parametric sediment-echosounder PARASOUND (PARAmetric sediment survey echoSOUNDer, Atlas Elektronik GmbH, Bremen), shallow sediment structures down to a depth of about 100 mbsf can be imaged.

Parasound works differently from traditional 3.5 kHz echosounders and uses a sound beam resulting from the interference of two high frequency narrow waves of similar frequency (18 - 23 kHz) forming a low frequency part of the signal. The depth of penetration of the parametric 2.5 to 5.5 kHz echo is as great as that of 3.5 kHz systems, but due to the narrower beam width, a clearer and more differentiated image of multi-layer structures is obtained. The opening angle of the sound wave is about 4° acoustically illuminating a spot with a diameter of 7% of the water depth. Therefore, information quality depends to a large amount on the morphology of the ocean bottom, in case of steep slopes, the image often is lost due to configuration reasons. Slopes steeper than 4° cannot be imaged, areas with a slope of more than 2° normally are only poorly imaged.

During SO143-3, Parasound war mostly operated in the parametric mode using a frequency of 4 kHz. Raw analogue data have been written to a black and white as well as a colour printer. A large portion of the data were also stored on DAT tape using the program PARADIGMA (PARAsound DIGitalisierungs- und Mehrkanal Auswertesystem, V. Spieß (1993), U Bremen).

Facies Types

Based on a first overview of the seismic inventory of the PS colour prints we classified the seismic facies in two main categories. We used surface reflectivity, lateral continuity of the surface signal, acoustic penetration, continuity and reflectivity of subsurface reflectors and their geometry for the differentiation of the seismic facies types. In a first step we classified sections of individual profiles and combined this information after some reinterpretation and additional refinement on the bathymetric map. The main problem for a more direct and faster interpretation is the change seismic attributes with the different inclination of the sea floor.

The depth of penetration of the seismic signal and the reflectivity or presence of reflectors near the seafloor defines the two main types. Penetration of up to 50 m and good lateral continuity of subbottom reflectors define the first category of youngest sediment cover. The seismic inventory of the second category of outcropping older

deformed or diagentically altered sediments are high surface reflectivity and no continuous or very short and discontinuous subsurface reflectors.

Seismic facies I (young sediments)

Seismic facies I a (drift deposits):
continuous, regular and closely spaced reflectors, sometimes with thick transparent sections, forming overlapping lenses with local unconformities, pinching out on outcrops or draping outcrops, locally erosional depressions along steep outcropping elevations, penetration from 10 m up to 60 m, small acoustic penetration and high reflectivity indicate strong impedance contrasts probably indicating well bedded sand-mud sequences (Fig. 70).

Seismic facies I b (ponded sediments):
continuous, irregularly spaced reflectors with various reflectivity, no internal deformation or unconformities,
individual layers with maximum thickness at the bottom of depression and reduced thickness over elevations, marginal draping of elevations, penetration from 10 m up to 80 m (Fig. 71).

Seismic facies II (outcrops)

The various seismic subfacies types could not clearly defined as frequent transitions do not allow a reliable assignment, only the end members are described.

Seismic facies II a (rocky outcrops)
high reflectivity of an irregular surface or rough topography, penetration usually less than 30 m, at some locations in shallow water indicative of the tectonic deformation (Fig. 72)

Seismic facies II b (outcrops of semiconsolidated sediments with carbonate slabs or gashydrate) (Fig. 73)

prolonged surface reflector of high amplitude indicating a penetration of several meters, reflectivity of the surface reflector decreases rapidly with increasing inclination, which indicates a hard bottom deflecting the signal, punctual dispersed high-amplitude reflectors, which might be caused by subbottom reflection points or numerous good reflectors at the surface within the acoustic foot print at the surface.

Seismic facies II c (outcrops of semiconsolidated sediments)
prolonged surface reflector of high amplitude as in subfacies II b, irregular or short high-amplitude subbottom reflectors (Fig. 72)

Seismic facies III (slump deposits)
transparent up to 20 m-thick lens shaped sections with a mound-like surface (Fig. 72)

a) 44° 29.393N / 124° 55.762W

44° 29.117N / 124° 55.163W

b) 44° 29.680N / 124° 45.180W   44° 29.388N / 124° 46.298W
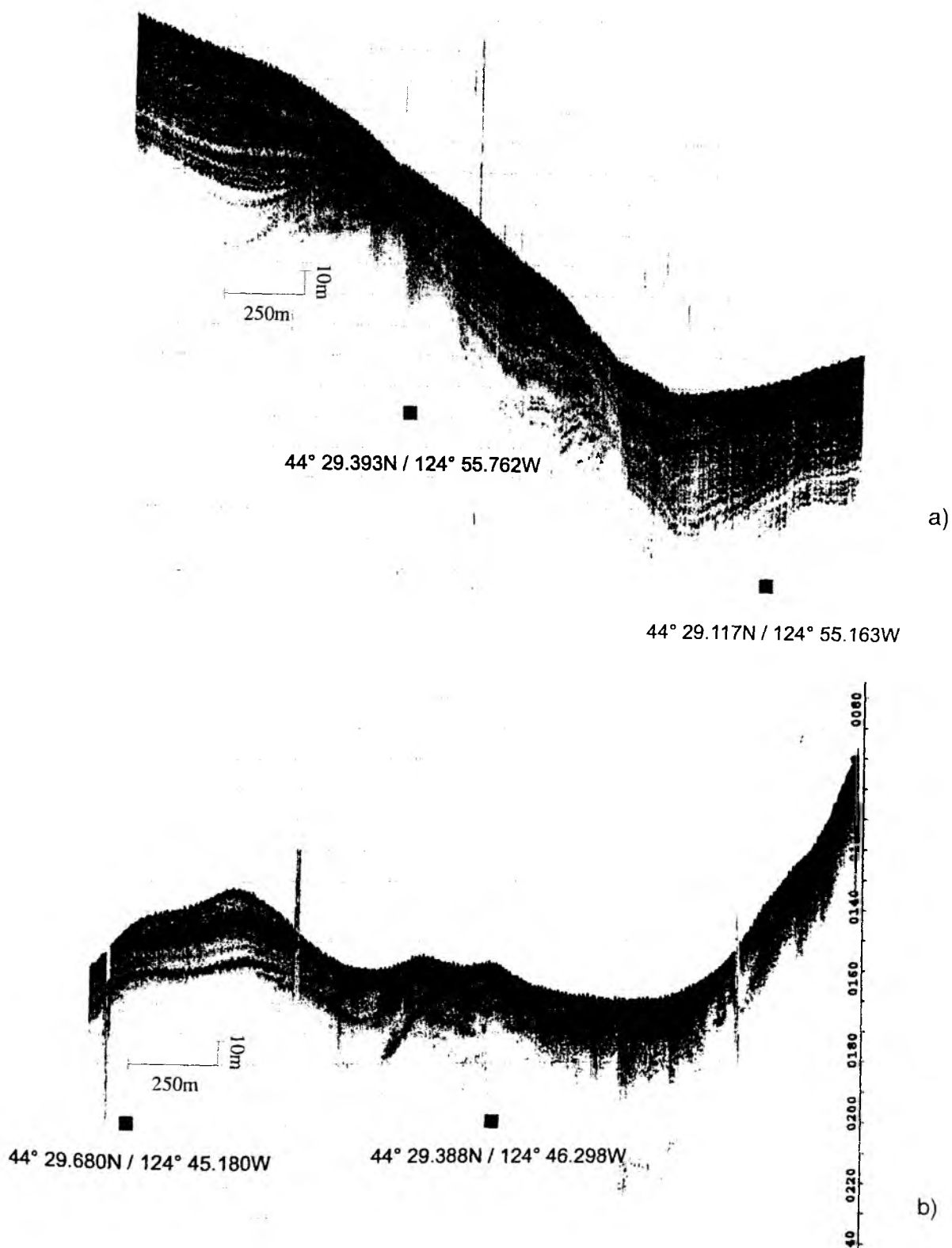
Fig. 70: Sediment facies at the Oregon accretionary prism. a) drift deposits (facies Ia), b)facies IIa (left) and IIc (right).
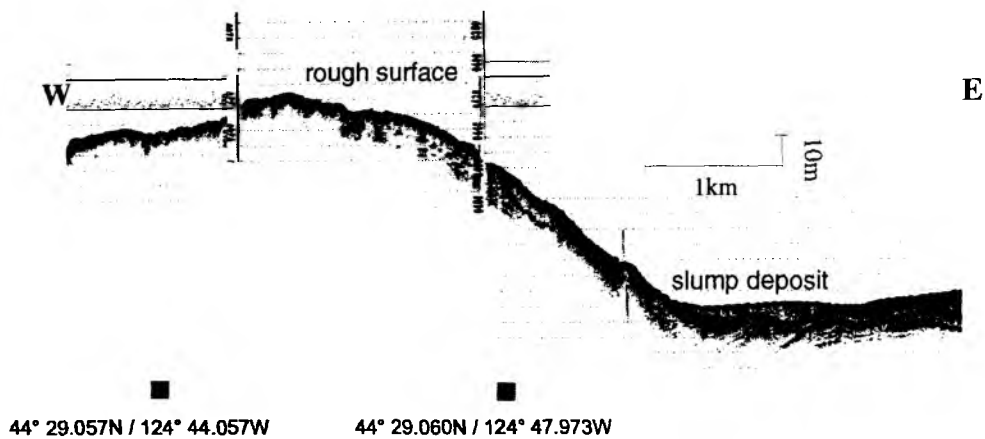
Fig. 72: Rough surface on top of a morphological high southeast of Hydrate Ridge. In the depression,slump deposits overly the layered sediment.
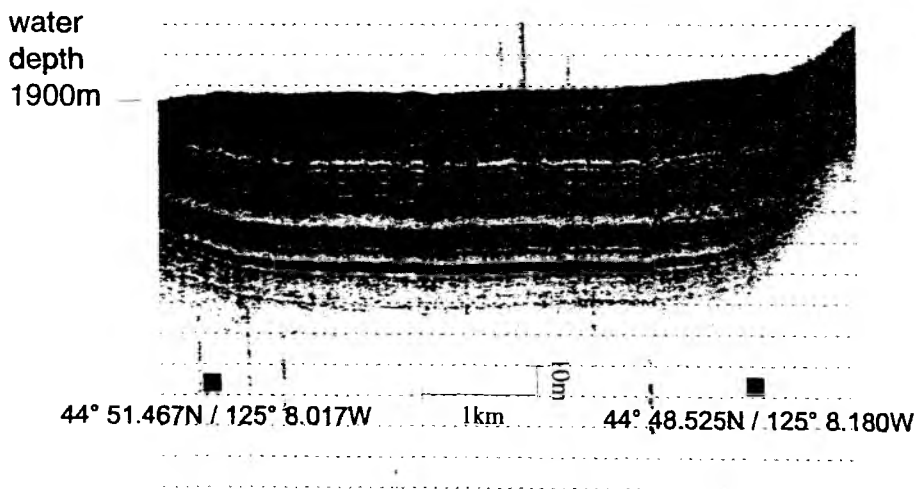
Fig. 71: Parasound profile across a basin structure in the Oregon accretionary prism. Penetration down to about 80mbsf, sequence of undisturbedly layered sediments of different reflectivity.

SSW

NNW

44° 36.260N / 125° 8.122W

44° 38.877N / 125° 7.075W
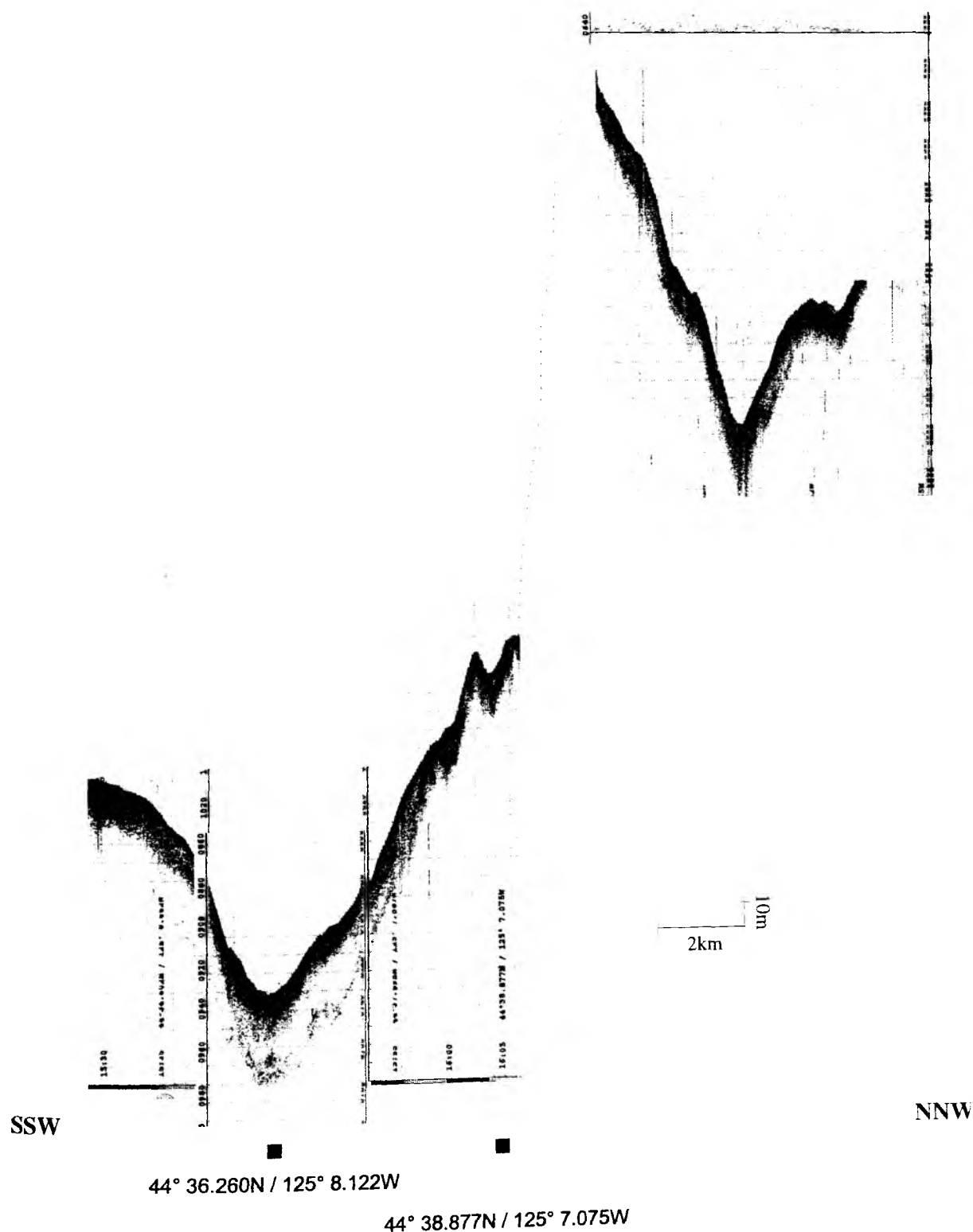
Fig. 73: Parasound profile along the crest of Hydrate Ridge.

Interpretation

The PS records offer additional information on the distribution of young sediments and the deformation, alteration and erosion of older sequences.
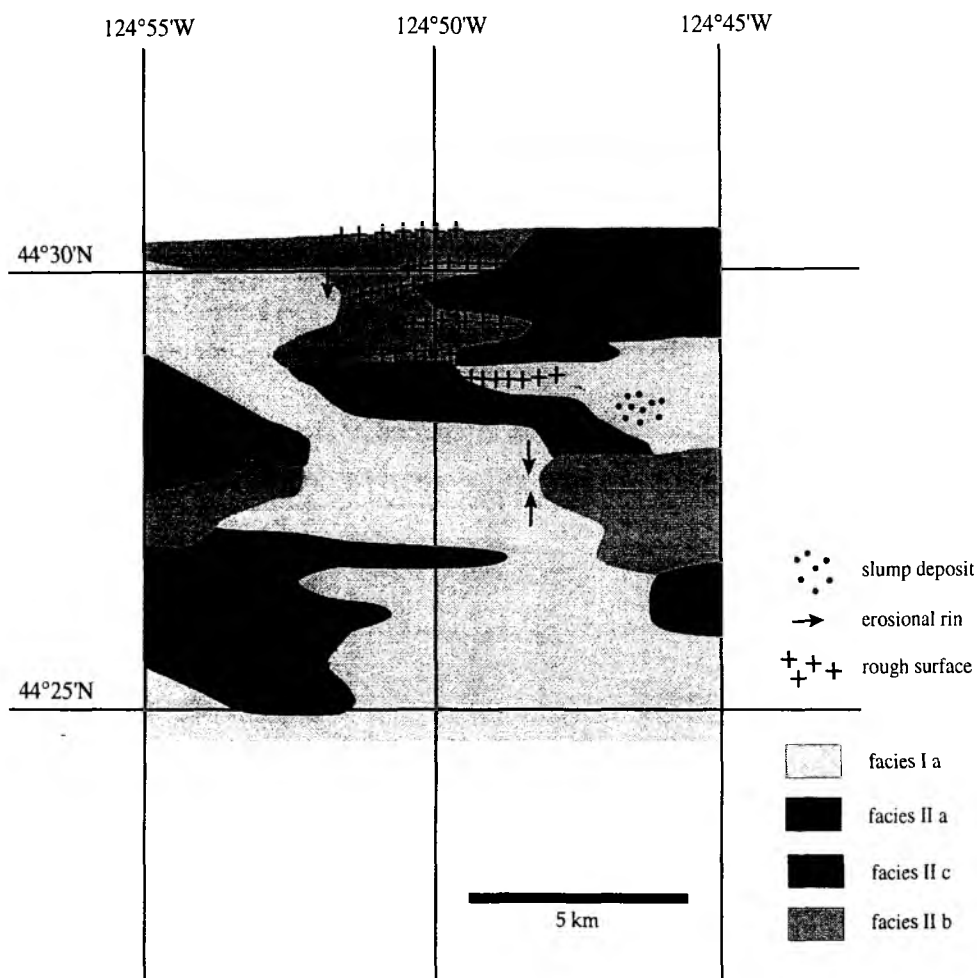
Fig 74: Facies map of the southeastern area surveyed systematically with Hydrosweep and Parasound.

At the deeper continental slope young sediments of seismic facies I b are accumulating in isolated basins, where probably a mixture of turbidites and hemipelagic sediments is deposited. About 80 m-thick sequences seem to be uneffected by tectonic deformation (Fig. 71). Accumulation in these ponded basins are clearly restricted to overdeepened or isolated basins, while other valley-type depressions are not trapping sediment which apparently bypasses into the deep-sea trench. The ponded basin north and southeast of the Hydrate Ridge may contain a record of the late Pleistocene formation of chemoherms and erosion and thus may contain some very valuable information on the long-term history of methane emanations.

Long continuous evenly spaced reflectors and the internal architecture with thick lens-shaped packages, which are separated by internal angular unconformities of the seismic facies I a are interpreted as drift deposits (Fig. 70). They mainly occur in water depths of about 500 m on the upper continental slope, where the supply of terrigenous

44° 23.958N / 125° 0.605W   44° 19.992N / 125° 0.602W
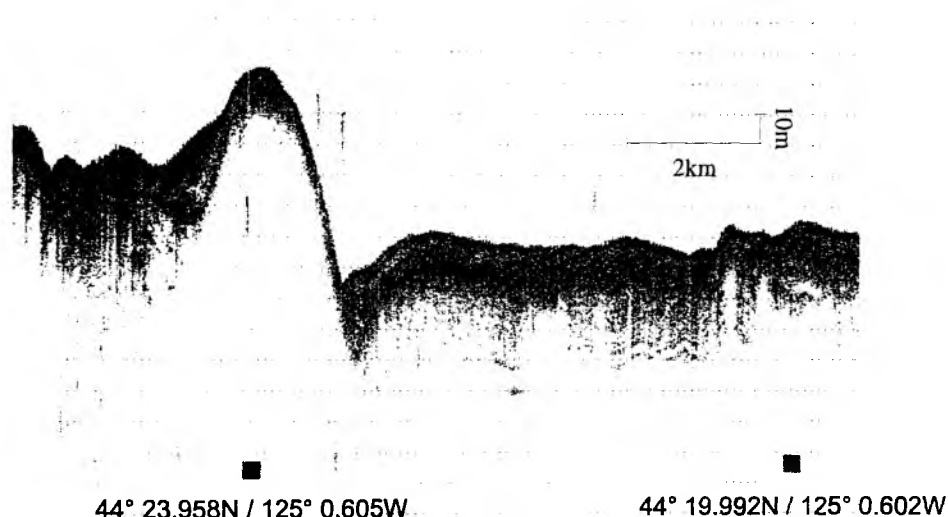
Fig. 75: Morphology of a knoll southeast of the summit of Hydrate Ridge.

gas in the
water column

water
depth
380m —

44° 36.620N / 124° 45.000W

44° 34.720N / 124° 43.160W

44° 34.835N / 124° 41.323W
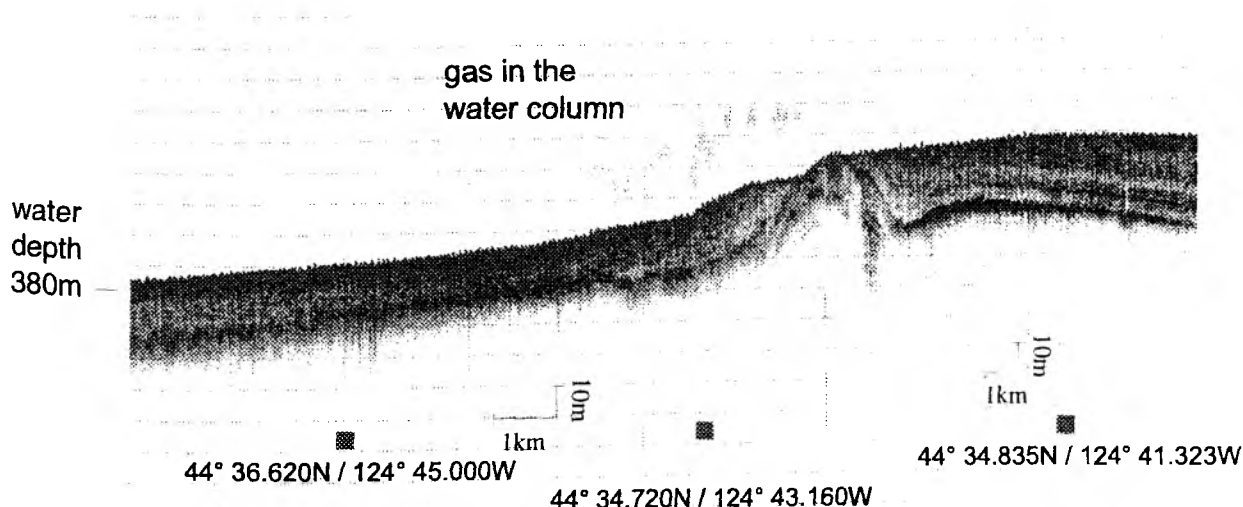
Fig. 76: Parasound profile across parts of Daisy Bank. Note evidence for gas in the water column at the flank of the pop-up structure.

particles from the continent is large enough to form these deposits. A deep contour following current must flow along the slope distributing and accumulating these deposits. The morphologically controlled change of a thick sequence to pinch out at the foot of an elevation often associated with a marginal erosional channel is also typical for a current controlled deposition (Fig. 74).

Most of the elevations and ridge are not covered by thick young sediments indicating either permanent current winowing and/or a small supply of sediment. Extensive signs of erosion are also manifested on the side-scan sonar records of most areas of the Hydrate Ridge where long-range striation of slightly higher reflectivity marks outcropping layered and partial deformed sediments of probably Neogene age. Seismic facies types II a and b are typical for these areas. At places, outcropping of higher consolidated sediments or chemoherms as high-amplitude mounds are also recorded. In the saddle between the northern and southern peaks of the Hydrate Ridge a weak diffuse subsurface reflector mimics in 50 m distance the sea floor topography (Fig. 73). This unique reflector may be caused by cementation related to fluids or fluid fronts associated with the gashydrates.

Close spacing of E-W running profiles are used for a map of the seismic facies between 44°25′/44°30′N and 125°45′/125°55′W (Fig. 74). Most of the area is covered by drift deposits (seismic facies Ia). Along the marginal slopes of the northern elevation several erosional channels mark the transition from the older sediments of the elevation to the drift deposit in the depression. Some slumps have been flown into the depression. The very top of the elevations is characterized by a rough surface and seismic facies II a, b and c.

In one profile across the Daisy Bank at the uppermost continental slope off Newport a 3 km-long zone of weak reflectivity in the water column indicates the vigorous expulsion of methane(?) bubbles (Fig. 75). The distinct wavy outline of the reflectivity zone and its distribution along a depth transect between 370 m and 345 m points to different gas exits which are probably related to a pop-up structure of older sediments damming the 30 m thick sandy sediments sequence on the landward side. Several methane sources are known along a transform fault demarking the western limit of the Daisy Bank. The obvious small depth distribution of only 20 m where the bubbles are reflecting the 4 kHz PS signal is probably determined by the expanding bubble size. Methane bubbles at deeper sites were detected at the previous cruise only by the higher PS frequency of 18 kHz.

4.4   Ocean Floor Observation System (OFOS)

C. Jung, J. Johnson, B. Teichert, C. Bartlett, A. Kopf, M. Elvert, G. Bohrmann

4.4.1   Introduction and equipment

The main OFOS objectives on SONNE 143-3 were to conduct additional OFOS surveys of Hydrate Ridge and to identify the locations of gas hydrates and active fluid venting sites in the surrounding region (Fig. 77, Table 22). The OFOS surveys were designed and conducted to map the distinct morphological, geological, and biological features that occur in gas hydrate and active fluid venting regions. Eight OFOS surveys were completed on this leg. The locations of the eight surveys are dispersed throughout the Hydrate Ridge region in order to determine and understand the differences between sites with or without gas hydrates and sites of active or inactive fluid venting. The results of the OFOS mapping will be used in conjunction with other sedimentological, geochemical, and geophysical results to better understand the distribution and behavior of gas hydrates in continental slope environments.

Table 22: OFOS deployments during Leg SO143-3.

SO 143-3 OFOS-tracks									
Date	Stat. No.	Time (UTC) at bottom	Time (UTC) off bottom	Start Lat. (NS) at bottom	Long. (EW)	End Lat. (NS) off bottom	Long. (EW)	Working area	Observation
	143-3								
27.8.99	211-1	14:16	0:21	45° 35,83'	125° 08,55'	45° 35,77'	125° 15,00'	North Area, R1 structure	chemoherm carbonates, carbonate boulders, carbonate outcrops, clam fields
28.8.99	213-1	16:49	23:21	44° 39,49'	125° 00,82'	44° 39,72'	125° 08,16'	Northern summit of Hydrate Ridge, eastern slope	carbonate crust and outcrops, carbonate boulders and chimneys, some clams,
29.8.99	216-1	17:16	22:04	44° 40,46'	125° 04,97'	44° 40,44'	125° 09,99'	Northern summit of Hydrate Ridge, Seismic line 9	chemoherm carbonates, carbonate crust and boulders, clam fields
31.8.99	223-1	20:26	4:28	44° 35,14'	125° 04,28'	44° 35,16'	125° 12,95'	Southern summit of Hydrate Ridge, Seismic line 2	carbonate crust and boulders near the crest, soft sediment, some pogonophorans at the slope
1.9.99	224-1	7:05	10:07	44° 41,01'	124° 51,90'	44° 42,80'	124° 49,67'	Daisy Bank Fault, eastern of Hydrate Ridge	at the top carbonate crust, boulders and slabs with doughnut and chimney feature
1.9.99	225-1	11:21	13:00	44° 49,50'	124° 48,43'	44° 48,61'	124° 50,47'	South of the BSR-outcrop	soft sediment, some carbonate boulders, clam fields at the top
2.9.99	231-1	4:45	9:00	44° 27,02'	125° 01,54'	44° 26,80'	125° 02,45'	Southeastern of Hydrate Ridge, SE-knoll	chemoherm carbonates, clam fields
2.9.99	232-1	10:09	11:53	44° 23,98'	125° 00,14'	44° 24,00'	125° 00,14'	Southeastern of Hydrate Ridge, southern part of SE-knoll	extensive chemoherm carbonates, clam fields and bacterial mats

4.4.2   Survey areas and results

North of Hydrate Ridge, R1 structure

The first survey, OFOS 211, was conducted across the first ridge, the R1 structure, located north of Hydrate Ridge. The OFOS track begins at 45° 35.86' N, 125° 08.60' W and ends at 45°35.76' N of 125° 15.00' W. The starting water depth was 744 m and the depth of water at the end of the track was 1714 m. The seafloor in this area is characterized by soft bioturbated sediments and harder, rocky carbonate crust with little to no sediment drape. Dispersed clams, sea anenomaes, crinoides, corals, sea stars, crabs, rattail fish, rockfish, and flounders were identified on the seafloor throughout the area. The corals typically attach themselves to hard substrates, usually exposed boulders. The corals and crinoids are also orientated in the direction

direction of the dominant sea bottom current. At a water depth of 700 m, extensive carbonate boulder fields and some carbonate outcrops exist. The carbonate surfaces are rough and irregular and generally covered by a thin layer of sediment. Black boulders, which are likely carbonate boulders coated with a manganese oxide, occur in patches and are sometimes mixed within the lighter colored carbonates.
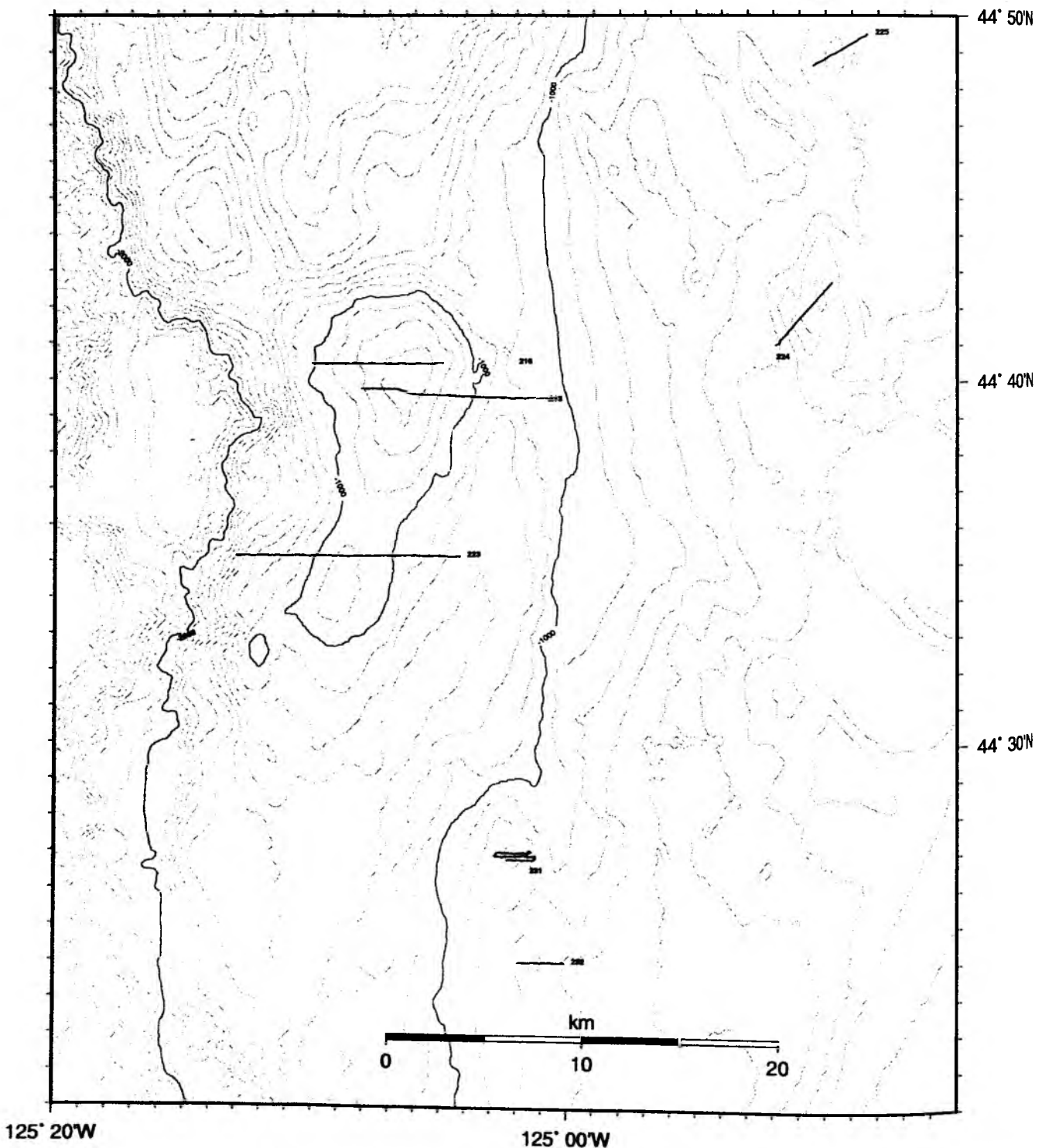
Fig. 77: Location of OFOS deployments during leg SO143-3 on Hydrate Ridge.
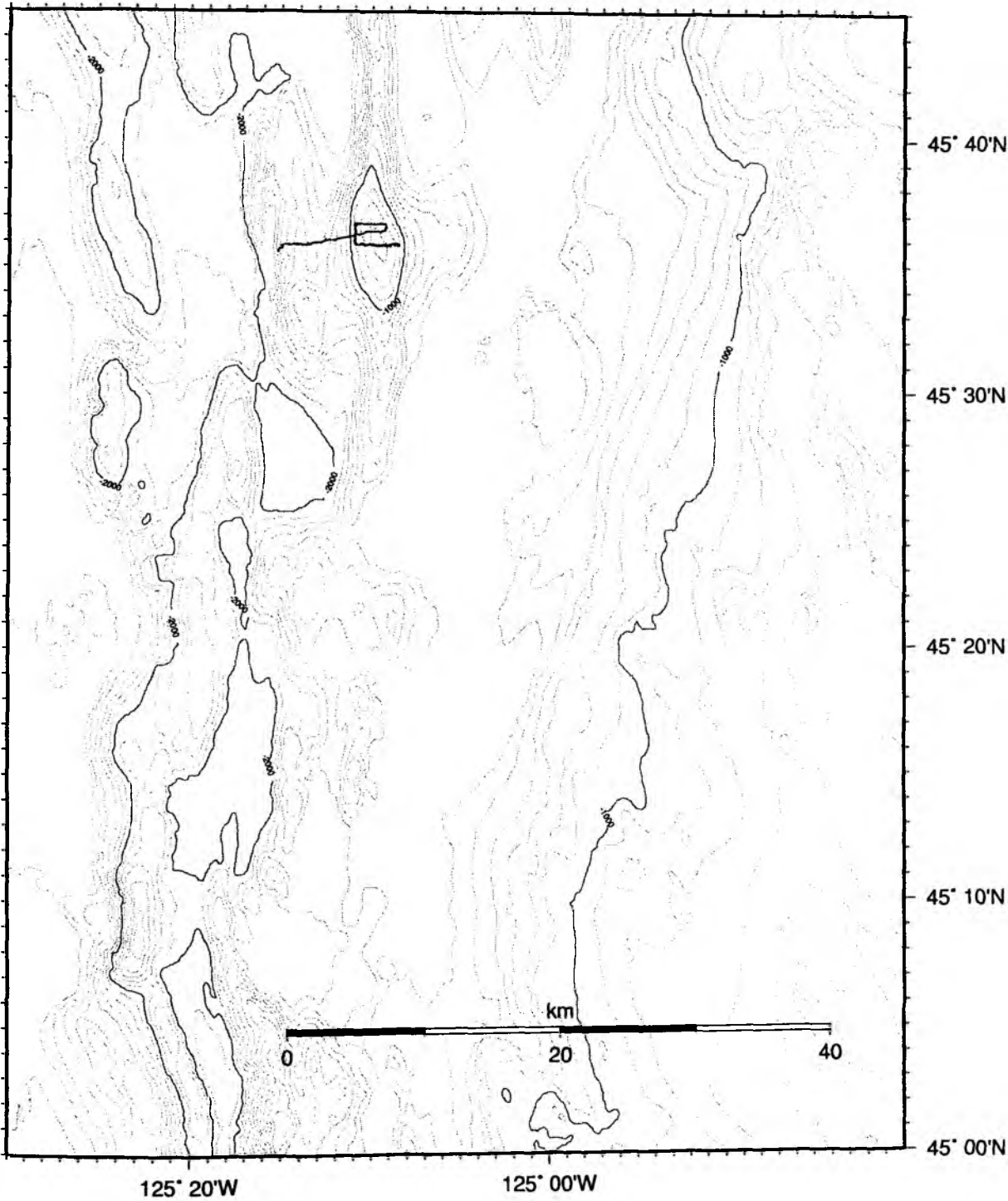
Fig. 78: OFOS deployment 211-1 at accretionary Ridge "R1", a similar structure like Hydrate Ridge.

OFOS-track 216
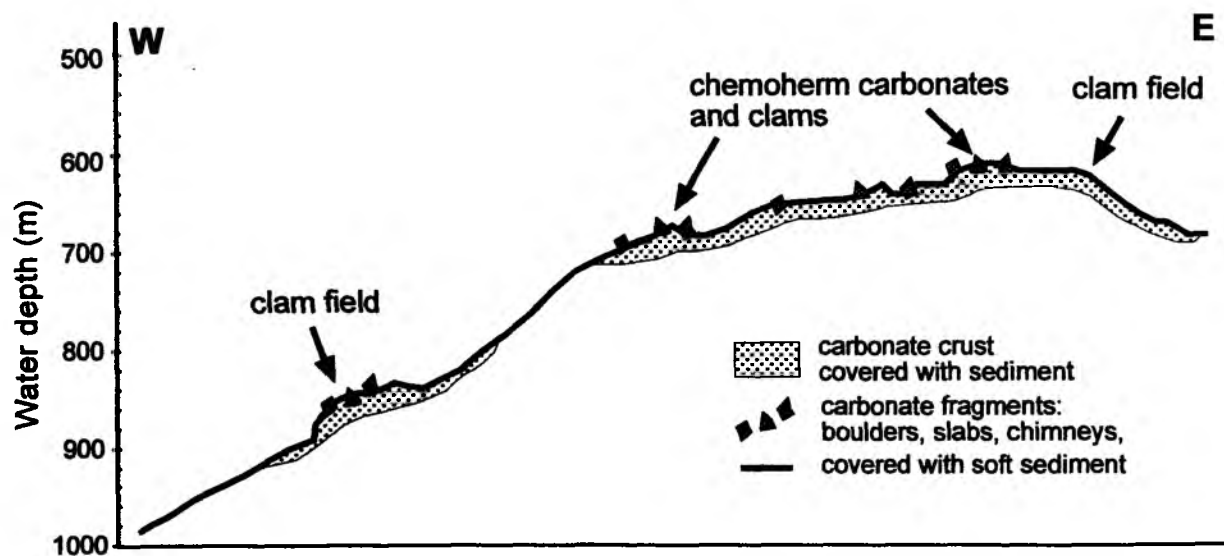
OFOS-track 232
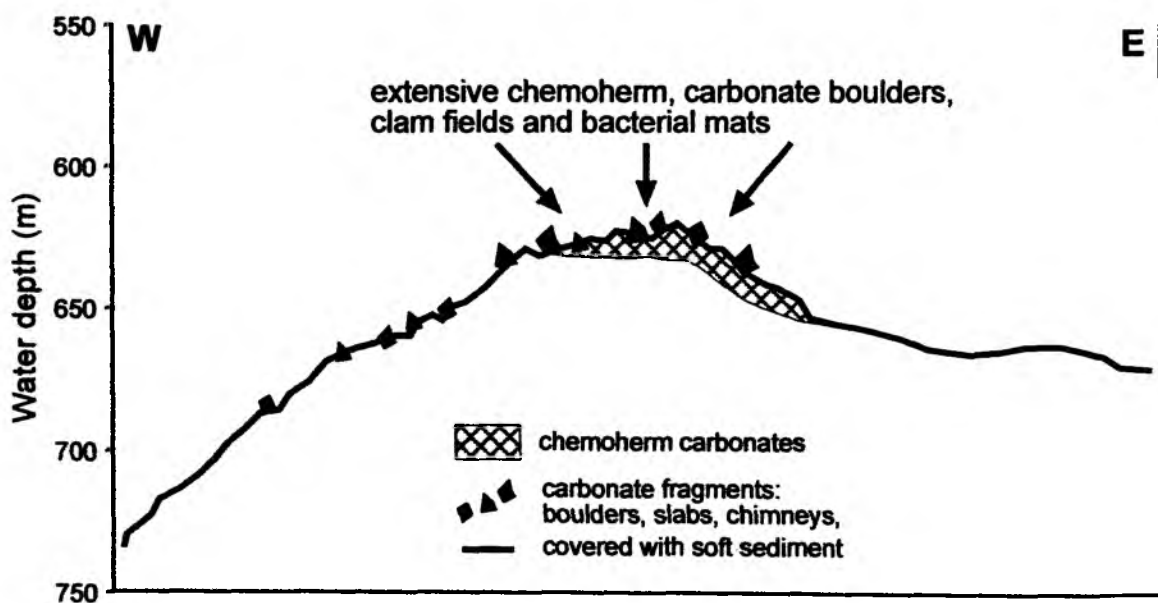
Fig. 79: The OFOS-track 216 was located at the northern summit of Hydrate Ridge and follows along MCS line 9. The seafloor is characterised by carbonate outcrops and some clam fields. The OFOS-track 232 was conducted south of the Southeast Knoll. Clam fields and bacterial mats indicate an active vent site. Water depth data were transferred from the CTD of the sled.

At a water depth of 680 m, a living clam field was observed, however there were no bacterial mats in the vicinity. A large chemoherm also exists in this area at 45°36.70' N, 125°9,70' W. The carbonates of this chemoherm are very rough and porous and appear to be highly fractured. Clam shells are also cemented within the carbonates of the chemoherm.

Northern summit of Hydrate Ridge

The second survey, OFOS 213, was conducted across the northern summit of Hydrate Ridge. The track begins at 44° 39.44' N, 125° 0.86' W and ends at 44° 39.16' N, 125° 8.15' W. The starting depth was 1004 m and the depth at the end of the track was 815 m. The seafloor in this area is characterized by soft bioturbated sediments on the eastern slope and hard carbonate crust , composed of slabs, cobbles, and boulders, near the crest of the ridge. The seafloor on the western slope of the ridge is also characterized by hard carbonate crust, which is composed of slabs, cobbles, and boulders, and in addition, doughnut, chimney, and skeletal carbonate structures. The carbonate crust, where present, is often covered by a thin layer of sediment and shows evidence of current formed structures. Benthic life on the seafloor consist of crinoids, sea anenomaes, sea cucumbers, sea stars, corals, crabs, and a few clams and snails. Jelly fish, rockfish, rattail fish, and flounders were observed. Several sea urchin fields are also present, but limited to the uppermost part of the western slope and the crest of the ridge. At a depth of 650 m on the western slope of the ridge, several clam shells are present within a large field of carbonate boulders. The carbonate boulders on the western slope are both dark, coated with manganese oxide, and light in color.

The third survey, OFOS 216 (Figs. 77 and 79), was also conducted across the northern summit of Hydrate Ridge. It lies north of the OFOS 213 survey and is coincident with multichannel seismic line 9. The track begins at 44° 40.43' N, 125° 4.99' W and ends at 44° 40.44' N, 125° 9.99' W. The trackline begins at the crest of Hydrate Ridge and extends downslope to the west. The starting depth was 686 m and the depth at the end of the track was 1026 m. The seafloor near the crest of the ridge is characterized by hard carbonate crust, composed of slabs, cobbles, boulders, and skeletal carbonate structures. On the western slope, the sea floor is dominated by soft sediments with scattered carbonate cobbles and boulders. Benthic life on the seafloor consits of crinoids, sea anenomaes, sea stars, crabs, and snails. Rattail fish, rays, eels, and flounders were only observed in the deeper water of the western slope. Sea urchin fields are also present, but limited to the crest of the ridge. Clam fields and abundant carbonate boulders and chemoherm carbonates are present near the crest of the ridge. We identified two species of clam within these fields, Acharax and Calyptogena.

Southern summit of Hydrate Ridge

The fourth survey, OFOS 223, was conducted across the northern part of the southern summit of Hydrate Ridge. It is coincident with multichannel seismic line 2. The track begins at 44° 35.17' N, 125° 4.12' W and ends at 44° 35.15' N, 125° 12.95' W. The starting depth was 1203 m and the depth at the end of the track was 1716 m.

The seafloor on the eastern and western slopes of the ridge is characterized by very soft, semi-suspended, bioturbated sediments. The seafloor near the crest is characterized by a hard carbonate crust, composed of slabs, cobbles, and boulders. Benthic life on the seafloor consits of crinoids, sea anenomaes, sea cucumbers, abundant sea stars, and crabs. Jelly fish, rockfish, rattail fish, rays, a single octopus, and flounders were are observed. The slope increases drammatically in a stepwise nature near the western end of the track producing large cliff faces and caves which are inhabited by several colonies of tube worms (pogonophorans), crinoids, sea anenomaes, and a single octopus.

Daisy Bank region, northeast of Hydrate Ridge

The fifth survey, OFOS 224, was conducted across two ridges within the Daisy Bank fault zone. The track begins at 44° 40.96' N, 125° 51.87' W and ends at 44° 42.79' N, 125° 49.67' W. The starting depth was 472 m and the depth at the end of the track was 349 m. The seafloor in this area is characterized by soft bioturbated sediments and carbonate cobbles, boulders, and blocks. Benthic life on the seafloor consits of crinoids, sea anenomaes, sea cucumbers, sea stars, sponges, crabs, and a few clams, snails, and sea urchins. The tops of the two ridges are each characterized by hard carbonate crust, composed of slabs, cobbles, boulders, and typical vent carbonates displaying donut, chimney, and skeletal carbonate structures.

The sixth survey, OFOS 225, was conducted across a ridge within the Daisy Bank Fault zone, and located north of the OFOS 224 survey. The track begins at 44° 49.51' N, 125° 48.36' W and ends at 44° 48.61' N, 125° 50.46' W. The starting depth was 421 m and the depth at the end of the track was 433 m. The seafloor in this area is characterized by soft bioturbated sediments and scattered carbonate cobbles, boulders, and blocks. Benthic life on the seafloor consits of crinoids, sea anenomaes, sea cucumbers, sea stars, octopus, and sponges. The top of the ridge is characterized by soft sediment, carbonate cobbles, and a few doughnut structures.

Southeast of Hydrate Ridge, SE-knoll

The seventh survey, OFOS 231, was conducted over the Southeast Knoll, located southeast of Hydrate Ridge, and consisted of three E-W tracklines. The survey begins at 44° 27.00' N, 125° 01.52' W and ends at 44° 26.79' N, 125° 02.44' W. The starting depth was 674 m and the depth at the end of the track was 652 m. The seafloor in this area is characterized by soft bioturbated sediments and scattered black carbonate cobbles, boulders, and chimney and donut structures. Benthic life on the seafloor consits of crinoids, sea anenomaes, sea stars, corals, crabs, and a few clams, snails, and sea urchins. Rockfish and rattail fish were also identified. A small chemoherm structure exists on the eastern end of the middle trackline at 44° 26.90' N, 125° 01.65' W. The carbonates of this chemoherm are very rough and porous and appear to be highly fractured. Carbonate boulders, donut structures, and scattered clams surround the chemoherm.

The eighth survey, OFOS 232 (Figs. 77 and 79), was conducted south of the Southeast knoll, across a small plateau. The survey begins at 44° 24.02' N, 125° 00.15' W and ends at 44° 24.00' N, 125° 01.95' W. The starting depth was 678 m and the depth at the end of the track was 832 m. The seafloor in this area is characterized by soft bioturbated sediments and scattered black carbonate cobbles, boulders, and chimney and donut structures. Benthic life on the seafloor consits of crinoids, sea stars, corals, sponges, crabs, and a few clams, snails, and sea urchins. Abundant jelly fish were also identified. A large chemoherm structure exists on the eastern edge of the plateau. The carbonates of this chemoherm are very rough and porous and appear to be highly fractured and eroded, forming large canyons. Carbonate boulders, doughnut structures, abundant clam fields, and bacterial mats surround the chemoherm. This was a previously an undiscovered chemoherm and thus, represents a new active vent site.

4.5   Autoclave tools

4.5.1   Autoclave piston corer

H. Kudrass

The autoclave piston corer of BGR is designed to preserve in situ conditions of sediment samples from the deep sea. The corer should collect cores from sediment, which has to be kept at low temperature and high pressure of the deep sea until analysis onboard or transfer into a pressurized chamber for a later analysis in an onshore laboratory (see following chapter). The corer is especially built to preserve in situ pressure and temperature of sensitive gas hydrate-bearing sediments. The prototype of the corer was lost during its first employment on the Hydrate Ridge off Oregon.

Design and Technique

The corer uses the common technique of piston coring. Dimensions and technical design of the coring unit are based on the widely used BGR piston corer, which consists of a 9 cm core barrel with a core cutter, a core catcher, a PVC liner inside a steel core barrel, a split piston, a tension release unit for the core barrel, a trigger weight and a release mechanism. The stiff steel core barrel usually has a length of 5 m which allows the employment of the corer even on consolidated sediments, usually without damage and especially without bending of the core barrel. A second 5 m long barrel can be added to obtain longer cores from less consolidated sediments. Penetration is achieved by a 5 m - free fall acceleration of the one tonne mass of the whole corer. The end velocity of about 7 m/sand the great mass, which could be enlarged by adding more lead weight, pushes the core barrel into the bottom. During the short period of the penetration the piston is fixed by the straight wire connected to the ship´s winch, thereby overcoming the internal friction of the incoming core along the inner walls of the core liner.

The coring process of the AKL is identical with the usual piston coring. The recovery of the core, however, is different. After penetration the heave of the wire is used to lift the core liner with the cored sequence into the autoclave chamber mounted on top of the core barrel. After completion the top part of the piston tightly seals the upper opening of the pressure chamber and at the same time closes by a system of wires and levers the conical valve at the bottom of the chamber. Both valves are additionally secured by adding 100 bar pressure from a small permanent pressure reservoir. Further heave of the wire will tear the now empty core barrel from the bottom and the autoclave unit can be hauled on deck.

The pressure chamber, the conical and piston valves are made from steel and are tested to withstand an internal pressure of 650 bar. A 5 cm thick thermal isolation made from epoxy resin embedded glass microspheres with a low thermal conductivity protects the chamber from being warmed. Some change of in situ temperature cannot be avoided. A first estimation predicts an increase by maximum of 8° C, which occurs mainly when the device with the common deep-water temperature of 2° C is recovered during the last 20 minutes ascent through a 23° C warm surface water. Further thermal isolation of the two valves can be easily achieved if this estimation proves to be too optimistic.

The employment of the corer is done with the corer handling unit onboard of RV SONNE, which was slightly modified to handle the larger diameter of the pressure chamber. Two 5 m sections of core barrels and pressure chamber can be combined to sample cores with a maximum length of a little less than 10 m.

Operation

The AKL was as easily deployed as a normal piston corer at the 29 of September its the southern tip of the Hydrate Ridge in water depth of 788 m. Gravity coring with one tonne of top weight at more or less the identical position had recovered about 1 m of slightly consolidated mud clasts with subrounded carbonate concretions and numerous 1 cm thick irregular carbonate slabs. The corer was correctly triggered and the tension record indicated no overpenetration, bending or sidewards fall of the corer (Fig. 80).
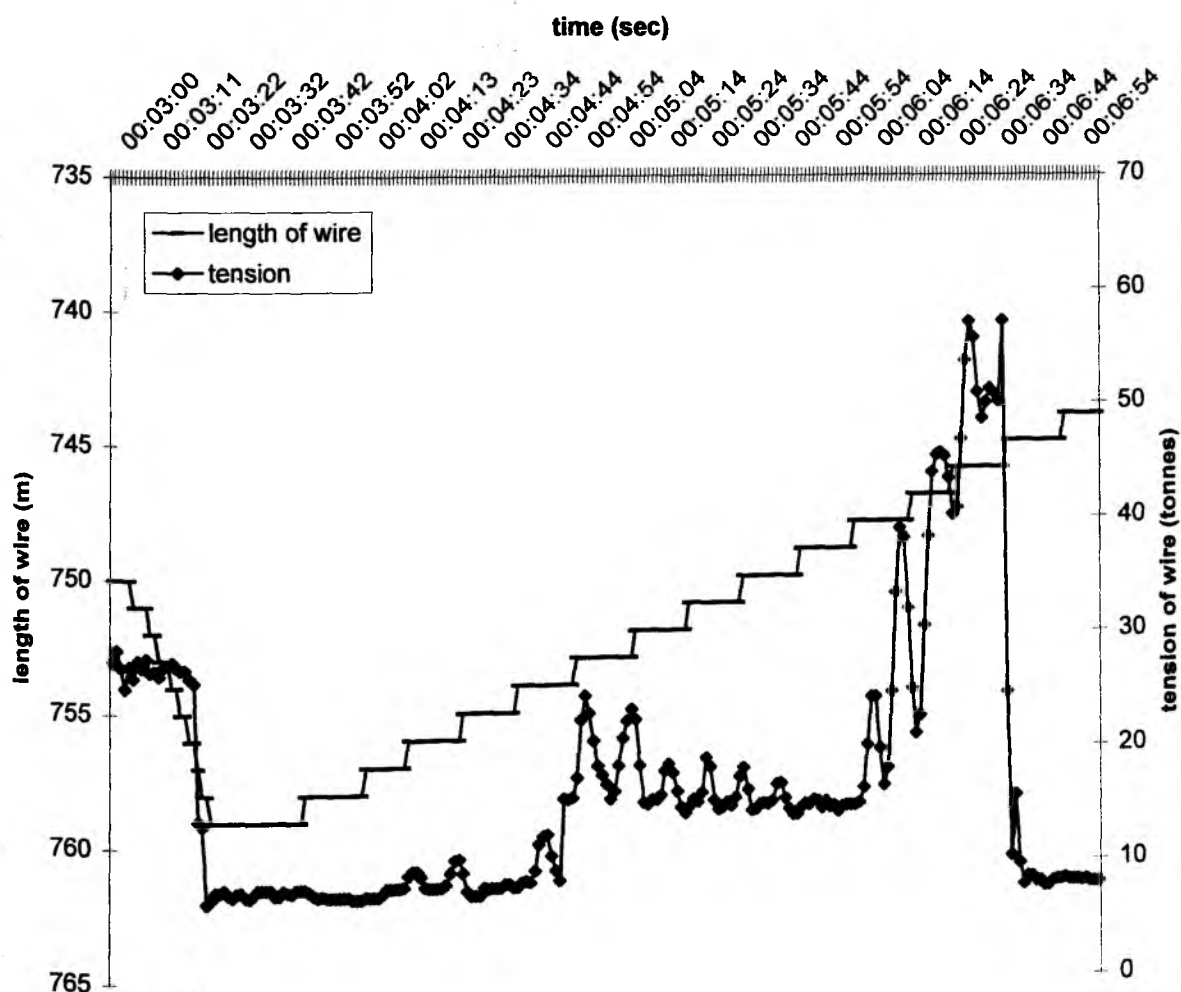
Fig. 80: Lenght and tension of wire during the loss of the AKL.

During the following slow heave with less than 0.1 m/s the first tension spikes occurred after 2,5 m which are probably related to the slow lift of the core liner into the pressure chamber. Later analysis indicate that some of the tension probably also resulted from the pilot corer being entangled below the round plate of the piston release mechanism. After heaving additional 7 m the tension of the wire increased

constantly. The variation in the tension record is mainly due to the heave of the ship. At 5,72 tonnes the wire broke and tension was suddenly reduced to the pure 0.7 tonne weight of the 750 m long wire. Pilot corer weight and release mechanism were retrieved, but the whole coring unit was lost at the bottom. The DGPS-position of the site is 44° 34,2120'N 125° 08,8603'W at the 30 of August 1999 00:03:22 (UTM). As the ship's heading at the time of the release was about 340° the exact position of the corer is about 20 m to SSE. The piston wire, which connects the coring unit to the ship's wire, had been torn out its socket with only a few wires actually sheared and shortened. Apparently the welding of these wires designed for a pulling force of more than 10 tonnes was not perfectly done. Tests with a slightly larger wire sockets for the little larger BGR piston corer did not break up to a pull force of 15 tonnes.

At the following day the AKL site was surveyed by the OFOS and the corer was found standing vertically on the core barrel, which had penetrated about 4 m into the bottom. The piston had been correctly moved to the top of the pressure chamber thereby closing the conical valve. Motivated by the intact and vertically standing device we attempted the following day to retrieve the corer. A 5 m high trapezoidal sling of heavy-load bands which were spread at its bottom by a 5 m long steel barrel was hooked by a 1,5 m broad steel pipe into the TV grab and lowered to the sea floor. During the fourth search profile the lost corer was detected and the sling hanging from the TV grab moved tangentially along the corer. In an attempt to override the about 6 m high corer, the TV grab was heaved and the upper part of the sling released by opening the grab claws. Unfortunately the upper sling fall to the same side as the lower part and the sling closed at the bottom without catching the corer. Thus the corer could not be retrieved. Later attempts with an improved sling design were impossible as weather conditions changed to high swell (sea state 5) and as the damage of the glassfiber wire during the last employment of the TV grab prevented its use.

It is planned to try a retrieval of the intact corer during the next SONNE cruise to the Hydrate Ridge in July / August 2000, possibly using the ROV ROPOS to assist the salvage operation.

4.5.2   Pressure and temperature preservation of gas hydrates

H.-J. Hohnberg

Samples collected by devices which preserve in situ pressure, temperature conditions can be stored in appropriate pressurized and temperature stable environments for several weeks or months. Thus samples can be preserved on board and transported to the relevant laboratory for later analysis. 80 cm long core sections with a diameter of 90 mm should be immediately transferred after the decompression of the pressurized corer into the pressure preservation box (PPB). 4 boxes are available. After insertion of the capped liner seawater is added and the ambient in-situ pressure is applied. A defined concentration of methane is added applying a partial pressure of 10 bar into the seawater filling the inner space of the sample box. The final pressure is created by adding seawater. The PPB must be stored under cold conditions.
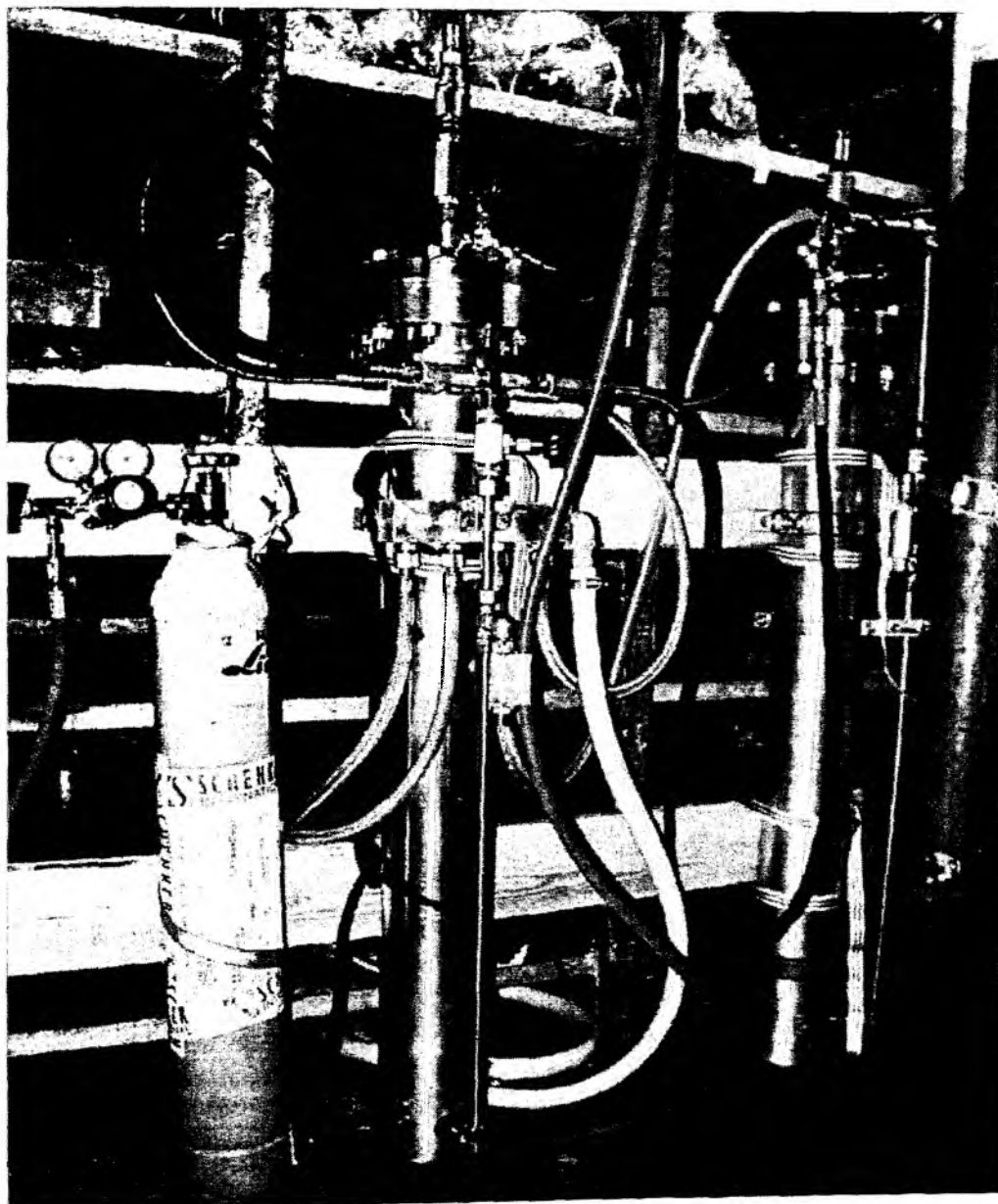
Fig. 81: Design of the pressure preservation system on bord of RV SONNE.

Function

The PPB (Fig. 81) is developed to preserve the high pressure, low temperature in situ conditions of seafloor sediments, which is important for the later analysis of chemical components or biological activity. The PPB is specially designed to preserve gashydrate in up to 80 cm long core sediments. After a short period of decompression of the corer in the coring device, when the core liners are cut into 80 cm sections, capped and the core should immediately transferred in a vertical position into the PPB.

After 80% filling the pressure chamber with seawater, the pressure chamber is closed, charged with a 10 bar methane pressure and finally pressurized to 100 bar. During the charging of CH4, which stream through a filter as gas bubbles into the chamber, part of the methane is dissolved, the other part is gathering in the compressed volume on the top of the PPB.

The final CH4 partial pressure is achived some hours later under a pressure of 100bar and a temperature of 2°C. The pressure is maintained by a central, water-filled pressure chamber (accumulator), which is fed by a controled pressure reducing device which its supplied from a pressurized air cylinder (10l-cylinder; 200bar). The pressurized air in the accumulator is seperated by a piston from the seawater. The PPB must be stored in a cool room at temperature of less than 10°C. In case the temperature rises above 14 °C rising internal pressure will open a safety valve and release methane into a gas tight plastic bag which is large enough to allow to store of 4x2 l decomposed gashydrate.

Operation on board RV SONNE

After installation of the PPB onboard RV SONNE in Astoria the pipe couplings of the hole system were checked and tightened to close possible transport leckages of the system. The following pressure tests were done with air at 4 bar pressure and with water at 100 bar. Small leckages were found and tightened. Initially it was planned to store the 4 PPB in a crate assembly in the cool room of SONNE, but with the restricted height of the cool room a vertical transfer of 80 cm long core would have been impossible. Therefore the PPB were mounted and fixed in a row along the wall of the cool room and connected with highly flexible pressure tubes (Fig. 81).

No pressurized core samples could be collected as the AKL was lost during its first employment at the 29. of August 99. Therefore at the 31 of August a certifical 75 cm long core was mixed by filling large pieces of gashydrate (totally 1,5-2 kg) and muddy sediment from the TV-grab (SO143-217). The core liner was capped and about 5 minutes after opening of the TV grab the core was tranferred into the PPB. Methane was added and a pressure of 100 bar was applied. The PPB showed no sign of leckage or a decrease of the pressure until the arrival of SONNE in San Diego at the 5 of September. The PPG remain onboard until G. Bohrmann will open it during one of the next cruises or will it transfer in a cooled container for transport to Germany. The three other empty PPBs will be transported by the BGR container back to Hannover and Berlin.

4.6   Geological sampling and sedimentology

4.6.1   Performance of equipment and sampling

E. Bracker, O. Klaus, A. Kopf, B. Teichert

During cruise SO143-3 of RV SONNE, the main attention regarding sampling of sediments, gas hydrates, pore water and carbonate precipitates was drawn towards the southern summit of Hydrate Ridge (see Fig. 56). In fact, the entire sampling with the various devices was carried out between 44°34.00'N and 44°35.00'N latitude and 125°08.00' and 125°09.50' W longitude. Three sampling tools were used to recover sediment, rock, and gas hydrate samples:

Table 23: Sample list of gravity cores taken during SO143-3 (Abbreviations: Biom.= biomarker, CD = core description, Meth.= methane, Pp.= physical properties, Pw.= porewater).

Station SO143-	Date [UTC]	Lat./Long.	Depth [m]	Recovery [m]	Analyses	Recovered samples
212	28. Aug	44°34.217°N 125°08.862°W	786.1	0.85	CD	meth., Pp, Biom., Pw.
215-1	29. Aug	44°34.205°N 125°08.830°W	785.2	-	-	Carb.
215-2	29. Aug	44°34.207°N 125°08.813°W	784.0	-	-	Carb.
219-1	30. Aug	44°34.207°N 125°08.866°W	785.0	1.38	CD.	Meth., Biom., Carb., Pp., Pw.
219-2	30. Aug	44°34.210°N 125°08.861°W	785.1	1.32	-	Carb.
219-3	30. Aug	44°34.213°N 125°08.867°W	788.0	0.90	-	-
221-1	31. Aug	44°34.210°N 125°08.814°W	784.5	1.05	CD	Pp., Pw.
221-2	31. Aug	44°34.211°N 125°08.811°W	785.1	1.18	CD	Meth., Biom., Pp., Pw.
229-1	02. Sep	44°34.211°N 125°08.810°W	786.1	1.10	CD	Pw., Piom., Carb.
229-2	02. Sep	44°34.207°N 125°08.813°W	786	0.30	CD	-
237	02. Sep	44°34.665°N 125°09.004°W	836.4	1.38	CD	Pp., Pw., Meth.
238	02. Sep	44°34.443°N 125°09.130°W	833.7	0.83	CD	Pp., Pw., Meth.

Gravity corer

A gravity corer was used at Stations 212, 215, 219, 221, 229, 237 and 238, with repeat runs depending on core recovery and quality. A core barrel segment of approximately 3.5 m length and 10 cm in diameter was used with a weight of 1200 kg. Both penetration and recovery varied considerably, which was mainly a result of sediment induration and the presence of gas hydrates in near surface layers. Penetration varied

between 1.5 mbsf (meters below seafloor) and 3.3 mbsf (Table 23). Consequently, core recovery also ranged from 0.3 to 1.38 meters (see Fig. 82). Cores recovered were mostly undisturbed, and are described below. A full list of samples taken for the different analyses can be found in:

Chapter 4.6.5:   Methane, biomarkers
Chapter 4.6.3:   Carbonates, physical properties, gas hydrates
Chapter 5:   Pore water geochemistry

Multicorer

A conventional multicorer was equipped with a deep-sea telemetry and one B&W and one colour video camera. The TV unit on RV SONNE is used both on the TV-multicorer and on the TV-grab (see below). The TV-guided multicorer (TV-MUC) was used four times, twice with and twice without the TV system operating. At Station 218, the mechanism to lock the core liners failed so that no samples were recovered. However, at Stations 220, 235 and 236, the TV-MUC was used successfully (Table 23). Up to four fibre glass tubes were filled at the time, gaining recovery of cores up to 30 cm (for details, see Table 24). One liner was sampled for pore fluid chemistry whilst the other three were dedicated to methane and biomarker sampling, physical properties sampling, sedimentary core description, and carbonate sampling (see below). A detailed list of samples taken with the MUC is given below (Table 26).

Table 24: Sample list of MUC stations. Abbreviations: bio = biomarker, me = methane, pp = physical properties, pw = pore water.

Station SO143-	Date [UTC]	Lat./Long.	Depth [m]	Cores [cm]	Analyses	Recovered samples
218	30. Aug	44°34.210°N 125°08.856°W	785.1	-	-	-
220	31. Aug	44°34.224°N 125°08.872°W	790.0	B - 22 F - 28	pw Bio, me, core descrip.	aragonite (6) carbonates (11)
				H - 23	pp	carbonates (9), clams (2)
235 non-TV	02. Sep	44°34.229°N 125°09.136°W	833.3	B - 18 D - 18 F - 19 H - 23	pw pp me, bio -	- core descrip. - -
236 non-TV	02. Sep	44°34.656°N 125°09.000°W	834.7	B - 31 D - 30	pw pp, me, bio	- -

TV-guided grab

The TV-grab onboard RV SONNE is equipped with two lights (150 W each) and the telemetry unit and two cameras, as described above. Power for lighting and the hydraulic unit is supplied by two deep-sea batteries. The sample size is roughly 100 x 170 cm.
The TV-grab was lowered from RV SONNE on four occasions, namely at Stations 214, 222, 228 and 233. As a consequence of technical problems and flat batteries, the

operation at Station 228 could not be completed and the use of the grab was unsuccessful. In each of the other three cases, more than 1000 kg of bulk rock sample were recovered (see Table 25 for details). The first two sampling stations focussed on gas hydrate recovery whilst at station 233, authigenic carbonates were aimed for. For sedimentological and gas hydrate description, see Chapters 4.6.2, 4.6.3. and 4.6.4. below).

Table 25: List of samples taken with the TV-grab.

Station SO143-	Date [UTC]	Lat./Long.	Depth [m]	Analyses	Samples
214	29. Aug	44°34.208°N 125°08.825°W	744	-	carbonates, clams (49), gastropods (17), gas hydrates
222	31. Aug	44°34.238°N 125°08.843°W	772	-	carbonates
227	01. Sep	-	-	-	-
228	01. Sep	-	-	-	-
233	02. Sep	44°34.263°N 125°08.889°W	908	-	carbonates, clams (13 living Acharax)

4.6.2 Preliminary sedimentological results

A. Kopf, B. Teichert, C. Jung, J. Johnson, A. Stüber, M. Elvert

In this section, we will give a brief overview of the sediments recovered by mainly TV-MUC and gravity corer; TV-G does not allow recovery of intact sedimentary surfaces. In total, seven longer cores and a set of short push cores (TV-MUC) in three locations recovered sediments up to 138 cm thick (see Table 23).

The main lithology found is mud of olive grey colours. The muds recovered are dominated by clay minerals, with considerable amounts of fine to medium silt. These sediments are soft near the sediment-water interface, but rapidly undergo compaction and induration. Their uppermost part (generally uppermost 20-25 cmbsf) is fairly homogeneous and does not exhibit sedimentary or deformational structures. Here, occasional clam shells (often Acharax) are found. Below this homogeneous interval, the muds and mudstones are indurated to semi-consolidated, and apparently have undergone pervasive fracturing.

Depending on their water content, the lithologies either have a broken, scaly texture with subangular shards and fragments, or appear mousse-like with gaseous pockets and soupy intervals. The latter is interpreted to be a result of gas hydrate dissociation (see also section 6.4.4.), whilst dry, fragmented intervals seem to originate from water loss in the vicinity of gas hydrate layers. This hypothesis is supported by pore fluid chlorinity and, to a lesser extent, alkalinity (see chapter 5 below). Independent of the fragmented (dry) or moussy (wet) nature, both types of sediments are accompanied by strong smells of hydrogen sulfide. In addition to the described textures, a bedding-plane parallel compaction fabric can be seen. Occasional slickensides are found on some of the fragments and mudclasts, suggesting some tectonic deformation. In one

core (SL 229-1), a gradational change from clay near the mudline over slightly consolidated to firm clay can be seen. In the slightly consolidated clay, pieces with intact internal structure are >10 cm long, while further below in the more consolidated part of the succession, fragments reach generally 2-3 cm or less. In all the other cores recovered, the change from unconsolidated highly porous clays and silts near the seafloor to clay(stone) beneath is rather abrupt (e.g. SL 219-1, 52 cmbsf; see Fig. 82) Here, the difference in induration suggests a hiatus to the overburden.

Table 26. List of station localities where sediment sampling was conducted during cruise SO143-3. Regarding the equipment used, the following abbreviations are: TV-G = TV-grab, SL = gravity corer, and TV-MUC = TV-operated multicorer. The carbonate classification follows the one in the text (see below). The occurrence of solid gas hydrates when the core came on deck is indicated by a „X".

Station No. SO143-	Device	Carbonates						Physical properties	Gas hydrates
		I	II	III	IV	V	VI		
212	SL	x						x	
214	TV-G	x		x	x				x
215-1	SL			x					
215-2	SL			x					
219-1	SL	x	x					x	
219-2	SL	x	x						
220	TV-MUC			x	x			x	x
221-1	SL							x	x
221-2	SL							x	x
222	TV-G	x	x	x	x				x
229-1	SL		x						x
233	TV-G	x	x	x	x	x	x		
235	MUC							x	
236	MUC							x	
237	SL							x	
238	SL							x	

Occasionally, the clayey succession is overlain by silts or clay-bearing fine sands (Stations 235, 237, and 238). These deposits are of olive grey to dark grey colour (see Fig. 82). Their thickness ranges from only 4 cm (SL 238-1) to up to 22 cm (SL 237-1). The homogeneity suggests accumulation as proximal deposits on the Astoria Fan prior to incorporation into the accretionary prism. No evidence has been found for a turbiditic origin or mass wasting processes. Silty layers, which have been recovered at Stations 237 and 238, are dominated by quartz and dark grey to black, largely subrounded particles. The latter may represent lithic fragments, which were derived from recycled orogenic crust of the Washington-Oregon margin, and which now are frequently found in the Cascadian forearc (see Behrmann et al., 1995).

In some of the gravity cores, indurated to well cemented calcareous layers were penetrated, the most prominent of which occurred at 61-69 cmbsf in Core SL 219-1 (see Fig. 82). These layers are homogeneous in texture, olive grey in colour, and

Fig. 82:. Graphic representation of gravity cores.
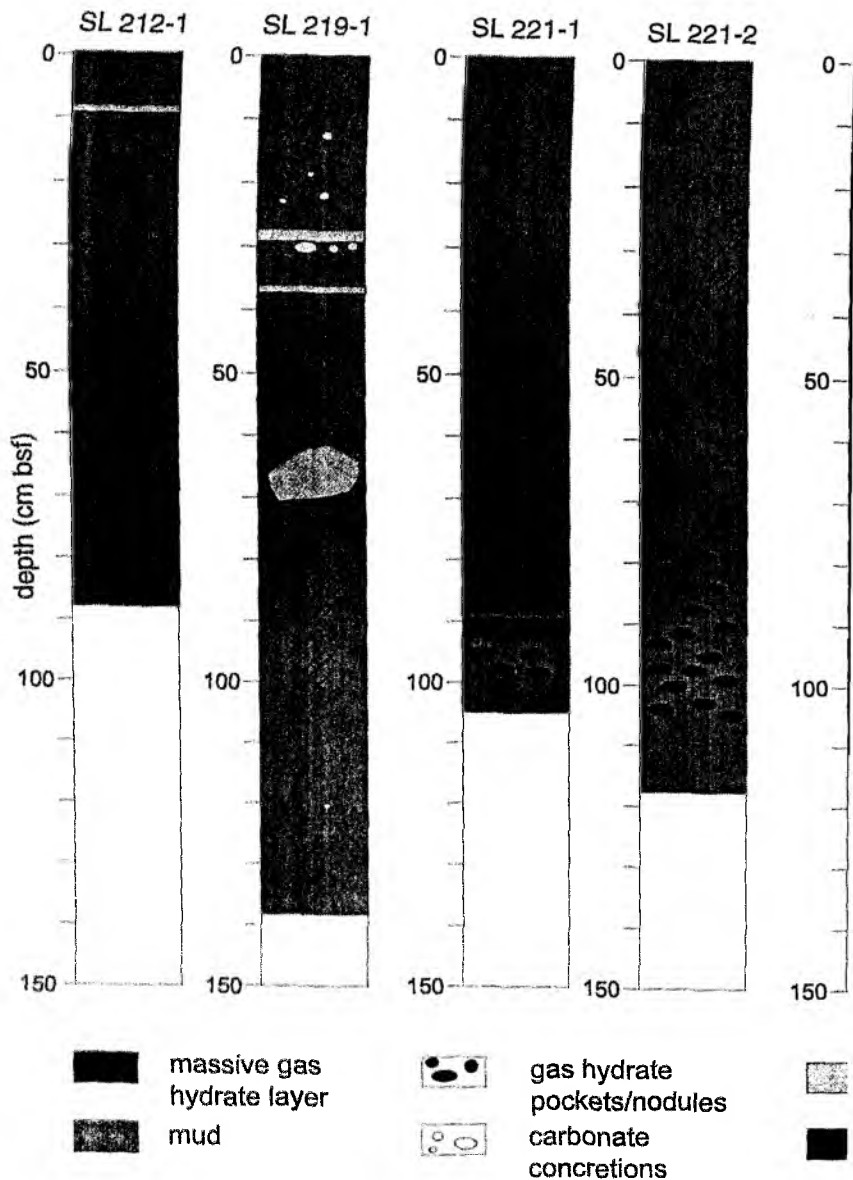
SL 229-1   SL 237-1   SL 238-1   TV-MUC 220

depth (cm bsf)

TV-MUC 235

depth (cm bsf)
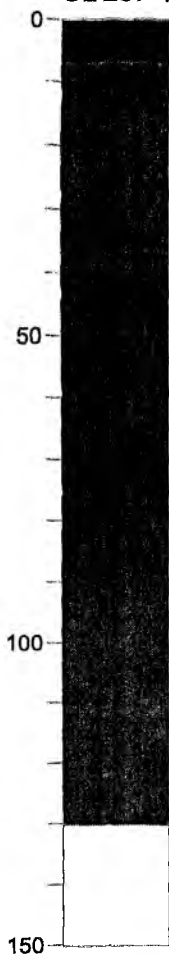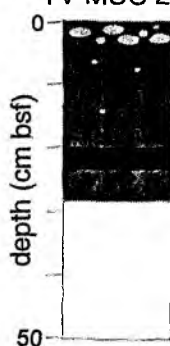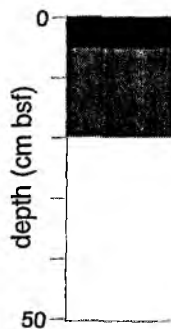
carbonate-cemented layers

silt/fine sand layers

shell fragments

broken formation, scaly clay
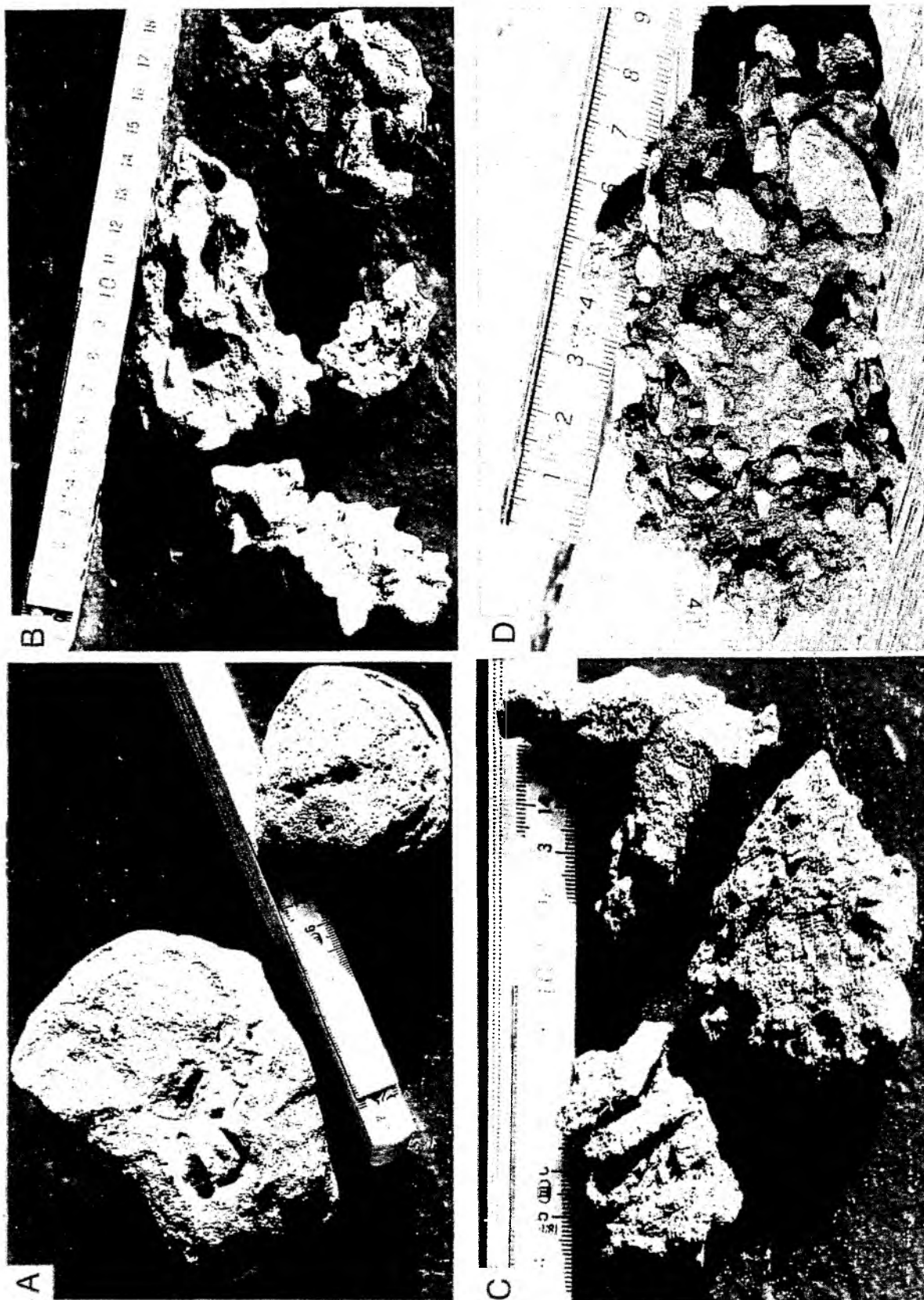
Fig. 83: Photographs of carbonate rock fragments recovered during R/V Sonne cruise SO143-3. Four major type examples are shown: (A) Massive carbonate concretions; (B) Aragonite crusts: (C) Carbonate sinter, and (D) Chimney precipitates with subrounded clasts. These particular specimens were all found in TV-G 233, however, similar rocks were observed in samples taken in the vicinity.

largely 1-2 cm in thickness (e.g. SL 212-1. Because of the cementation, they are described with the carbonate rocks (section 6.4.3.). Small (< 1cm in diameter) carbonate nodules are found scattered within muds and mudstones. They are light grey to yellowish in colour, and subrounded in shape.

Massive gas hydrate pockets, platy fragments, and layers were also recovered in gravity cores and TV-multicorer (e.g. in Cores SL 221-1, 221-2, and 229-1, or TV-MUC 220; see Fig. 82). A separate chapter (section 4.6.4.) is dedicated to their detailed description.

Despite no biostratigraphic dating has been done aboard RV SONNE, a comparison with previous cores (and namely ODP Leg 146 drillcores; see Westbrook et al., 1994) suggests an age from Quaternary to late Pliocene. Whilst the uppermost part of the succession is generally undisturbed, unconsolidated fine-grained muds and silts, the mud at depths of a couple of decimeters already shows considerable overconsolidation. This induration is a result of both compaction-driven dewatering and cementation due to carbonate precipitation. Indurated muds and mudstones are often fragmented to subangular chips and bisquits, with two mechanisms regarding its deformation being discussed: Either the already indurated mud has undergone pore fluid expulsion and tectonic deformation (e.g. hydrofracture) in the accretionary setting, as is suggested from scaly fabrics and slickensides seen along some of the chips (e.g. Clennell and Maltman, 1995); Or alternatively, the presence of solid gas hydrate may have caused destruction of the fabrics, as seems likely when the texture is compared to sections where massive gas hydrates interbedded with the sediments are recovered (see section 4.6.4. and Fig. 82). This relationship between destroyed, sometimes mousse-like textures, and the former occurrence of gas hydrates has been tried to establish elsewhere in the Cascadia forearc (Kastner et al., 1995).

4.6.3   Carbonates

A. Kopf, B. Teichert, C. Jung

Authigenic carbonates have been associated with fluid venting, which is well-documented in the Cascadia accretionary prism (e.g. Ritger et al., 1987; Sample and Kopf, 1995). Studies related to cruises SO109/110 have provided evidence for a great variety of carbonate precipitates in the area (Greinert, 1999). Carbonate concretions, calcareous crusts, and carbonate-cemented mustones occur throughout the sediments recovered at stations 212, 214, 219, 220, 222, 228, 233, but not in cores from the reference sites west of the Hydrate Ridge southern summit (Stations 235-238; see Figs. 5 and 82). Carbonate occurrences were as patches or layers (usually slighly lighter colours than the surrounding muds/mudstones), i.e. of primary origin, but mainly as cemented or precipitated crusts (incorporating the clayey matrix nearby as mudclasts) or lensy concretions. Based on their texture and composition, a preliminary distinction into six types of carbonate deposits has been performed:

1) Carbonate layers and patches (e.g. SL 212-1, SL 219-1) are the only carbonate deposits found which are believed to be of primary origin (i.e. containing considerable amounts of biogenic carbonate). These deposits occur usually as thin (c1-2 cm thick)

layers of light grey to olive grey colour, and are characterised by their increased firmness in comparison to the surrounding sediment. In general, these continuous beds follow the sedimentary layering and do not cross-cut bedding planes, so that a primary origin is suggested. However, at this preliminary stage we cannot exclude formation in the vicinity to gas hydrate layers (where removal of pore water may have led to brine-like pore water chemistry, and consequently carbonate cementation due to precipitation; see section 4.6.4. below).

2) Carbonate concretions are found at stations 214, 219, 222 and 233 (Fig. 83 and Table 26). In places, they can reach up to 45 cm in length (TV-G 222-1). In general, the concretions are massive, fine-grained carbonates of subrounded to rounded shape (Fig. 83A). Colours range from light grey to olive grey when fresh surfaces are regarded, however, some specimens show a brown and dark olive grey patina which may originate from exposure on the seafloor. Most of the samples are moderately bioturbated, with the burrows not having been filled. In places, layering on a mm-scale (most likely a result of concentric growth) is preserved during carbonate replacement. A total of c15 samples of this type was found during SO143-3.

3) Aragonite crusts of variable geometry and colour were mainly found sampling with the TV-grab at stations 222, 228 and 233. They occur largely (>25 samples altogether) as crusts or rocks of irregular shape (Fig. 83B), and rarely (<5 samples) are seen as elongated precipitates of former burrows. The colours range from white to very light grey. Two types of aragonite crusts are observed: (a) The typical crusts exhibit odd geometries and have mud and mudstone clasts up to 3 cm across incorporated. The aragonite can be easily distiguished from mudclasts, but also other calcareous components by its light, off-white colour. The largest crusts found were 20 x 15 cm in size. (b) On occasion (especially in TV-G 222-1), the aragonite crusts showed two generations of precipitation. The generally platy specimens revealed a 1- to 2-mm-thick yellow aragonite layer over their surface, which itself got precipitated as a coat on top of a white layer of aragonite cement. Both coats got cemented on top of a well-indurated calcareous layer of c2 cm thickness.

4) Micritic cement carbonates are the most common calcareous deposits observed during SO143-3 (Fig. 83C). It is interpreted as the precipitate from sulfate- and methane-rich pore fluids, which can occupy most of the remaining pore space of their host sediment. A total of >>150 samples was recovered at stations 215, 222, 228, and 233 (see Fig. ?). Almost half of the „sinter“ rocks are irregular in shape while the other half is platy and resembles sedimentary layering. Less common, sinter is precipitated in bioturbated areas and burrows, leading to bone-shaped, elongated rocks. The majority of the carbonate sinter is olive grey (5Y 4/2) after recovery, but fades slightly when dried. Often, subangular mudclasts (of the same olive grey colour) are incorporated into the rocks. Clast sizes are generally small (0.5 to 2 cm in diameter). The specimen size varies widely, but rarely exceeds 15 cm in length. It remains under debate whether the smaller pieces recovered were previously part of a bigger aggregate (especially likely for platy, layer-type samples). The size may be also a function of induration, because both well lithified rocks are found next to semi-consolidated ones.

5) Light grey carbonate crusts are one of the less commonly found carbonate rocks on the southern summit of the Hydrate Ridge. However, four pieces of considerable size (the largest c20 x 15 x 3 cm in size) were grabbed with TV-G 233-1. By comparison with sinter (type 4, see above), they show a considerably reduced specific weight (porous internal structure?) and a significantly paler colour (light grey as supposed to olive grey). Their texture is homogeneous with only a few mudclasts incorporated, so that a preliminary conclusion would be a formation at the seafloor, and not within the sediment pile. On the other hand, no lamination (from e.g. step-wise growth or several generations of precipitation events) is seen.

6)"Chimneys" (i.e. precipitated fluid conduits) are distinguished from both carbonate sinter and light carbonate crusts (types 4 and 5, see above) by two characteristics: their shape and the clasts they have imbedded (Fig. 83D). They were recovered only at station 233, however, nine pieces of up to 12 cm length were seen. Concerning their shape, some specimens are typical concentric micro-chimneys with a tubular structure which has preserved a conduit in the centre (like the example in Fig. 83D).

Samples with irregular geometries may be parts broken out of the walls of bigger chimneys. Second, the size and the shape of the clasts which were incorporated into the chimney wall are very different from the sinter specimens. The main characteristic is the subrounded to sometimes rounded shape, which suggests either abrasion due to transport from depth within a conduit (or along a fault plane), or dissolution processes. At this preliminary stage, none of the hypothesis can be favoured, and additional investigation is needed. Application of 0.1N hydrocloric acid revealed that not the entire set of clast lithologies is calcareous so that an explanation of the shape by dissolution appears unlikely. Also, the clast size is fairly homogeneous, which may be envisaged as an effect of sorting due to transport. At present, we lack geophysical evidence of a prominent fault cropping out at or adjacent to the southern summit.

4.6.4   Gas hydrates

G. Bohrmann

During Leg SO143-3 several gas hydrate samples were recovered by gravity corer and by TV-guided grab from southern summit of Hydrate Ridge (Fig. 56; Table 26). Pure gas hydrate occurred in layers or joints several millimeters to decimenters thick. The layers are generally oriented parallel to bedding planes obliquely (Fig. 84). Gas hydrate often filled large pore space either as fractures or joints, or seemed to create its own space during growth by fracturing or pushing apart the sediment framework, most often along bedding planes. The internal fabric of pure gas hydrate showed a peculiar structure with large pores which remember to methan bubbles. Such pores occured in variable sizes and indicated that free methane gas was intimitely involved with the formation of these hydrates. A collection of various fabrics is shown in Fig. 84.

Fig. 84: Images of gas hydrate specimens with layered remnants of mud.

4.6.5   Methane in sediment cores from Hydrate Ridge

M. Elvert, A. Stüber

Introduction

Upward-diffusion of methane in marine sediments is stimulated by fluid venting along subduction zones all over the world. Critical regions for fluid escape are trenches, deformation fronts, and initial accretionary ridges. Tectonic compaction, heating and volatile generation pressurize the pore fluids and drive much of the interstitial fluids and gases of the prism sediments upward. Parts of the methane-charged fluids escape into the seawater, either by diffuse pore fluid expulsion or by focused venting along tectonic fractures, resulting in near-bottom water methane anomaly patterns which directly indicate dewatering and degassing sites in subduction zones. Such "cold seeps" have been known for more than a decade now and are still an intriguing process for marine geoscientists and ocean scientists. Venting affects the presence and abundance of benthic communities and precipitates of authigenic carbonates which result from biogeochemical turnover and interaction between fluids and ambient bottom water. Growth and metabolism of the vent fauna are based on a chemosynthetic food chain which starts with the microbially-mediated oxidation of reduced inorganic and organic compounds such as hydrogen sulfide or methane.

At Hydrate Ridge, the accelerated discharge of fluids dramatically stimulates benthic material turnover that is in orders of magnitude higher than normally found at comparable ocean depths (Suess et al., 1999) Generally, gas hydrates form in methane-rich sediments as "ice-like" clathrate structures in which methane is occluded within a water lattice under conditions of high pressure and low temperature. The stability of methane-hydrates in marine sediments is limited to bottom-water depths exceeding 300 to 500 m (Kvenvolden, 1995). In addition, hydrate stability is influenced by porewater salinity, the geothermal gradient and the inclusion of other gases in the clathrate structure such as ethane, propane or hydrogen sulfide. Gas hydrates are widespread in sediments of the world's oceans with amounts of carbon which may exceed that of all fossil fuel deposits (Kvenvolden, 1988). Because methane hydrates contain so much methane and occur at moderate water depths within the geosphere, they are of special interest as a potential source of atmospheric methane released by global warming.

Materials and methods

Sediment analysis used for the determination of methane concentrations have been described previously (see SO 143 1a/1b and SO 143-2 for details). Briefly, at each station 3 ml of sediment were taken from different depths within a core to obtain a methane depth profile. Sediments were transferred into 20 ml vials, mixed with 5 ml of 1 M KOH, and sealed gas tight. For faster equilibration between the sediment-water and gas phase the vials were shaken for 24 to 36 h. Finally, analysis of an aliquot of headspace methane (100 µl) was performed using a Shimadzu gas chromatograph equipped with an flame ionization detector. Additionally, some stations were sampled for carbon isotope analysis using gas chromatography-combustion-isotope ratio mass spectrometry (GC-C-IRMS) on shore.

a)

b)
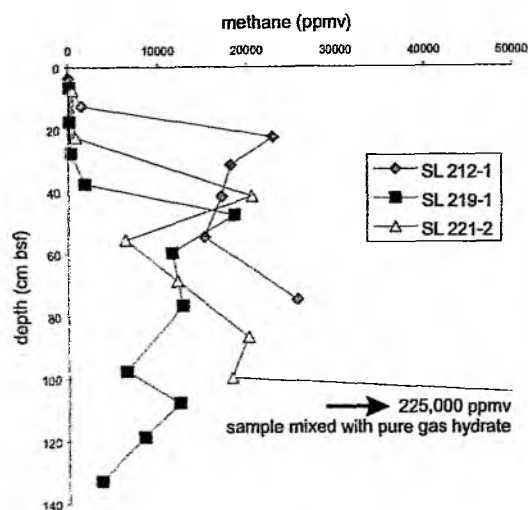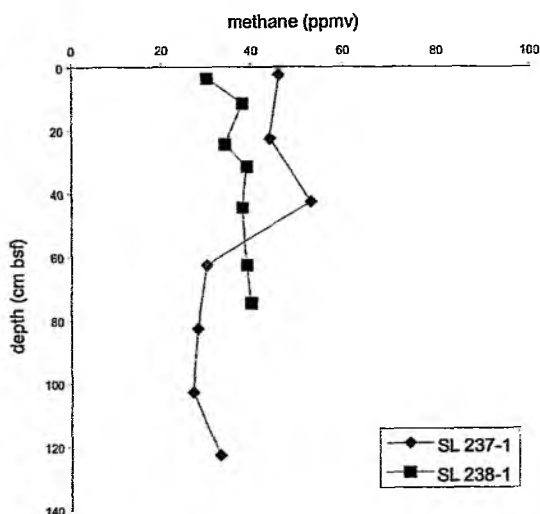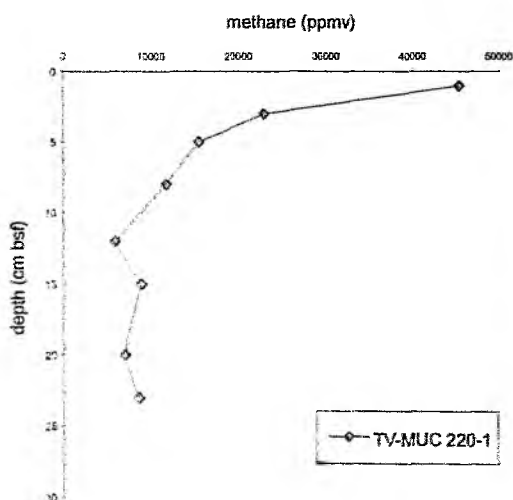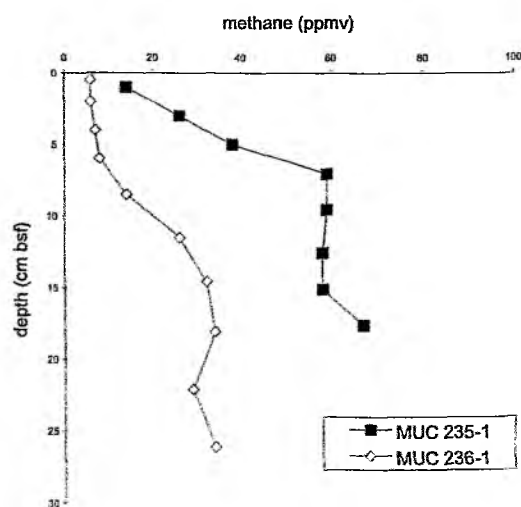
Fig. 85: Methane depth profiles within sediment cores recovered from the southern summit of Hydrate Ridge and various background stations. (a) gravity cores, (b) TV-guided multicorer cores. Please note the different scales used for sediment cores with and without gas hydrates.

Preliminary results

Sediment cores analyzed during SO143-3 were taken either directly from the southern summit of Hydrate Ridge or background stations located northeast from the southern summit. Whereas the cores from the southern summit contained evidence of abundant gas hydrates they were completely absent from the background cores. This results in different methane concentrations and depth profiles (Fig. 85 a, b).

For all gravity cores from the southern summit, methane concentrations increase dramatically up to 3 orders of magnitude at a depth where the sediment starts to show gas hydrate pockets (SL 221-2; 60 cm bsf) or where carbonate-cemented layers occur (SL 212-1 and 219-1; 20 cm or 30 cm, respectively) (for details see Fig. 85). These distinct depths might correlate with a depth at which gas hydrates are at their destabilization boundary. Concentrations for these sediments are usually up to 25,000 ppmv whereas the background cores show very low concentrations of around 50 ppmv (Fig. 85a). Even higher concentrations of over 200,000 ppmv were obtained for a sample which was mixed with pure gas hydrate. But generally, further downcore all methane profiles within gravity cores from the southern summit of Hydrate Ridge slowly decrease in concentration what indicates gas hydrate stability more than destabilization.

In contrast, gas hydrate containing surface sediments recovered with a TV-guided multicorer reveal an inversed methane depth profile with maximum methane concentrations of up to 45,000 ppmv (Fig. 85b). Mostly, such locations are indicated by bacterial mats overlying the sediment surface, abundant small scale carbonate concretions at the first centimeters of the core, and the occurence of gas hydrates very close to the sea floor. This probably explains the reversion of the methane depth profile because gas hydrates within these depths lay outside their field of stability. Again, background stations with none of these features contain methane concentrations not higher than 60 ppmv.

4.7   Pore water chemistry

D. Rickert, B. Domeyer, R. Surberg

Introduction

During the third leg of SONNE cruise 143 (SO143-3) geological sampling was planed to extend to a new sampler, the autoclave piston corer of BGR Hannover (Chapter 4.5.1). Long sediment cores containing gas hydrates should be collected under in-situ pressure conditions with this technology. It would have been interesting to study the pore water chemistry since the data would have provided more information about the mechanisms and consequences of hydrate formation and decomposition at actively venting sites.

The outstanding feature in the pore waters during SO143/1b cruise were the concentrations of chloride at the bottom of the core where we recovered extremely dry sediment surrounding almost undecomposed gas hydrate so that dilution of the pore waters was minimized. Through extraction of fresh water from the pore waters massively enriched chloride concentrations (~ 800 mM), almost 50 % enrichment compared to mean seawater concentrations were observed (see Chapter 2.7). A possible limitation of gas hydrate formation through the water content of the surrounding sediments is possible. Unfortunately, the recovery of the piston core failed during the first deployment so that we gained no pore water data under almost *in-situ* conditions.

Nevertheless, TV-controlled multiple corer as well as gravity corers were sucessfully deployed during this cruise and complemented the data base of the geochemical environment on the southern summit of Hydrate Ridge.

Samples and analytical methods

Table 27: Types of analysis performed on pore water.

ANALYSIS STATION	PO$_4$ [µM]	NO$_2$ [µM]	NO$_3$ [µM]	NH$_4$ [µM]	H$_2$S [mM]	Cl [mM]	TA [mM]	SiO$_2$ [mM]	pH pore-water	core depth [cm]	number of samples
I. Hydrate Ridge											
Southern summit											
212-1-SL	x			x	x	x	x	x	x	85	10
214-TVG	x			x	x	x	x	x	x	–	2
219-1-SL	x			x	x	x	x	x	x	138	14
221-1-SL	x			x	x	x	x	x	x	105	11
221-2-SL	x			x	x	x	x	x	x	118	26
229-1-SL					x	x	x	x		110	21
II. Reference sites											
NW southern summit											
235-1-MUC	x	x	x	x		x	x	x		18	13
236-1-MUC	x	x	x	x		x	x	x		28	17
237-1-SL	x	x	x	x		x	x	x		154	15
238-1-SL	x	x	x	x		x	x	x		83	10
										total of samples :	139

for most MUCs oxygen of bottomwater was measured (titration)
TA, Cl. = titration; PO$_4$, NO$_2$, NO$_3$, NH$_4$ = autoanalyser; H$_2$S, SiO$_2$ = photospectrometer

Pore water

Pore waters were recovered and processed as described in the previous Cruise Reports (SO143-1b, and 2). Since we were especially interested to characterize the pore water signature in the vicinity of almost undecomposed gas hydrates which should have actually been realized with the autoclaved piston corer rapidity was important with the recovery of gravity cores in which gas hydrates continuously decompose. Techniques used for pore water analysis and modifications due to high hydrogen sulfide concentrations are described inChapter 2.7.

Acidified subsamples (10 µl HCl (30 %)/1 ml sample) were prepared for ICP analyses of major cations (Na, K, Li, Mg, Ca, Sr, and Mn). Sulphate, bromide, DIC and $\delta^{13}C$ will be determined on selected subsamples in the shore-based laboratory.
A synopsis of cores, numbers of samples, subsampling, and geochemical analysis performed on board is listed in Table 27.

Results and discussion

Preliminary results about the distribution of nutrients, chloride and total alkalinity in the pore water of gravity cores and TV-guided multiple cores either at on-vent or off-vent sites are given and discussed in the following. Results performed on board are illustrated in Figs. 1-10.

Pore water composition at on-vent and off-vent sites

During Legs SO143-1b and 2 sampling strategies were concentrated on TV-guided multicorer and TV-grabs in order to monitor the pore water situation of surface sediments at an on-vent area with a full scale of biological phenomena which are associated with the occurence of pore water enriched in hydrogen sulphide and methane in contrast to off-vent sites. Here, only two reference stations on Hydrate Ridge were analysed by multicorer (Figs. 86 and 97).

Typically for these reference sites are non-detectable concentrations of H_2S and consequently low TA values. During this cruise pore water sampling was focussed on gravity corer deployments and should provide more information about the occurence of gas hydrates and geochemical environment in deeper zonations of the sediments on the Southern Summit of Hydrate Ridge in comparison to slightly northwestern reference sites.
In Figure 88 the pore water data of the surficial sediments (~130 cm) of two sites are directly compared. The pore water on the Southern Summit (219-1 SL) show high total alkalinity and sulfide values whereas at the reference site (237-1 SL) concentrations are almost equal to the overlying water column. Figs. 89 and 90 show further results of gravity cores deployed on active venting sites of the Southern Summit, in Fig. 91 results from a second reference site are illustrated. Relatively low ammonia/alkalinity and ammonia/sulfide ratios on the Southern Summit can only be explained by mainly anaerobic methane oxidation that produces sulfide and alkalinity without generating ammonia and other organic matter degradation products:

$$CH_4 + SO_4^{2-} \rightarrow HCO_3^- + HS^- + H_2O \tag{1}$$
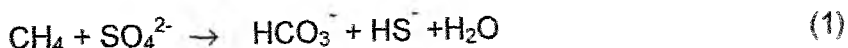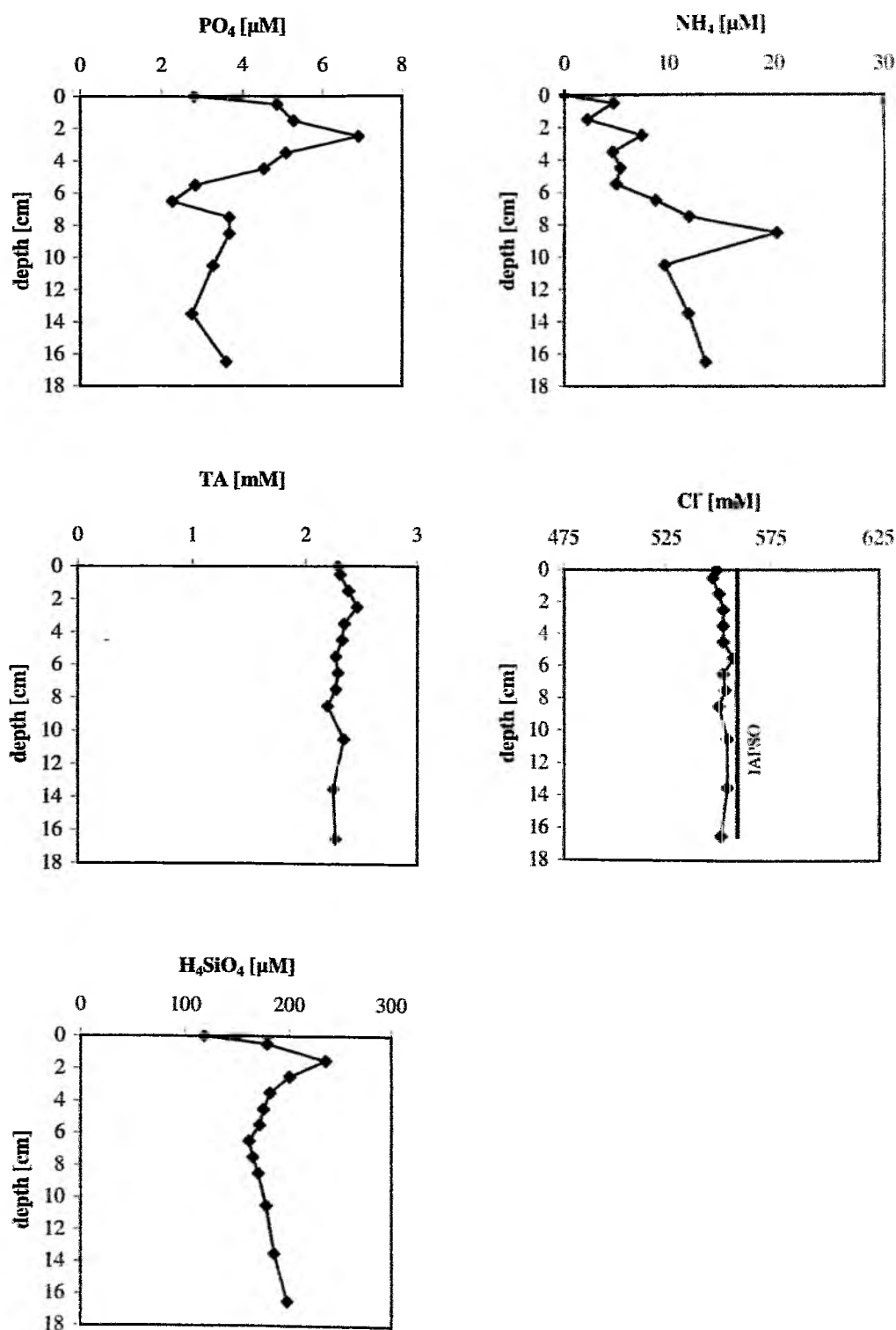
Fig. 86: Pore water chemistry of 235-1-MUC. H$_2$S was not detectable.
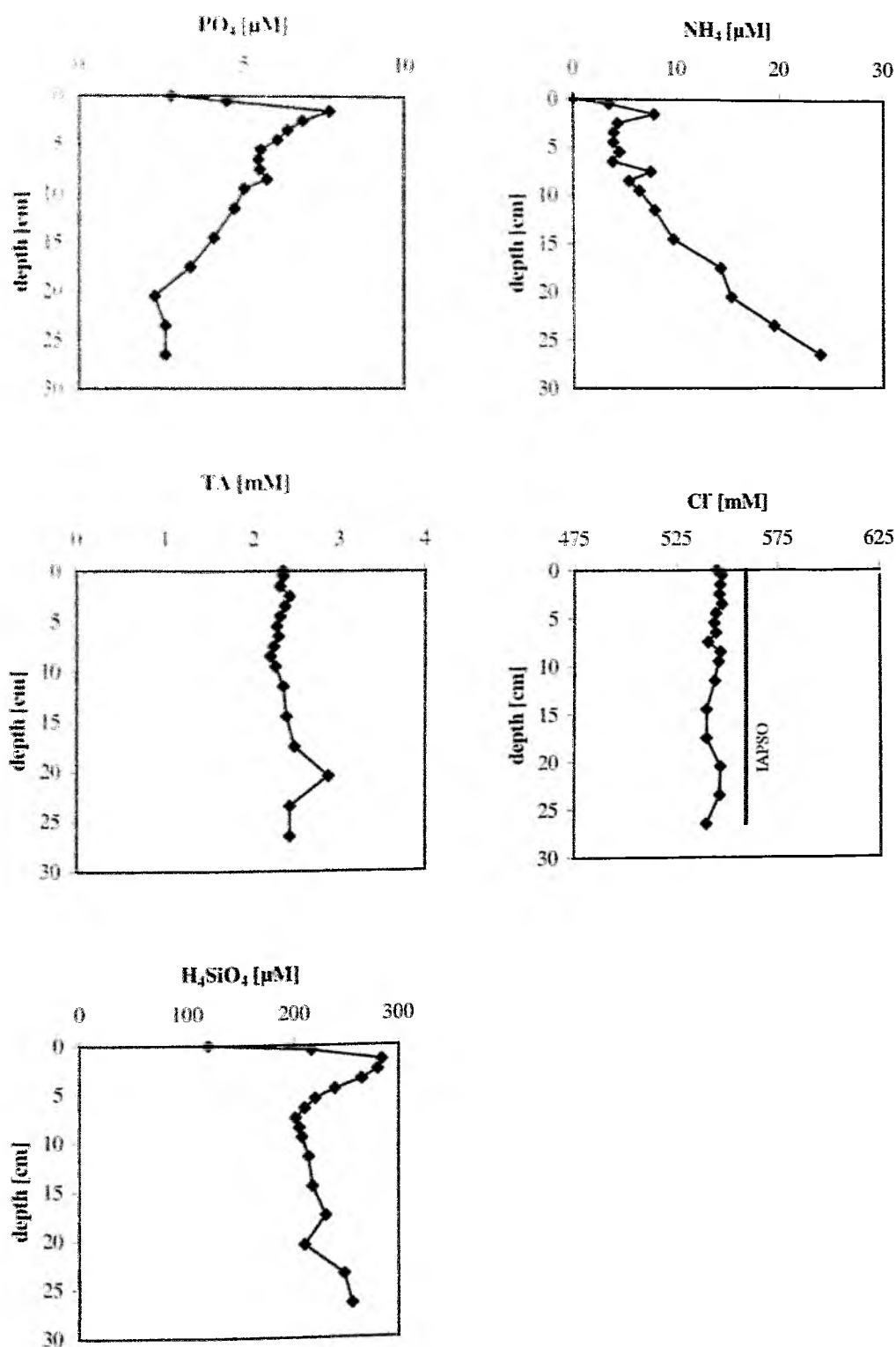
Fig. 87: Pore water chemistry of 236-1-MUC. H₂S was not detectable.
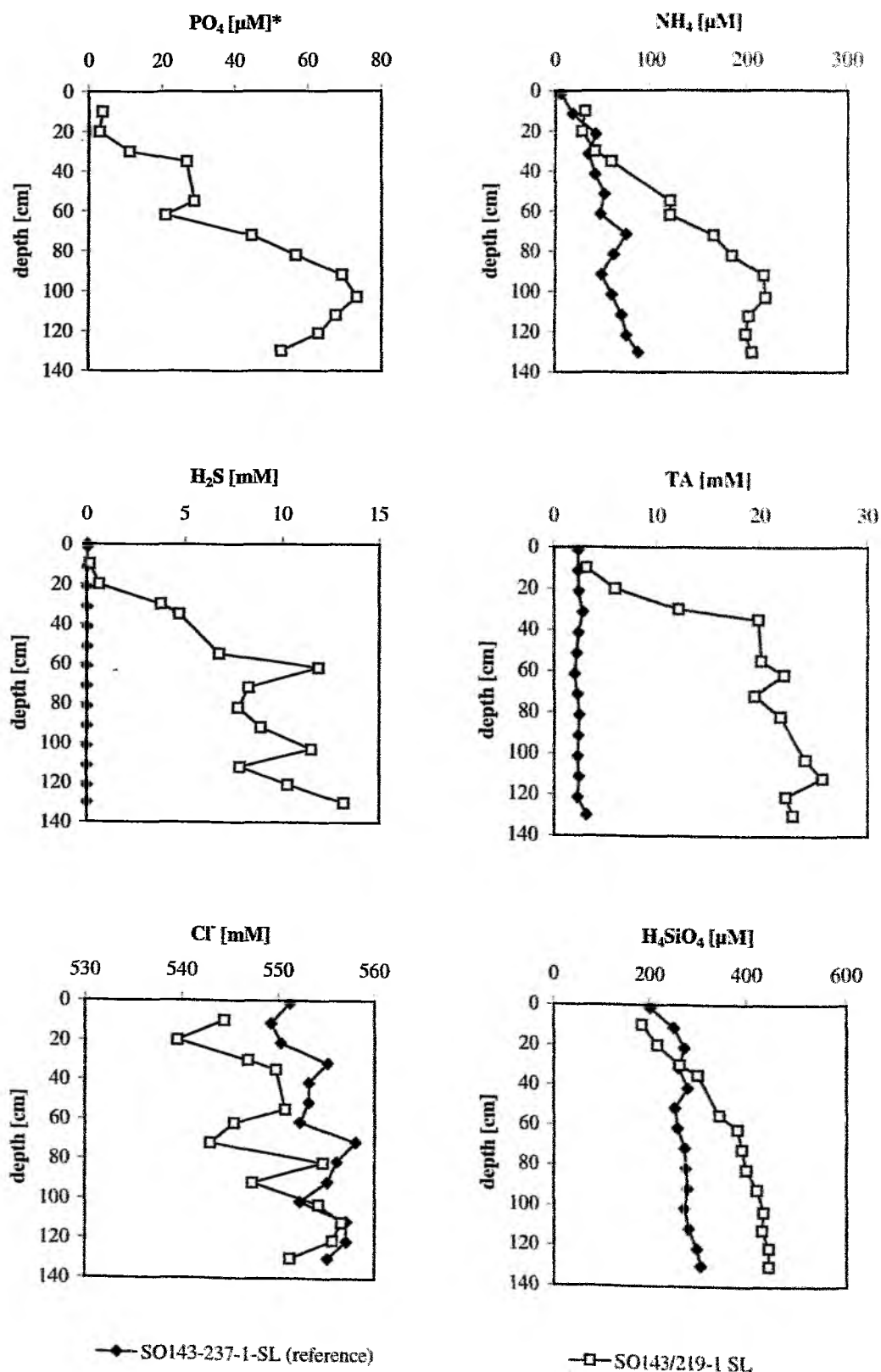
Fig. 88: Pore water chemistry of 237-1-SL and 219-1-SL. * No data available for SO143-237-1-SL due to analytical problems.
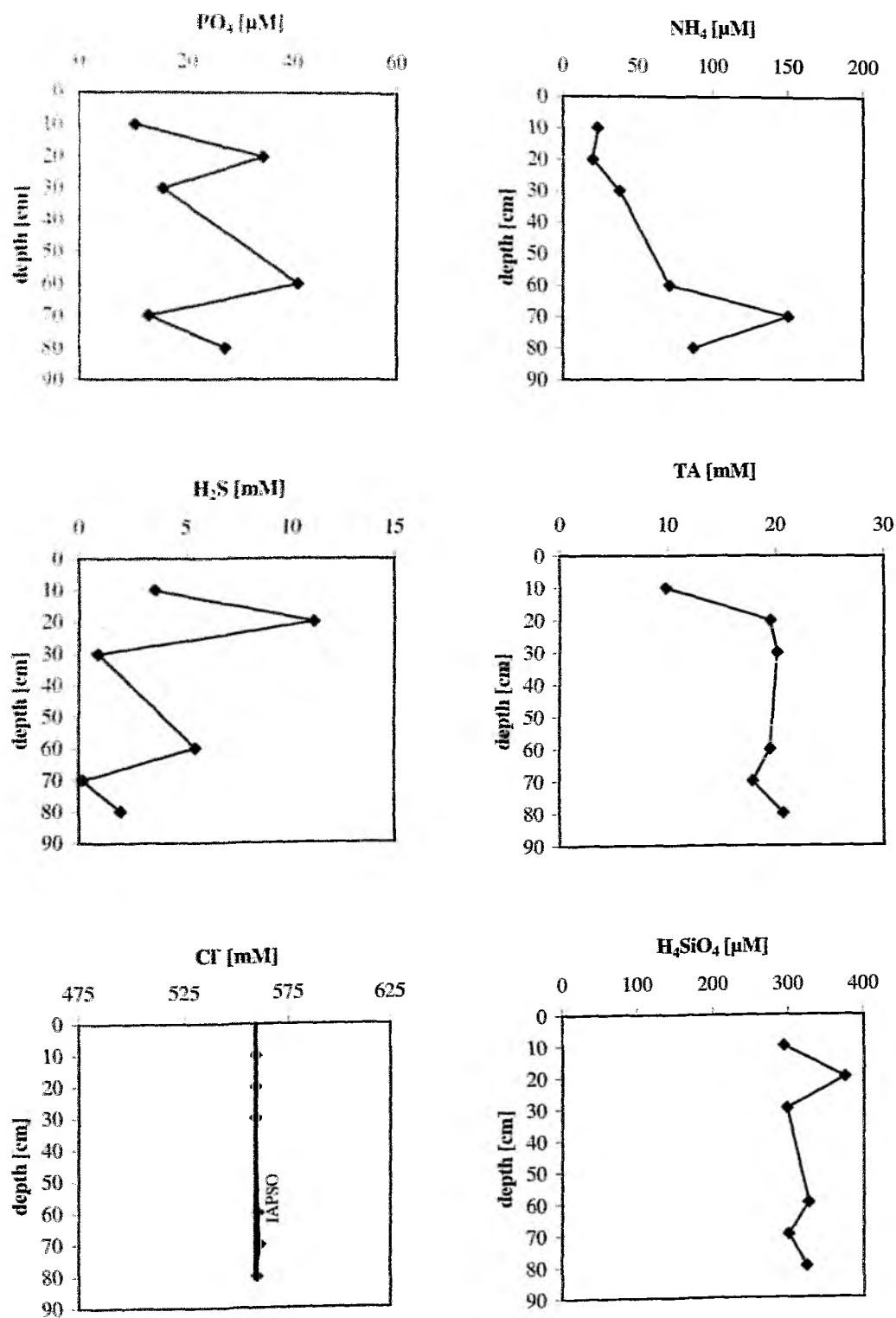
Fig. 89: Pore water chemistry of 212-1-SL.

H₂S [mM] → H_2S [mM]

TA [mM]

Cl⁻ [mM] → Cl^- [mM]

H₄SiO₄ [µM] → H_4SiO_4 [µM]
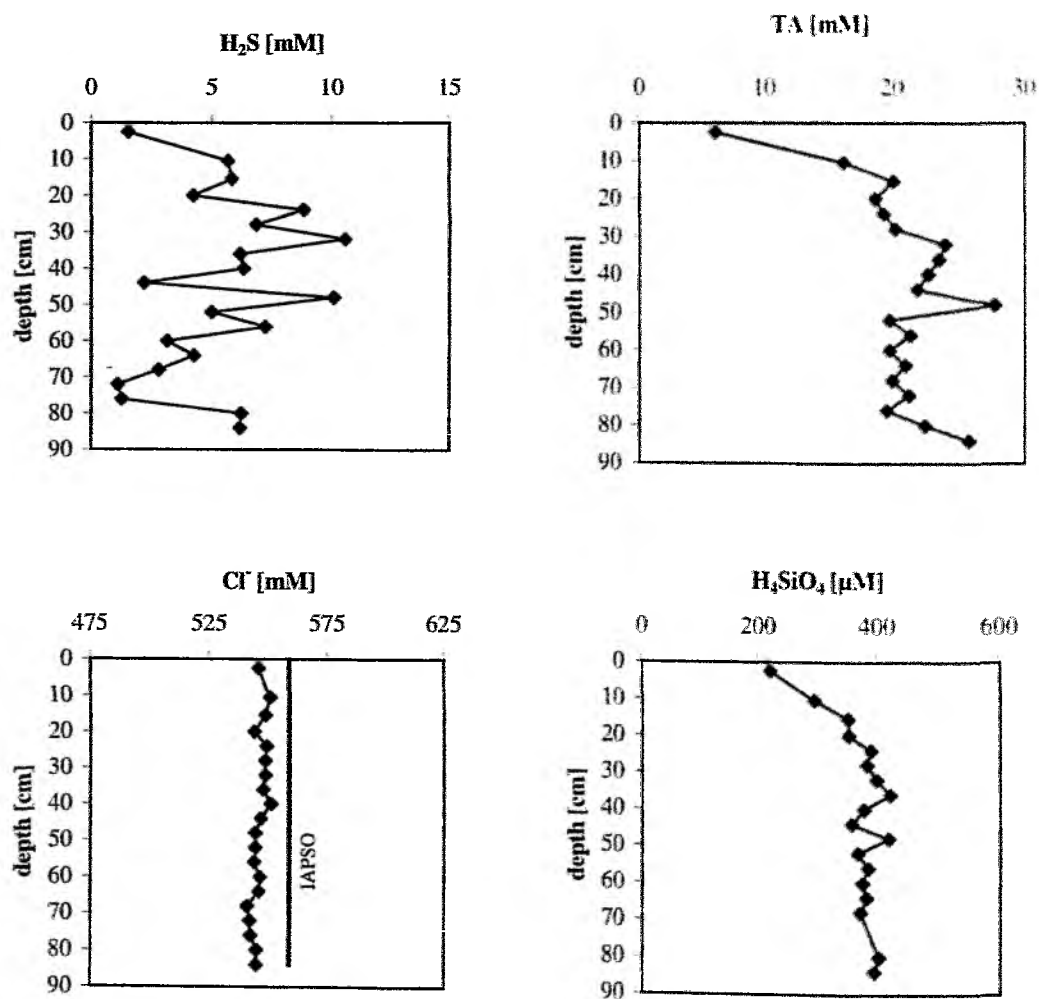
Fig. 90: Pore water chemistry of 239-1-SL. NH₄ and PO₄ were not determined due to analytical problems.
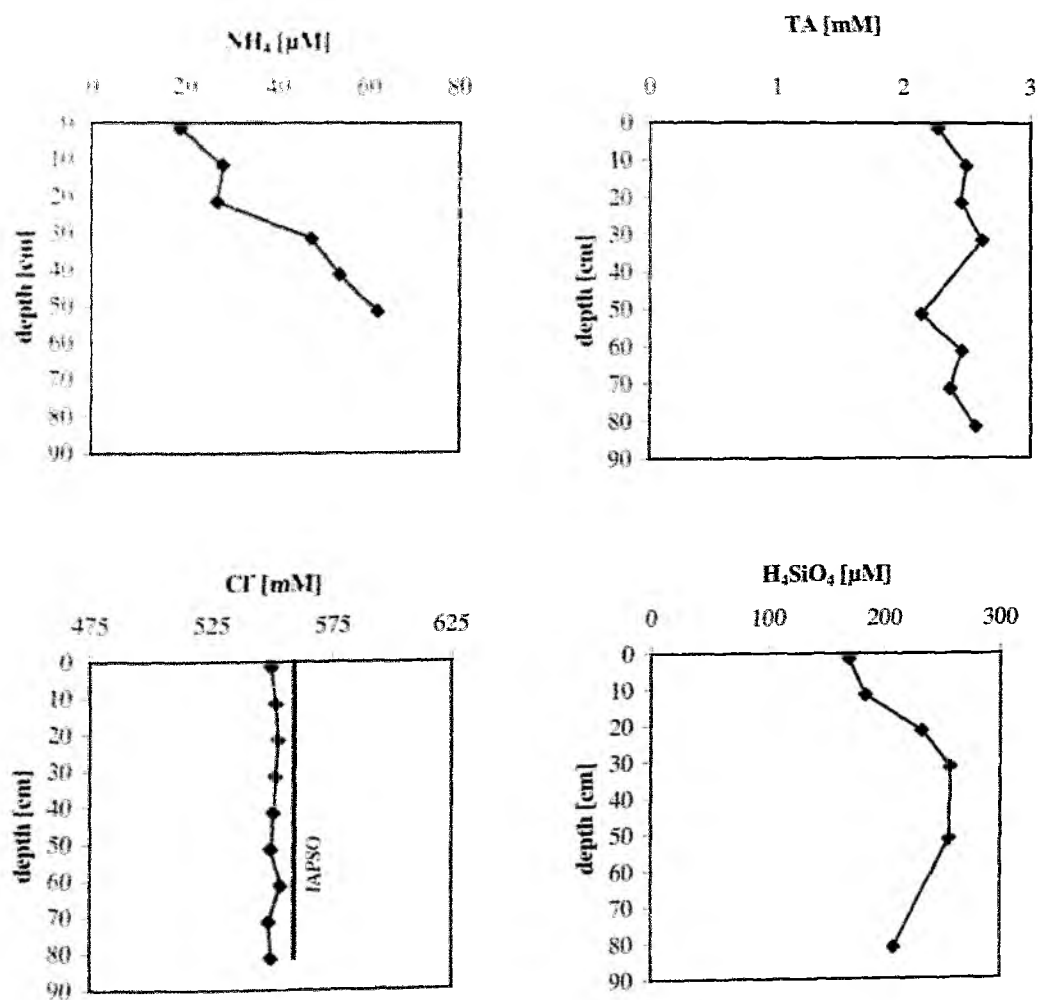
Fig. 91: Pore water chemistry of 238-1-SL. PO$_4$ was not determined due to analytical problems. H$_2$S was not detectable.
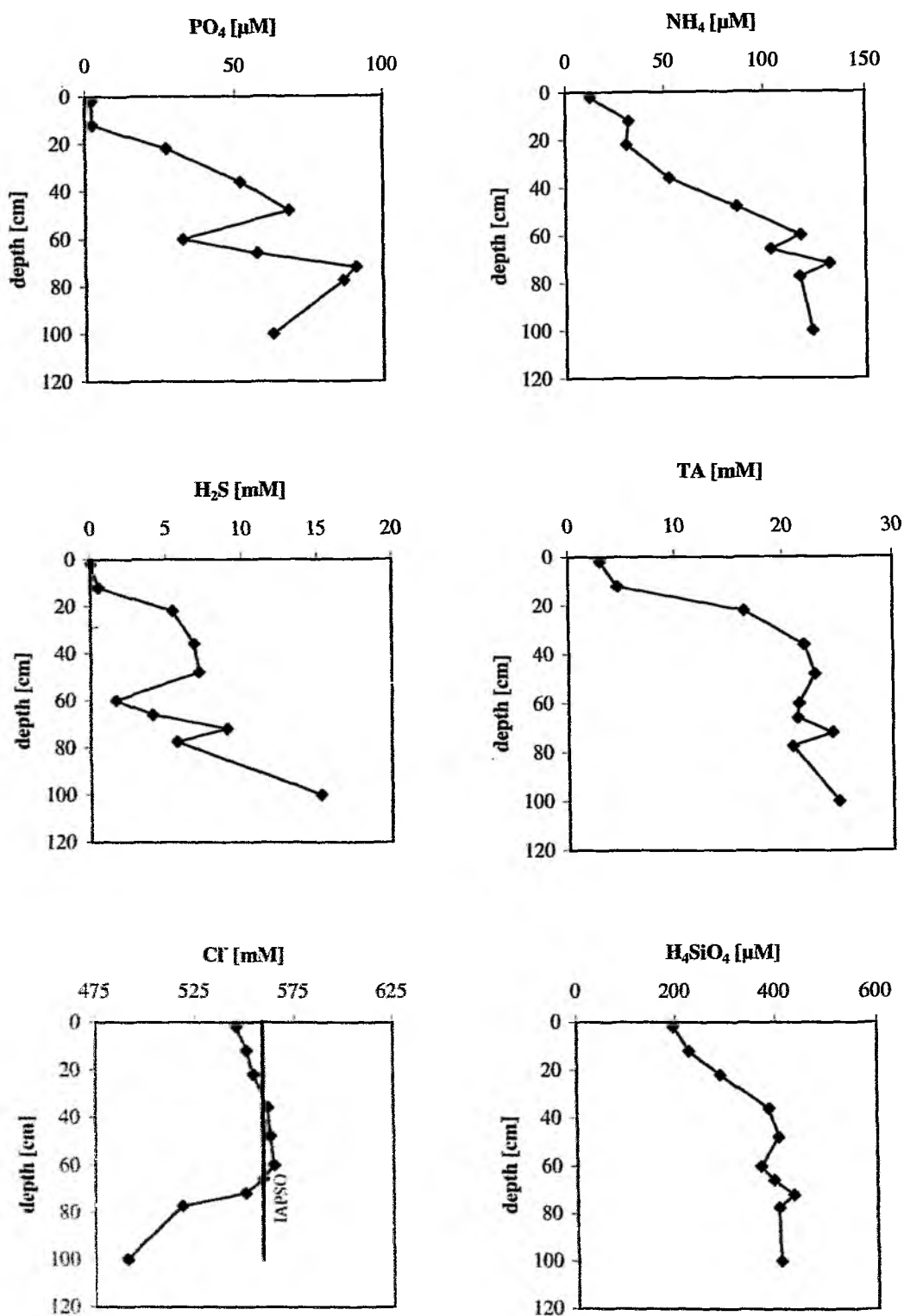
Fig. 92: Pore water chemistry of 221-1-SL. Two pore-water anomalies are shown: slightly increasing chlorinity trend (ca. 30-70 cmbsf) due to salt exclusion during hydrate formation and decreasing chlorinity trend (> 70 cmbsf) due to fresh water dilution of pore water caused by decomposed gas hydrates (compare to Fig. 90).
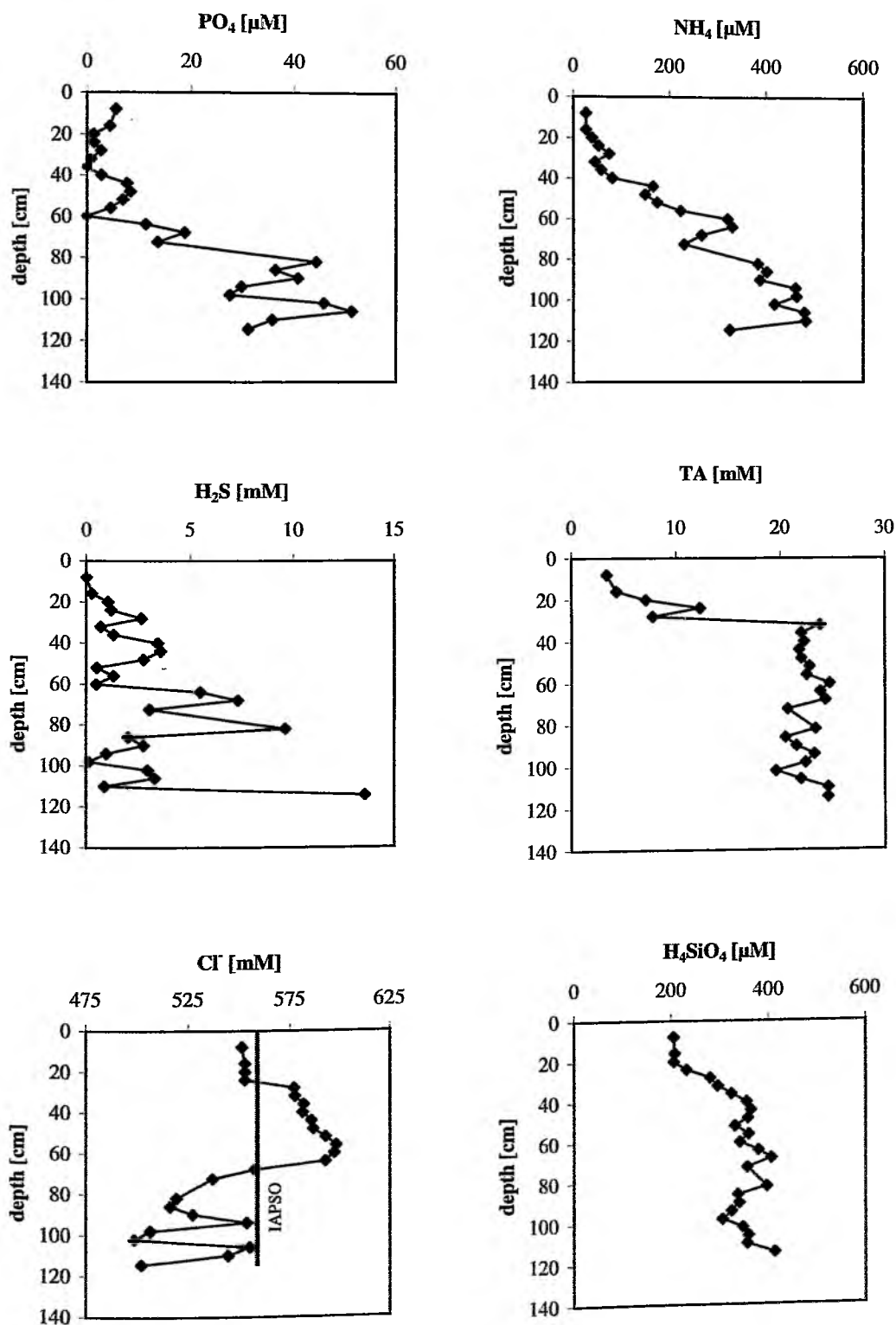
Fig. 83: Pore water chemistry of 221-1-SL. Two significant pore-water anomalies are shown: increasing chlorinity trend (ca. 30-70 cmbsf) due to salt exclusion during hydrate formation and decreasing chlorinity trend (> 70 cmbsf) due to fresh water dilution of pore water caused by decomposed gas hydrates (compare to Fig. 90).

Salt exclusion

The phenomenon of salt exclusion during gas hydrate formation has already been observed in gravity core 55-5-SL during expedition SO143/1b. During this cruise it was again possible to determine a pore water signature which is less affected by the sampling artifact of decreased chlorinities after hydrate decomposition.

As salt free water is produced during gas hydrate dissociation, fluids with a gas hydrate component have characteristically lower salt contents. Chloride concentrations are indeed slightly lower at on-vent site compared to off-vent site (Fig. 88) but can not be interpreted as significantly lower. The pore water chemistry, especially the chlorinity of gravity core 221-2-SL (Fig. 93) and 221-1-SL (Fig. 92) to a lower extent however is significantly affected by both phenomena, salt exclusion and pore water freshening through gas hydrate decomposition. Salt exclusion was detected ~ 30-70 cmbsf where fresh water is withdrawn from the pore water reservoir in the course of hydrate crystallization and the remaining interstitial water becomes progressively more saline.

In 221-2-SL (Fig. 93) chloride concentrations of up to ~ 600 mM were measured, almost 10% more saline than IAPSO seawater standard. This effect however is mostly overcompensated by the decomposition of hydrates, an artifact of the sampling procedure as shown at depth below 70 cmbsf in both cores. Injection of hydrate water dilutes the pore water over the entire length of the core resulting in significantly lower chloride concentrations compared to IAPSO.

A slight chlorinity increase may also result from the burial of saltier sea water during glacial epochs (Hesse, 1989). This effect, however, can be differentiated isotopically from the hydrate effect, because it would be associated with a positive $\delta^{18}O$ anomaly in the pore water wheras the hydrate effect should cause a negative $\delta^{18}O$ anomaly. This is just the opposite of the hydrate sampling artifact due to which the downhole chloride decrease should be coupled with a $\delta^{18}O$ increase.

Summarizing, the hydrate-formation and -decomposition mechanism still provides the most successfull explanation for the chamical porewater anomalies but could be confirmed by complementary $\delta^{18}O$ measurements in the home laboratories.

Additionally, carbon isotope measurements will be used to differentiate between biogenic and thermogenic gas hydrates.

5   References

Aller, R.C. (1980) Quantifying solute distributions in the bioturbated zone of marine sediments by defining an average microenvironment. Geochim. Cosmochim. Acta 44: 1955-1965.

Bange, H.W., Ramesh, R., Rapsomanikis, S. and M.O. Andreae (1998) Methane in surface waters of the Arabian Sea. Geophys. Res. Lett. 25: 3547-3550.

Behrmann, J.H., Bauer, P., and A. Kopf (1995) Provenance of Quaternary sands and sandstones, ODP Leg 146, Cascadia Margin. In: Carson, B., Westbrook, G.K., Musgrave, R.J., and Suess, E. (eds.), Proc. ODP, Sci. Results 146: College Station, TX (Ocean Drilling Program): 425-430.

Bohrmann, G., Greinert, J., Suess E., and M. Torres (1998) Authigenic carbonates from Cascadia Subduction Zone and their relation to gas hydrate stability. Geology 26(7): 647-650.

Boulegue J., Lijama, J.T., Charlou, J.L., and J. Jedwab (1987) Nankai Trough, Japan Trench and Kuril Trench: Geochemistry of fluids sampled by submersible „Nautile". Earth Planet. Sci. Lett. 83: 363-375.

Brewer, P.G., Orr Jr, F.M., Friedrich, G., Kvenvolden K.A., Orange, D.L., McFarlane, J., and W. Kirkwood (1997) Deep-ocean field-test ofmethane hydrate formation from a remotely operating vehicle. Geology 25, 407-410.

Brown, K.M., Sauter, A. W., and L.M. Dorman (1995) Diffusive flux measurement in convergent margin and ridge flank environments: A new sea-floor fluid flux meter system. EOS Transactions, Am. Geophys. Union 76, 563.

Burton, E.A. and L.M. Walter (1987) Relative precipitation rates of aragonite and Mg calcite from seawater: Temperature or carbonate ion control? Geology 15: 111 - 114.

Caress, D.W. and D.N. Chayes (1996): Improved processing of Hydrosweep DS multibeam data on the R/V Maurice Ewing. Mar. Geophys. Res. 18: 631-650.

Carson, B., Suess, E., and J.F. Strasser (1990) Fluid flow and mass flux determinations at vent sites on the Cascadian margin accretionary prism. J. Geophys. Res. 95 (B6): 8891-8897.

Carson, B., Erol, S., Paskevich, V., and M.L. Holmes (1994) Fluid expulsion sites on the Cascadia accretionary prism: Mapping disgenetic deposits with processed GLORIA imagery. J. Geophys. Res. 99: 11959-11969.

Clennell, M.B. and A. Maltman (1995) Microstructures in accreted sediments of the Cascadia margin: examples from ODP Leg 146. In: Carson, B., Westbrook, G.K., Musgrave, R.J., and Suess, E. (eds.), Proc. ODP, Sci. Results 146, TX (Ocean Drilling Program): 201-216.

Cremer, A., Maßnahmen zur Realisierung eines videogeführten Lander-Systems für die Langzeitmessung und Beprobung submariner Quellen: Diplomarbeit an der Fachhochschule Kiel, 1995.

Dickson, A.G. (1993) pH buffers for sea water media based on the total hydrogen ion concentration scale, Deep Sea Res. I (40): 107-118.

Flueh, E.R. and R. von Huene (1994) FS Sonne Fahrtbericht SO96, KODICA SEIS, GEOMAR Forschungszentrum.

Fossing, H., Gallardo, B.B., Jørgensen, B.B., Huttel, M., Nielsen, L.P., Schulz, H., Canfield, D.E., Forster, S., Glud, R.N., Gundersen, J.K., Kuver, J., Ramsing, N.B., Teske, A., Thamdrup, B., and O. Ulloa (1995) Concentration and transport of nitrate by the mat-forming sulphur bacterium Thioploca. Nature 374: 713-715.

Gallardo, V.A. (1977) Large benthic microbial communities in sulphide biota under Peru-Chile subsurface countercurrent: Nature, 268: 331-332.

Gieskes, J.M., Gamo, T., and H. Brumsack (1991) Chemical methods for interstitial water analyses on Joides Resolution, Ocean Drill. Program, Texas A&M Univ., College station.

Goldsmith, J.R., Graf, D.L., and H.C. Heard (1961) Lattice constants of the calcium-magnesium carbonates. Am. Mineral. 46: 453 - 457.

Gornitz, V. and I. Fung (1994) Potential distribution of methane hydrates in the world's ocean. Glob. Biogeochem. Cycl. 8: 335-347.

Grasshoff, M., Ehrhardt, K., and K. Kremling (1983) Methods of seawater analysis, 2nd edition, Verlag Chemie, Weinheim: 419pp.

Greinert J. (1999) Rezente submarine Mineralbildungen: Abbild geochemischer Prozesse an aktiven Fluidaustrittstellen im Aleuten- und Cascadia-Akkretionskomplex. Dissertation, University of Kiel.

Greinert, J. (1999) Rezente submarine Mineralbildungen: Abbild geochemischer Prozesse an aktiven Fluidaustrittsstellen im Aleuten- und Cascadia-Akkretionskomplex. Geomar Report 87: 210 pp.

Henry, P., J.-P. Foucher, X. Le Pichon, K. Kobayashi, P. Tarits, N. Chamot-Rooke, T. Furuta, and P. Schultheiss (1992) Interpretation of temperature measurements from the Kaiko-Nankai cruise: Modeling of fluid flow in clam colonies. Earth Planet. Sci. Lett. 109: 355-371.

Herzig, P. (1997) FS Sonne Fahrtbericht SO109-2, Geomar Report 58: 98-213.

Hesse, R. (1990) Pore water anomalies in gas-hydrate-bearing sediments of the deeper continental margins: facts and problems. J. of Inclusion Phenomena and Molecular Recognition in Chemistry 8: 117-138.

Hyndman, R.D. and G.C. Spence (1992) A seismic study of methane hydrate seafloor bottom simulating reflectors. J. Geophys. Res. 97: 6683-6698.

Hyndman R. D. and E. E. Davis (1992) A mechanism for the formation of authigenic carbonates along the Cascadia continental margin: Implications for the global Ca-cycle. Paleography Paleoclimatology 71: 97-118.

Ivanenkov, V.N. and Y.I. Lyakhin (1978) Determination of total alkalinity in seawater, In: O.K. Bordovsky, and V.N. Ivanenkov (eds.), Methods of hydrochemical investigations in the ocean, Nauka Publ. House, Moscow, 110-114 (in Russian).

Jannasch, H.W., Nelson, D.C., and C.O. Wirsen (1989) Massive natural occurrence of unusually large bacteria (Beggiatoa sp.) at the hydrothermal deep-sea vent site. Nature 342, 834-836.

Jørgensen, B.B. (1977) Bacterial sulfate reduction within reduced microniches of oxidized marine sediments: Mar. Biol., 41: 7-17.

Kastner, M., Kvenvolden, K.A., Whiticar, M.J., Camerlenghi, A., and Lorenson, T.D., 1995A. Relation between pore fluid chemistry and gas hydrates asociated with bottom simulating reflectors at the Cascadia Margin, Sites 889 and 892. In: Carson, B., Westbrook, G.K., Musgrave, R.J., and Suess, E. (eds.), Proc. ODP, Sci. Results 146: College Station, Texas, 175-187

Kulm L.D., Suess, E., Moore, J.C., Carson, B., Lewis, B.T., Ritger, S.D., Kadko, D.C., Thornburg, T.M., Embley, R.W., Rugh, W.D., Massoth, G.J., Langseth, M.G., Cochrane, G.R., and R.L. Scamann (1986) Oregon subduction zone: venting, fauna, and carbonates. Science 231: 561-566.

Kulm L.D. and E. Suess (1990): Relationship between carbonate deposits and fluid venting: Oregon accretionary prism. J. Geophys. Res. 95(B6): 8889-8915.

Kvenvolden, K.A. (1988) Methane hydrate - a major reservoir of carbon in the shallow geosphere? Chem. Geol. 71: 41-51.

Kvenvolden, K.A. (1995) A review of the geochemistry of methane in natural gas hydrate. Org. Geochem. 23(11/12): 997-1008.

Lammers, S. and Suess, E., 1994. An improved head-space analysis method for methane in seawater. Mar. Chem., 47: 115-125.

Linke, P., Suess, E., Torres, M., Martens, V., Rugh, W.D., Ziebis, W., and L.D. Kulm (1994) In situ measurement of fluid flow from cold seeps at active ccontinental margins: Deep-Sea Res. 41: 721-739.

Lumsden, D.N. (1979) Error in X-Ray Diffraction Estimates of Dolomite in Carbonate Rocks- Causes and Cures. AAPG Bulletin 63: 488.

MacDonald, G. (1990) Role of methane clathrates in past and future climates. Clim. Change 16: 247-281

McKay, M.E., Jarrad, R.D., Westbrook, G.K., Hyndman, R.D., et al. (1994) Origin of bottom simulating reflectors : Geophysical evidence from the Cascadia accretionary prism. Geology 22, 459-462.

Moore W. S. (1996) Large groundwater inputs to coastal water revealed by ^{226}Ra enrichments. Nature 380: 612-614.

Moore C. and P. Vrolijk (1992) Fluids in accretionary prisms. Revue Geophys. 30, 113-135.

Rehder, G., Keir, R.S., Suess, E. and M. Rhein, (1999) Methane in the northern Atlantic controlled by oxidation and atmospheric history. Geophys. Res. Lett., 26: 587-590.

Rimek, R. (1999) Konstruktion eines Probennehmers zur Gewinnung von Fluidproben aus untermeerischen kalten und warmen Quellen. Diplomarbeit, Fachhochschule Kiel: 1-104.

Ritger, S., Carson, B., and Suess, E. (1987) Methane-derived authigenic carbonates formed by subduction-induced pore-water expulsion along the Oregon/Washington margin. Geol. Soc. Am. Bull. 98: 147-156.

Sample, J.C. and Kopf, A. (1995). Occurrences and geochemistry of syntectonic carbonate cements and veins from ODP Leg 146: Implications for hydrogeologic evolution of the Cascadia margin. In: Carson, B., Westbrook, G.K., Musgrave, R.J., and Suess, E. (eds.), Proc. ODP, Sci. Results 146, TX (Ocean Drilling Program), 137-150.

Sample JC and Reid MR (1998): Contrasting hydrogeologic regimes along strike-slip and thrust faults in the Oregon convergent margin: Evidence from the chemistry of syntectonic carbonate cements and veins. GSA Bulletin 110(1): 48-59.

Schreiber, R., and H. W. Schencke (1990) Efficient hydrographic surveying of EEZ with new multibeam echosounder technology for shallow and deep water. Ocean Resources 1: 73-87.

Schulz, H.N., Brinkhoff, T., Ferdelman, T.G., Hernadéz Mariné, M., Teske, A., and B.B. Jørgensen (1999) Dense populations of a giant sulfur bacterium in Namibian shelf sediments. Science 284: 493-495.

Shipley, T.H., Houston, M.H., Buffler, R.T., Shaub, F.J., McMillen, K.J., Ladd, J.W., and J.L. Worzel (1979) Seismic reflection evidence for the widespread occurrence of possible gas-hydrate horizons on continental slopes and rises. Amer. Ass. Petrol. Geol. Bull. 63: 2204-2213.

Suess E., Carson, B., Ritger, S.D., Moore, J.C., Kulm, L.D., and G. R. Cochrane (1985) Biological communities at vent sites along the subduction zone off Oregon. In: The hydrothermal vents of the Eastern Pacific: an overview, M. C. JONES (ed.). Bull. Biol. Soc. Wash. 6: 475-484.

Suess, E. and M.J. Whiticar (1989) Methane-derived CO_2 in pore fluids expelled from the Oregon subduction zone. Palaeogeogr. Palaeoclimatol. Palaeoecol. 71: 119-136.

Suess, E. and G. Bohrmann (1997) FS Sonne Fahrtbericht SO 110 SO-RO, Geomar Report 59: 181 pp.

Suess E., Torres, M. E., Bohrmann, G., Collier, R. W., Greinert, J., Linke, P., Rehder, G., Trehu, A., Wallmann, K., Winckler, G., and E. Zuleger (1999) Gas hydrate destabilization: enhanced dewatering, benthic material turnover and large methane plumes at the Cascadia convergent margin. Earth Planet. Sci. Lett. 170(1-2): 1-15.

Torres, M., Bohrmann, G., Suess, E., Boulege, J., and J. Bourgois (1996) Authigenic barites and fluxes of barium associated with fluid seeps in the Peru subduction zone, Earth Planet. Sci. Lett. 144: 469-481.

Torres, M., Bohrmann, G., Brown, K., de Angelis, M., Hammond, D., Klinkhammer, G., McManus, J., Suess, E., and A. Trehue (1999). Geochemical observations on Hydrate Ridge, Cascadia Margin during R/V-ATLANTIS-cruise AT3-35b, July 1999: Oregon State Univeristy, COAS-Data Report 174.

Trehu, A.M., Lin, G., Maxwell, E., and C. Goldfinger (1995) A seismic reflection profile across the Cascadia subduction zone offshore central Oregon: New constraints on the deep crustal structure and/or the distribution of methane in the accretionary prism. J. Geophys. Res. 100:15101-15116.

Trehu, A., Torres, M., Moore, G., Suess, E., and G. Bohrmann (1999). Temporal and spatial evolution of a gas hydrate-bearing accretionary ridge on the Oregon continental margin: Geology, 27(10): 939-942.

Wallmann, K., Linke, P., Suess, E., Bohrmann, G., Sahling, H., Schlüter, M., Dählmann, A., Lammers, S., Greinert, J., and N. von Mirbach (1997) Quantifying fluid flow, solute mixing, and biogeochemical turnover at cold vents of the eastern Aleutian subduction zone, Geochim. Cosmochim. Acta 61(24): 5209-5219.

Weinrebe, W. (1997) Fahrtbericht SO112 HIRESBAT, Geomar Report 64.

Weiss, R.F. (1970) The Solubility of Nitrogen, Oxygen and Argon in Water and Seawater. Deep-Sea-Res., 17: 721-735.

Weiss, R.F. (1981) Determinations of carbon dioxide and methane by Dual Catalyst Flame Ionisation Chromatography and nitrous oxide by Electron Capture Chromatography. J. Chrom. Sci., 19: 611-616.

Wessel, P., and W.H.F. Smith (1991) Free software helps map and display data. EOS Transaction, Am. Geophys. Union 72(441): 445-446.

Westbrook, G.K., Carson, B. Musgrave, R.J., et al. (1994). Proc. ODP, College Station, TX, Ocean Drilling Program, Init. Repts. 146 (I).

Whiticar, M.J., Hovland, M., Kastner, M., and J.C. Sample (1995) Organic geochemistry of gases, fluids, and hydrates at the Cascadia Accretinary Margin. In: Carson, B., Westbrook, G.K., Musgrave, R.J., and Suess, E. (eds.), Proc. ODP, Sci. Results 146. TX (Ocean Drilling Program), 385-397.

Appendix

A1   Station list SO143-1a

Station list

SONNE 143-1a

Date 1999	Station No. SO143/	Instrument	Time (UTC) Begin	on seafloor	off seafloor	End	Duration hh:mm	Begin / on seafloor Latitude N°	Begin / on seafloor Longitude W°	End / off seafloor Latitude N°	End / off seafloor Longitude W°	Water depth (m)	Recovery	Remarks
08. Jul	1-1	CTD	06:08			10:23	4:15	44°32.850	125°23.380	44°32.910	125°23.420	2931	7 bottles	test
08. Jul	2-1	HS	10:22			11:07	0:45	44°32.880	125°23.340	44°34.140	125°15.720			
08. Jul	3-1	HS	11:09			13:08	1:59	44°34.140	125°15.720	44°50.340	124°53.520	1330		
08. Jul	4-1	OFOS	13:21	13:41	21:16	21:45:05	8:23	44°50.240	124°53.670	44°50.153	125°01.324			
08. Jul	4-2	HS/PS	13:42			21:20	7:38	44°50.340	124°53.520	44°50.000	125°01.500			test
08. Jul	5-1	VESP-II	23:17	23:38		00:20:00	1:03	44°50.420	124°53.070	44°50.420	125°53.180	538.6		
09. Jul	5-2	VESP-I	01:08	01:28		02:05:00	0:57	44°50.376	124°57.290	44°50.363	125°53.320	551		test
09. Jul	6-1	HS	03:16			04:12	0:56	44°50.340	124°53.520	40°50.100	125°03.240			
09. Jul	6-2	HS	04:12			06:02	1:50	40°50.100	125°03.240	40°50.100	125°23.000			
09. Jul	6-3	HS	06:02			06:12	0:10	40°50.100	125°23.000	44°48.920	125°23.000			
09. Jul	6-4	HS	06:12			08:04	1:52	44°48.920	125°23.000	44°48.920	125°03.000			
09. Jul	6-5	HS	08:04			08:10	0:06	44°48.920	125°03.000	44°47.760	125°03.000			
09. Jul	6-6	HS	08:10			09:55	1:45	44°47.760	125°03.000	44°47.760	125°23.000			
09. Jul	6-7	HS	09:55			10:03	0:08	44°47.760	125°23.000	44°46.560	125°23.000			
09. Jul	6-8	HS	10:03			11:06	1:03	44°46.560	125°23.000	44°46.560	125°10.000			
09. Jul	7-1	OFOS	13:25	13:44	18:38	19:00:24	5:35	44°26.990	125°02.440	44°27.010	124°59.980	885		
09. Jul	8-1	VESP-I	21:18	22:29	22:41	07:37	10:18	44°41.108	125°17.003	44°40.760	125°16.970	2094		not deployed
10. Jul	9-1	HS	09:00			09:08	0:08	44°34.140	125°15.720	44°33.120	125°15.180			
10. Jul	9-2	HS	09:08			09:53	0:45	44°33.120	125°15.180	44°30.480	125°22.620			
10. Jul	9-3	HS	09:53			10:09	0:16	44°30.480	125°22.620	44°28.020	125°22.620			
10. Jul	9-4	HS	10:09			10:58	0:49	44°28.020	125°22.620	44°31.380	125°14.700			
10. Jul	9-5	HS	10:58			11:06	0:08	44°31.380	125°14.700	44°30.300	125°13.980			
10. Jul	9-6	HS	11:06			11:36	0:30	44°30.300	125°13.980	44°28.000	125°18.400			
10. Jul	10-1	OFOS	13:08	13:32	22:41	23:09:14	10:00	44°36.880	125°00.240	44°36.880	125°10.210	1332		
11. Jul	11-1	VESP-I	00:11	00:44	01:47		1:35	44°39.998	125°05.806	44°40.060	125°05.890			
11. Jul	12-1	HS	03:52			04:22	0:30	44°28.100	125°18.200	44°25.800	125°22.620	609		on bacterial mat
11. Jul	12-2	HS	04:22			04:43	0:21	44°25.800	125°22.620	44°25.280	125°22.620			
11. Jul	12-3	HS	04:43			05:43	1:00	44°25.280	125°22.620	44°30.000	125°14.700			
11. Jul	12-4	HS	05:43			05:52	0:09	44°30.000	125°11.700	44°29.100	125°10.620			
11. Jul	12-5	HS	05:52			06:42	0:50	44°29.100	125°10.620	44°24.480	125°17.160			
11. Jul	12-6	HS	06:42			07:02	0:20	44°24.480	125°17.160	44°24.480	125°14.160			
11. Jul	12-7	HS	07:02			07:41	0:39	44°24.480	125°14.160	44°27.840	125°10.020			
11. Jul	12-8	HS	07:41			08:00	0:19	44°27.840	125°10.020	44°30.000	125°10.020			

Date	Station No.	Instrument	Time (UTC)					Begin / on seafloor		End / off seafloor				
1999	SO143/		Begin	on seafloor	off seafloor	End	Duration hh:mm	Latitude N°	Longitude W°	Latitude N°	Longitude W°	Water depth (m)	Recovery	Remarks
11. Jul	12–9	HS	08:00			09:25	1:25	44°30.000	125°10.020	44°30.000	124°55.000			
11. Jul	12–10	HS	09:28			10:18	0:50	44°30.546	124°55.000	44°30.546	125°04.500			
11. Jul	12–11	HS	10:32			11:29	0:57	44°33.092	125°04.500	44°31.092	124°55.000			
11. Jul	12–12	HS	11:37			12:00	0:23	44°31.638	124°55.000	44°31.638	124°59.500			
11. Jul	13–1	OFOS	13:04	13:28	16:32	16:59	3:28	44°44.680	125°06.990'	44°40.670	125°02.730	1067		Laser not correct
11. Jul	14–1	OFOS	18:04	18:25	22:51	23:23	5:19	44°35.140	124°56.490	44°35.130	125°02.150	1239		
12. Jul	15–1	HS	00:03			00:25	0:22	44°31.638	124°59.500	44°31.638	125°03.500			
12. Jul	15–2	HS	00:33			01:20	0:47	44°32.184	125°03.500	44°32.184	124°55.000			
12. Jul	15–3	HS	01:27			02:11	0:44	44°32.730	124°55.000	44°32.730	125°00.300			
12. Jul	15–4	HS	02:21			03:05	0:44	44°33.402	125°03.000	44°33.402	124°55.000			
12. Jul	15–5	HS	03:14			03:56	0:42	44°34.000	124°55.000	44°34.000	125°02.500			
12. Jul	16–1	TP	04:40			05:10	0:30	44°34.190	125°09.240	44°34.190	125°09.210			
12. Jul	16–2	TP	05:20			05:40	0:20	44°34.310	125°08.220	44°34.300	125°08.210			
12. Jul	16–3	TP	05:50			06:01	0:11	44°34.810	125°08.920	44°34.800	125°08.900			
12. Jul	16–4	TP	06:15			07:18	1:03							transponder calibration
12. Jul	17–1	HS	07:52			08:34	0:42	44°34.668	125°02.500	44°34.668	124°55.000			
12. Jul	17–2	HS	08:34			09:14	0:40	44°34.668	124°55.000	44°29.200	124°55.000			
12. Jul	17–3	HS	09:14			10:49	1:35	44°29.200	124°55.000	44°29.200	125°12.000			
12. Jul	17–4	HS	10:49			10:58	0:09	44°29.200	125°12.000	44°28.420	125°13.000			
12. Jul	17–5	HS	10:58			12:42	1:44	44°28.420	125°13.000	44°28.420	124°55.000			
12. Jul	17–6	HS	12:49			14:34	1:45	44°27.640	124°55.000	44°27.640	125°14.000			
12. Jul	17–7	HS	14:34			14:42	0:08	44°27.640	125°14.000	44°26.860	125°15.000			
12. Jul	17–8	HS	14:42			16:41	1:59	44°26.860	125°15.000	44°26.860	124°55.000			
12. Jul	17–9	HS	16:50			18:34	1:44	44°26.070	124°55.000	44°26.070	125°13.500			
12. Jul	18–1	TP	19:15			21:33	2:18							transponder calibration
12. Jul	19–1	TP	00:04			00:18	0:14	44°39.890	125°05.500	44°39.890	125°05.500			
12. Jul	19–2	TP	00:37			00:52	0:15	44°39.690	125°06.700	44°39.700	125°06.690			
12. Jul	19–3	TP	01:03			02:15	1:12	44°40.500	125°06.420	44°40.490	125°06.410			no signals

Abbreviations: CTD (Conductivity temperature depth)
HS (Hydrosweep)
OFOS (Ocean floor observation system)
PS (Parasound)
TP (Transponder)
VESP (Vent sampler)

Annotations: OFOS: time beginn   = OFOS into water
time off seafloor = end of profil time
time end   = on deck time
water depth   = end of profile depth

all Lat./Long. positions   = ship positions, except end Lat./Long. of 11-1 which is SSBL position

Water depth: OFOS   = end of profile
VESP   = deployed

SONNE 143-1b — Station list

Date 1999	Station No. SO143/	Instrument	Time (UTC) Begin	on seafloor	off seafloor	End	Duration hh:mm	Begin / on seafloor Latitude N°	Longitude W°	End / off seafloor Latitude N°	Longitude W°	Water depth (m)	Recovery	Remarks
15 Jul	20–1	OFOS	13:05	13:24		14:17	1:11	44°34.150	125°08.500	44°34.220	125°09.050	798		
15 Jul	20–2	OFOS	14:17			15:09	0:52	44°34.220	125°09.050	44°34.230	125°09.080	856		
15 Jul	20–3	OFOS	15:09			16:11	1:01	44°34.230	125°09.080	44°34.180	125°08.660	814		
15 Jul	20–4	OFOS	16:11		16:51	17:13	1:02	44°34.180	125°08.660	44°34.195	125°08.356	828		
15 Jul	21–1	TV-G	18:05	18:25	18:30	19:01	0:56	44°34.240	125°08.820	44°34.222	125°08.827	786	2 subcores 40cm (1 pw.)	drop at 18:30:10
15 Jul	21–2	TV-G	21:30	21:48	21:48	22:15	0:44	44°34.221	125°08.828	44°34.221	125°08.818	788	3 subcores (20-33cm; 2 parallel cores; 2 pw.)	drop at 21:48:32
16 Jul	22-1-59	18kHz	00:52			16:32	15:40							details on separate sheet
16 Jul	23–1	CTD	17:55	17:55		18:43	0:47	44°40.100	125°05.870	44°40.120	125°05.830	601	13 bottles	lat./long. of deployment
16 Jul	23–2	CTD	19:43	20:10	20:10	20:10	0:27	44°40.002	125°06.172	44°40.000	125°06.170	612	24 bottles	lat./long. of deployment
16 Jul	24–1	MUC	23:20	23:49		00:09	0:49	44°34.229	125°08.806	44°34.215	125°08.796	788	3 cores (23-27cm)	
17 Jul	24–2	MUC	00:23	00:49		01:07	0:44	44°34.222	125°08.801	44°34.223	125°08.805	787.4	4 cores (24-28cm)	
17 Jul	24–3	MUC	01:21	01:44		02:05	0:44	44°34.229	125°08.809	44°34.254	125°08.798	787	4 cores (28-29cm)	
17 Jul	25–1	ZAPS-I	03:10			06:10	3:00	44°39.918	125°06.234	44°40.237	125°05.696	615		
17 Jul	26–1	HS	07:36			07:51	0:15	44°26.070	125°13.500	44°26.070	125°16.000			
17 Jul	26–2	HS	07:51			07:59	0:08	44°26.070	125°16.000	44°25.284	125°17.000			
17 Jul	26–3	HS	07:59			09:52	1:53	44°25.284	125°17.000	44°25.284	124°55.000			
17 Jul	26–4	HS	09:58			10:57	0:59	44°25.680	124°55.000	44°25.680	125°05.000			
17 Jul	26–5	HS	11:04			11:56	0:51	44°26.466	125°05.000	44°26.466	124°55.000			
17 Jul	27–1	OFOS	13:58	14:20	16:58	17:24	3:26	44°34.710	124°58.480	44°34.690	125°01.130	1161		
17 Jul	28–1	OFOS	18:13	18:31	21:21	21:45	3:31	44°33.897	125°08.506	44°34.647	125°11.188	821.3		
17 Jul	29–1	TV-MUC	22:40	23:50	00:19	00:54	2:13	44°34.243	125°08.798	44°34.264	125°08.815	776.0	no core	drop at 00:17
18 Jul	29–2	TV-MUC	01:41	02:07	02:30	03:11	1:30	44°34.212	125°08.793	44°34.264	125°08.827	773.0	4 cores (11-22cm)	drop at 02:29
18 Jul	29–3	TV-MUC	03:15	03:45	04:01	04:40	1:25	44°34.210	125°08.800	44°34.258	125°08.833	789.1	3 cores (24-44cm)	drop at 03:58:31
18 Jul	29–4	TV-MUC	04:50	05:12	05:22	06:04	1:14	44°34.213	125°08.788	44°34.222	125°08.817	786.9	4 cores (27-34cm)	drop at 05:21:13
18 Jul	30–1	HS	07:36			08:32	0:56	44°27.252	124°55.000	44°27.252	125°05.000			
18 Jul	30–2	HS	08:38			09:31	0:53	44°28.038	125°05.000	44°28.038	124°55.000			
18 Jul	30–3	HS	09:38			10:30	0:52	44°28.824	124°55.000	44°28.824	125°05.000			
18 Jul	30–4	HS	10:35			11:33	0:58	44°29.610	125°05.000	44°29.610	124°54.120			
18 Jul	30–5	HS	11:33			12:17	0:44	44°29.610	124°54.120	44°35.000	124°54.120			
18 Jul	31–1	TV-MUC	13:07	13:27	14:02	14:47	1:40	44°34.695	124°59.385	44°34.732	124°59.330	886	4 cores (29-39cm)	drop at 14:00
18 Jul	32–1	SL	15:08	15:26		16:00	0:52	44°34.720	124°59.340	44°34.723	124°59.341	905	no core	
18 Jul	32–2	SL	16:29	16:53		17:22	0:53	44°34.730	124°59.340	44°34.724	124°59.340	905.2	1 core (5.55m)	
18 Jul	33–1	OFOS	18:05	18:28	22:30	22:59	4:54	44°35.950	124°57.331	44°35.460	125°01.810	1209		
18 Jul	34–1	TV-MUC	23:36	00:07	00:12	00:46	1:09	44°35.600	124°59.100	44°35.600	124°59.090	922.8	6 cores (36-42cm)	drop at 00:09
19 Jul	35–1	SL	00:54	01:17		01:50	0:56	44°35.590	124°59.090	44°35.580	124°59.100	921	1 core (1.40m)	

Date 1999	Station No. SO143/	Instrument	Time (UTC)					Begin / on seafloor		End / off seafloor		Water depth (m)	Recovery	Remarks
			Begin	on seafloor	off seafloor	End	Duration hh:mm	Latitude N°	Longitude W°	Latitude N°	Longitude W°			
19. Jul	36–1	CTD	03:33	04:30		05:10	1:37	44°34.178	125°08.784	44°34.180	125°08.799	780	16 bottles / 16 water depths	
19. Jul	36–2	ZAPS–I	05:32			09:01	3:29	44°34.190	125°08.792	44°34.183	125°08.782	800		
19. Jul	36–3	CTD	09:30	10:19		11:17	1:47	44°34.189	125°08.790	44°34.189	125°08.786	770	16 bottles / 16 water depths	
19. Jul	36–4	CTD	13:35	14:06		15:00	1:25	44°34.187	125°08.786	44°34.189	125°08.785	787	17 bottles / 17 water depths	
19. Jul	36–5	CTD	17:30	18:01		19:30	2:00	44°34.192	125°08.784	44°34.194	125°08.782	784	16 bottles / 16 water depths	
19. Jul	37–1	OFOS	20:31	20:45	23:01		3:28	44°40.156	125°05.143	44°40.188	125°02.598	1132		
19. Jul	37–2	OFOS		23:18	01:26		2:08	44°40.375	125°02.708	44°40.391	125°05.239	648		
20. Jul	37–3	OFOS		01:26	04:05	04:54	3:27	44°40.391	125°05.239	44°40.598	125°02.497	1071		
20. Jul	38–1	HS	05:38			07:06	1:28	44°46.560	125°22.000	44°46.560	124°55.000			
20. Jul	38–2	HS	07:12			10:16	3:04	44°47.160	124°55.000	44°47.160	125°20.000			
20. Jul	38–3	HS	10:25			11:49	1:24	44°48.333	125°20.000	44°48.333	125°05.000			
20. Jul	39–1	SL	13:10	13:37		14:15	1:05	44°37.800	125°02.990	44°37.800	125°02.990	1200	1 core (0.83m)	
20. Jul	40–1	TV-G	15:42	15:55	17:08	17:55	2:12	44°40.100	125°03.200	44°40.180	125°03.280	945.7	no subcores	drop at 17:02:42
20. Jul	40–2	TV-G	18:52	19:22	20:48		1:56	44°40.161	125°03.312	44°40.164	125°03.298	908	3 subc. (47-48cm; 2 pw., 1 meth.+phys. prop.)	drop at 20:48
20. Jul	41–1	TV-G	23:42	00:06	00:36	01:57	2:15	44°39.842	125°06.219	44°39.957	125°06.091	609,5	2 subcores (45-46cm; 1pw., 1 phys. prop.)	drop at 00:34:40
21. Jul	41–2	TV-G	02:41	03:02	04:39	05:09	2:27	44°39.856	125°06.222	44°40.305	125°05.760	615		not dropped
21. Jul	42–1–51	18kHz	05:31			18:28	12:56							details on separate sheet
21. Jul	43–1	CTD	19:10	19:45		20:55	1:45	44°40.120	125°05.781	44°40.126	125°05.791	603	17 bottles / 17 water depths	
21. Jul	43–2	ZAPS–I	14:08			17:30	3:22	44°40.123	125°05.794	44°40.064	125°05.958	603		
22. Jul	43–3	CTD	00:57	01:23		02:19	1:22	44°40.121	125°05.789	44°40.121	125°05.791	603	16 bottles / 16 water depths	
22. Jul	43–4	CTD	05:20	05:43		06:42	1:22	44°40.119	125°05.790	44°40.120	125°05.790	603	19 bottles / 19 water depths	
22. Jul	43–5	CTD	08:56	09:36		10:20	1:24	44°40.123	125°05.788	44°40.123	125°05.788	601	16 bottles / 16 water depths	
22. Jul	44–1	OFOS	12:57	13:08	20:37	21:02	8:05	44°50.107	124°47.948	44°50.205	124°59.713	1046		
22. Jul	45–1	TV-MUC	21:25	22:00	22:41	23:34	2:08	44°50.210	124°59.370	44°50.290	124°59.370	993,5	8 cores (30-31cm)	dropped at 22:40:00
22. Jul	45–2	TV-MUC	23:41	00:06	00:45	01:13	1:31	44°50.220	124°59.363	44°50.291	124°59.364	996		not dropped
23. Jul	45–3	TV-MUC	01:26	01:52	02:25	02:44	1:17	44°50.244	124°59.316	44°50.202	124°59.542	1020		not dropped
23. Jul	46–1	TV-MUC	03:09	03:28	03:48	04:20	1:10	44°50.335	124°58.356	44°50.335	124°58.356	840	8 cores (35-40cm)	dropped at 03:52:15
23. Jul	47–1	HS	05:07			05:29	0:22	44°50.500	124°55.000	44°50.500	124°59.000			
23. Jul	47–2	HS	05:29			06:07	0:38	44°50.500	124°59.000	44°51.500	125°09.000			
23. Jul	47–3	HS	06:07			07:20	1:13	44°51.500	125°09.000	44°51.500	125°20.000			
23. Jul	47–4	HS	07:20			07:34	0:14	44°51.500	125°20.000	44°49.500	125°20.000			
23. Jul	47–5	HS	07:34			10:31	2:57	44°49.500	125°20.000	44°49.500	124°55.000			
23. Jul	47–6	HS	10:35			11:01	0:25	44°48.917	124°55.000	44°48.917	125°00.000			
23. Jul	47–7	HS	11:04			11:34	0:29	44°48.333	125°00.000	44°48.333	124°55.000			
23. Jul	47–8	HS	11:38			12:32	0:53	44°47.750	124°55.000	44°47.750	125°05.000			
23. Jul	47–9	HS	12:38			13:07	0:28	44°48.625	125°05.000	44°48.625	125°00.000			
23. Jul	48–1	SL	13:30	14:00		15:19	1:49	44°50.320	124°58.370	44°50.282	124°58.460	827,8	1 core (9m)	
23. Jul	48–2	SL	15:31	15:58		16:31	0:59	44°50.330	124°58.380	44°50.330	124°58.380	830	1 core (6m)	

Date 1999	Station No SO143/	Instrument	Time (UTC)					Begin / on seafloor		End / off seafloor		Water depth (m)	Recovery	Remarks
			Begin	on seafloor	off seafloor	End	Duration hh:mm	Latitude N°	Longitude W°	Latitude N°	Longitude W°			
23 Jul	49-1	TV-G	17:27	17:41	18:06	18:26	0:59	44°50.292	124°58.029	44°50.191	124°50.089	344		dropped at 18:01:50
23 Jul	49-2	TV-G	18:58	19:12	19:34	20:04	1:05	44°50.176	124°50.077	44°50.201	124°50.202	340		dropped at 19:34:56
23 Jul	50-1	TV-G	20:32	20:46	21:03	21:24	0:52	44°50.307	124°52.622	44°50.308	124°52.661	429		dropped at 21:03:34
23 Jul	50-2	TV-G	22:07	22:20	22:39	23:03	0:55	44°50.301	124°52.663	44°50.327	124°52.716	490		dropped at 22:39:25
24 Jul	51-1	TP	00:35			01:00	0:25	44°40.090	125°06.310	44°40.470	125°06.410			transponder deployed
24 Jul	52-1	TP	01:10			02:40	1:30							transponder calibration
24 Jul	53-1	OFOS	03:31	03:52	05:02	05:23	1:52	44°33.909	125°08.835	44°34.751	125°08.756	829,2		
24 Jul	54-1	MS	05:55			08:30	2:35	44°37.000	125°08.650	44°37.000	124°40.000			
24 Jul	54-2	MS	08:30			08:57	0:26	44°37.000	124°40.000	44°40.500	124°40.000			
24 Jul	54-3	MS	08:57			12:22	3:24	44°40.500	124°40.000	44°40.500	125°18.000			
24 Jul	54-4	MS	12:22			13:03	0:41	44°40.500	125°18.000	44°34.700	125°18.000			
24 Jul	54-5	MS	13:03			13:54	0:50	44°34.700	125°18.000	44°34.700	125°08.700			
24 Jul	55-1	TV-MUC	14:08	14:34	14:56	15:31	1:22	44°34.210	125°08.800	44°34.201	125°08.854	785,9	4 cores (23-32cm)	dropped at 14:55
24 Jul	55-2	TV-MUC	15:43	16:05	16:26	17:05	1:22	44°34.150	125°08.730	44°34.230	125°08.840	788,1	3 cores (15-34cm)	dropped at 16:25
24 Jul	55-3	TV-MUC	17:12	17:34	18:29	19:09	1:56	44°34.080	125°08.730	44°34.250	125°08.880	791,5	3 cores (24-27cm)	dropped at 18:27:03
24 Jul	55-4	SL	19:12	19:40		20:13	1:00	44°34.250	125°08.880	44°34.250	125°08.880	791,8	55cm	
24 Jul	55-5	SL	20:44	21:11		21:42	0:57	44°34.210	125°08.809	44°34.210	125°08.830	787,1	105cm	
24 Jul	56-1	TV-G	22:01	22:23	23:16	00:53	2:51	44°34.198	125°08.794	44°34.230	125°08.840	787,1		dropped at 23:14:51
25 Jul	56-2	TV-G	01:18	01:43	02:44	03:06	1:47	44°34.189	125°08.781	44°34.199	125°08.799	693		not dropped
25 Jul	57-1	OFOS	04:05	04:18	06:46	07:25	3:20	44°39.923	125°09.976	44°36.971	125°12.860	1847		
25 Jul	58-1	OFOS	08:14	08:31	10:22	10:44	2:29	44°37.560	125°06.000	44°37.600	125°03.888	1050		
25 Jul	59-1	OFOS	11:32	11:53	18:18	18:42	7:09	44°44.027	125°01.817	44°44.022	125°52.884	543		
25 Jul	60-1	TV-G	20:05	20:28	20:38	21:31	1:25	44°37.560	125°04.730	44°37.560	125°04.670	922,2		dropped at 20:36:37
25 Jul	61-1	TV-G	21:43	22:02	23:19	23:43	2:00	44°37.564	125°02.291	44°37.560	125°04.660	924,1		not dropped
26 Jul	62-1	SL	00:12	00:36		01:02	0:49	44°37.010	125°03.010	44°37.010	125°03.010	1201	110cm	
26 Jul	63-1	MUC	01:25	01:57		02:49	1:24	44°37.010	125°03.010	44°37.010	125°03.010	1201,0	7 cores (43-51cm)	
26 Jul	64-1	HS	03:47			04:30	0:43	44°34.667	124°55.000	44°34.667	125°03.000			
26 Jul	64-2	HS	03:38			05:22	1:44	44°34.000	125°03.000	44°34.000	124°55.000			
26 Jul	64-3	HS	05:28			06:11	0:43	44°33.333	124°55.000	44°33.333	125°03.000			
26 Jul	64-4	HS	06:19			07:02	0:43	44°32.667	125°03.000	44°32.667	124°55.000			
26 Jul	64-5	HS	07:02			07:15	0:13	44°32.667	124°55.000	44°30.667	124°55.000			
26 Jul	64-6	HS	07:15			07:31	0:16	44°30.667	124°55.000	44°30.667	124°58.000			
26 Jul	64-7	HS	07:37			07:54	0:17	44°30.000	124°58.000	44°30.000	124°55.000			
26 Jul	64-8	HS	08:00			08:27	0:27	44°29.167	124°55.000	44°29.167	125°00.000			
26 Jul	64-9	HS	08:33			09:00	0:27	44°28.417	125°00.000	44°28.417	124°55.000			
26 Jul	64-10	HS	09:07			09:34	0:27	44°27.583	124°55.000	44°27.583	125°00.000			
26 Jul	64-11	HS	09:59			10:28	0:29	44°27.583	125°00.000	44°28.417	125°05.000			
26 Jul	65-1	20kHz	12:00			12:18	0:18	44°44.900	125°13.640	44°44.000	125°13.370			
26 Jul	65-2	20kHz	12:18			12:39	0:21	44°44.000	125°13.370	44°43.130	125°14.620			

Date 1999	Station No. SO143/	Instrument	Begin	on seafloor	off seafloor	End	Duration hh:mm	Latitude N°	Longitude W°	Latitude N°	Longitude W°	Water depth (m)	Recovery	Remarks
								Begin / on seafloor		**End / off seafloor**				
26. Jul	65–3	20kHz	12:49			13:18	0:29	44°43.130	125°14.620	44°44.000	125°13.380			
26. Jul	65–4	20kHz	13:18			13:49	0:31	44°44.000	125°13.380	44°44.900	125°13.640			
26. Jul	66–1	OFOS	14:15	14:40	16:10		1:55	44°43.134	125°14.584	44°43.947	125°13.520	972		
26. Jul	66–2	OFOS		16:13	19:46	20:06	3:53	44°43.931	125°13.481	44°44.762	125°14.406	1056		
26. Jul	67–1	ZAPS-I	13:44			16:27	2:43	44°43.826	125°13.711	44°44.054	125°14.222	965		not dropped
26. Jul	67–2	CTD	23:55	01:11		01:32	1:37	44°43.838	125°13.687	44°43.824	125°13.704	957	24 bottles / 24 water depths	
27. Jul	68–1	TV–G	01:55	02:11	03:02	03:06	1:10	44°43.830	125°13.690	44°43.970	125°14.070	980,8		not dropped
27. Jul	68–2	TV–G	03:20	03:20	03:49	05:05	3:09	44°43.686	125°13.833	44°43.880	125°13.864	946		dropped at 03:46
27. Jul	69–1	HS	06:13			07:04	0:50	44°32.148	125°15.200	44°29.323	125°22.617			
27. Jul	69–2	HS	07:04			07:25	0:20	44°29.323	125°22.617	44°26.900	125°22.617			
27. Jul	69–3	HS	07:25			08:27	1:01	44°26.900	125°22.617	44°31.148	125°13.617			
27. Jul	69–4	HS	08:27			08:37	0:10	44°31.148	125°13.617	44°30.323	125°12.617			
27. Jul	69–5	HS	08:37			09:43	1:06	44°30.323	125°12.617	44°25.000	125°21.617			
27. Jul	69–6	HS	09:43			10:00	0:17	44°25.000	125°21.617	44°24.775	125°18.158			
27. Jul	69–7	HS	10:00			11:03	1:03	44°24.775	125°18.158	44°30.000	125°10.617			
27. Jul	69–8	HS	11:03			11:15	0:12	44°30.000	125°10.617	44°29.333	125°09.000			
27. Jul	69–9	HS	11:15			11:40	0:25	44°29.333	125°09.000	44°29.333	125°09.000			
27. Jul	70–1	SL	13:17	14:05		15:22	2:05	44°38.500	125°14.500	44°38.500	125°14.500	2307	2.40m	
27. Jul	70–2	MUC	15:31	16:26		17:55	2:23	44°38.500	125°14.500	44°38.490	125°14.500	2307	7 cores (35-41cm)	
27. Jul	71–1	TV–G	18:26	19:03	20:40	21:15	2:46	44°34.190	125°08.790	44°34.200	125°08.840	786,3		dropped at 20:38:11
27. Jul	71–2	TV–G	22:19	22:36	23:33	23:56	1:36	44°34.194	125°08.775	44°34.172	125°08.826	786		not dropped
27. Jul	72–1	ZAPS-I	17:09			18:58	1:49	44°34.190	125°08.850	44°34.189	125°08.847	773		
28. Jul	73–1~11	18 kHz	02:47			06:27	3:39							details on separate sheet
28. Jul	74–1	CTD	07:00	07:26		08:15	1:15	44°40.121	125°05.774	44°40.122	125°05.787	605	14 bottles / 14 water depths	
28. Jul	74–2	CTD	09:55	10:25		11:15	1:19	44°40.127	125°05.799	44°40.126	125°05.789	602	15 bottles / 15 water depths	
28. Jul	74–3	ZAPS-I	06:08			09:42	3:34	44°40.125	125°05.788	44°40.123	125°05.793	598		
28. Jul	74–4	CTD	17:02	17:20		18:25	1:23	44°40.126	125°05.790	44°40.120	125°05.790	603	23 bottles / 23 water depths	
28. Jul	74–5	CTD	19:49	20.10		20:58	1:09	44°40.125	125°05.792	44°40.120	125°05.790	604	17 bottles / 17 water depths	
28. Jul	75–1	OFOS	21:47	22:09	02:37		4:28	44°43.649	125°13.109	44°40.493	125°07.297	749		
29. Jul	75–2	OFOS		03:17	04:30	05:12	1:54	44°41.213	125°05.691	44°42.890	125°05.760	1194,0		

CTD (Conductivity temperature depth)
HS (Hydrosweep)
MS (Surface-methane survey)
MUC (Multicoran)
OFOS (Ocean floor observation system)
HS (Parasound)
SL (Schwerelot / gravity core)
TP (Transponder)
TV–G (TV–Grab sampler)

TV–MUC (TV–Multicorer)
ZAPS-I (Zero angle photon spectrometer)
18 kHz (18 kHz array)
20 kHz (Elac fishfinder)

OFOS: time begin   = OFOS into water
   time off seafloor = end of profil time
   time end   = on deck time
   water depth   = end of profile depth

all Lat./Long. positions   = ship positions
CTD: end Lat./Long. = on deck position
SL   end Lat./Long. = end of station position

Water depth
OFOS: end of profile
MUC: at bottom
TV-MUC: drop (except 34-1/45-2/45-3 which is off bottom depth)
CTD: at bottom
SL: at bottom
TV-G: drop (except 41-2/56-2/61-1/68-1/71-2 which is off bottom depth)
ZAPS-I: average depth

SONNE 143–2 | **Station list**

Date 1999	Station No SO143/	Instrument	Time (UTC) Begin	on seafloor	off seafloor	End	Duration hh:mm	Begin / on seafloor Latitude N°	Longitude W°	End / off seafloor Latitude N°	Longitude W°	Water depth (m)	Recovery	Remarks
01 Aug	76-1	VESP-LL				15:04				44°40.060	125°05.890	604		Device Recovered
01 Aug	77-1	CTD – 16	17:01	18:02		19:57	2:56	44°38.984	125°20.016	44°39.019	125°19.819	2684	24 Bottles / 10 WaterDepths	
01 Aug	78-1	missing				21:45				44°38.499	125°06.382	613		Device Recovered
01 Aug	79-1	VESP-L?	23:34	00:13			0:39	44°34.090	125°08.970			786.9		Device Deployed
02 Aug	80-1	TV-G	01:34	01:57	02:30	02:55	1:21	44°34.112	125°08.783	44°34.249	125°08.808	779		
02 Aug	81-1	OFOS	03:54	04:12	07:29	08:04	4:08	44°33.560	125°08.030	44°34.807	125°09.509	934		
02 Aug	82-1	OFOS	09:33	09:51	13:21	13:44	4:11	44°34.160	125°08.610	44°34.201	125°08.878	791		
02 Aug	83-1	TV-MUC	15:18	16:26	16:28	17:30	2:12	44°38.500	125°14.500			2304		
02 Aug	83-2	TV-MUC	18:01	18:58	19:00	19:58	1:57	44°38.500	125°14.500			2305		
02 Aug	84-1	TP	21:30			22:43	1:13	44°39.560	125°06.830					Cancelled
02 Aug	85-1	18kHz	22:23			23:28	1:05	44°40.170	125°06.600	44°40.000	125°05.500			
03 Aug	86-1	CTD – 17	00:06	01:14		02:10	2:04	44°39.966	125°05.937	44°40.006	125°05.983	610	24 Bottles / 24 WaterDepths	
03 Aug	86-2	CTD – 18	04:36	05:17		06:06	1:30	44°39.984	125°05.996	44°39.942	125°05.993	612	22 Bottles / 21 WaterDepths	
03 Aug	87-1	OFOS	07:15	07:52	13:03	13:45	6:30	44°40.090	125°18.020	44°40.500	125°18.090	2107		
03 Aug	88-1	VESP-LL	14:45	15:29			0:44	44°34.189	125°08.820			785		Device Deployed
03 Aug	89-1	18kHz	16:08			18:46	2:38	44°34.007	125°09.159	44°34.338	125°08.782			
03 Aug	90-1	BCL-1	20:35	22:00			1:25	44°38.488	125°14.472			2311		Device Deployed
04 Aug	91-1	TV-MUC	00:14	00:44	00:46	01:10	0:56	44°33.880	125°08.290			852		
04 Aug	91-2	TV-MUC	01:33	01:54	01:56	02:32	0:59	44°33.900	125°08.310			848		
04 Aug	92-1	GKG	03:30	04:10		04:55	1:25	44°38.580	125°14.480			2311		
04 Aug	93-1	OFOS	06:00	06:20	09:42	10:15	4:15	44°44.212	125°13.818	44°44.033	125°15.031	1184		
04 Aug	94-1	OFOS	12:01	12:20	15:44	16:05	4:04	44°32.731	125°08.788	44°34.517	125°07.656	900		
04 Aug	95-1	GKG	17:05	17:54		18:40	1:35	44°38.580	125°14.510			2307		
04 Aug	96-1	18kHz	19:43			20:20	0:37	44°34.240	125°09.000	44°34.200	125°09.000	810		
04 Aug	97-1	CTD – 19	21:15	21:51		23:32	2:17	44°34.185	125°08.811	44°34.192	125°08.828	786	17 Bottles / 17 WaterDepths	
05 Aug	98-1	AN	00:25			01:00	0:35	44°38.770	125°14.430			50		
05 Aug	98-2	BCL-1			01:00	02:06	1:06			44°38.060	125°14.440	2311		Device Recovered
05 Aug	99-1	CTD – 20	03:33	03:43		04:41	1:08	44°34.185	125°08.798	44°34.168	125°08.816	787	24 Bottles / 23 WaterDepths	
05 Aug	100-1	HS	05:46			06:51	1:05	44°35.152	124°53.919	44°35.152	124°45.198			
05 Aug		HS	06:56			08:00	1:04	44°34.830	124°45.198	44°34.830	124°54.198			
05 Aug	100-3	HS	08:06			09:12	1:06	44°34.530	124°54.198	44°34.530	124°45.198			
05 Aug	100-4	HS	09:18			10:21	1:03	44°34.224	124°45.198	44°34.224	124°54.198			
05 Aug	100-5	HS	10:27			11:31	1:04	44°33.924	124°54.198	44°33.924	124°45.198			
05 Aug	100-6	HS	11:37			12:41	1:04	44°33.624	124°45.198	44°33.624	124°54.198			
05 Aug	100-7	HS	12:47			13:53	1:06	44°33.318	124°54.198	44°33.318	124°45.198			

Date 1999	Station No. SO143/	Instrument	Time (UTC)				Duration hh:mm	Begin / on seafloor		End / off seafloor		Water depth (m)	Recovery	Remarks
			Begin	on seafloor	off seafloor	End		Latitude N°	Longitude W°	Latitude N°	Longitude W°			
05. Aug	101–1	BCL–2	15:36	16:16			0:40	44°33.904	125°08.299			848		Device Deployed
05. Aug	102–1	GKG	17:17	17:35		18:10	0:53	44°33.794	125°08.297			858		
05. Aug	103–1	BEAMT	20:10	21:45	22:45	00:11	4:01	44°37.880	125°15.070	44°41.910	125°14.960	2295		
06. Aug	104–1	BCL–2			01:35	02:07	0:32			44°33.890	125°08.370	858		Device Recovered
06. Aug	105–1	TV–MUC	02:33	02:51	03:03	03:27	0:54	44°34.140	125°08.810	44°34.218	125°08.823	787		
06. Aug	105–2	TV–MUC	03:45	04:06	04:09	04:31	0:46	44°34.220	125°08.821	44°34.181	125°08.767	787		
06. Aug	106–1	TV–G	05:35	06:15	08:55	09:58	4:23	44°40.955	125°16.633	44°41.120	125°17.740	2088		Not Dropped
06. Aug	107–1	HS	12:28			13:30	1:02	44°33.018	125°54.198	44°33.018	125°45.198			
06. Aug	107–2	HS	13:35			14:39	1:04	44°32.760	125°45.198	44°32.760	125°54.198			
06. Aug	107–3	HS	14:44			15:48	1:04	44°32.496	125°54.198	44°32.496	125°45.198			
06. Aug	107–4	HS	15:55			17:00	1:05	44°32.238	125°45.198	44°32.238	125°54.198			
06. Aug	108–1	BCL–3	18:09	18:38			0:29	44°34.201	125°08.802			786		Device Deployed
06. Aug	109–1	VESP	20:45	22:33		23:35	2:50	44°34.146	125°08.743	44°34.191	125°08.813	786		
07. Aug	110–1	Foto–L1	00:45	02:03			1:18	44°34.200	125°08.799			788		
07. Aug	111–1	OFOS	05:00	05:19	08:42	09:21	4:21	44°37.700	125°07.670	44°38.494	125°11.368	1725		
07. Aug	112–1	OFOS	10:56	11:11	13:50	14:28	3:24	44°40.107	125°05.351	44°40.477	125°07.381	684		
07. Aug	113–1	GKG	15:36	15:51		16:20	0:44	44°34.000	125°08.600			807		
07. Aug	114–1	TV–MUC	16:56	17:20	17:27	17:45	0:49	44°34.210	125°09.850	44°34.202	125°08.813	786		
07. Aug	115–1	GKG	18:27	18:46		19:15	0:48	44°33.600	125°08.100			887		
07. Aug	116–1	BEAMT	19:48	20:38	21:08	22:15	2:27	44°32.330	125°08.940	44°33.800	125°06.920	970		
07. Aug	117–1	BCL–3			22:16	22:50	0:34			44°34.240	125°08.750	796		Device Recovered
07. Aug	118–1	VESP	23:35	00:14		01:16	1:41	44°34.191	125°08.800	44°34.209	125°08.806	786		
08. Aug	119–1	BCL–4	05:20	06:04		06:24	1:04	44°34.200	125°08.870	44°34.200	125°08.800	787		Device Deployed
08. Aug	120–1	CTD – 21	08:23	08:56		09:49	1:26	44°50.199	124°57.802	44°50.234	124°57.774	750	20 Bottles / 20 WaterDepths	
08. Aug	121–1	OFOS	10:21	10:38	13:58	14:16	3:55	44°50.519	124°56.761	44°48.983	124°57.548	696		
08. Aug	122–1	BCL–4			16:30	17:00	0:30			44°34.170	125°08.780	787		Device Recovered
08. Aug	123–1	TV–MUC	17:05	17:30	17:55	18:22	1:17	44°34.180	125°08.810	44°34.203	125°08.805	787		
08. Aug	124–1	CTD – 22	19:18	20:38		22:45	3:27	44°39.000	125°14.430	44°39.010	125°14.500	2311	20 Bottles / 20 WaterDepths	
09. Aug	125–4	HS	14:39			14:49	0:10	44°41.500	125°39.000	44°42.150	125°39.250			
09. Aug	125–5	HS	14:49			15:36	0:47	44°42.150	125°39.250	44°39.100	125°35.000			
09. Aug	125–6	HS	15:36			15:54	0:18	44°39.100	125°35.000	44°37.850	125°36.800			
09. Aug	125–7	HS	15:54			16:38	0:44	44°37.850	125°36.800	44°40.900	125°41.000			
09. Aug	126–1	GKG	17:10	18:04		19:05	1:55	44°40.000	125°37.990			2889		
09. Aug	126–2	TV–MUC	20:08	21:07	21:09	22:20	2:12	44°39.990	125°38.020	44°40.000	125°37.990	2892		
09. Aug	127–1	TV–MUC	23:50	00:41	00:43	01:40	1:50	44°38.450	125°14.520	44°38.500	125°14.490	2321		
10. Aug	128–1	VESP 4.1				02:35				44°34.189	125°08.820	785		Device Recovered
10. Aug	129–1	OFOS	03:47	04:14	06:45	07:12	3:25	44°36.542	125°11.082	44°38.540	125°10.333	1191		

Date 1999	Station No. SO143/	Instrument	Time (UTC)				Duration hh.mm	Begin / on seafloor		End / off seafloor		Water depth (m)	Recovery	Remarks
			Begin	on seafloor	off seafloor	End		Latitude N°	Longitude W°	Latitude N°	Longitude W°			
10. Aug	130–1	CTD – 23	08 05	08 47		09 37	1:32	44°34.180	125°08.773	44°34.238	125°08.851	787	15 Bottles / 15 WaterDepths	
10. Aug	130–2	CTD – 24	12:00	12:37		13 26	1:26	44°34.190	125°08.804	44°34.213	125°08.817	784	16 Bottles / 16 WaterDepths	
10. Aug	130–3	CTD – 25	16 03	16:55		17:44	1:41	44°34.192	125°08.815	44°34.185	125°08.835	784	16 Bottles / 16 WaterDepths	
10. Aug	130–4	CTD – 26	20:04	20 36		21:35	1:31	44°34.191	125°08.838	44°34.180	125°08.830	787	24 Bottles / 24 WaterDepths	
10. Aug	131–1	TV–MUC	22:54	23:11	23:14	23 25	0 31	44°34.180	125°08.800	44°34.187	125°08.803	785		
11. Aug	131–2	TV–MUC	00 00	00 20	00:23	00:50	0:50	44°34.180	125°08.830	44°34.196	125°08.819	786		
11. Aug	131–3	VESP	01:45	02:23	02:28	03:31	1.46	44°34.195	125°08.837	44°34.215	125°08.801	783		
11. Aug	132–1	OFOS	05.11	05.36	08:58	09:25	4:14	44°44.079	125°12.599	44°44.381	125°14.735	1087		
11. Aug	133–1	OFOS	10:46	11:04	15:30	15:55	5:09	44°34.170	125°07.930	44°33.710	125°12.702	1299		
11. Aug	134–1	BCL–5	16:50	18:10			1:20	44°38.562	125°14.485			2307		Device Deployed
11. Aug	135–1	TV–MUC	19:51	20:15	20:18	20:48	0:57	44°34.190	125°08.830	44°34.200	125°08.819	787	Nothing	1st try – in vain (malfunction)
11. Aug	135–1	TV–MUC	20:58	21:29	21:32	22:15	1:17	44°34.200	125°08.810	44°34.197	125°08.818	787		2nd try
11. Aug	135–2	TV–MUC	22:23	22:59	23:02	23:30	1:07	44°34.190	125°08.830	44°34.186	125°08.822	786		
11. Aug	135–3	TV–MUC	23:50	00:24	00:27	00:45	0:55	44°34.200	125°08.850	44°34.196	125°08.825	783	Acharax	
12. Aug	135–4	TV–MUC	01:05	01:32	01:35	01:55	0:50	44°34.200	125°08.790	44°34.196	125°08.801	785		
12. Aug	135–5	TV–MUC	02:17	02:33	02:36	03:00	0:43	44°34.200	125°08.790	44°34.207	125°08.802	784	Acharax	
12. Aug	135–6	TV–MUC	03:11	03:39	03:42	04:02	0:51	44°34.190	125°08.820	44°34.193	125°08.806	785	Acharax	
12. Aug	136–1	HS	04:59			05:58	0:59	44°31.974	124°54.198	44°31.974	124°45.198			
12. Aug	136–2	HS	06:03			07:00	0:57	44°31.721	124°45.198	44°31.721	124°54.198			
12. Aug	137–1	CTD – 27	08:28	08:57	13:36	14:00	5:32	44°39.741	125°05.508	44°39.427	125°06.643	610	17 Bottles	ToYo
12. Aug	138–1	BCL–6	14:57	15:38			0:41	44°34.171	125°08.885			784		Device Deployed
12. Aug	139–1	MUC	17:55	18:19		18:45	0:50	44°34.100	125°08.380	44°34.080	125°08.400	826		
12. Aug	140–1	TV–GKG	19:45	20:13		20:40	0:55	44°34.200	125°08.810	44°34.190	125°08.830	786		
12. Aug	141–1	BCL–5			21:26	22:16	0:50			44°38.550	125°14.480			Device Recovered
12. Aug	142–1	VESP–L1	23:10	00:15			1:05	44°34.209	125°08.758			786		Device Deployed
13. Aug	143–1	VESP–L2				00:47				44°34.090	125°08.970	786.9		Device Recovered
13. Aug	144–1	BCL–6			01:20	01:47	0:27			44°34.060	125°08.800	787		Device Recovered
13. Aug	145–1	CTD – 28	03:10	03:43		05:40	2:30	44°37.561	125°04.693	44°37.560	125°04.700	920	19 Bottles / 19 WaterDepths	
13. Aug	146–1	18kHz	05:27			08:29	3:02	44°40.070	125°06.250	44°40.200	125°06.200			
13. Aug	147–1	CTD – 29	08:54	10:13		11:00	2:06	44°40.144	125°06.520	44°40.144	125°06.546	625	11 Bottles / 11 WaterDepths	
13. Aug	148–2	CTD – 30	13:00	13:28		14:12	1:12	44°40.900	125°06.560	44°40.899	125°06.468	710	21 Bottles / 21 WaterDepths	
13. Aug	149–1	TV–GKG	15:15			16:30	1:15	44°34.170	125°08.810			765		chancelled due to bad TV–Pic.
13. Aug	150–1	VESP	18:10	18:29	18:40	20:40	2:30	44°34.172	125°08.764	44°34.231	125°08.803	786		
13. Aug	151–1	MUC	21:55	23:02		23:40	1:45	44°33.010	125°04.020	44°33.000	125°04.000	1284		
14. Aug	151–2	MUC	00:08	00:39		01:10	1:02	44°33.000	125°04.000	44°33.000	125°04.000	1285		
14. Aug	152–1	Foto–L1			01:47	02:12	0:25			44°34.060	125°08.900	782		Device Recovered

Date 1999	Station No. SO143/	Instrument	Time (UTC) Begin	on seafloor	off seafloor	End	Duration hh:mm	Begin / on seafloor Latitude N°	Longitude W°	End / off seafloor Latitude N°	Longitude W°	Water depth (m)	Recovery	Remarks
14. Aug	153–1	VESP–L2			02:40	03:04	0:24	44°34.210	125°08.810			785		chancelled: Grndweight dropped
14. Aug	154–1	OFOS	05:53	06:05	09:52	10:10	4:17	44°49.523	124°53.140	44°51.144	124°55.713	676		No CTD
14. Aug	155–1	OFOS	12:30	12:47	16:00	16:19	3:49	44°45.771	124°55.511	44°48.810	124°59.750	846		
14. Aug	156–1	VESP–L2	18:58	19:32			0:34	44°34.234	125°08.832			786		Device Deployed
14. Aug	157–1	BCL–7	21:30	22:20			0:50	44°34.189	125°08.830			787		Device Deployed
15. Aug	158–1	VESP	00:05	01:10	02:50	03:41	3:36	44°40.185	125°05.875	44°40.198	125°05.867	605		
15. Aug	159–1	CTD – 31	04:37	04:55	10:28	10:35	5:58	44°39.603	125°05.702	44°38.630	125°05.865			ToYo
15. Aug	160–1	HS	12:10			13:16	1:06	44°31.461	124°54.198	44°31.461	124°45.198			
15. Aug	160–2	HS	13:22			14:27	1:05	44°31.202	124°45.198	44°31.202	124°54.198			
15. Aug	160–3	HS	14:33			15:36	1:03	44°30.943	124°54.198	44°30.943	124°45.198			
15. Aug	160–4	HS	15:45			16:48	1:03	44°30.727	124°45.198	44°30.727	124°54.198			
15. Aug	161–1	TV–GKG	18:10	18:35	18:45	19:10	1:00	44°34.190	125°08.830	44°34.208	125°08.809	784		
15. Aug	162–1	Foto–L2	20:00	20:36			0:36	44°34.176	125°08.822			785		Device Deployed
15. Aug	163–1	TV–MUC	21:42	21:58	22:16	22:36	0:54	44°34.170	125°08.840	44°34.196	125°08.804	786		
15. Aug	163–2	TV–MUC	23:50			00:09	0:19	44°34.180	125°08.760			787		chancelled due to bad TV–Pic.
16. Aug	164–1	BCL–7			01:35	02:05	0:30			44°33.910	125°08.780	784		Device Recovered
16. Aug	165–1	VESP	03:18	03:51	05:05	05:51	2:33	44°40.100	125°05.810	44°40.180	125°05.885	608		
16. Aug	166–1	CTD – 32	06:42	07:04		07:51	1:09	44°39.612	125°05.685	44°39.598	125°05.590	638	20 Bottles / 20 WaterDepths	
16. Aug	167–1	TV–G	10:01	10:16	12:48	13:10	3:09	44°50.550	125°55.827	44°50.263	125°55.681	567		
16. Aug	168–1	BCL–8	16:06	16:59			0:53	44°34.201	125°08.833			784		Device Deployed
16. Aug	169–1	GKG	17:52	18:14		18:45	0:53	44°34.410	125°08.790	44°34.390	125°08.790	793		
16. Aug	170–1	GKG	19:00	19:15		19:45	0:45	44°34.600	125°08.810	44°34.600	125°08.800	812		
16. Aug	171–1	BEAMT	20:30	21:30	22:30	23:30	3:00	44°34.130	125°10.940	44°38.320	125°09.840	1220		
17. Aug	172–1	mooring	00:34	01:22			0:48	44°38.660	125°06.190					Device Deployed
17. Aug	173–1	TV–MUC	02:48	03:05	03:27	03:50	1:02	44°34.160	125°08.850	44°34.195	125°08.800	785		
17. Aug	174–1	TV–MUC	04:23	04:40	04:51	05:15	0:52	44°34.200	125°08.840	44°34.202	125°08.804	786		
17. Aug	174–2	TV–MUC	05:32	05:49	06:01	06:30	0:58	44°34.200	125°08.850	44°34.198	125°08.801	787		
17. Aug	175–1	CTD – 33	07:28	07:54		08:38	1:10	44°39.848	125°05.120	44°39.843	125°05.153	690	20 Bottles / 20 WaterDepths	
17. Aug	176–1	HS	09:54			11:55	2:01	44°52.400	125°08.000	44°52.400	125°25.000			
17. Aug	176–2	HS	12:10			14:12	2:02	44°53.529	125°25.000	44°53.529	125°08.000			
17. Aug	176–3	HS	14:24			16:26	2:02	44°54.658	125°08.000	44°54.658	125°25.000			
17. Aug	176–4	HS	16:41			17:00	0:19	44°55.522	125°25.000	44°55.522	125°22.268			Time–Out
17. Aug	177–1	GKG	18:58	19:13		19:30	0:32	44°34.900	125°08.780	44°34.890	125°08.810	840		
17. Aug	178–1	BCL–8			20:00	20:27	0:27			44°34.040	125°08.600	790		Device Recovered
17. Aug	179–1	TV–MUC	20:55	21:13	21:23	21:45	0:50	44°34.180	125°08.860	44°34.188	125°08.821	786		
17. Aug	179–2	TV–MUC	22:08	22:26	22:38	23:00	0:52	44°34.180	125°08.830	44°34.179	125°08.824	786		
17. Aug	179–3	TV–MUC	23:26	23:44	00:14	00:30	1:04	44°34.210	125°08.740	44°34.221	125°08.843	786		
18. Aug	179–4	TV–MUC	00:50	01:08	01:30	02:00	1:10	44°34.200	125°08.780	44°34.216	125°08.871	791		

Date 1999	Station No SO143/	Instrument	Time (UTC) Begin	on seafloor	off seafloor	End	Duration hh:mm	Begin / on seafloor Latitude N°	Longitude W°	End / off seafloor Latitude N°	Longitude W°	Water depth (m)	Recovery	Remarks
18 Aug	180-1	BCL-9	02:31	03:22			0:53	44°34.193	125°08.821			787		Device Deployed
18 Aug	181-1	VESP	04:25	05:30	06:42	07:01	2:36	44°34.180	125°08.820	44°34.216	125°08.848	788		
18 Aug	182-1	CTD-34	08:52	09:26		10:06	1:11	44°40.124	125°04.522	44°40.089	125°04.650	756	20 Bottles / 20 WaterDepths	
18 Aug	183-1	HS	12:02			14:37	2:35	44°55.522	125°22.240	44°55.522	125°00.000			
18 Aug	183-2	HS	14:44			17:00	2:16	44°56.396	125°00.000	44°56.386	125°18.900			
18 Aug	184-1	BCL-9			18:57	19:24	0:27			44°34.040	125°08.690	795		Device Recovered
18 Aug	185-1	TV-MUC	17:43	20:03	20:13	20:35	00:52	44°34.190	125°08.830	44°34.202	125°08.834	787		
18 Aug	185-2	TV-MUC	20:53	21:15	21:40	22:20	1:27	44°34.170	125°08.850	44°34.211	125°08.839	788		
19 Aug	186-1	CTD-35	00:05	00:45		01:37	1:32	44°40.189	125°03.246	44°40.168	125°03.264	938	20 Bottles / 20 WaterDepths	
19 Aug	187-1	TV-MUC	02:43	03:11	03:12	03:30	0:47	44°36.160	125°08.860	44°36.186	125°08.819	786		
19 Aug	187-2	TV-MUC	03:47	04:14	04:31	04:50	1:03	44°34.180	125°08.860	44°34.180	125°08.820	786		
19 Aug	187-3	TV-MUC	05:06	05:28	06:17	06:45	1:45	44°34.170	125°08.830	44°34.193	125°08.833	785		
19 Aug	187-4	TV-MUC	06:54	07:22	07:35	08:00	1:06	44°34.190	125°08.820	44°34.204	125°08.814	785		
19 Aug	188-1	CTD-36	09:40	10:10		10:45	1:05	44°39.280	125°06.253	44°39.282	125°06.303	624		
19 Aug	189-1	BCL-10	21:55	23:33			1:38	44°34.200	125°08.830			786		Device Deployed
20 Aug	190-1	TV-MUC	00:03	00:20	00:26	00:45	0:42	44°34.050	125°08.410	44°34.044	125°08.480	824		
20 Aug	191-1	VESP	01:45	02:46	04:20	05:00	3:15	44°34.180	125°08.870	44°34.213	125°08.807	786		
20 Aug	192-1	OFOS	06:16	06:21	10:52	11:06	4:50	44°40.015	125°06.473	44°40.176	125°06.652	634		
20 Aug	192-2	OFOS	12:10	12:25	15:52	16:00	3:50	44°39.956	125°06.434	44°40.353	125°06.593	642		
20 Aug	193-1	TV-MUC	16:59	17:24	17:26	17:56	0:57	44°37.490	124°55.990	44°37.509	124°55.970	686		
20 Aug	193-2	GKG	18:50	19:12		19:40	0:50	44°37.500	124°55.980	44°37.500	124°55.990	684		
20 Aug	194-1	SIO-Bf	20:36			01:15	4:39	44°34.150	125°08.670					Device Recovered
21 Aug	195-1	VESP-L2			01:18	01:45	0:27			44°34.234	125°08.832	786		Device Recovered
21 Aug	196-1	BCL-10			01:47	02:15	0:28			44°34.200	125°08.830	768		Device Recovered
21 Aug	197-1	CTD-37	04:19	04:56				44°39.005	125°14.491			2307	10 Bottles / 1 WaterDepth	
21 Aug	198-1	VESP	06:34	07:19	08:33	09:15	2:49	44°34.180	125°08.820	44°34.237	125°08.826	786		
21 Aug	199-1	CTD-38	10:50	11:26		12:09	1:19	44°39.107	125°06.898	44°39.098	125°06.896	698		
21 Aug	200-1	SIO-Bf			13:15	16:47	3:32	44°40.001	125°05.800			616		
21 Aug	201-1	SIO-Bf			16:47	19:27	2:40	44°34.150	125°05.670					
21 Aug	202-1	VESP			20:09	20:37	0:28	44°34.150	125°05.670	44°34.130	125°08.650	807		
21 Aug	203-1	Foto-L2			20:38	21:02	0:24			44°34.130	125°08.650	807		Device Recovered
21 Aug	204-1	TV-MUC	21:57	22:24	23:05	23:30	1:33	44°34.210	125°08.900	44°34.233	125°08.865	785		
22 Aug	205-1	HS	01:37			02:19	0:42	44°56.386	125°18.900	44°56.386	125°25.000			
22 Aug	205-2	HS	02:30			05:30	3:00	44°57.250	125°25.000	44°57.250	125°00.000			
22 Aug	205-3	HS	05:40			08:38	2:58	44°58.114	125°00.000	44°58.114	125°25.000			
22 Aug	205-4	HS	08:52			11:51	2:59	44°58.978	125°25.000	44°58.978	125°00.000			
22 Aug	205-5	HS	12:03			14:59	2:56	44°59.842	125°00.000	44°59.842	125°25.000			
22 Aug	205-6	HS	15:15			16:00	0:45	45°00.706	125°25.000	45°00.706	125°19.020			
22 Aug	206-1	TV-MUC	18:30	18:47	19:06	19:35	1:05	44°34.230	125°08.840	44°34.247	125°08.814	787		

Date 1999	Station No. SO143/	Instrument	Time (UTC) Begin	on seafloor	off seafloor	End	Duration hh:mm	Begin / on seafloor Latitude N°	Longitude W°	End / off seafloor Latitude N°	Longitude W°	Water depth (m)	Recovery	Remarks
22. Aug	206–2	TV–MUC	19:45	20:07	20:41	21:05	1:20	44°34.270	125°08.870	44°34.182	125°08.835	787		
22. Aug	206–3	TV–MUC	21:11	21:42	21:54	22:20	1:09	44°34.230	125°08.880	44°34.472	125°08.842	786		
22. Aug	207–1	TP			22:38	01:15	2:37			44°34.300	125°08.200			Device Recovered
23. Aug	208–1	NLC–K	02:20	02:50	03:50	04:05	1:45	44°39.013	125°14.496			2300		
23. Aug	209–1	TV–G	05:49	06:00	07:10	07:36	1:47	44°40.008	125°06.082	44°40.421	125°06.018	618		Not dropped
23. Aug	210–1	HS	12:47			14:41	1:54	45°30.000	125°16.000	45°41.000	125°16.000			
23. Aug	210–2	HS	14:53			16:42	1:49	45°41.000	125°14.500	45°30.000	125°14.500			
23. Aug	210–3	HS	16:59			18:45	1:46	45°30.000	125°13.000	45°41.000	125°13.000			
23. Aug	210–4	HS	18:54			20:42	1:48	45°41.000	125°11.800	45°30.000	125°11.800			
23. Aug	210–5	HS	20:52			22:42	1:50	45°30.000	125°10.900	45°41.000	125°10.900			
23. Aug	210–6	HS	22:51			00:41	1:50	45°41.000	125°10.000	45°30.000	125°10.000			
24. Aug	210–7	HS	00:51			02:38	1:47	45°30.000	125°09.100	45°41.000	125°09.100			
24. Aug	210–8	HS	02:46			04:35	1:49	45°41.000	125°08.200	45°30.000	125°08.200			
24. Aug	210–9	HS	04:44			06:30	1:46	45°30.000	125°06.900	45°41.000	125°06.900			

Abbreviations

CTD (Conductivity temperature depth)
HS (Hydrosweep)
MUC (Multicorer)
OFOS (Ocean floor observation system)
PS (Parasound)
TP (Transponder)
TV–G (TV–Grab sampler)
TV–MUC (TV–Multicorer)
18 kHz (18 kHz array)
20 kHz (Elac fishfinder)
VESP (Vent sampler)
AN (Apstein Netz)
GKG (Gross Kasten Greifer)
BEAMT (Beam–trawl)
SIO–Bt (SIO–Benthic–turameter)

Annotations:

OFOS: time beginn = OFOS into water
    time off seafloor = end of profil time
    time end = on deck time
    water depth = end of profile depth

all Lat./Long. positions = ship positions
CTD: end Lat./Long. = on deck position
SL: end Lat./Long. = end of station position
TV–G: end Lat./Long. = drop position

Water depth
OFOS: end of profile
MUC: at bottom
TV–MUC: drop (except 34–1/45–2/45–3 which is off bottom depth)
CTD: at bottom
SL: at bottom
TV–G: drop (except 106–1 which is off bottom depth)
AN : Tiefe bei Hols

SONNE 143–3 — Station list

Date 1999	Station No. SO143/	Instrument	Time (UTC) Begin	on seafloor	off seafloor	End	Duration hh:mm	Begin / on seafloor Latitude N°	Longitude W°	End / off seafloor Latitude N°	Longitude W°	Water depth (m)	Recovery	Remarks
27. Aug	211	OFOS	13:50	14:16	00:21	01:05	11:15	45°35.830	125°08.550	45°35.766	125°15.003	1714		
28. Aug	212	SL	14:07	14:44		15:10	1:03	44°34.217	125°08.862			786	85 cm	
28. Aug	213	OFOS	16:16	16:49	23:21	23:48	7:32	44°39.494	125°00.815	44°39.723	125°08.160	816		
29. Aug	214	TV-G	01:02	02:11	02:29	03:00	1:58	44°34.169	125°08.736	44°34.212	125°08.827	774	dropped at 44°34.208N/125°08.825W	
29. Aug	215–1	SL	13:23	13:52		14:15	0:52	44°34.205	125°08.830			785	no core	
29. Aug	215–2	SL	14:43	15:04		15:29	0:46	44°34.207	125°08.813			784	no core, carbonates	
29. Aug	216	OFOS	16:48	17:16	22:04	22:05	5:17	44°40.460	125°04.970	44°40.441	125°09.993	1026		
29. Aug	217	AKL	23:20	00:03		00:28	1:08	44°34.216	125°08.864	44°34.2131	125°08.865	788	dropped at 44°34.2118N/125°08.8603W	AKL lost
30. Aug	218	TV-MUC	13:35	13:53	14:05	14:31	0:56	44°34.175	125°08.782	44°34.215	125°08.856	785	dropped at 44°34.210N/125°08.856W, no core	
30. Aug	219–1	SL	15:38	16:01		16:29	0:51	44°34.207	125°08.866			785	138 cm	
30. Aug	219–2	SL	16:56	17:20		17:46	0:50	44°34.210	125°08.861			785	132 cm	
30. Aug	219–3	SL	18:07	18:20		18:34	0:27	44°34.213	125°08.867			788	90 cm	
31. Aug	220	TV-MUC	13:13	13:48	14:03	14:40	1:27	44°34.172	125°08.802	44°34.222	125°08.852	790	dropped at 44°34.224N/125°08.872W, 3 cores (22–28 cm)	
31. Aug	221–1	SL	15:15	15:31		15:52	0:37	44°34.210	125°08.814			785	105 cm	
31. Aug	221–2	SL	16:05	16:21		16:40	0:35	44°34.211	125°08.811			785	118 cm	
31. Aug	222	TV-G	17:05	17:27	18:45	19:14	2:09	44°34.167	125°08.770	44°34.260	125°08.850	772	dropped at 44°34.238N/125°08.843W	
31. Aug	223	OFOS	19:59	20:26	04:28	05:04	9:05	44°35.140	125°04.280	44°35.156	125°12.953	1716		
01. Sep	224	OFOS	06:49	07:05	10:07	10:06	3:17	44°41.014	124°51.903	44°42.795	124°49.674	349		
01. Sep	225	OFOS	11:09	11:21	13:00	13:00	1:51	44°49.495	124°48.430	44°48.611	124°50.466	433		
01. Sep	226	TP	14:37			16:15	1:38	44°38.800	125°05.500					
01. Sep	227	TV-G	16:57	17:28	21:54	22:30	5:33	44°34.170	125°08.770	44°34.234	125°08.892	792	unsuccessful attempt to retrieve the AKL	
01. Sep	228	TV-G	22:39	23:00	00:17	00:40	2:01	44°34.160	125°08.780	44°34.184	125°08.759	790		grab didn't close
02. Sep	229–1	SL	01:10	01:26		01:41	0:31	44°34.211	125°08.810			786	110 cm	
02. Sep	229–2	SL	01:58	02:13		02:27	0:29	44°34.207	125°08.813			786	30 cm	
02. Sep	230	TP	02:31			03:24	0:53	44°34.370	125°08.000					
02. Sep	231	OFOS	04:28	04:45	09:00	09:18	4:50	44°27.020	125°01.540	44°26.797	125°02.445	652		
02. Sep	232	OFOS	09:52	10:09	11:53	12:16	2:24	44°23.977	125°00.135	44°24.004	125°01.952	832		
02. Sep	233	TV-G	13:36	13:54	15:07	15:38	2:02	44°34.144	125°08.740	44°34.269	125°08.887	792	dropped at 44°34.263N/125°08.689W	
02. Sep	234	TP	16:30			17:16	0:46	44°39.530	125°06.860					
02. Sep	235	MUC	17:59	18:21		18:37	0:38	44°34.452	125°09.136			833	4 cores (18–23 cm)	
02. Sep	236	MUC	18:56	19:13		19:30	0:34	44°34.656	125°09.000			835	2 cores (30–31 cm)	
02. Sep	237	SL	19:45	19:58		20:15	0:30	44°34.665	125°09.004			836	154 cm	
02. Sep	238	SL	20:43	21:02		21:20	0:37	44°34.443	125°09.130			834	83 cm	

AKL (Autoklaven–Kolbenlot / autoclave piston–corer)
MUC (Multicorer)
OFOS (Ocean floor observation system)
SL (Schwerelot / gravity core)
TP (Transponder)
TV-G (TV–Grab sampler)
TV–MUC (TV–Multicorer)

OFOS: time beginn = OFOS into water
    time off seafloor = end of profil time
    time end = on deck time
    water depth = end of profile depth

all Lat./Long. positions = ship positions

Water depth (hydrosweep):
AKL: at bottom
MUC: at bottom
OFOS: end of profile
SL: at bottom
TV-G: drop
TV–MUC: drop

A5 **Vent acrivity on Hydrate Ridge South**

Lat-	Long.	Sta.	Remark
SONNE 143 observations 1999			
44° 34.199	125° 08.786	20-3 OFOS	bacteria & clam
44° 34.215	125° 08.818	20-3 OFOS	bacteria & clam
44° 34.243	125° 08.801	20-3 OFOS	bacteria
44° 34.217	125° 08.699	20-3 OFOS	clam
44° 34.227	125° 08.713	20-3 OFOS	clam
44° 34.208	125° 08.802	53-1 OFOS	marker No. 7
44° 34.262	125° 09.083	20-4 OFOS	Alvin track
44° 34.255	125° 08.915	20-4 OFOS	Alvin track
44° 34.222	125° 08.791	20-4 OFOS	pinnacle
44° 34.244	125° 08.799	53-1 OFOS	2 pinnacles
44° 34.231	125° 08.766	20-4 OFOS	pinnacle
44° 34.192	125° 08.819	20-4 OFOS	bacteria
44° 34.197	125° 08.802	53-1 OFOS	bacteria on rock
44° 34.213	125° 08.802	53-1 OFOS	biggest mat field
44° 34.221	125° 08.801	53-1 OFOS	biggest mat field
44° 34.235	125° 08.799	53-1 OFOS	bacteria
44° 34.248	125° 08.864	20-4 OFOS	SIO/FM
44° 34.212	125° 08.802	21-2 TVG	bact. & hydrate
44° 34.195	125° 08.802	71-2 TVG	hydrate
44° 34.244	125° 08.801	28-1 OFOS	Alvin weight
44° 34.292	125° 08.860	28-1 OFOS	SIO/FM
44° 34.222	125° 08.775	28-1 OFOS	bacteria
44° 34.207	125° 08.769	28-1 OFOS	bacteria
44° 34.199	125° 08.772	28-1 OFOS	clams
44° 34.258	125° 08.801	53-1 OFOS	N clam limit
44° 34.105	125° 08.805	53-1 OFOS	S clam limit
44° 34.181	125° 08.800	53-1 OFOS	big clam field
44° 34.258	125° 08.795	53-1 OFOS	clam
SONNE 110 observations 1996			
44° 34.23	125° 08.89	TV-G 18	hydrate
ALVIN 3-35 observations 1999			
44° 34.206	125° 08.826	3428	bubbles
44° 34.199	125° 08.812	3421	orange bacteria
44° 34.188	125° 08.822	3421	white bacteria
44° 34.176	125° 08.803	3421	S limit vents
44° 34.197	125° 08.818	3430	bubble site No.7

A6　Sonar tracks 18kHz

SONNE 143-1b			18 kHz Sonar Tracks				

		Time (UTC)			Begin		End	
Date 1999	Stat. No. SO143/	Begin	End	Duration hh:mm	Latitude N°	Longitude W°	Latitude N°	Longitude W°
16. Jul	22–1	00:52	01:04	0:12	44°39.631	125°06.833	44°39.631	125°05.500
16. Jul	22–2	01:06	01:21	0:15	44°39.755	125°05.500	44°39.755	125°06.833
16. Jul	22–3	01:26	01:38	0:12	44°39.879	125°06.833	44°39.879	125°05.500
16. Jul	22–4	01:44	01:55	0:11	44°40.003	125°05.500	44°40.003	125°06.833
16. Jul	22–5	02:02	02:13	0:11	44°40.127	125°06.833	44°40.127	125°05.500
16. Jul	22–6	02:19	02:36	0:17	44°40.252	125°05.500	44°40.252	125°06.833
16. Jul	22–7	02:37	02:49	0:12	44°40.376	125°06.833	44°40.376	125°05.500
16. Jul	22–8	02:53	03:05	0:12	44°40.500	125°05.500	44°40.500	125°06.833
16. Jul	22–9	03:06	03:16	0:10	44°40.500	125°06.833	44°39.631	125°06.833
16. Jul	22–10	03:25	03:36	0:11	44°39.631	125°06.667	44°40.500	125°06.667
16. Jul	22–11	03:40	03:51	0:11	44°40.500	125°06.499	44°39.631	125°06.499
16. Jul	22–12	03:57	04:08	0:11	44°39.631	125°06.334	44°40.500	125°06.334
16. Jul	22–13	04:12	04:23	0:11	44°40.500	125°06.167	44°39.631	125°06.167
16. Jul	22–14	04:30	04:41	0:11	44°39.631	125°06.000	44°40.500	125°06.000
16. Jul	22–15	04:44	04:55	0:11	44°40.500	125°06.833	44°39.631	125°06.833
16. Jul	22–16	05:02	05:13	0:11	44°39.631	125°06.666	44°40.500	125°06.666
16. Jul	22–17	05:17	05:27	0:10	44°40.500	125°06.500	44°39.631	125°06.500
16. Jul	22–18	05:27	05:41	0:14	44°39.631	125°05.500	44°39.631	125°06.833
16. Jul	22–19	05:45	05:57	0:12	44°39.755	125°06.833	44°39.755	125°05.500
16. Jul	22–20	06:02	06:13	0:11	44°39.879	125°05.500	44°39.879	125°06.833
16. Jul	22–21	06:18	06:30	0:12	44°40.003	125°06.833	44°40.003	125°05.500
16. Jul	22–22	06:34	06:46	0:12	44°40.127	125°05.500	44°40.127	125°06.833
16. Jul	22–23	06:51	07:04	0:13	44°40.252	125°06.833	44°40.252	125°05.500
16. Jul	22–24	07:07	07:20	0:13	44°40.376	125°05.500	44°40.376	125°06.833
16. Jul	22–25	07:25	07:36	0:11	44°40.500	125°06.833	44°40.500	125°05.500
16. Jul	22–26	07:36	07:47	0:11	44°40.500	125°05.500	44°39.631	125°05.500
16. Jul	22–27	07:52	08:04	0:12	44°39.631	125°05.666	44°40.500	125°05.666
16. Jul	22–28	08:07	08:18	0:11	44°40.500	125°05.833	44°39.631	125°05.833
16. Jul	22–29	08:23	08:34	0:11	44°39.631	125°06.000	44°40.500	125°06.000
16. Jul	22–30	08:38	08:48	0:10	44°40.500	125°06.167	44°39.631	125°06.167
16. Jul	22–31	08:54	09:05	0:11	44°39.631	125°06.334	44°40.500	125°06.334
16. Jul	22–32	09:09	09:20	0:11	44°40.500	125°06.499	44°39.631	125°06.499
16. Jul	22–33	09:25	09:36	0:11	44°39.631	125°06.667	44°40.500	125°06.667
16. Jul	22–34	09:40	09:50	0:10	44°40.500	125°06.833	44°39.631	125°06.833
16. Jul	22–35	09:50	10:02	0:12	44°39.631	125°06.833	44°39.631	125°05.500
16. Jul	22–36	10:07	10:20	0:13	44°39.755	125°05.500	44°39.755	125°06.833
16. Jul	22–37	10:25	10:37	0:12	44°39.879	125°06.833	44°39.879	125°05.500
16. Jul	22–38	10:42	10:54	0:12	44°40.003	125°05.500	44°40.003	125°06.833
16. Jul	22–39	10:58	11:10	0:12	44°40.127	125°06.833	44°40.127	125°05.500
16. Jul	22–40	11:15	11:27	0:12	44°40.252	125°05.500	44°40.252	125°06.833
16. Jul	22–41	11:33	11:44	0:11	44°40.376	125°06.833	44°40.376	125°05.500
16. Jul	22–42	11:49	12:01	0:12	44°40.500	125°05.500	44°40.500	125°06.833
16. Jul	22–43	12:01	12:12	0:11	44°40.500	125°06.833	44°39.631	125°06.833
16. Jul	22–44	12:17	12:29	0:12	44°39.631	125°06.667	44°40.500	125°06.667
16. Jul	22–45	12:33	12:43	0:10	44°40.500	125°06.499	44°39.631	125°06.499
16. Jul	22–46	12:48	12:59	0:11	44°39.631	125°06.334	44°40.500	125°06.334
16. Jul	22–47	13:03	13:14	0:11	44°40.500	125°06.167	44°39.631	125°06.167
16. Jul	22–48	13:19	13:30	0:11	44°39.631	125°06.000	44°40.500	125°06.000
16. Jul	22–49	13:34	13:44	0:10	44°40.500	125°06.833	44°39.631	125°06.833
16. Jul	22–50	13:50	14:01	0:11	44°39.631	125°06.666	44°40.500	125°06.666
16. Jul	22–51	14:04	14:15	0:11	44°40.500	125°06.500	44°39.631	125°06.500
16. Jul	22–52	14:15	14:28	0:13	44°39.631	125°05.500	44°39.631	125°06.833
16. Jul	22–53	14:31	14:43	0:12	44°39.755	125°06.833	44°39.755	125°05.500
16. Jul	22–54	14:48	15:00	0:12	44°39.879	125°05.500	44°39.879	125°06.833
16. Jul	22–55	15:05	15:16	0:11	44°40.003	125°06.833	44°40.003	125°05.500
16. Jul	22–56	15:22	15:34	0:12	44°40.127	125°05.500	44°40.127	125°06.833
16. Jul	22–57	15:41	15:53	0:12	44°40.252	125°06.833	44°40.252	125°05.500
16. Jul	22–58	16:01	16:13	0:12	44°40.376	125°05.500	44°40.376	125°06.833
16. Jul	22–59	16:20	16:32	0:12	44°40.500	125°06.833	44°40.500	125°05.500
21. Jul	42–1	05:31:17	05:42:15	0:10	44°39.631	125°06.833	44°39.631	125°05.500
21. Jul	42–2	05:46:53	05:58:19	0:11	44°39.755	125°05.500	44°39.755	125°06.833
21. Jul	42–3	06:03:11	06:14:37	0:11	44°39.879	125°06.833	44°39.879	125°05.500
21. Jul	42–4	06:18:55	06:30:37	0:11	44°40.003	125°05.500	44°40.003	125°06.833

A6   Sonar tracks 18kHz

21. Jul	42–5	06:30:37	06:47:04	0:16	44°40.127	125°06.833	44°40.127	125°05.500
21. Jul	42–6	06:51:12	07:02:55	0:11	44°40.252	125°05.500	44°40.252	125°06.833
21. Jul	42–7	07:07:31	07:18:59	0:11	44°40.376	125°06.833	44°40.376	125°05.500
21. Jul	42–8	07:23:30	07:34:00	0:10	44°40.500	125°05.500	44°40.500	125°06.833
21. Jul	42–9	07:34:00	07:44:10	0:10	44°40.500	125°06.833	44°39.631	125°06.833
21. Jul	42–10	07:49:30	07:59:28	0:09	44°39.631	125°06.667	44°40.500	125°06.667
21. Jul	42–11	08:03:05	08:13:18	0:10	44°40.500	125°06.499	44°39.631	125°06.499
21. Jul	42–12	08:17:42	08:28:40	0:10	44°39.631	125°06.334	44°40.500	125°06.334
21. Jul	42–13	08:32:29	08:42:46	0:10	44°40.500	125°06.167	44°39.631	125°06.167
21. Jul	42–14	08:48:02	08:58:28	0:10	44°39.631	125°06.000	44°40.500	125°06.000
21. Jul	42–15	09:02:02	09:12:40	0:10	44°40.500	125°06.833	44°39.631	125°06.833
21. Jul	42–16	09:17:27	09:28:12	0:10	44°39.631	125°06.666	44°40.500	125°06.666
21. Jul	42–17	09:31:55	09:42:29	0:10	44°40.500	125°06.500	44°39.631	125°06.500
21. Jul	42–18	09:42:29	09:54:59	0:12	44°39.631	125°05.500	44°39.631	125°06.833
21. Jul	42–19	09:58:03	10:10:21	0:12	44°39.755	125°06.833	44°39.755	125°05.500
21. Jul	42–20	10:14:19	10:25:53	0:11	44°39.879	125°05.500	44°39.879	125°06.833
21. Jul	42–21	10:29:58	10:41:45	0:11	44°40.003	125°06.833	44°40.003	125°05.500
21. Jul	42–22	10:46:39	10:57:51	0:11	44°40.127	125°05.500	44°40.127	125°06.833
21. Jul	42–23	11:03:20	11:13:55	0:10	44°40.252	125°06.833	44°40.252	125°05.500
21. Jul	42–24	11:18:30	11:29:50	0:11	44°40.376	125°05.500	44°40.376	125°06.833
21. Jul	42–25	11:34:50	11:46:30	0:11	44°40.500	125°06.833	44°40.500	125°05.500
21. Jul	42–26	11:47:00	11:57:30	0:10	44°40.500	125°05.500	44°39.631	125°05.500
21. Jul	42–27	12:01:00	12:12:30	0:11	44°39.631	125°05.666	44°40.500	125°05.666
21. Jul	42–28	12:16:35	12:27:40	0:11	44°40.500	125°05.833	44°39.631	125°05.833
21. Jul	42–29	12:31:26	12:42:00	0:10	44°39.631	125°06.000	44°40.500	125°06.000
21. Jul	42–30	12:46:12	12:57:00	0:10	44°40.500	125°06.167	44°39.631	125°06.167
21. Jul	42–31	13:00:20	13:10:50	0:10	44°39.631	125°06.334	44°40.500	125°06.334
21. Jul	42–32	13:15:00	13:26:00	0:11	44°40.500	125°06.499	44°39.631	125°06.499
21. Jul	42–33	13:30:00	13:40:16	0:10	44°39.631	125°06.667	44°40.500	125°06.667
21. Jul	42–34	13:44:00	13:54:52	0:10	44°40.500	125°06.833	44°39.631	125°06.833
21. Jul	42–35	13:54:52	14:06:00	0:11	44°39.631	125°06.833	44°39.631	125°05.500
21. Jul	42–36	14:10:20	14:21:20	0:11	44°39.755	125°05.500	44°39.755	125°06.833
21. Jul	42–37	14:25:44	14:37:40	0:11	44°39.879	125°06.833	44°39.879	125°05.500
21. Jul	42–38	14:41:50	14:52:40	0:10	44°40.003	125°05.500	44°40.003	125°06.833
21. Jul	42–39	14:57:22	15:08:20	0:10	44°40.127	125°06.833	44°40.127	125°05.500
21. Jul	42–40	15:14:20	15:26:58	0:12	44°40.252	125°05.500	44°40.252	125°06.833
21. Jul	42–41	15:33:01	15:44:57	0:11	44°40.376	125°06.833	44°40.376	125°05.500
21. Jul	42–42	15:52:02	16:04:02	0:12	44°40.500	125°05.500	44°40.500	125°06.833
21. Jul	42–43	16:15:29	16:26:17	0:10	44°40.500	125°06.833	44°39.631	125°06.833
21. Jul	42–44	16:33:37	16:43:51	0:10	44°39.631	125°06.667	44°40.500	125°06.667
21. Jul	42–45	16:50:59	17:01:53	0:10	44°40.500	125°06.499	44°39.631	125°06.499
21. Jul	42–46	17:06:05	17:15:58	0:09	44°39.631	125°06.334	44°40.500	125°06.334
21. Jul	42–47	17:19:56	17:30:26	0:10	44°40.500	125°06.167	44°39.631	125°06.167
21. Jul	42–48	17:34:26	17:44:44	0:10	44°39.631	125°06.000	44°40.500	125°06.000
21. Jul	42–49	17:48:32	17:59:12	0:10	44°40.500	125°06.833	44°39.631	125°06.833
21. Jul	42–50	18:03:02	18:13:22	0:10	44°39.631	125°06.666	44°40.500	125°06.666
21. Jul	42–51	18:17:35	18:28:07	0:10	44°40.500	125°06.500	44°39.631	125°06.500
27. Jul	73–1	02:47:30	03:03:10	0:15	44°39.631	125°06.833	44°39.631	125°05.500
27. Jul	73–2	03:09:00	03:25:11	0:16	44°39.755	125°05.500	44°39.755	125°06.833
27. Jul	73–3	03:30:09	03:46:19	0:16	44°39.879	125°06.833	44°39.879	125°05.500
27. Jul	73–4	03:51:41	04:08:15	0:16	44°40.003	125°05.500	44°40.003	125°06.833
27. Jul	73–5	04:12:45	04:29:15	0:16	44°40.127	125°06.833	44°40.127	125°05.500
27. Jul	73–6	04:34:31	04:50:45	0:16	44°40.252	125°05.500	44°40.252	125°06.833
27. Jul	73–7	04:55:33	05:12:05	0:16	44°40.376	125°06.833	44°40.376	125°05.500
27. Jul	73–8	05:16:41	05:32:55	0:16	44°40.500	125°05.500	44°40.500	125°06.833
27. Jul	73–9	05:32:55	05:47:52	0:14	44°40.500	125°05.500	44°39.631	125°05.500
27. Jul	73–10	05:52:44	06:08:00	0:15	44°39.631.	125°05.666	44°40.500	125°05.666
27. Jul	73–11	06:12:10	06:27:18	0:15	44°40.500	125°05.833	44°39.631	125°05.833

A7   Foram sampling list

Foram Sampling: A total of 7 multicores were used in sampling for foramanifers. This accounts for one core from every multicoring site on this cruise. Aside from the first two coring sites each core was sliced into 1/2cm intervals for the first 6 cm and then at 1cm intervals from 6-12 cm. A piston and measuring rings aided in this process. No samples were taken after 12 cm. From each slice the sediment was placed into 125 ml Nalgene bottles labeled with coring site and centimeter depth from core. After all samples were taken formalin containing rose bengal stain was added, about a half an inch per bottle, to preserve and stain the forams. Each bottle was then stored in the cold room awaiting to be analyzed at OSU.

AT9906-3MC-2

Date: July 1-99
Core Diameter: 9.5cm
Number of Samples: 15
Sample Depths: 0-12cm at 1cm intervals
12-18cm at 2cm intervals

Notes:
Observed at channel-looking feature beginning at 5.5cm and at 1cm in diameter. Black/sandy possibly made up of iron.

AT 9906-7MC-3

Date: July 3-99
Core Diameter: 9.5cm
Number of Samples: 11
Sample Depths: 0-10cm at 1cm intervals
10-10.5cm

Notes:
Beginning at 6cm core was split down the middle. One side was harder, lighter in color, and clay. The other side was darker, softer, and containing more water.

AT 9906-13MC-8

Date: July 5-99
Core Diameter: 9.5cm
Number of Samples: 18
Sample Depths: 0-6cm at 1/2cm intervals
6-12cm at 1cm intervals

Notes:
Core was virtually containing no sea life on surface through observation. No clams or carbonates. Clay appeared from 10cm on out.

AT 9906-20MC-3

Date: July 7-99
Core Diameter: 9.5cm
Number of Samples: 18
Sample Depths: 0-6cm at 1/2cm intervals
6-12cm at 1cm intervals

Notes:
Removed a red-orange colored Amphipod/Crustacea. Mud turned to clay at 8cm on out.

AT 9906-22MC-5

Date: July 7-99
Core Diameter: 9.5cm
Number of Samples: 18
Sample Depths: 0-6cm at 1/2cm intervals
6-12cm at 1cm intervals

Notes:
A lot of mud in this core, saved the remaining. AT 7-8cm observed an orange rust-colored cylinder about 1/3cm in diameter. It stood vertical and was hollow.

AT 9906-30MC-5

Date: July 10-99
Core Diameter: 9.5cm
Number of Samples: 18
Sample Depths: 0-6cm at 1/2cm intervals
6-12cm at 1cm intervals

Notes:
Mud became firmer about 6cm down. Also saved remaining core.

AT 9906-35MC-5

Date: July 11-99
Core Diameter: 9.5cm
Number of Samples: 18
Samples Depths: 0-6cm at 1/2cm intervals
6-12cm at 1cm intervals

Notes:
Sample a little disturbed, water was drained in freezer. Saved remaining mud and stored in cold room.

Date	Stat. No.	Time (UTC) at bottom	Time (UTC) off bottom	Start Lat. (NS) at bottom	Long. (EW)	End Lat. (NS) off bottom	Long. (EW)	Working area	Remarks	Tapes color (c'), black & white (b'/w')	Slides slides/quality/processing
	SO143-1a										
8.7.99	4-1	13:41	21:16	44° 50,24'	125° 53,67'	44° 50,15'	125° 01,32'	BSR Outcrop, SL 100	winch works incorrect	2 c' & 2 b'/w'	527 / + / a & b
9.7.99	7-1	13:44	18:38	44° 26,99'	125° 02,44'	44° 27,01'	124° 53,98'	SE of HR	winch works incorrect	1 c' & 1 b'/w'	764 / + / a
10.7.99	10-1	13:32	22:41	44° 36,88'	125° 00,24'	44° 36,86'	125° 10,21'	HR, Vents, Fauna		3 c' & 3 b'/w'	600 / + / a
11.7.99	13-1	13:28	16:32	44° 44,68'	125° 06,99'	44° 40,67'	125° 02,73'	Kontinental side of N-HR	laser incorrect	1 c' & 1 b'/w'	757 / + / a (incomplete) & b
11.7.99	14-1	18:25	22:51	44° 35,14'	124° 56,49'	44° 35,13'	125° 02,15'	E of HR, pockmarks	winch works incorrect	2 c' & 2 b'/w'	504 / + / a
	SO143-1b										
15.7.99	20-1	13:24	16:51	44° 34,15'	125° 8,49'	44° 34,20'	125° 08,36'	S-HR		1 c' & 1 b'/w'	770 / - / a
17.7.99	27-1	14:27	16:58	44° 34,69'	124° 58,48'	44° 34,69'	125° 01,13'	E of HR		1 c' & 1 b'/w'	613 / - / a
17.7.99	28-1	18:31	21:21	44° 33,90'	125° 08,51'	44° 34,65'	125° 11,19'	SW of HR		1 c' & 1 b'/w'	678 / - / a
18.7.99	33-1	18:28	22:30	44° 35,95'	124° 57,33'	44° 35,46'	125° 01,81'	SE of HR, pockmarks		1 c' & 1 b'/w'	653 / - / a
19.7.99	37-(1-3)	20:45	4:05	44° 35,97'	124° 57,31'	44° 40,60'	125° 02,50'	N-HR		2 c' & 2 b'/w'	799 / - / a
22.7.99	44-1	13:08	20:37	44° 50,11'	124° 47,95'	44° 50,21'	124° 59,71'	BSR Outcrop, SL 100		2 c' & 2 b'/w'	800 / + / a
23.7.99	53-1	3:58	5:02	44° 33,91'	125° 08,84'	44° 34,75'	125° 08,75'	S-HR		1 c' & 1 b'/w'	524 / - / a
25.7.99	57-1	4:23	6:46	44° 36,91'	125° 09,95'	44° 36,97'	125° 12,86'	Saddle HR, 10-1 continue		1 c' & 1 b'/w'	575 / + / a
25.7.99	58-1	8:37	10:22	44° 37,56'	125° 06,00'	44° 37,60'	125° 03,89'	E slope of Northern Summit		1 c' & 1 b'/w'	526 / + / a
25.7.99	59-1	11:53	18:18	44° 44,01'	125° 01,86'	44° 44,02'	125° 52,88'	Seismic Line 8a		2 c' & 2 b'/w'	790 / - / b
26.7.99	66-(1-2)	14:40	19:46	44° 43,13'	125° 14,58'	44° 44,05'	125° 14,34'	NW Knoll	stop at 17:12:27	2 c' & 2 b'/w'	784 / + / a
28.7.99	75-(1-2)	3:17	4:30	44° 43,65'	125°13,11'	44° 40,49'	125° 07,30'	NW Knoll		2 c' & 2 b'/w'	710/+/ a
	SO143-2										
2.8.99	81-(1-2)	4:12	7:29	44° 33,56	125° 08,03'	44° 34,81'	125° 09,51'	Beaver Mounts	no compass correction	1 c' & 1 b'/w'	800
2.8.99	82-1	9:51	13:21	44° 34,16'	125° 08,61'	44° 34,20'	125° 08,88'	Beaver Mounts	no compass correction	1 c' & 1 b'/w'	805
3.8.99	87-1	7:52	10:03	44° 40,09'	125° 18,02'	44° 40,50'	125° 18,09'	First Ridge	no compass correction	2 c' & 2 b'/w'	780
4.8.99	93-1	6:20	9:42	44° 44,21'	125° 13,82'	44° 44,03'	125° 15,03'	NW-Knoll	no compass correction	1 c' & 1 b'/w'	800
4.8.99	94-1	12:20	15:44	44° 32,73'	125° 08,79'	44° 34,52'	125° 07,66'	South HR		1 c' & 1 b'/w'	800
7.8.99	111-1	5:19	8:42	44° 37,70'	125° 07,67'	44° 38,49'	125° 11,37'	Incipient Headwall	no compass correction	1 c' & 1 b'/w'	800, camera defect
7.8.99	112-2	11:11	13:50	44° 40,11'	125° 05,35'	44° 40,48'	125° 07,38'	N-HR		1 c' & 1 b'/w'	644
8.8.99	121-1	10:38	13:58	44° 50,52'	124° 56,76'	44° 48,98'	124° 57,55'	BSR Outcrop, SL 100		1 c' & 1 b'/w'	802
10.8.99	129-1	4:14	6:45	44° 36,54'	125° 11,08'	44° 38,54'	125° 10,33'	Saddle w-basin		1 c' & 1 b'/w'	604
11.8.99	132-1	5:36	8:58	44° 44,08'	125° 12,60'	44° 44,38'	125° 14,74'	NW-Knoll		1 c' & 1 b'/w'	802
11.8.99	133-1	11:04	15:30	44° 34,17'	125° 07,93'	44° 33,71'	125° 12,70'	S-HR		2 c' & 2 b'/w'	831
14.8.99	154-1	6:05	9:52	44° 49,52'	124° 53,14'	44° 51,14'	124° 55,71'	BSR Outcrop, SL 100	without CTD	1 c' & 1 b'/w'	800
14.8.99	155-1	12:47	16:00	44° 45,77'	124° 55,51'	44° 48,81'	124° 59,75'	BSR Outcrop	without CTD	1 c' & 1 b'/w'	766
20.8.99	192-1	6:31	10:52	44° 40,02'	125° 06,47'	44° 40,18'	125° 06,65'	N-HR		2 c' & 2 b'/w'	792
20.8.99	192-2	12:25	15:52	44° 39,96'	125° 06,43'	44° 40,35'	125° 06,59'	N-HR		1 c' & 1 b'/w'	800
	SO143-3										
27.8.99	211-1	14:16	0:21	45° 35,83'	125° 08,55'	45° 35,77'	125° 15,00'	North Area, R1		3 c' & 3 b'/w'	329
28.8.99	213-1	16:49	23:21	44° 39,49'	125° 00,82'	44° 39,72'	125° 08,16'	N-HR		2 c' & 2 b'/w'	458
29.8.99	216-1	17:16	22:04	44° 40,46'	125° 04,97'	44° 40,44'	125° 09,99'	N-HR, SL 9		2 c' & 2 b'/w'	535
31.8.99	223-1	20:26	4:28	44° 35,14'	125° 04,28'	44° 35,16'	125° 12,95'	S-HR, SL 2		3 c' & 3 b'/w'	499
1.9.99	224-1	7:05	10:07	44° 41,01'	124° 51,90'	44° 42,80'	124° 49,67'	Daisy Bank Fault	Data-online interrupt	1 c' & 1 b'/w'	356
1.9.99	225-1	11:21	13:00	44° 49,50'	124° 48,43'	44° 48,61'	124° 50,47'	South of the BSR Area		1 c' & 1 b'/w'	450
2.9.99	231-1	4:45	9:00	44° 27,02'	125° 01,54'	44° 26,80'	125° 02,45'	SE-Knoll		2 c' & 2 b'/w'	326
2.9.99	232-1	10:09	11:53	44° 23,98'	125° 00,14'	44° 24,00'	125° 00,14'	SE-Knoll, southern Area		1 c' & 1 b'/w'	573

Summary 46 tracks

Vortrag über Aufsehen erregen
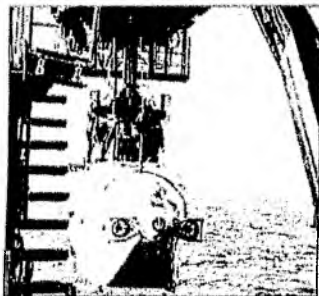
Das Tiefseetauchboot „Alvin", das auch bei der Suche nach dem Wrack der „Titanic" eingesetzt war, wird zu Wasser gelassen, um „brennbares Eis" zu orten. Foto: ARCHIV

hl Bönningstedt – Sieben Hochschullehrer der Kieler Christian-Albrechts-Universität – darunter eine Professorin – haben der Bönningstedter Sektion der Schleswig-Holsteinischen Universitäts-Gesellschaft (SHUG) ihre Zusage gegeben, im Frühjahr Vorträge aus ihren jeweiligen Fachbereichen zu halten. Die Themen wurden von den SHUG-Mitgliedern ausgewählt und mit einem brandaktuellen Vortrag ergänzt.

Tiefseeforscher des Geomar-Instituts der Kieler Uni haben nämlich im Pazifischen Ozean eine sensationelle Entdeckung gemacht: große Mengen „gefrorenes Gas" oder auch „brennbares Eis" – wissenschaftlich: „Methan-Hydrate". Es handelt sich also um Methangas, das unter tiefen Temperaturen und hohem Druck zu festen Körpern zusammengepresst wird.

Das Vorkommen vor der amerikanischen Westküste ist etwa so groß wie der Harz und stellt eine unerschöpfliche Energiequelle dar – sofern der wirtschaftliche Abbau gelingt. Das Methangas stellt allerdings auch eine nicht zu unterschätzende Gefahr für das Weltklima dar. Außerdem werden riesige Methangas-Vorkommen inzwischen auch mit dem bisher unerklärlichen Verschwinden von Schiffen und Flugzeugen im Bermuda-Dreieck in Verbindung gebracht.

Am Mittwoch, 19. Januar, berichtet Dr. Gerhard Vohrmann über diese Aufsehen erregende Entdeckung. Der Wissenschaftler war an Bord des Forschungsschiffes und spricht aus unmittelbarem Erleben. Zudem ist er bereit, auf Fragen einzugehen.

Weitere Vorträge: Am Montag, 31. Januar, referiert Dr. Peter

'UNG 8./9. Jan Sonnabend/S

den Fund im Pazifik

Rautenberg über „Neue gefährliche Viruserkrankungen", am Donnerstag, 10. Februar, spricht Dr. Peter Nitsche über „Deutsche und Polen – das deutsch-polnische Verhältnis seit den Teilungen" und am Mittwoch, 23. Februar, steht der hundertste Vortrag der SHUG in Bönningstedt auf dem Programm. Dann spricht Professorin Regina Mronski über „Gifte in Haus und Garten".

„Im Schatten von Maastricht – Gedanken zum britischen Deutschlandbild nach der Wiedervereinigung" lautet das Thema, das Dr. Jürgen Elvert am Dienstag, 7. März, behandelt. Am Mittwoch, 15. März, spricht Professor Dr. Johannes Schilling über „Die Reformation in Schleswig-Holstein", und am Mittwoch, 15. März, erläutert Professor Dr. Johannes Verreet Modelle zur „Sicherung der Welternährung".

Die Vorträge finden in der Schule Rugenbergen an der Ellerbeker Straße in Bönningstedt statt und beginnen jeweils um 20 Uhr. Die Teilnahmegebühr beträgt fünf Mark. SHUG-Mitglieder haben freien Eintritt.

„Brennbares Eis"
in der Amtsschule

Kieler Wissenschaftler klären auf

Bönningstedt (fra). Sieben Hochschullehrer der Christian-Albrechts-Universität zu Kiel haben zugesagt, im Frühjahr Vorträge aus ihrem Fachbereich in Bönningstedt zu halten. Die Themen wurden von den Mitgliedern der Sektion ausgewählt. Die Themenvielfalt reicht von neuen gefährlichen Viruserkrankungen über die Sicherung der Welternährung bis zu der sensationellen Entdeckung der Tiefseeforscher vom GEOMAR-Institut. Heute berichtet Dr. Gerhard Bohrmann über die aufsehenerregende Entdeckung. Die Veranstaltung beginnt um 20 Uhr in der Bönningstedter Schule Rugenbergen an der Ellerbeker Straße. Der Eintritt kosten fünf Mark.

Bohrmann und seine Kollegen von der Uni Kiel haben im Pazifischen Ozean „gefrorenes Gas" oder „brennbares Eis",

wissenschaftlich „Methan-Hydrate" in großen Mengen entdeckt. Es handelt sich um Methangas, das unter tiefen Temperaturen und hohem Druck zu festen Körpern zusammengepresst wird. Das Vorkommen vor der amerikanischen Westküste ist etwa so groß wie der Harz und stellt damit eine schier unerschöpfliche Energiequelle dar – sofern der wirtschaftliche Abbau gelingt. Aber auch die Gefahr für das Weltklima ist nicht zu unterschätzen. Methan ist ein Treibhausgas. Wird es freigesetzt, kann dies katastrophale Auswirkungen für die Umwelt haben.

Methanhydrate, kommen in vielen Weltmeeren vor. Sie werden auch in Verbindung gebracht mit Phänomenen wie dem Verschwinden von Schiffen und Flugzeugen im Bermudadreieck.
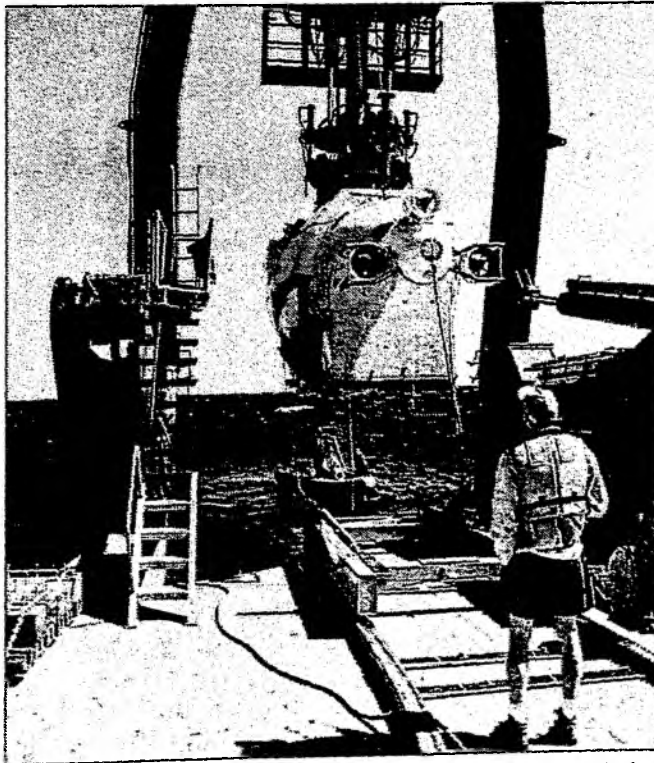
Das Tiefseetauchboot „Alvin", das auch bei der Suche nach der Titanic eingesetzt wurde, ortet im Pazifik das „brennende Eis".

IN DER ERDKRUSTE LAGERN GEWALTIGE MENGEN
METHANHYDRAT. DER ROHSTOFF KANN VIELE
ENERGIEPROBLEME LÖSEN – ABER AUCH DAS WELTKLIMA
ZUM KIPPEN BRINGEN

VON GERALD TRAUFETTER

Energie
ohne Ende

stoff bildet sich besonders an den Kontinentalschelfkanten", hat Geologe Bohrmann entdeckt. Dort wirkt er wie Mörtel und bindet bei seiner Entstehung das lockere Sediment an den Felsuntergrund. So verhindert er das Abrutschen des Gesteins in die Tiefsee.

Dennoch ist das Stoffgemisch sehr instabil. Die Methanmoleküle sind nur so lange im Kristallgitter des gefrorenen Wassers eingebunden, wie der Druck von 800 bis 900 Meter Wassertiefe und eine Temperatur um 4 Grad herrschen. Das Meerwasser darf sich nicht erwärmen, ansonsten löst sich die Eisstruktur auf – in einem Kubikmeter Eis sind 164 Kubikmeter Gas komprimiert. Unterhalb des Methanhydrat-Schildes sitzt häufig ein riesiger Pfropf gasförmigen Methans, weil an vielen Stellen des Meeresbodens Erdwärme aufsteigt. „Ein Horror-Szenario wäre es, wenn beim Anbohren eines Methanhydrat-Feldes das große Stück eines Kontinentalschelfhanges abrutscht", warnt Jürgen Mienert, deutscher Professor an der Universität von Trondheim: „Ein Szenario, für dass es in der Erdgeschichte einige Beispiele gibt."

Vor rund 15 000 Jahren rutschten entlang der gesamten norwegischen Küste über 100 Meter der Kontinentalschelfkante ab. Überall an Land hat Mienert Spuren der riesigen Tsunami-Flutwelle gefunden, die von einer derart gewaltigen Unterwasserlawine ausgelöst wurde. „In den Fjorden schaukelte sich die Flutwelle bis zu einer Höhe von 20 Metern auf", hat Mienert berechnet.

Nicht nur Förderplattformen wären bedroht. Weitaus dramatischer könnten die Folgen für das Weltklima sein. Vor rund 55 Millionen Jahren soll schlagartig freigesetztes Methanhydrat für eine in der Klimageschichte der Erde einzigartige Erwärmung des Planeten verantwortlich gewesen sein. Diese These vertritt der australische Paläo-Ozeanograf Gerald Dickens nach Auswertung von Bohrkernen aus Meeressediment. 1 Billion Tonnen Methanhydrat, so schätzt Dickens, seien plötzlich freigesetzt worden und auf dem Weg zur Wasseroberfläche zum Treibhausgas Kohlendioxid oxidiert.

Andere Klimaforscher vermuten, die Erderwärmung war nicht Wirkung des freigesetzten Methanhydrats, sondern dessen Ursache. „Schließlich könnte sich das Methanhydrat auch wegen der in der Wärmeperiode gestiegenen Temperatur des Ozeans aufgelöst haben", erklärt Mienert und fordert angesichts dieses sich selbst verstärkenden Mechanismus die Klimamodelle für die kommenden Jahrhunderte neu zu berechnen: „Wenn es weltweit immer wärmer wird, könnten die Methanhydrat-Speicher zerstört werden."

Viele Wissenschaftler halten Methanhydrat für die Büchse der Pandora und würden das brennende Eis lieber als ewige Energiereserve unangetastet lassen. Mögliche Fördertechniken sind wegen des Risikos Treibhausgase freizusetzen sehr teuer. „Am einfachsten wäre sicherlich, das gasförmige Methan unter der Hydrat-Schicht anzuzapfen. Das funktioniert wahrscheinlich sogar mit der heutigen Technik", sagt Statoil-Ingenieur Helge Kongsjorden. Viel mehr Aufwand kostet es, das Hydrat selbst aufzulösen. „Denkbar wäre, warmes Wasser oder ein Taumittel in die Hydrat-Schicht zu pumpen", sagt Christian Beckervordersandforth vom Essener Ruhrgas-Konzern. Das ausströmende Methangas müsste mit Trichtern aufgefangen werden, ehe es sich zu Kohlendioxid zersetzt.

Alle diese Abbaustrategien sind derzeit preislich nicht mit denen bei Erdgas und Öl konkurrenzfähig. „Doch wenn die Reserven zur Neige gehen, schießen die Preise in die Höhe", sagt Volker Meyn vom Clausthaler Erdölinstitut. „Innerhalb kurzer Zeit könnte sich der Methanhydrat-Abbau rechnen." Selbst für Peter Hennicke, Vizepräsident des Wuppertal-Institutes für Klima, Umwelt und Energie, der auf eine effiziente Energienutzung und Wind- und Sonnenkraft setzt, könnte Methanhydrat im künftigen Energiemix durchaus eine Rolle spielen: „Interessant wäre es nach entsprechender Risikoabschätzung auch als Ersatz für die Atomenergie. Im Übrigen," findet Hennicke, „sollte man das Fördergeld für die Kernfusion eher in die Methanhydrat-Forschung stecken."

An der Wasseroberfläche schäumen die weißen Brocken. Auf dem Deck des Forschungsschiffs knacken und zerspringen sie wie Eiswürfel im Whisky-Glas. Doch dann hält Gerd Bohrmann eine Feuerzeugflamme unter den Klumpen aus milchigem Eis und bringt das physikalische Weltbild der Beobachter ins Wanken: Der gefrorene Block brennt plötzlich mit roter Flamme.

Was die Geologen des Kieler Geomar-Zentrums vom Grunde des Pazifiks hochgefördert haben, ist Methanhydrat – eine Verbindung des Sumpfgases Methan mit Wasser. „Bei einem ganz bestimmten Verhältnis von Druck und Temperatur wird das Methan in einen Molekülkäfig aus gefrorenem Wasser eingeschlossen", beschreibt Bohrmann die Hydrat-Bildung. In allen Weltmeeren lagern mächtige Schichten aus Methanhydrat, die aus verrottenden Mikroorganismen entstanden sind. Auch in den Dauerfrostböden Sibiriens, Alaskas und Kanadas hat man den rätselhaften Stoff entdeckt.

Wissenschaftler schätzen das Gesamtvolumen auf fast 10 Trillionen Kubikmeter. „Das ist ein doppelt so großer Energiespeicher wie alle Erdöl-, Kohle- und Gasreserven auf diesem Planeten zusammen". rechnet Bohrmann vor. Deshalb halten einige Forscher den erst seit wenigen Jahrzehnten entdeckten Rohstoff für die Lösung aller irdischen Energieprobleme. Kritische Kollegen betrachten Methanhydrat allerdings als Zeitbombe.

Bei der Verbrennung von Methan entsteht das Klimagas Kohlendioxid. Mehr Gefahr droht dem Temperaturhaushalt der Erde allerdings durch reines Methangas, das aus den Ozeanen emporsteigt. „Methan hat ein 30-mal höheres Treibhaus-Potenzial als Kohlendioxid", warnt Bohrmann. Auch deswegen spielen Energiekonzerne das Interesse am noch jungen und umstrittenen Energieträger herunter. „Wirtschaftlich", erklärt Helge Kongsjorden vom norwegischen Statoil-Konsortium, „ist die Förderung noch uninteressant." Die weltweit bekannten Öl- und Gasreserven seien viel billiger zu fördern und halten selbst bei stetig steigendem Verbrauch weitere 60 Jahre.

Doch ohne großes Aufsehen zu erregen erforschen die Unternehmen, wie an die Vorkommen aus der Tiefsee heranzukommen ist. „Das Energie-Potenzial ist einfach zu gewaltig, als dass die Konzerne es ignorieren könnten", sagt Volker Meyn vom Institut für Erdöl- und Erdgasforschung in Clausthal. Allen voran Japan: In Zukunft, so hofft die Industrienation, könnte sie dank riesiger Methanhydrat-Vorkommen vor ihrer Küste unabhängig von Energieimporten werden.

In diesen Wochen startet die Japan National Oil Corporation mit einem Forschungsaufwand von etwa 120 Millionen Mark (61,4 Mio. €) eine Bohrung vor der Halbinsel Omasaki. „In fünf bis zehn Jahren müssten wir technisch in der Lage sein, die Vorkommen abzubauen", prophezeit Hydrat-Forscher Ryo Matsumoto von der Tokioer Universität. Nach einer Testbohrung in Alaska hatte der Staatskonzern 1998 einen weiteren Anlauf im Permafrostboden Kanadas gestartet.

Echte Pionierarbeit leistet derzeit das russische Gasimperium Gasprom, dessen Ingenieure per Zufall auf eine Methanhydrat-Schicht gestoßen sind. Im sibirischen Permafrostboden zapften die Russen eine konventionelle Gaslagerschicht an, die aber nach oben durch eine Lage aus Methanhydrat abgedichtet ist. Durch die Erdgasförderung verringerte sich der Druck auf das Methanhydrat, das sich jetzt langsam zersetzt und nun abgeschöpft wird.

Unvergleichlich schwerer ist an die Vorkommen aus der Tiefsee zu kommen. Viele noch ungeklärte Rätsel über die Eigenschaften der mysteriösen Eisklumpen verhindern ihre Gewinnung. Ölbohrfirmen fürchten die Tücken des Untersee-Hydrats. Anfang der 90er Jahre wäre im Golf von Mexiko eine Bohrplattform beinahe umgekippt, als die Ingenieure versehentlich eine Methanhydrat-Schicht angebohrt hatten. Alptraum jeder Besatzung von Bohrschiffen ist eine plötzlich aufsteigende Methanblase. Schlagartig verringert sich dann die Tragkraft des Wassers, das Boot sinkt binnen Minuten – so könnte sich auch das mysteriöse Verschwinden von Schiffen im methanhydratreichen Bermuda-Dreieck erklären lassen.

Noch ist Grundlagenforschung nötig, denn erst in den 40er Jahren stießen die Chemiker auf Gashydrate. Zuerst entdeckte man sie in Gas-Pipelines. Das eisige Material ver-

ZUR SACHE

Methanhydrat-Vorräte
Schätzung in Milliarden Kubikmeter

Offshore-Gebiete	5756
Permafrost-Landgebiete	3003
Permafrost-Schelfgebiete	632

Ein Brocken **METHANHYDRAT** *(Foto oben); die weltweiten Vorkommen dieses Rohstoffs könnten doppelt so viel Energie liefern wie alle Reserven an Öl, Kohle und Erdgas zusammen*

stopfte die Leitungen und ließ sie platzen. 30 Jahre später stießen russische Forscher in den Permafrostböden Sibiriens auf Methanhydrat. In den 80er Jahren förderten amerikanische Geologen erstmals kleine Klumpen des Stoffs vom Meeresboden. „Der Roh-
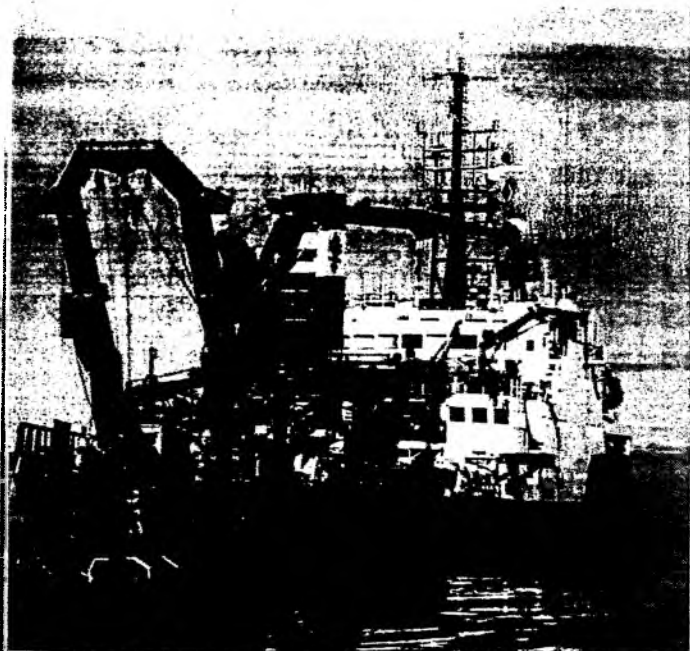
Foto: GEOMAR/Bornfeld

46

NEUE ENERGIE LEW

So heiß wie vor 55 Millionen Jahren war es seitdem nie wieder auf der Erde: in der Arktis wuchsen damals subtropische Wälder, in Alaska lebten Krokodile. Auslöser dieser Klimaveränderung, so vermuten Santo Bains und Kollegen von der Oxford University in England in der aktuellen Ausgabe des Wissenschaftsmagzins Science, war Sumpfgas Methan: In einer eisähnlichen Verbindung mit Wasser, dem sogenannten Methanhydrat, lagerte es in riesigen Mengen im Meeresboden. Wie Untersuchungen der Forscher zeigen, muss das Treibhausgas durch einen noch unbekannten Mechanismus in die Atmosphäre gelangt sein und stellenweise eine globale Erwärmung ausgelöst haben.

Diese Zeitbombe schlummert auch heute im Ozean: Zehntausend Milliarden Tonnen Kohlenstoff, schätzen selbst konservative Geologen, lagern als Methanhydrat an den Kontinentalhängen, am Boden der Polarmeere und in den Permafrostgebieten – das ist doppelt soviel Kohlenstoff, wie alle bekannten Erdöl-, Kohle- und Erdgasreserven der Welt enthalten. Würden nur acht Prozent des eisigen Methans freigesetzt, berechneten Forscher um Gerald Dickens von der Universität von Michigan in einem Modell, würde das ausreichen, um die Erdoberfläche um zwei Grad zu erwarmen.

Schlote, aus denen Gasblasen perlen

Dass das Methaneis keineswegs stabil ist, zeigt die Expedition des deutschen Forschungsschiffes „Sonne". Vor der Küste des US-Bundesstaates Oregon untersuchen deutsche und amerikanische Forscher seit Wochen den „Hydratrücken", ein Unterwasser-Gebirge von der Größe des Harz, das besonders reich an Methanhydrat ist. Bei Tauchgängen mit dem Drei-Mann-Forschungs-U-Boot „Alvin" entdeckten die Wissenschaftler mehrere 15 Zentimeter große Schlote, aus denen Gasblasen perlten. „Wir konnten jetzt zum ersten Mal dokumentieren, dass aus Hydratrücken großen Mengen Methan ins Meer gelangt", sagt Gerhard Bohrmann vom Geomar-Forschungszentrum an der Universität Kiel. Das Gas, vermuten er und seine Kollegen, kommt nicht aus den obersten Zentimetern des Meeresbodens, sondern aus größerer Tiefe. In den obersten 140 Metern herrschen am südlichen Gipfel des Hydratrückens ein genügend hoher Druck und eine genügend niedrige Temperatur, damit sich aus Methan und Wasser die Käfigverbindung Methanhydrat bildet (siehe nächste Seite). Weiter unten wird es dem Eis zu heiß. Die Erdwärme löst die Verbindung in Wasser und gasformiges Methan auf, das unter der Schicht aus dem festen Hydrat gefangen ist. Am Südgipfel hat es sich offenbar seinen Weg nach oben gebahnt. „Das Methan muss schlagartig durch die Hydratzone schießen – sonst würde es ja dort gefrieren", erläutert Bohrmann seine Theorie.

Bevor das Gas in die Atmosphäre gelangen könnte, muss es allerdings noch viele hundert Meter Meerwasser durchqueren. Dort sind noch Kapazitäten vorhanden, um reichlich Methan zu lösen. Im Wasser wird Methan zudem schnell zu Kohlendioxid oxidiert und ist eine beliebte Nahrung für Bakterien. Trotzdem erscheint es Bohrmann möglich, dass das Treibhausgas vor Oregon die Barriere überwindet.

2 cm

1,25 mm

Methanhydrat am Meeresboden ist eine unermessliche Rohstoffreserve – und eine Gefahr für das Klima
von Ute Kehse

"Das Potenzial, dass es in die Atmosphäre gelangt, ist gegeben." Die Auswertung von entsprechenden Messungen erwartet der Kieler Forscher mit Spannung.

Hydrat wird durch Erosion freigelegt

An den Flanken des Hydratrückens stießen die Kieler Forscher auf Methanhydrat, das offen zu Tage trat: Größere, weiße Brocken, vermischt mit dem grauen Meeresschlamm. *„Das Hydrat wird durch Erosion freigelegt"*, erklärt Bohrmann, *„das zeigt, dass der Meeresboden wenige Millimeter bis Zentimeter unter der Oberfläche von dem Zeug durchtränkt ist."* Dorthin gelangt das Methan durch Bakterien: An Stellen, wo viel organisches Material zum Meeresboden sinkt, wird der Sauerstoff schnell verbraucht. Die Tier- und Pflanzenreste müssen dann anaerob abgebaut werden, wobei Methan entsteht. Ab Wassertiefen von 300 Metern und bei Temperaturen um den Gefrierpunkt verbindet sich das Gas mit dem Meerwasser im Porenraum zu einem Feststoff – eben Methanhydrat. Bevorzugte Lagerstätten sind die Kontinentalhänge – dort, wo der Meeresboden vom flachen Schelf zur Tiefsee hin abfällt. Auch in sogenannten „Akkretionskeilen" – Stellen, wo die ozeanische Meereskruste gegen einen Kontinent stößt und die aufliegenden Sedimente abgeschabt und zwischen

den Platten keilförmig verdickt werden – ist oft Methanhydrat zu finden. Rund um den Pazifik, vor der Ostküste der USA, vor Norwegen, Pakistan, Südafrika – weltweit vor den Küsten durchsetzt das Treibhausgas den Meeresboden vor den Küsten.
Neben den Klimaforschern, die noch nicht so recht wissen, wie sich Warm- und Kaltzeiten auf das merkwürdige

Organische Kohlenstoffe der Erde

Gashydrate enthalten weltweit mehr organischen Kohlenstoff als alle anderen irdischen Vorräte zusammen. Sie übertreffen sogar die Menge der fossilen Energieträger um das Doppelte.
(Angaben in Milliarden Tonnen)

Erdöl, Kohle, Erdgas: 5.000

Böden: 1.400
gelöste organische Substanzen: 980
terrestrische Biosphäre: 830
Torf: 500
partikuläre organische Substanzen: 60
Atmosphäre und marine Biosphäre: 6,6
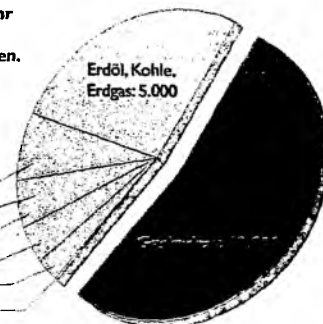
Eis auswirken und umgekehrt, interessieren sich allmählich auch Erdölindustrie und Politiker für Methanhydrat. Die unermesslichen Mengen sind eine verlockende, verhältnismäßig saubere Rohstoffquelle – Methan ist schließlich der Hauptbestandteil von Erdgas. So hat das amerikanische Department of Energy im letzten Frühjahr ein Programm konzipiert, das die kommerzielle Förderung von Methanhydrat bis zum Jahr 2015 ermöglichen soll. Die

Japan National Oil Company hat im vergangenen Jahr zusammen mit dem Konzern Exxon erste Versuche in Alaska unternommen, den Stoff abzubauen.
Das ist allerdings nicht einfach. Erdölingenieure haben noch keine Ahnung, wie sich Methanhydrat schnell und effektiv auflösen lässt. Im Prinzip gibt es drei Möglichkeiten: Man könnte

Chemikalien in den Meeresboden spritzen, die den Schmelzpunkt herabsetzen, die Temperatur erhöhen – etwa mit heißem Wasser –, oder den Druck erniedrigen. *„Alles zu teuer oder zu langwierig"*, winkt Volker Meyn vom Institut für Erdöl- und Erdgasforschung in Clausthal-Zellerfeld ab. Chemikalien wie Methanol oder Glykol könnten Methaneis zwar zum Schmelzen bringen, aber nicht schnell genug, als dass es sich für die gewinnorien-

**Schatzsuche:**
Mit einem „Staubsauger" sammeln Wissenschaftler Methaneis am Meeresboden.

48

tierte Industrie lohnen würde. Da das Methanhydrat im Gegensatz zu konventionellen Erdöllagerstätten nicht durch eine undurchlässige Gesteinsschicht abgeschlossen ist, müsste man eventuell einen künstlichen Deckel über die Hydratfelder legen, damit das aufgelöste Methan nicht einfach ins Meerwasser entweicht.

Die Hydratnutzung ist bisher ungewiss

Vielversprechender erscheint es da, Gebiete wie den Hydratrücken anzubohren, wo freies Gas unter der Hydratzone liegt. Dabei würde sich wahrscheinlich auch ein Teil des Hydrats mit auflösen, weil der Druck von unten nachlässt. Diese Methode hält der Chemiker Dendy Sloan vom Zentrum für Hydratforschung an der Colorado School of Mines für die Vielversprechendste. Mit Hilfe dieser Druckentlastung haben die Russen anscheinend in den Siebzigerjahren im sibirischen Messoyakha-Gasfeld auch Methan aus Hydraten gefördert. Im dortigen Permafrostboden überdeckt eine Schicht aus Gashydrat eine Erdgaslagerstätte. Sloan gibt an, dass bis zu 36 Prozent des in Messoyakha geförderten Gases aus Hydrat stammen. Noch aus einem dritten Grund weckt Methanhydrat das Interesse der Geologen: Es ist wahrscheinlich für gewaltige Rutschungen am Meeresboden verantwortlich. Das Eis wirkt in den Porenräumen als Zement für den breiigen Meeresschlamm und stabilisiert dadurch die steilen Kontinentalhänge. Löst es sich auf, kommt die Pampe ins Rutschen. Das kann die gefürchteten Tsunamis auslösen, meterhohe Flutwellen, die auch bei Seebeben entstehen – so geschehen vor 8400 Jahren vor der Küste von Norwegen bei der sogenannten Storegga-Rutschung. Eine besonders gewagte Theorie macht solche Rutschungen für das geheimnisvolle Verschwinden von Schiffen und Flugzeugen im Bermuda-Dreieck verantwortlich: An den fraglichen Stellen vor der Küste Floridas stimmen die Zonen, in denen man Rutschungen beobachtet hat, und Gashydratfelder fast genau überein. Wenn sich nun eine Gashydrat-Schicht in Bewegung setzt, so die Überlegung, könnte freies Gas aus darunter liegenden Schichten in großen Blasen emporquellen. Gerät ein Schiff oder auch ein Flugzeug in eine solche Blase, hat es nicht mehr genügend Auftrieb und wird ohne Vorwarnung in die Tiefe gesogen.
Für die Geologen-Gemeinde sind solche Szenarien schlicht Unsinn. In kleinerem Maßstab kann sich das Gas
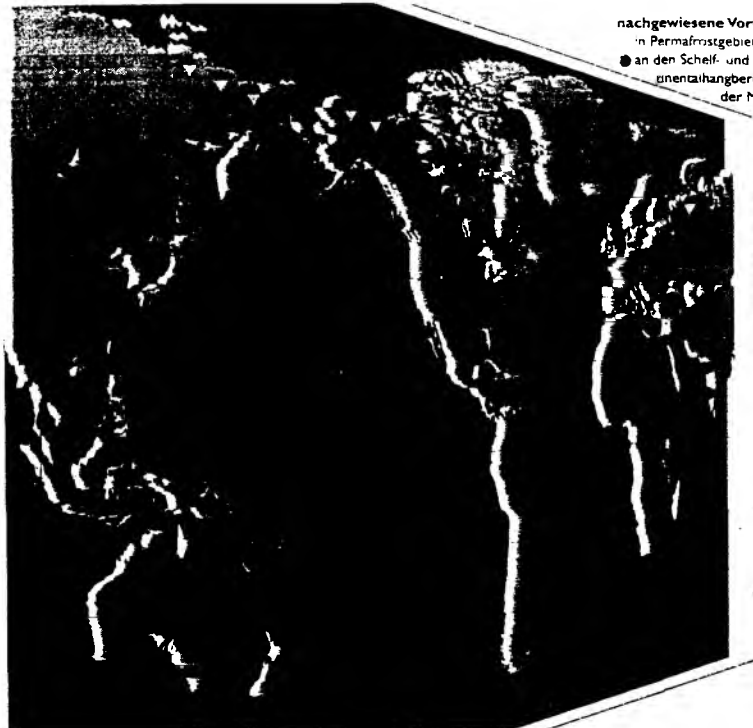
aber durchaus gewaltsam den Weg bahnen: Geologen der Bundesanstalt für Geowissenschaften und Rohstoffe fanden in der arktischen Laptewsee und am Makkran-Akkretionskeil vor Pakistan am Meeresboden sogenannte Pockmarks: Krater von 20 bis 30 Metern Durchmesser, die offenbar durch Gasausbrüche entstanden waren. Eine
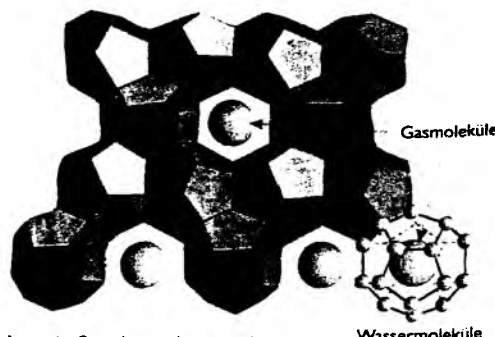
Methanhydrat

... sieht aus wie gewöhnliches Eis. Dass es das nicht ist, beweist ein Streichholz: Die Klumpen verbrennen mit einer gelblich-blauen Flamme. In dem brennenden Eis ist eine Menge Energie gespeichert, mehr als in Erdgas unter den gleichen Druckbedingungen: Die Moleküle liegen näher zusammen als im gasförmigen Zustand. Unter Atmosphärendruck hätte das in einem Kubikmeter Methaneis gespeicherte Gas ein Volumen von 164 Kubikmetern.
Methanhydrat ist eine sogenannte Einschlussverbindung, in der Fachsprache ein „Clathrat": Wasser und Methan gehen keine chemische Bin-

andere Gefahr halten viele Geowissenschaftler für viel wahrscheinlicher: Ein Ausgasen könnte den Treibhauseffekt verstärken und so die globalen

Klimaveränderungen beschleunigen, warnt beispielsweise auch Andreas Troge, Präsident des Umweltbundesamtes. Das immer größere Wissen über diese „alte Energiequelle" entschärfe die Energieprobleme also nicht. Troge: „Eher das Gegenteil ist der Fall." Auch Geomar-Forscher Gerhard Bohrmann stimmt dieser Einschätzung

Gasmoleküle

Wassermoleküle

dung ein. Stattdessen lagert sich das Methan in Hohlräumen im Kristallgitter des Wassereises ab. Ob das Methaneis stabil ist, hängt vom Druck, von der Temperatur, vom Verhältnis zwischen Wasser und Gas und von der Anwesenheit anderer Stoffe ab. Im Meer entsteht Methanhydrat ab etwa 500 Metern Tiefe bei Temperaturen kurz über dem Gefrierpunkt.

zu: „Methanhydrat ist keine alternative Energiequelle. Wer es als solche betrachtet, der vergisst, an die wirklich alternativen Energieträger zu denken." ●

Die Autorin
Ute Kehse arbeitet als Journalistin in Delmenhorst.

nachgewiesene Vorkommen
in Permafrostgebieten
● an den Schelf- und Kontinentalhangbereichen der Meere

In der Tiefe blubbert es

Welche Bedeutung hat das Methan-Gas für das Klima? Geomar-Forscher ziehen erste Bilanz

Wie Kohlensäure im Wasserglas perlen die Blasen aus dem Meeresboden. Doch was da so harmlos aus den Ritzen in 600 Metern Tiefe blubbert, hat es in sich: Die von Kieler Geomar-Forschern erstmals be- *obachtete Ausströmung von Methan-Gas könnte wesentlich zum Treibhauseffekt, der weltweit registrierten Erwärmung der Atmosphäre, beitragen. „Genaueres wissen wir aber erst, wenn wir den Weg des* *Gases aus der Meerestiefe bis in die Atmosphäre besser verstehen", sagt Geomar-Direktor Prof. Erwin Suess, der nach sieben von insgesamt acht Expeditionen in den Pazifik (wir berichteten) nun Bilanz zog.*

„Brennendes Eis" halten die Forscher Prof. Harry Klinkhammer, Katja Heeschen und Geomar-Direktor Prof. Erwin Suess (von links) in ihren Händen. Das aus 600 Metern Tiefe vor der Küste Oregons geborgene Gashydrat enthält Methan, das sich entzünden lässt. In insgesamt acht Expeditionen soll Entstehung und Bedeutung der Gashydrate vor allem für das Weltklima genauer erforscht werden.   Foto hfr

Seit Mai diesen Jahres versuchen Biologen, Ozeanographen, Geologen und Chemiker dem Geheimnis des *Methans vor der Küste* des US-Staates Oregon im wörtlichen Sinn auf den Grund zu gehen. Gemeinsam mit Kollegen der Oregon State University entdeckten sie mit dem in den USA entwickelten Tauchboot „Alvin" stark sprudelnde Gas-Austrittszonen in einem Unterwasser-Gebirge von der Größe des Harzes.

„Die Menge der ausströmenden Gase ist abhängig von den Gezeiten", beschreibt Suess eines der wichtigsten Forschungser-

gebnisse der Expeditionen: „Denn bei Ebbe sinkt der Druck des Wassers auf die ‚kalten Quellen'. Die Folge ist *ein stärkerer Austritt der Gase* als bei Flut." Dass dieses bislang noch nicht dokumentierte Phänomen überhaupt beobachtet werden konnte, führen die Forscher auf eine „tektonische Störung" im Meeresboden zurück. Das heißt: Die gewaltigen Kräfte sich verschiebender Erdkrusten erzeugen Risse im Meeresboden, *durch die das Gas* ins Wasser austreten kann.

Einen Hinweis auf die riesigen Dimensionen solcher frei werdenden Methan-Mengen erhielten die For-

scher durch ausgedehnte Kalkstein-Vorkommen. Denn Kalk entsteht als Nebenprodukt bei einer Mineral-Ausfällung, sobald Methan in das Wasser gelangt. Als Folge dieser chemischen Reaktion bildeten sich am *Meeresboden Kalkschlote* von bis zu 50 Metern Höhe, aus denen das Gas perlte. „Auf dem Monitor erschien uns diese Unterwasserlandschaft mit ihren Kratern wie ein Wald mit lauter abgestorbenen Bäumen", schwärmt Suess von den Eindrücken der Expeditionen.

Und noch etwas wird den *Wissenschaftlern wohl unvergesslich* bleiben: Die

dampfenden und sich an der Luft zersetzenden Gashydrat-Brocken, die die Greifer der stählernen Proben-Nehmer aus dem Meeresboden bohrten. „Brennendes Eis" tauften die Forscher die Mischung aus gebundenem Methan, Salz und Ablagerungen des Meeresbodens, denn das austretende Gas ist brennbar. „Auch wenn die Methan-Vorkommen *mit Sicherheit* die Menge aller anderen fossilen Brennstoffe wie Öl, Kohle oder Erdgas weit übersteigen, hält sich die Industrie bislang noch zurück", sagt Geomar-Meeresbiologe Dr. Gerhard Bohrmann. „Denn der Abbau wäre auf-

wendig und teuer. Außerdem reichen Gas- und Ölvorräte noch für einige Jahrzehnte."

Und noch eine wenn auch verheerende Eigenschaft besitzt das Methan: Bei entsprechender Menge verringert es die Dichte des Wassers. Folge: Schiffe haben nicht mehr genug Auftrieb und drohen zu sinken. An dieser vor allem in Boulevard-Blättern kolportierten „Lösung" des Rätsels um das Schiffe verschlingende Bermuda-Dreieck will sich Bohrmann aber nicht beteiligen. „Rein theoretisch mag das funktionieren, aber wissenschaftliche Beweise dafür gibt es bislang nicht." (kup)

Brennendes Eis

Forscher suchen im Tiefseeboden nach Erdgasvorräten

Tief unten im Meeresboden liegen große Erdgasvorräte. Sie enthalten nach Einschätzung von Geowissenschaftlern mehr Kohlenstoff, als in allen bekannten fossilen Quellen zusammen gelagert ist. In dieser Woche diskutieren Experten aus zehn Ländern an der Technischen Universität Berlin darüber, wie sich diese Erdgasvorkommen zunächst zu Forschungszwecken anzapfen und dereinst möglicherweise für die Energiegewinnung nutzen lassen.

Mit der herkömmlichen Erdgasgewinnung hat dies nicht allzu viel zu tun. Denn die Gasvorräte verbergen sich in den Sedimenten der Ozeane in kleinen Eiskristallen. Diese schneeähnlichen Gashydrate findet man in nahezu allen Weltmeeren, vor allem aber an Kontinentalabhängen, wo der Boden langsam abfällt.

Vor der Südostküste des US-Bundesstaates South Carolina zum Beispiel sind die Bedingungen besonders günstig. Unter dem nährstoffreichen, kalten Wasser haben die Bodenbakterien mit dem Abbau organischer Substanzen, etwa von Plankton, allerhand zu tun. Das schließlich in der Tiefe bei der Methangärung entstandene Gas, das Methan, wird in einer Art Käfig festgehalten: bei den niedrigen Temperaturen und hohen Drücken, wie sie am Meeresboden herrschen, schließen Wassermoleküle die Gast-Atome ein.

„Die Erdgeschichte hat diese Vorräte geschaffen", sagt Claus Marx vom Institut für Tiefbohrtechnik, Erdöl- und Erdgasgewinnung der Technischen Universität Clausthal. „Und was sich da zusammenballt, stellt alle Vorkommen die wir sonst haben, gewaltig in den Schatten."

Nun rätseln Forscher nicht nur über den vermutlich beträchtlichen Einfluss dieses Methans auf das Erdklima, sondern auch darüber, wie sie den Schatz am Meeresgrund eines Tages bergen könnten, wenn andere Quellen versiegen. Denn bei Wärmeentwicklung oder Druckänderung schmelzen die Eiskristalle, und das Gas verflüchtigt sich. Gelingt es jedoch, sie aus mehreren tausend Metern Tiefe an die Oberfläche zu holen, kann man einen interessanten Effekt beobachten: Die feste Masse brennt, wenn sie angezündet wird. Sie wird deshalb auch als „brennendes Eis" bezeichnet.

Unter Leitung von Hans Amann vom Fachgebiet Maritime Technik der Technischen Universität Berlin entwickeln acht Firmen und Institute aus sechs EU-Staaten derzeit ein neues Probe-Entnahmesystem. „Wir müssen im Sediment schneiden, ohne dass es zur Wärmeentwicklung oder zu Verschiebungen kommt", sagt Amann. Die Probe müsse anschließend in ein Druckgefäß gepackt, hochgezogen und in ein Laborgefäß verfrachtet werden.

„Es ist im Grunde genommen noch nicht mehr, als eine Sprudelwasserflasche zuzukriegen und nach oben zu bringen." Doch unter Experten gilt schon dies als sehr diffizil. „Wir stehen immer noch am Anfang", sagt Amann. Zuerst gehe es darum, das Vorkommen der Gashydrate zu studieren, aber auch, auf welche Weise zerfallende Gashydrate gewaltige Unterwasser-Hangrutsche auslösen können. „Es ist langfristig auch eine Energieressource, die aber nur angegangen werden kann, wenn die offenbar erheblichen ökologischen Implikationen bekannt sind." THOMAS DE PADOVA

Geomar-Forscher im Pazifik unterwegs

Auf der Suche nach der Energie von morgen

Im Meeresboden lagert mehr Energie in Form von Methan, als alle Erdöl-, Erdgas- und Kohlevorräte weltweit zusammengerechnet. Wissenschaftler der Kieler Universität erforschen gegenwärtig an Bord des Forschungsschiffes „Sonne" die Methanvorkommen im östlichen Pazifik.

KIEL

Ullrich Meißner

Noch ist nicht sicher, ob die Wissenschaftler vom Forschungszentrum für marine Geowissenschaften (Geomar) auf die Energiequelle der Zukunft gestossen sind. Gemeinsam mit amerikanischen Kollegen entdeckten sie vor der amerikanischen Westküste, im Pazifik, eine 125 Meter hohe Gasblase. An acht verschiedenen Stellen trat in dem Seegebiet Gas aus, berichtete der Direktor von Geomar, Professor Erwin Suess. Die Blase im südlichen Teil des sogenannten Hydratrückens, besteht aus brennbarem Methan.

Der Hydratrücken ist ein unterseeisches Gebirgsmassiv von der Grösse des Harzes. Darin gebunden sind Methanhydrate, die sehr viel Energie enthalten und auch als brennendes Eis bezeichnet werden (siehe Kasten unten rechts). Die Hydrate dürften weltweit mehr Energie speichern als Kohle, Erdgas und Erdöl zusammen. Doch noch stehen die Forschungen über die Nutzung ganz am Anfang.

Im Zentrum der deutschen Gashydratforschung steht die „Sonne", ein 1969 als Fabrikschiff für den Nordatlantik gebauter Heckfänger, der 1977 zum Forschungsschiff umgebaut wurde. 1991 gab es den zweiten Komplettumbau des knapp 100 Meter langen Schiffes — Stammbesatzung 30 Mann und Platz für 25 Wissenschaftler. Gechartert hat Geomar die „Sonne", die seit Anfang Juni besonders im Raum vor Newport im Pazifik nach den Gashydraten sucht. Erstmals gelang es 1996 mit dem Spezialgreifer der „Sonne", Gashydrate, die nur unter ganz bestimmten Temperatur- und Druckbedingungen stabil sind, an die Oberfläche zu holen. Die an Eis erinnernden Gesteinsbrocken leuchten am Meeresboden schneeweiß und enthalten soviel Methan, das sie mit leicht violetter Flamme an der Oberfläche verbrennen.

Methan-Eis blendete die Videokameras

Aufgefallen waren den Geomar-Forschern die weissen Flecken auf dem Meeresgrund, die förmlich die Objektive der an Kabeln geschleppten gesteuerten Videokameras blendeten. Die Hoffnung, dass es sich dabei um Gashydrate handeln könnte, bestätigte sich nach dem Einsatz des Greifers, der aus mehreren hundert Metern Tiefe erstmals den Stoff an die Oberfläche beförderte.

Um die Entwicklungen der Gashydratfelder im Meeresboden besser verfolgen zu können, will Geomar ein Langzeit-Observatorium vor der Westküste der USA installieren. Erstmals wurden daher von der „Sonne" aus sogenannte Landersysteme am Hydratrücken im Nordostpazifik abgesenkt. Sie messen die ausgetretenen Methangase und Fluide und gleichzeitig deren Langzeitwirkung auf das Ökosystem.

Bis zum erfolgreichen Einsatz im Pazifik konnten die High-Tech-Geräte nur in der Ostsee getestet werden. Mit Begeisterung registrierte Peter Linke, Fahrtleiter der Expedition, den Einsatz der Geräte. Die von Geomar selbst entwickelten Tiefsee-Lander messen ferngesteuert und mehrere Wochen lang selbständig chemische und physikalische Werte. Auf ein akustisches Signal hin kehren sie wieder an die Oberfläche zurück und bringen Proben vom Meeresboden wie Sedimente, Karbonat und Organsimen mit.

Erfolgreich verlief auch der Einsatz des kamerabestückten Videoschlitten, der Bilder von der räumlichen Ausdehnung der Gashydratfelder in rund 1000 Meter Tiefe lieferte. Bei mehreren Fahrten mit dem Tauchboot „Alvin", das unter anderem auch bei der Suche nach der „Titanic" eingesetzt worden war, stellten die Kieler Geologen fest, dass der Hydratrücken von Oregon bei Newport mit schneeweißen Hydratfeldern geradezu gepflastert ist. Bei niedriger Tide sei zudem eine regelrechte Methan-Wolke aus Quellen im Meeresboden aufgestiegen.

Damit sich Methanhydrat in den Ozeanen bilden kann, müssen vier Faktoren zusammenpassen. Methan, das in der Regel aus der Zersetzung organischer Substanz entsteht. Wasser, das an dem Gas übersättigt ist, tiefe Temperaturen von höchstens einigen Grad über dem Gefrierpunkt und ein hoher Druck, wie er ab 500 Meter Wassertiefe vorherrscht. Genau diese Bedingungen finden sich vorrangig an den Schelf und Kontinentalhangbereichen der Meere. Dort findet sich in fast allen Meeren eine Methan-Hydrat Schicht, die vom Boden aus etliche hundert Meter tief in das Sediment hinein reicht. In der Tiefsee hingegen fehlt es an Methan, weil zuwenig organische Substanz vorhanden ist. Auch in den flachen Schelfmeeren, wie etwa der Nordsee, fehlen diese Strukturen, da die Temperaturen nicht tief genug und der Druck nicht hoch genug sind. Ausnahmen gibt es: in den polaren Schelfgebieten wird der eigentlich viel zu geringe Druck durch die sehr niedrigen Temperaturen kompensiert.

Katastrophen durch Hydrate

Auch Ausnahmen für die Tiefsee kommen nach Geomar-Angaben vor, etwa wenn durch ein Randmeer sehr viel organische Substanz in die Tiefe getragen wird.

Die Methan-Hydrate könnten nicht nur ein Segen für die Energiesicherung der Zukunft sein, sondern sich auch ganz schnell in einen regelrechten Fluch verwandeln. Dann nämlich, wenn durch den anthropogenen Treibhauseffekt die Wassertemperaturen steigen. Schon kleinere Schwankungen können dann ausreichen, das Methangas freizusetzen. Die Folge wäre ein erheblicher Zustrom des Treibhausgases in die Atmosphäre und eine rasante Beschleunigung der globalen Klimaänderung, beziehungsweise Aufheizung, ein unheilvoller Kreislauf wäre in Gang gesetzt.

Bedrohlich für fast alle Küsten wären dann aber nicht nur der steigende Wasserspiegel wegen der thermischen Ausdehnung der Meere. Wenn die in den Untergrund eingebettete stabile Struktur durch das Schmelzen des Methaneises plötzlich instabil wird, können ganze Hänge von den unterseeischen Höhenzügen abstürzen und gewaltige Wellen — sogenannte Tsunamis — verursachen. Eines der beeindruckendsten Zeugnisse eines solchen Ereignisses wird im „Spektrum der Wissenschaft - Juni 1999" geschildert. Vor der Küste Norwegens rasten bei der sogenannten Storegga-Rutschung 5600 Kubikkilometer Sedimente als Schlammströme 800 Kilometer weit vom oberen Hang des Kontinentalhanges bis in das Norwegische Becken hinunter. Gewaltige Tsunamis mussen nach Einschätzung der Wissenschaftler die Folge der Katastrophe vor rund 8000 Jahren gewesen sein. Auslöser der Rutschung waren vermutlich Gashydrate in 400 bis etwa 1500 Meter Tiefe, die durch Temperatur- oder Druckveränderungen instabil wurden. Auch natürliche geothermische Vorgänge, wie etwa unterseeische Vulkanausbrüche oder tektonische Plattenverschiebungen können also dazu führen, dass das Methaneis schmilzt.

Flensburger Tageblatt 08.10.99

Gefrorener Schatz aus dem Meer

Brennendes Eis in den Händen von Kieler Geomar-Wissenschaftern an Bord der „Sonne". Die weißen Brocken vom Meeresgrund zerfallen relativ schnell unter dem normalen atmosphärischen Druck. Noch ist ungeklärt, wie die riesigen Energiereserven ausgenutzt werden können. Foto: Geomar

Gashydrate sind eisähnliche Substanzen, die nur bei hohem Druck und niedrigen Temperaturen stabil bleiben. Sie kommen im Meeresboden aller Ozeane oder im Permafrost von Polargebieten vor. Unter normalen Bedingungen (etwa Atmosphärendruck) zerfallen die Gashydrate relativ schnell.

Methan entsteht in der Tiefsee aus der Zersetzung von organischem Material. Übersteigt die Konzentration einen bestimmten Schwellenwert, kommt es im Wasser bei Temperaturen knapp über dem Gefrierpunkt zur Ausbildung der Hydrate. Die Gasmoleküle sitzen eingekapselt im Kristallgitter des gefrorenen Wassers wie winzige Käfige.

Neben Methan enthalten die Hydrate 1,5 bis 3 Prozent Schwefelwasserstoff sowie Spuren von Ethan, Propan und Kohlendioxid. Schätzungen zufolge sollen die Energievorräte in den Methanhydraten die sämtlicher Kohle-, Erdöl- und Erdgasvorkommen der Erde weit übertreffen. Gelangt das Methan in die Atmosphäre, wirkt es als starkes Treibhausgas. Noch ist aber ungeklärt, wie das sehr instabile Methaneis zur Energiegewinnung gewonnen und transportiert werden kann.

Die „Sonne" wurde 1969 als Fabrikschiff für den Nordatlantik von der Bremer Rickmers Werft gebaut. Acht Jahre später erwarb die Bremer RF Reedereigemeinschaft Forschungsschifffahrt GmbH den Heckfänger und baute ihn zu einem Forschungsschiff aus. 1978 ging es dann zur ersten Reise ins Rote Meer, wo Erzschlämme erforscht wurden, anschließend in den Nordatlantik und durch den Panama-Kanal in den Pazifik, auch heute noch das Hauptarbeitsgebiet der „Sonne".

1991, nach 13 Jahren im Dienst der Forschung, lief die „Sonne" dann erstmals wieder einen deutschen Hafen an, um von März bis September in Bremerhaven komplett umgebaut zu werden. Dabei wurde unter anderem eine 10,8 Meter lange neue Schiffssektion eingesetzt, die „Sonne" ist jetzt genau 97,6 Meter lang. Geschätzt wird das Forschungsschiff mit einer Breite von 14,2 Meter und einem Tiefgang von 6,8 Metern wegen seiner sehr guten Seeeigenschaften. „Das Schiff wurde ja für den Einsatz auf dem Nordatlantik — bei jedem Wetter — gebaut", sagt Rainer Duthel, Chefelektroniker und an Bord „Häuptling" der technischen Mannschaft.

Seit genau zehn Jahren fährt der 56jährige von der Bergstraße stammende Duthel auf der „Sonne". Und er weiß wovon er spricht, denn vorher ist er jahrelang auf „normalen Schiffen" zur See gefahren. Daher hat es auch in seiner aktiven „Sonne"-Nordzeit, wie er meint, noch keine brenzlige Situation gegeben, „das Schiff ist absolut sicher, auch wenn die „Sonne"

schon mal vor den Ausläufern eines Hurrikans ablaufen oder aber in schwerster Pazifikwelle gegenan bolzen musste. Die Arbeit an Bord eines Forschungsschiffes ist seiner Einschätzung nach kein Zuckerschlecken, denn der Betrieb läuft rund um die Uhr, 24 Stunden, auch an den Feiertagen, einschließlich Weihnachten und Sylvester. In diesem Jahr allerdings hofft der jetzt in Schafflund (Kreis Schleswig-Flensburg) wohnende Duthel, dass er das Weihnachtsfest bei seiner Familie verbringen kann.

Und mit einem Klischee, weil die „Sonne" ausschließlich im Pazifik fährt, will der vollbartige Duthel aufräumen. „Die aus Hollywoodfilmen hinlänglich bekannten Südseeschönheiten treffen wir nie." Das liegt seiner An-

sicht nach nicht nur daran, dass die Filmdamen durchweg zierliche, auf exotisch geschminkte Schönheiten waren, sondern auch daran, dass Forschungsschiffe nur ganz selten Häfen anlaufen. „Wenn die „Sonne" einmal im Hafen liegt, dann haben wir alle Hände voll zu tun". Die Gebühren für die verschiedenen Institute und Wissenschaftler seien einfach zu hoch, als das lange Hafenliegezeiten bezahlt werden könnten. Allerdings: Jedes Jahr geht die „Sonne" für drei Wochen in die Werft — Safety first.

Duthel, der an Bord unter anderem für den Einsatz von Greifern, Fotoschlitten und der Echtzeitvideoübertragung mit Glasfaserkabeln zuständig ist, hat auch die jüngsten Forschungsfahrten vor der amerikanischen Westküste

zum sogenannten Hydratrücken mitgemacht. Während die Wissenschaftler über das „Methaneis" jubelten, „haben mich die vielfältigen Lebensformen am Meeresgrund am meisten fasziniert", sagt der Schafflunder, der besonders stolz auf seine zwei Röntgenspektrometer ist. „Damit", so Duthel, „ist die Sonne das einzige deutsche Forschungsschiff, das Gesteinsfunde unmittelbar an Bord genau untersuchen kann." Sollte es an Bord einmal zu einem Unfall oder einem Krankheitsfall kommen, gibt es einen Arzt und ein Bordhospital, wo notfalls sogar kleine Operationen vorgenommen werden können.

Duthel bedauert, dass es zwar auf wissenschaftlicher Ebene laufend Austauschprogramme gibt, im technischen

Bereich jedoch gar nicht. „Wir wissen vielfach gar nicht, was für Geräte die Kollegen der anderen Nationen zur Verfügung haben", beklagt er. Reizen würde es ihn daher, einmal auf einem amerikanischen Forschungsschiff mitzufahren, weil dort angeblich eine nicht schlagbare Ansammlung von High-Tech-Geräten versammelt sein soll.

Auch in seinem Urlaub, der nach deutschem Tarif gewährt wird, ist der Schafflunder der See treu. Seit nunmehr drei Jahren ist er Eigner einer hölzernen Ketsch, die in Flensburg beheimatet ist. Die Arbeit an Bord eines Forschungsschiffes mit all der Top-Technik „verdirbt aber auch im Privatbereich." An Bord der Segelyacht finden nur Profigeräte und „kein Spielkram" Platz.

Als Heckfänger für den harten Einsatz im Nordatlantik wurde die „Sonne" einst gebaut. Heute ist sie eines der modernsten Forschungsschiffe und fährt fast ausschließlich im Pazifik. Foto: RF-Reederei

Meeresgeologe Bohrmann zeigt einen Fund aus dem Nordostpazifik: ein Stück Gashydrat mit Meeresablagerungen. Foto aug

Riesige Gasblase in der Tiefsee
Geomar-Forscher entdeckten Bakterienkolonien und Methanvorkommen

Bei Tauchfahrten vor der Küste des US-Bundesstaates Oregan haben Geowissenschaftler aus Kiel einen ausgedehnten Bereich mit einer überdurchschnittlich hohen Methankonzentration im Wasser und größere Bakterienmatten entdeckt; beides Indizien für größere Vorkommen von Gashydraten im Meeresboden. In einem Gemeinschaftsprojekt mit der Oregon State University wollen die Wissenschaftler jetzt weitere Erkenntnisse über die Gasvorkommen in der Tiefsee gewinnen, die als Energiequelle Bedeutung bekommen könnten, die aber auch für Meeresbiologen und Klimaforscher interessant sind (KN berichteten).

Vom deutschen Forschungsschiff „Sonne" aus, das abwechselnd mit der „Atlantis" der Universität von Oregon im Einsatz ist, wurden erstmals sogenannte „Lander"-Systeme am Hydratrücken im Nordostpazifik ausgesetzt. Die bei Geomar in Kiel entwickelten, käfigartigen Gestelle sind mit Meßfühlern, Sonden, Probennehmern und Videokameras bestückt. Sie messen jetzt drei Wochen lang beispielsweise Methan, Sauerstoff, Temperatur und Salzgehalt des Wassers.

Die riesige „Gasblase" liegt im südlichen Teil des Hydratrückens, eines Unterwassergebirges von der Größe des Harzes. „Wir konnten sehen, daß an acht verschiedenen Stellen Gas austritt." berichtete Prof. Erwin Suess, Direktor des Geomar Forschungszentrums für marine Geowissenschaften. Es sei richtig aufgeschwommen und habe sich vom Sediment (den Ablagerungen am Meeresboden) gelöst. Ein deutsch-amerikanisches Forscherteam will nun die Ursachen für den Zerfall der Gashydrate untersuchen.

Dr. Gerhard Bohrmann, Mitarbeiter in der von Prof. Suess geleiteten Abteilung Marine Umweltgeologie, hatte bei zwei Tauchgängen mit dem Tauchboot „Alvin" Gelegenheit, die schneeweißen Hydratfelder zu untersuchen. Spannender, schilderte er, seien jedoch die Gasausdünstungen. „Auf dem nördlichen Gipfel entdeckten wir Schlote von etwa fünfzehn Zentimetern Durchmesser, aus denen massiv Gasblasen aufstiegen – soweit im Wasser erkennbar 15 bis bis 20 Meter hoch." Vom Schiff aus beobachteten die Wissenschaftler mit dem Echolot „Gasfahnen" im Wasser, die bis zu 140 Metern Höhe erreichten. Durch weitere Messungen soll festgestellt werden, ob dieses Methan auch in die Atmosphäre gelangt.   (IN)

Berliner Zeitung

❖

Wissenschaft

·Ein brennendes Problem

Methaneis ist eine unermesslich große Energiereserve – und eine Gefahr für das Klima

Energiegeladenes Eis: Methanhydrat
verbrennt an der Luft mit einer rötlichen Flamme.
Das darin enthaltene Methan ist auch ein
wichtiger Bestandteil von Erdgas.

VON UTE KEHSE

So heiß wie vor 55 Millionen Jahren war es seither auf der Erde nie wieder: In der Arktis wuchsen damals subtropische Wälder, in Alaska lebten Krokodile. Der Grund dafür, so vermuten Santo Bains und Kollegen von der Oxford University in der aktuellen Ausgabe des Fachjournals „Science", war das Sumpfgas Methan. Riesige Mengen davon lagerten in einer eisähnlichen Verbindung mit Wasser, dem „Methanhydrat", im Meeresboden. Wie Analysen der Forscher zeigen, muss das Treibhausgas auf noch unbekanntem Wege in die Luft gelangt sein und die Erwärmung ausgelöst haben.

Diese Zeitbombe schlummert auch heute im Ozean: Zehntausend Milliarden Tonnen Kohlenstoff, schätzen Geologen, lagern als Methanhydrat im Meer und in Dauerfrostgebieten. Das ist doppelt so viel Kohlenstoff, wie alle bekannten Erdöl-, Kohle- und Erdgasvorkommen der Welt enthalten. Würden nur acht Prozent des eisigen Methans freigesetzt, berechneten Forscher um Gerald Dickens von der Universität von Michigan, würde das ausreichen, um die Welt um zwei Grad Celsius zu erwärmen.

Dass das Methaneis keineswegs für immer im Meeresboden bleiben muss, zeigt die Expedition des deutschen Forschungsschiffes „Sonne". Vor der Küste des US-Bundesstaates Oregon untersuchen deutsche und amerikanische Forscher zurzeit den „Hydratrücken", ein Unterwasser-Gebirge von der Größe des Harzes, das besonders reich an Methanhydrat ist. Bei Fahrten mit dem Tiefsee-Tauchboot „Alvin" entdeckten die Wissenschaftler mehrere 15 Zentimeter große Schlote, aus denen Gas perlte. „Wir können jetzt zum ersten Mal dokumentieren, dass am Hydratrücken größere Mengen Methan ins Meer gelangen", sagt Gerhard Bohrmann vom Forschungszentrum Geomar in Kiel. Das Gas kommt vermutlich tief aus dem Meeresboden. In den Schichten darüber herrscht ein genügend hoher Druck und es ist kalt genug, um aus Methan und Wasser Methanhydrat entstehen zu lassen. Weiter unten wird es dem Eis zu heiß: Die Erdwärme löst die Verbindung in Wasser und gasförmiges Methan auf, das dann unter der Schicht aus dem festen Hydrat gefangen ist. Am Südgipfel hat sich das Gas offenbar über die Schlote einen Weg nach oben gebahnt: „Das Methan muss schlagartig durch die Hydratzone schießen – sonst würde es ja dort gefrieren", vermutet Bohrmann.

Bevor es in die Luft gelangen könnte, müsste das Gas aber erst durch viele hundert Meter Meerwasser emporsteigen. Dieses Wasser kann noch reichlich Methan aufnehmen. Mikroben im Ozean wandeln das Gas überdies schnell zu Kohlendioxid um. Trotzdem hält es Bohrmann für möglich, dass das Treibhausgas vor Oregon die Barriere überwindet. „Das Potenzial dafür ist gegeben." An den Flanken des Hydratrückens stießen die Forscher auf Methanhydrat, das offen hervortrat: weiße Brocken, vermischt mit grauem Schlamm. „Der Meeresboden ist von dem Zeug durchsetzt", so Bohrmann.

Der Rohstoff für das Methaneis wird von Bakterien gebildet. An Stellen, wo viel organisches Material zu Boden sinkt, beispielsweise
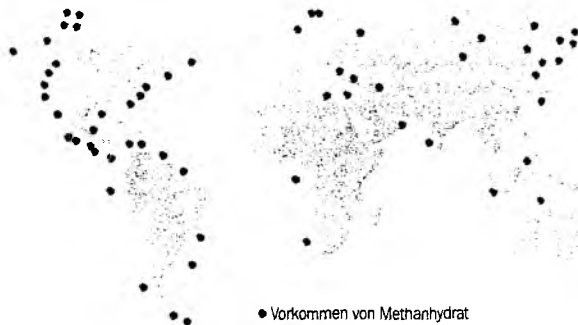
● Vorkommen von Methanhydrat

Methanhydrat kommt sowohl in Dauerfrostgebieten auf dem Land als auch am Boden der Ozeane vor. Im Meer findet man das Methaneis oft in Küstennähe.
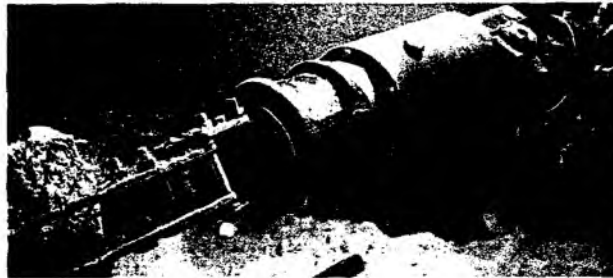
Mit einem Greifarm konnten Kieler Forscher bei früheren Expeditionen mit dem russischen Tauchboot „Mir" Methanhydrat vom Meeresboden nach oben holen.

METHANHYDRAT

Energiereicher als Gas

Im Meer entsteht Methanhydrat in Tiefen von etwa 500 Metern abwärts und bei Temperaturen knapp über dem Gefrierpunkt. Es sieht aus wie Eis und enthält mehr Energie als Erdgas. An der Luft hätte das in einem Kubikmeter Methaneis gespeicherte Gas ein Volumen von 164 Kubikmetern.

Ob Methaneis fest bleibt, hängt vom Druck, von der Temperatur, vom Verhältnis zwischen Wasser und Gas und von der Anwesenheit anderer Stoffe ab. (uk.)

vor großen Flussmündungen, ist der Sauerstoff schnell verbraucht. Die Tier- und Pflanzenreste müssen dann anaerob abgebaut werden, wobei Methan entsteht. In Ozeantiefen von mehr als 300 Metern und bei Temperaturen um den Gefrierpunkt verbindet sich das Faulgas mit Wasser zu Methanhydrat. Häufige Vorkommen gibt es an Kontinentalhängen, wo der Meeresboden vom flachen Schelf zur Tiefsee hin abfällt. Auch an Stellen, wo die ozeanische Erdkruste gegen einen Kontinent stößt, ist oft Methanhydrat zu finden. Ob rund um den Pazifik, vor der Ostküste der USA, vor Norwegen, Pakistan oder Südafrika – das Treibhausgas durchsetzt weltweit den Meeresgrund vor den Küsten (siehe Karte).

Neben den Klimaforschern, die noch nicht so recht wissen, wie Warm- oder Kaltzeiten mit dem merkwürdigen Eis zusammenhängen, interessieren sich auch Erdölindustrie und Politiker für Methanhydrat. Eine schier unermessliche Rohstoffquelle lockt. So hat das US-Department of Energy 1998 ein Programm vorgeschla-

gen, das die kommerzielle Förderung von Methanhydrat bis zum Jahr 2015 ermöglichen soll. Die Japan National Oil Company hat im vergangenen Jahr mit dem Konzern Exxon erste Versuche in Alaska unternommen, den Stoff abzubauen.

Das ist nicht einfach. Erdölingenieure haben noch keine Ahnung, wie sich Methanhydrat schnell und effektiv auflösen lässt. Im Prinzip gibt es drei Möglichkeiten: Man könnte Chemikalien in den Meeresboden spritzen, die den Schmelzpunkt des Methaneises herabsetzen, man könnte die Temperatur erhöhen – etwa mit heißem Wasser – oder den Druck verringern.

„All das ist zu teuer oder zu langwierig", urteilt Volker Meyn vom Institut für Erdöl- und Erdgasforschung in Clausthal-Zellerfeld. Chemikalien wie Glykol könnten Methaneis zwar zum Schmelzen bringen, aber nicht so schnell, dass es sich für die Industrie lohnen würde. Da das Hydrat im Gegensatz zu Erdöllagerstätten nicht durch eine Gesteinsschicht abgeschlossen ist, müsste man eventuell einen Deckel über die Hydratfelder legen, damit das aufgelöste Methan nicht ins Meer entweicht.

Einfacher erscheint es da, Gebiete wie den Hydratrücken anzubohren, wo freies Gas unter der Hydratzone liegt. Dabei würde sich wahrscheinlich auch ein Teil des Hydrats auflösen, weil der Druck von unten nachlässt. Diese Methode hält der Chemiker Dendy Sloan vom Zentrum für Hydratforschung an der Colorado School of Mines für die aussichtsreichste.

Geologen interessieren sich noch aus einem dritten Grund für das Methanhydrat: Es ist wahrscheinlich die Ursache für gewaltige Rutschungen am Meeresboden. Eigentlich wirkt das Methaneis als Zement für den breiigen Meeresschlamm und stabilisiert dadurch steile Kontinentalhänge. Ändern sich aber Druck oder Temperatur, so kann es sich auflösen, der Brei kommt ins Rutschen. Das kann die gefürchteten Tsunamis auslösen, meterhohe Flutwellen, die auch bei Seebeben entstehen.

Eine besonders gewagte Theorie führt das geheimnisvolle Verschwinden von Schiffen und Flugzeugen im Bermuda-Dreieck auf solche Rutschungen zurück. Vor der Küste Floridas stimmen die Zonen, in denen man Rutschungen beobachtet hat, und die Lage der Gashydratfelder fast genau überein. Wenn eine Hydratschicht in Bewegung gerät, so die Überlegung, könnte Gas in großen Blasen emporquellen. Gelangt ein Schiff oder Flugzeug in eine solche Blase, hat es nicht mehr genügend Auftrieb und wird blitzschnell in die Tiefe gesogen.

Viele Experten halten solche Szenarien für Unsinn. Sie sehen die Gefahr, die von Methanhydrat ausgeht, woanders: Ein Ausgasen könnte den Treibhauseffekt verstärken und dadurch die globalen Klimaveränderungen beschleunigen, warnt etwa Andreas Troge, Präsident des Umweltbundesamtes. Das immer größere Wissen über diese „alte Energiequelle" entschärfe die Energieprobleme der Welt also nicht. Troge: „Eher das Gegenteil ist der Fall." Gerhard Bohrmann stimmt diesem Urteil zu und ergänzt: „Methanhydrat ist eben keine alternative Energiequelle. Wer es als solche betrachtet, der vergisst, an wirkliche Alternativen zu denken."

Natur und Wissenschaft
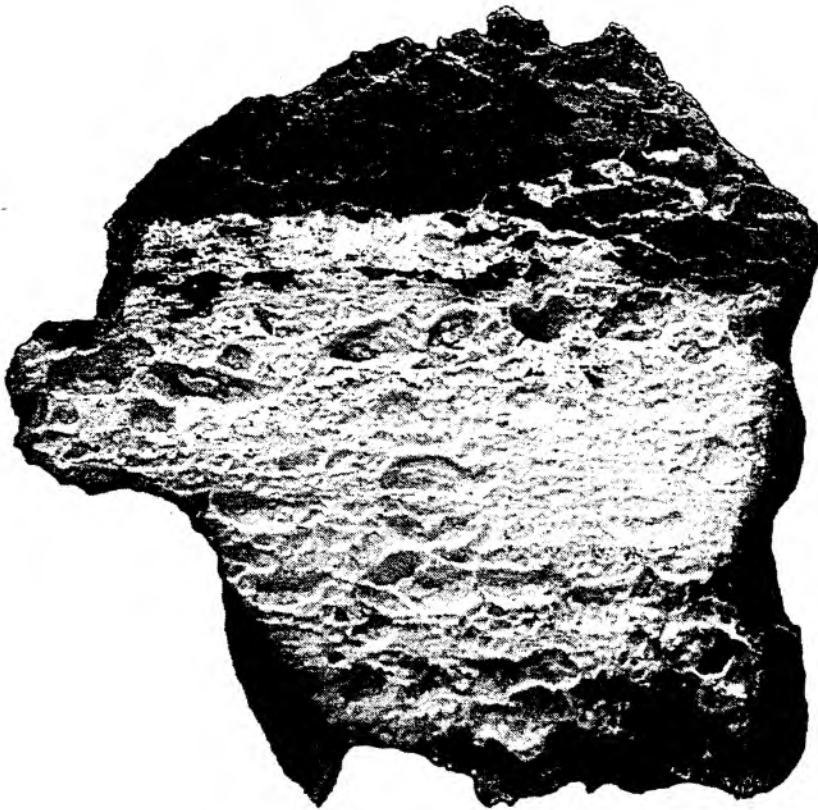
Ein etwa faustgroßer Gesteinsbrocken, der reichlich Methaneis enthält. Das Stück haben Kieler Forscher aus dem sogenannten Hydratrücken vor der Küste Oregons in rund 600 Meter Tiefe gewonnen.

Foto GEOMAR

Natur und Wissenschaft

Gashydrate gestalten Meer und Klima

Extrem unregelmäßige Abgabe von Methan / Lebensraum für Bakterien und Muscheln

Die Untersuchung von Gashydraten spielt inzwischen eine wichtige Rolle in vielen Zweigen der Meereskunde. Geologen interessieren sich für das Methaneis als fossiler Energieträger. Klimaforscher sehen die Gefahr, dass das Treibhausgas Methan möglicherweise im Laufe der Zeit aus auftauenden Gashydraten freigesetzt und damit das Erdklima verändert wird. Gashydrate tragen außerdem zur Stabilität der Hänge des Kontinentalschelfs bei. Schließlich sind sie ein wichtiges Element im Stoffkreislauf zwischen Meerwasser und den Sedimenten des Meeresbodens. Eine internationale Forschergruppe unter Leitung des Geomar-Instituts der Universität Kiel befasst sich in diesem Sommer mit der detaillierten Untersuchung eines Gashydratvorkommens vor der Küste Oregons im Nordostpazifik. Nach mehreren Fahrten mit drei Forschungsschiffen liegen nun erste Ergebnisse vor.

Gashydrate gehören chemisch zur Gruppe der Käfigverbindungen oder Clathrate. Moleküle von Kohlenwasserstoffen und Wasser bilden gemeinsam ein Kristallgitter. In Gashydraten können nicht nur Methan, sondern auch höhere Kohlenwasserstoffe bis zum Pentan gebunden sein. Sie entstehen nur bei hohem Druck und niedrigen Temperaturen. Ein Kubikmeter Gashydrat besteht zu etwa 80 Prozent aus Wassermolekülen. Methan ist darin so dicht gepackt, dass es als Gas bei normalem Luftdruck und Zimmertemperatur ein Volumen von 164 Kubikmetern einnehmen würde.

Im Rahmen der „Tecflux"-Expeditionen, an denen neben dem Geomar-Institut auch Mitarbeiter der Universität Heidelberg sowie mehrerer amerikanischer und kanadischer Institute beteiligt sind, wird der sogenannte Hydratrücken untersucht. Dieser Höhenzug am Meeresboden befindet sich auf dem Kontinentalschelf etwa 150 Kilometer vor der Küste Oregons in Wassertiefen zwischen 700 und 1000 Me-

tern. Der etwa 500 Quadratkilometer große Rücken wurde bei früheren Fahrten mit dem Forschungsschiff „Sonne" entdeckt und nach seinen großen Vorkommen an Gashydraten benannt. Die „Sonne" ist auch das wichtigste Schiff für die laufenden Untersuchungen.

Bei der Analyse zahlreicher, zum Teil mehrere Meter langer Proben, die mit verschiedenen Verfahren dem Meeresboden entnommen wurden, wurde deutlich, dass es im Meeressediment mindestens drei verschiedene Arten von Gashydratschichten gibt. In den obersten 10 bis 20 Zentimetern erinnern die Gashydrate an locker gefügtes Styropor. Zum Teil gibt es darin sogar Methanblasen von mehreren Zentimetern Durchmesser. Mit zunehmender Tiefe im Sediment nimmt auch die Dichte der Gashydratschichten zu. Es können dünne, folienartige Lagen ebenso wie kompakte, fest zementierte Schichten vorkommen. Fast immer bilden sich die Gashydrate an den Grenzen verschiedener Sedimentschichten.

Während der Expeditionen wurde erstmals nachgewiesen, dass die Gashydrate bei ihrer Entstehung das Meerwasser entsalzen. Weil zur Bildung der Käfigmoleküle reines Wasser nötig ist, werden das Chlorid und andere Ionen aus dem Salzwasser gedrängt. Das kann in unmittelbarer Nähe der Gashydratschichten eine erhebliche Erhöhung des Salzgehaltes des Porenwassers im Meeressediment zur Folge haben und damit zum Anfüllen von Mineralen und letztendlich zur Bildung von Gesteinen führen.

Die Zersetzung der Gashydrate vollzieht sich keineswegs mit konstanter Geschwindigkeit, sondern ist zeitlich unterschiedlich. Mit Sonargeräten und chemischen Sonden stellten die Meeresforscher fest, dass die Entgasungsraten einzelner Methanquellen auf dem Hydratrücken innerhalb von wenigen Stunden um den Faktor zehn oder mehr schwanken können.

Das Gashydrat zerfällt dabei in seine zwei Bestandteile, wobei das Methan in Form kleiner Bläschen im Meerwasser aufsteigt. Abhängig von der Wassertiefe und der Temperatur steigen die Bläschen zwischen 40 und 200 Meter über den Meeresboden. Dort löst sich das Methan im Wasser. Die Expeditionsteilnehmer fanden Hinweise darauf, dass die Entgasung möglicherweise von den Gezeitenströmen abhängig ist.

Ähnlich wie um die mineralreichen heißen Quellen in der Nähe der untermeerischen Spreizungszonen, hat sich auch um die Methanquellen auf dem Hydrat-Rücken ein einzigartiges Ökosystem entwickelt. Die meisten Austrittsstellen sind von Bakterienkolonien umgeben, die mehrere Quadratmeter große und einige Zentimeter dicke, weiße und orangefarbene Matten bilden. Über den Metabolismus dieser Bakterien ist noch wenig bekannt. Sicher ist, dass sie ihre Energie aus der Umsetzung von Methan oder Schwefelwasserstoff beziehen. Die Bakterienmatten sind wiederum von Muschelkolonien umgeben, die eine Ausdehnung von bis zu 15 Meter haben.

Welchen Einfluss die Gashydrate auf das Klima haben können, stellten britische und amerikanische Meeresgeologen jetzt unabhängig vom Tecflux-Programm fest. Sie untersuchten zwei Sedimentkerne, die im Rahmen des internationalen Meeresbohrprogramms ODP im Weddell-Meer in der Antarktis und im nordwestlichen Atlantik vor der Küste Südkarolinas erbohrt wurden. Wie die Gruppe um Santo Bains von der Universität Oxford in der Zeitschrift „Science" (Bd. 285, S. 724) schreibt, deuten Isotopenanalysen darauf hin, dass es vor 55 Millionen Jahren an beiden Stellen gewaltige Freisetzungen von Gashydraten gegeben haben muss. Sie könnten zu der starken globalen Erwärmung im Frühtertiär geführt haben. Das Paläozän gilt als die wärmste Epoche der Erdneuzeit.   HORST RADEMACHER

Brennbares Eis im Pazifik entdeckt

Kiel – Geowissenschaftler aus Kiel haben bei Tauchfahrten im nordöstlichen Pazifik vor der Küste des US-Bundesstaats Oregon eine 125 Meter hohe Gasblase entdeckt. „Das entweichende Methangas ist ein sicheres Indiz für größere Vorkommen an Gashydraten", so Prof. Erwin Suess, Direktor des Kieler Geomar Forschungszentrums für marine Geowissenschaften. Der Geomar-Direktor wechselte am Mittwoch vom US- Forschungsschiff „Atlantis" auf das deutsche Forschungsschiff „Sonne". Beide Schiffe sind beteiligt an einem Forschungsprojekt zur Erkundung der Gashydrate.

Von der „Sonne" aus wurde bereits ein neuartiges Tiefsee-Landersystem erfolgreich getestet. Damit sollen in Zukunft austretende Gase und Fluide über Hydratfeldern gemessen werden. Biologen wollen außerdem herausfinden, wie sich die Gasströme langfristig auf das Ökosystem im Meer auswirken.

Gashydrate sind eisähnliche, feste Substanzen, die nur bei hohem Druck und niedrigen Temperaturen stabil bleiben. Sie kommen im Meeresboden aller Ozeane oder im Permafrost von Polargebieten vor. Die Forscher bezeichnen Methanhydrat auch als brennbares Eis. Schätzungen zufolge sollen die Energievorräte in den Methanhydraten die sämtlicher Kohle-, Erdöl- und Erdgasvorkommen der Erde weit übertreffen.

Bis Oktober sind im Bereich des amerikanischen Hydratrückens westlich von Newport insgesamt neun Expeditionen mit vier Forschungsschiffen geplant. Das Großprojekt wird gemeinsam von Geomar in Kiel und der State University in Corvallis (US-Bundesstaat Oregon) getragen.

Von dem Forschungsschiff „Sonne" aus wird ein sogenannter Tiefsee-Lander getestet. Mit dem High-Tech-Gerät sollen ausströmende Gase gemessen werden FOTO: DPA

Brennbares Eis entdeckt

Rätsel um Gasblase im Pazifik

Kieler Forscher: „Das ist die wohl größte Energiequelle der Erde"

nr Kiel – Zeitbombe oder Energiequelle der Zukunft? Auf dem Grund des Pazifiks sind riesige Mengen eines Bodenschatzes entdeckt worden: Methanhydrat, ein eisartiger Stoff aus Methan und Wasser. Er soll energiereicher sein als alle Erdöl- und Kohlevorkommen der Welt, aber auch Naturkatastrophen auslösen können.

Jahrelang gab das „brennbare Eis" auf dem Meeresgrund den Forschern in aller Welt Rätsel auf. Jetzt haben Wissenschaftler des Kieler Geomar Forschungszentrums im nordöstlichen Pazifik eine 125 Meter hohe Gasblase in der Tiefsee entdeckt – der erste Fund dieser Art! Das daraus entweichende Methangas läßt auf noch größere Vorkommen nur 100 Kilometer vor der Küste des US-Staates Oregon schließen. Die Entdeckung des „gefrorenen Rülpsers" gelang mit dem Tiefsee-Tauchboot Alvin, das schon bei der Suche nach dem Wrack der Titanic im Einsatz war.

Die Gaseisblöcke, die bei hohem Druck und Kälte entstehen,

Wie einst bei der Suche nach dem Wrack der Titanic: Das Tiefseetauchboot Alvin wird zu Wasser gelassen. Sechs Forscher aus Kiel waren an der Suche nach dem „brennbaren Eis" auf dem Meeresgrund beteiligt.

sind aus einem unterseeischen Gebirgsmassiv (so groß wie der Harz) zu Tage getreten. Das Gebirge wird als „Hydrat-Rücken" bezeichnet, in dem sich unvorstellbare Mengen von Methanhydraten befinden sollen.

Geomar-Forscher Dr. Olaf Pfannkuche: „Das ist die wohl größte Energiequelle der Erde." Eine industrielle Nutzung sei noch offen. Aber solange das Erdöl auf der Welt nicht teurer werde oder versiege, lohne sich der Abbau des Gases wirtschaftlich noch nicht. Es sei mit dem Erdgas vergleichbar, das schon jetzt aus Sibirien zu uns kommt.

Pfannkuche weist jedoch auch auf die möglichen Gefahren hin. Besonders die Küstenländer seien von dem wundersamen Gasvorkommen aus mehr als 400 Meter Tiefe bedroht. „Die Schwankung des Meeresspiegels und der Wassertemperatur kann eine Explosion auslösen. Das könnte eine Kettenreaktion nach sich ziehen. Am Ende sind Rutschungen der Kontinentalhänge möglich." Schon in der Vergangenheit seien Hänge am Meeresboden durch zerfallenes Methanhy-

drat abgerutscht. Diese Prozesse verliefen ähnlich wie eine Schlammlawine in den Alpen – mit den fatalen Folgen eines Meeresbebens. Pfannkuche: „Es ist möglich, daß Tsunamis (Flutwellen aus dem Meer, d. Red.) auf diese Weise ausgelöst werden."

Ein weiteres Risiko: Methan ist ein sogenanntes Treibhausgas, das in der Atmosphäre zur globalen Erwärmung beiträgt – 30mal stärker als Kohlendioxid (CO_2). Ein Teufelskreis? Wenn sich der Meeresgrund erwärmt und die Gashydrate schmelzen, werden schnell auch große Mengen Methan aus natürlichen Quellen freigesetzt. Was dies aber im Detail für die globale Klimaverän-

derung bedeutet, ist laut Geomar noch weitgehend unbekannt. Andere Forscher machen aufsteigende Methangase sogar für das rätselhafte Verschwinden von Schiffen im Bermuda-Dreieck verantwortlich: Das zu dünne Wasser habe die Schiffe nicht mehr tragen können, vermuten sie. Angeblich könnten sogar Jets vom Himmel gefallen sein, weil Methanwolken in der Luft die Motoren entflammt hätten.

Die Kieler arbeiten mit Kollegen von der Oregon State University zusammen. Neun Expeditionen mit vier Forschungsschiffen und High-Tech-Bohrern sind in diesem Sommer geplant. Kosten: rund 14 Millionen Mark.

Untersucht wird auch das Ökosystem, insbesondere, wie die Organismen im Meer „ihre" Energiequelle nutzen. So können Muscheln mit Hilfe von Bakterien ohne Licht ihre Energie aus Methan und Wasserstoff gewinnen – eine seltene Symbiose.

Schon vor drei Jahren bargen Geomar-Forscher einen Zentner Methanhydrat aus dem Pazifik. Bevor es zerfiel, gelang es noch, einige Eiswürfel anzuzünden.

Flensburger Tageblatt 14.02.99

Methan-Eis Energieträger der Zukunft?

Eis aus der Tiefe: Fluch oder Segen?

Geowissenschaftler aus Kiel haben im Pazifik bei Tauchfahrten eine 125 Meter hohe Gasblase entdeckt. Das darin gefrorene Methangas könnte die Energiequelle der Zukunft sein, gleichzeitig aber auch den Treibhauseffekt noch verstärken.

KIEL/NEWPORT

(lno)

Sie sollen Naturkatastrophen ausgelöst haben und die Erklärung für das legendäre Bermuda-Dreieck sein. Bei der Klimaerwärmung wird ihnen eine unheilvolle Rolle zugeschrieben, doch neuerdings werden sie auch als riesige Energiequelle gehandelt: Methanhydrate, brennbare Formen von Eis im Meeresboden, sind seit Jahren Gegenstand blühender Spekulationen. Geowissenschaftler in aller Welt versuchen das Geheimnis der rätselhaften Gasvorkommen zu lüften, stehen aber noch ganz am Anfang. Im Pazifischen Ozean, 100 Kilometer westlich der Küste des US-Staates Oregon, haben Kieler Geomar-Forscher bei Tauchfahrten eine 125 Meter hohe Gasblase entdeckt.

Schauplatz ist ein Unterwassergebirge von der Größe des Harzes, das auf Anregung der Kieler Meeresforscher offiziell Hydratrücken getauft wurde. „Es war fast so, als ob wir einen Klumpen Eis durch die Wüste transportieren mußten", erinnert sich Prof. Erwin Suess, Direktor des Forschungszentrums Geomar der Universität Kiel, an den seltsamen Fund vor drei Jahren. Als sich der Greifer an Bord des Forschungsschiffes „Sonne" öffnete leuchtete schneeweiß aus dem dunklen Schlamm eine Substanz, die wie Brausepulver schäumte und dabei schmolz. Bevor die Brocken gänzlich zerfielen, wurden sie konserviert. Ver-

einzelt gelang es, Eiswürfel anzuzünden. Sie brannten mit violetter Flamme. Zurück blieb eine Wasserpfütze.

Methanhydrate brauchen tiefes und kaltes Wasser — bei normalen Außentemperaturen zerfallen sie in ihre Bestandteile. Hoher Druck, wie er ab 500 Metern Wassertiefe herrscht, und Temperaturen von höchstens einigen Grad begünstigen ihre Entstehung, sofern zwei weitere Dinge zusammenkommen: Methan aus der Zersetzung organischen Materials und Wasser, das an dem Gas angelagert ist. Daraus bilden sich am Ende die eisähnlichen, festen Stoffe. Reiche Methanhydratfelder finden sich in etwa 875 Meter Tiefe am Kontinentalrand vor Oregon, wo sich die pazifische Platte unter die nordamerikanische Platte schiebt. Dort treten Gase und Fluide in teilweise hoher Konzentration aus dem Meeresboden aus. Sie werden derzeit mit dem Forschungsschiff „Sonne" genau analysiert. Dabei fanden die Kieler auch die Gasblase bei Fahrten mit dem Tauchboot „Alvin", das auch bei der Suche nach der „Titanic" eingesetzt war.

Die riesigen Vorräte an festem Methan im nördlichen Pazifik lassen nach Ansicht der Forscher den Schluß zu, daß dieser Stoff weltweit in großen Mengen vorhanden ist. Mehr noch: Methanhydrate speichern vermutlich doppelt soviel Energie wie alle bekannten Kohle-, Erdöl- und Erdgaslagerstätten. Schon gibt es Pläne zum kommer-

ziellen Abbau der Hydrat-Vorkommen, doch davor warnen Wissenschaftler. Strömt Methan aus dem Ozean in die Atmosphäre, wirkt es als starkes Spurengas. Es trägt 30 Mal stärker zum Treibhauseffekt bei als Kohlendioxid (CO_2).

Das Methan soll auch den Bermuda-Dreieck-Effekt verursachen. Das Meerwasser sei durch aufsteigende Gasblasen zu dünn geworden und habe Frachter nicht mehr tragen können und Jets seien vom Himmel gefallen, weil Methanwolken in der Atmosphäre die Motoren in Brand gesetzt hätten. Wie auch immer — die energiereichen Methanhydrate warten noch auf ihre Erforschung.
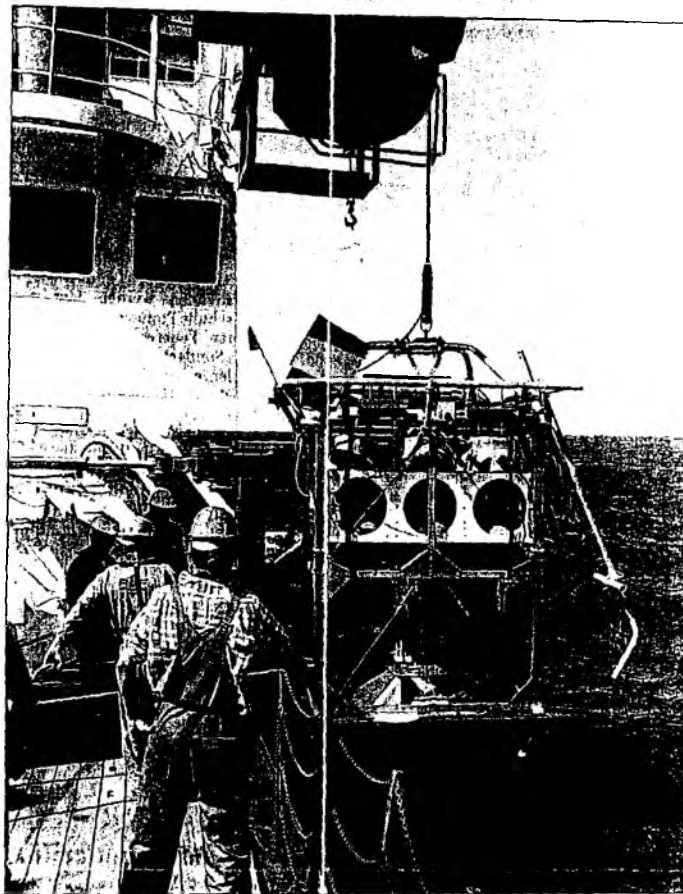
Titanic-erprobt: Der Tiefsee-Roboter der Kieler Forscher an Bord der „Sonne". Foto: dpa

STICHWORT
Moleküle gefangen im Eis

Gashydrate sind eisähnliche Substanzen, die nur bei hohem Druck und niedrigen Temperaturen stabil bleiben. Sie kommen im Meeresboden aller Ozeane oder im Permafrost von Polargebieten vor. Unter normalen Bedingungen (etwa Atmosphärendruck) zerfallen die Gashydrate relativ schnell.

Methan entsteht in der Tiefsee aus der Zersetzung von organischem Material. Übersteigt die Konzentration einen bestimmten Schwellenwert, kommt es im Wasser bei Temperaturen knapp über

dem Gefrierpunkt zur Ausbildung der Hydrate. Die Gasmoleküle sitzen eingekapselt im Kristallgitter des gefrorenen Wassers wie winzige Käfige.

Neben Methan enthalten die Hydrate 1,5 bis 3 Prozent Schwefelwasserstoff sowie Spuren von Ethan, Propan und Kohlendioxid. Schätzungen zufolge sollen die Energievorräte in den Methanhydraten die sämtlicher Kohle-, Erdöl- und Erdgasvorkommen der Erde weit übertreffen. Gelangt das Methan in die Atmosphäre, wirkt es als starkes Treibhausgas. (lno)

Rätsel Bermuda-Dreieck

Sind es Erd-Rülpser?

Es sind unheimliche Eisklumpen, die ohne Frost entstehen. Lösen sie sich auf, können ihre Gasblasen Schiffe versenken.

Wissenschaftler glauben, die Energiequelle der Zukunft entdeckt zu haben – und die Lösung des Rätsels um das Bermuda-Dreieck: die „gefrorenen Rülpser".

Seit Jahrhunderten erzählen sich Seefahrer wunderliche Geschichten aus dem 300 000 Quadratkilometer großen Seegebiet zwischen Florida, Puerto Rico und den Bermuda-Inseln. Allein in den letzten hundert Jahren gingen dort 100 Schiffe und 20 Flugzeuge verloren, mehr als 1000 Menschen.

Was war die Ursache?

Geowissenschaftler aus den USA, Japan und Kiel erforschen die riesigen Methangas-Vorkommen unter dem Meeresboden. Das Methan entsteht in der Tiefsee, wenn organisches Material (abgestorbene Pflanzen) verfault. Bei hohem Druck und Kälte (wenige Grad über Null) bilden sich Methanhydrate. Es sind feste, eisähnliche Klumpen, auch „gefrorene Rülpser" genannt.

Verändern sich die Temperaturen, zerfallen die Brocken in ihre Bestandteile Gas und Wasser. Ein höchst energiereicher, gefährlicher Vorgang mit Folgen:

▶ Das aufsteigende Gas verändert die Oberflächenspannung des Wassers – es trägt auf einmal keine Schiffe mehr. Dies könnte im Bermuda-Dreieck passiert sein.

▶ Unter Wasser rutschen ganze Berghänge ab – so entstehen riesige Flutwellen.

▶ Das Methan wirkt in der Atmosphäre wie ein Treibhausgas – es heizt sie auf, verändert das Klima.

Dennoch gibt es Pläne, die Methanhydrate unter Wasser im großen Stil abzubauen. Denn sie enthalten doppelt soviel Energie wie alle bekannten Kohle-, Erdöl- und Erdgasvorkommen der Welt zusammen.

So sieht ein Klumpen von Methanhydraten aus, brennbares Eis aus dem Meeresboden. Auf der Erde schmelzen die Gashydrate.

Methangas entweicht in die Atmosphäre und heizt sie auf.

Wenn Gashydrate zerfallen, dehnen sie sich aus und lösen unter dem Meer Erdrutsche aus. Das Gas zischt nach oben.

Die Gashydrate (gelbe Zone) schlummern im Meeresboden der Ozeane.

Brennendes Eis im Ozean

Methanhydrate gelten als riesige neue Energiequelle

Newport/Kiel (dpa) – Sie sollen Naturkatastrophen ausgelöst haben und der Grund dafür sein, daß im legendären Bermuda-Dreieck immer wieder Schiffe verschwunden sind. Neuerdings werden sie aber auch als riesige Energiequelle gehandelt: Methanhydrate, brennbare Formen von Eis im Meeresboden, sind seit Jahren Gegenstand blühender Spekulationen. Geowissenschaftler in aller Welt versuchen das Geheimnis der rätselhaften Gasvorkommen zu lüften, stehen aber noch ganz am Anfang.

Im Pazifischen Ozean, 100 Kilometer westlich der Küste des US-Bundesstaates Oregon, hat das Projekt „Tecflux 99" zur Erkundung der „gefrorenen Rülpser" begonnen. Schauplatz ist ein Unterwassergebirge von der Größe des Harzes, das auf Anregung von Kieler Meeresforschern offiziell Hydratrücken getauft wurde. „Es war fast so, als ob wir einen Klumpen Eis durch die Wüste transportieren mußten", erinnert sich Professor Erwin Suess, Direktor des Forschungszentrums Geomar der Universität Kiel, an den seltsamen Fund vor drei Jahren. Als sich der Greifer an Bord des Forschungsschiffes „Sonne" öffnete, kam mehr als ein Zentner Methanhydrat zum Vorschein - die größte Menge, die bis dahin aus dem Meer geholt worden war. Aus dem Schlamm leuchtete schneeweiß eine Substanz, die wie Brausepulver schäumte und schnell schmolz. Vereinzelt gelang es, Eiswürfel anzuzünden, sie brannten mit rötlich-violetter Flamme. Zurück blieb eine Wasserpfütze.

Die erste wissenschaftliche Beschreibung stammt aus dem Jahr 1811, doch erst in den 60er Jahren dieses Jahrhunderts wurden die ersten Vorkommen entdeckt. Die Forscher bezeichnen Methanhydrat auch als brennbares Eis. Methanhydrate brauchen tiefes und kaltes Wasser - bei normalen Außentemperaturen zerfallen sie in ihre Bestandteile. Hoher Druck, wie er ab 500 Metern Wassertiefe vorliegt, und Temperaturen am Gefrierpunkt ermöglichen ihre Entstehung, sofern Methan aus der Zersetzung organischen Materials und Wasser zur Verfügung stehen. Übersteigt die Konzentration einen Schwellenwert, bilden sich am Ende die eisähnlichen, festen Stoffe.

Die riesigen Vorräte an festem Methan im nördlichen Pazifik lassen nach Ansicht der Forscher den Schluß zu, daß dieser Stoff weltweit in großen Mengen vorhanden ist. Mehr noch: Methanhydrate speichern vermutlich doppelt soviel Energie wie alle bekannten Kohle-, Erdöl- und Erdgaslagerstätten. Schon gibt es Pläne zum kommerziellen Abbau. Doch Wissenschaftler mahnen: Strömt Methan in die Atmosphäre, wirkt es als starkes Treibhausgas. Seit langem ist bekannt, daß Methan die Atmosphäre aufheizt, wenn es etwa aus Sumpfgebieten und Reisfeldern oder als Rülpser aus dem Verdauungstrakt von Rindern entweicht. Daß aus Gashydraten freigesetztes Methan in der Vergangenheit bereits das Klima beeinflußt hat, gilt unter Fachleuten als sicher.

Meeresspiegel- und Temperaturschwankungen könnten den Zerfall der Hydrate verursacht haben. Nach Ansicht von Suess hat zerfallendes Methanhydrat unterseeische Hänge zum Abrutschen gebracht: „Das führte wahrschein-
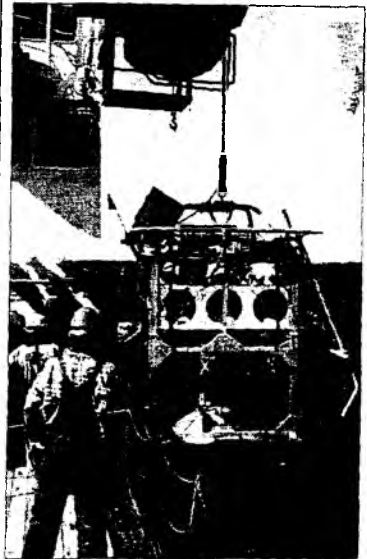
MISSION ERFOLGREICH: *Der von Wissenschaftlern und Technikern des Geomar-Forschungszentrums in Kiel gebaute „Tiefsee-Lander".* Photo: dpa

lich zu großen Flutwellen in Küstengebieten." Andere Forscher verweisen auf das unerklärliche Verschwinden von Schiffen und Flugzeugen im Bermuda-Dreieck: Das Meerwasser sei durch aufsteigende Gasblasen zu dünn geworden um die Frachter zu tragen.

Die USA und Japan wollen in den nächsten fünf Jahren mehr als 100 Millionen Dollar (200 Millionen Mark) für die Forschung an Methanhydraten ausgeben. Deutschland beteiligt sich mit 3,2 Millionen Mark pro Jahr. Die Kieler Hydratforscher wollen mit ihrem Langzeit-Observatorium am Ball bleiben. Bis Oktober sind zusammen mit der Oregon State University neun Unterwasser-Expeditionen geplant - mit vier Forschungsschiffen, einem Tauchboot sowie einem Tiefsee-Landesystem.

Forscher suchen den Schlüssel zum Klima

Größtes Geomar-Projekt startet im Juni

Geomar-Forscher sind zurückgekehrt

Gestern sind sie vom „brennenden Eis" nach Kiel zurückgekehrt: Geomar-Forscher unter der Leitung von Direktor Prof. Erwin Suess hatten während einer mehrwöchigen Expedition vor der Küste des US-Bundesstaates Oregon Methanhydrate aufgespürt. Die im Meeresboden lagernden Vorkommen gelten als Energiequellen der Zukunft, aber auch als tickende Zeitbomben: Da sie sich als Gase in plötzlichen Explosionen entladen können, vermuten Wissenschaftler in ihnen Auslöser für Naturkatastrophen wie Flutwellen. Die jüngsten Forschungsergebnisse hätten größte öffentliche und wissenschaftliche Aufmerksamkeit gefunden, lobte Wissenschaftsministerin Ute Erdsiek-Rave, als sie die Geomar-Mitarbeiter gestern begrüßte. Zum Zeigen hatte Dr. Olaf Pfannkuche sogar einen der „Eisklumpen" mitgebracht, den er und seine Kollegen an Bord des Forschungsschiffes „Sonne" vom Meeresgrund heraufgeholt hatten. (mad)
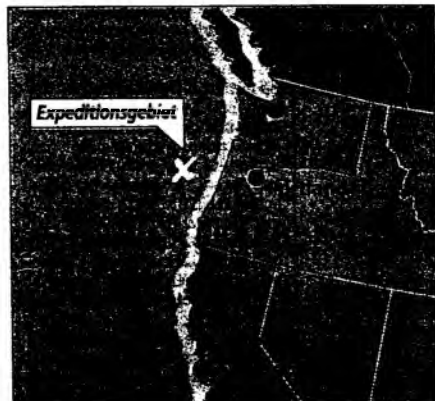
KN. Do, 2.7.1999

Seit einigen Jahren rückt Methan immer mehr ins Blickfeld der Wissenschaft. Kein Wunder, denn die Verbindungen von Wasser und Sumpfgas in der Tiefsee speichern nicht nur mehr Energie als alle Kohle- und Ölvorräte der Erde zusammen. Sie können auch Naturkatastrophen wie Flutwellen auslösen und, wenn sie in die Atmosphäre entweichen, die Erde weiter aufheizen. 1996 stieß eine Arbeitsgruppe des Kieler Forschungszentrums Geomar vor der Küste Oregons auf riesige Methanhydrat-Felder in einem untermeerischen Gebirge. In dieser Region beginnt am 1. Juni die erste von neun deutsch-amerikanischen Expeditionen. Für Geomar ist das mit 19 Millionen Mark geförderte Projekt „Tecflux" das bisher umfangreichste seiner elfjährigen Geschichte.

Geomar-Sprecher Gerhard Haass sparte gestern bei der Presse-Konferenz nicht mit Superlativen: Mit dem Gemeinschaftsvorhaben werde eine neue Dimension in der Methanhydrat-Forschung erreicht. Vier Schiffe, darunter die „Horizon" und die deutsche „Sonne", sind im Einsatz, von denen aus zum größten Teil neuentwickelte Hightech-

Vor der Küste Oregons liegt der von Kielern entdeckte Hydrat-Rücken. Dort beginnen die Expeditionen zur Erforschung von Methanhydrat. Karte KN

Geräte der Spitzenklasse zur Erkundung auf den Meeresgrund geschickt werden, so zum Beispiel das Tieftauchboot „Alvin".

Um Methan näher zu erforschen, brauche man „Tricks", erklärte Geomar-Direktor Prof. Erwin Suess. Denn der brennbare Stoff, der durch Fäulnis entsteht, ändert sich schnell: Unter dem hohen Druck und niedrigen Temperaturen am Meeresgrund bildet er relativ stabile Eiskristalle, doch auf dem Weg an die Wasseroberfläche zerfällt er in Gas-Wolken.

Wie sich diese Methan-Ausbrüche als Treibhausgas auf das Klima auswirken und ab wann sich eine wirtschaftliche Förderung lohnen würde, sind Fragen, die noch offen sind. Doch die Geowissenschaftler Suess, Dr. Olaf Pfannkuche, Dr. Peter Linke und Dr. Gerhard Bohrmann erhoffen sich durch die Expeditionen, mehr Aufschlüsse auf die Mechanismen, wie Methan entsteht, wie Änderungen der Meerwassertemperatur den Zerfall vorantreiben und wo Gefahrenpunkte lauern, weil riesige Austritte untermeeri-

sche Hänge zum Abrutschen bringen könnten.

In der Regel bilden sich Methan-Felder vor allem dort, wo wie vor Oregon Erd-Platten zusammenstoßen. In einer an sich lebensfeindlichen Umgebung schaffen sie noch nicht erforschte „Oasen", so Suess, wo sich Mineralien umbilden und bestimmte Organismen ansammeln. Ein solcher Bewohner ist eine Muschelart, die Methan als Energiequelle nutzt. Solchermaßen gewachsene Muschel-Felder dienten auf diese Weise zur Suche nach Methan-Gebieten, erklärte Linke. Gegenüber der „normalen" Tiefsee erhöhten die Methan-Austritte die Masse der Tiere um etwa das Tausendfache, führte sein Kollege Pfannkuche aus.

Um vor Oregon die Gashydrate zu erfassen, sind Bohrungen in bis zu 2000 Meter Wassertiefe nötig. Dafür wird nach Angaben von Bohrmann ein völlig neuartiges Bohr-System eingesetzt, das auch festes Gestein am Meeresgrund Proben entnehmen kann. Doch auch die von Geomar selbst entwickelten Lander-Geräte arbeiten ferngesteuert – meist in einer Tiefe von 600 bis 700 Metern – tage- und wochenlang auf dem Meeresboden, messen dort chemische und physikalische Daten und sammeln Proben.

Für ihren sensationellen „Gebirgsfund" 1996 haben die Kieler Forscher einen Namen beantragt und genehmigt bekommen: Nach ihrem Vorschlag wird das Gebiet, wo die erste Expedition von Newport (Oregon) aus startet, als „Hydrat-Rücken" künftig in den Seekarten verzeichnet. Die weiteren Expeditionen bis zum 7. Oktober führen dann bis nach San Francisco und Honolulu. Unterstützt wird das Projekt vom Bundesforschungsministerium und von der amerikanischen National Science Foundation. (mad)
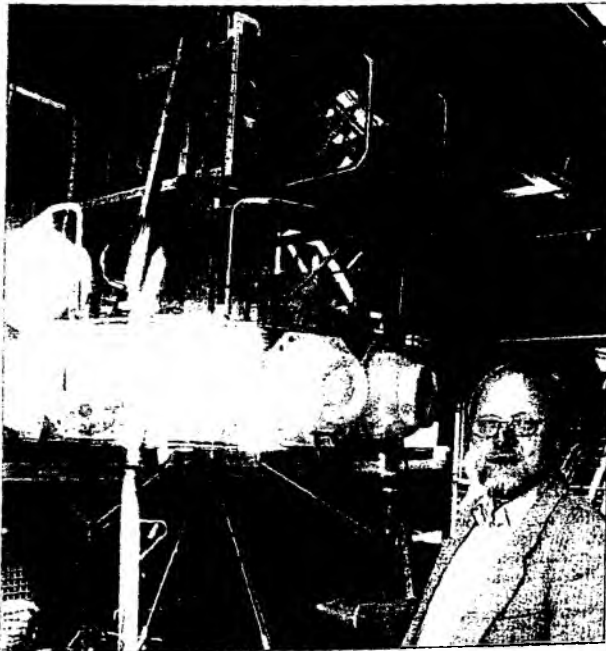
Das Rätsel um die „eisigen Rülpser"

Gas aus dem Meer: Fluch oder Segen?

Newport/Kiel – Was sind eigentlich „Metanhydrate"? Wenn man Wissenschaftlern der Uni Kiel glauben darf, sind diese eisähnlichen, gashaltigen Substanzen die Energiequelle der Zukunft. Man findet sie an Meeresböden aller Ozeane. Wie zum Beispiel im nordöstlichen Pazifik, wo die Forscher jetzt eine gigantische, 125 Meter hohe Eis-Gasblase entdeckten. Einen „gefrorenen Rülpser" von Mutter Erde, sozusagen. Methan birgt jedoch auch Gefahren. Strömt das Gas in die Atmosphäre, trägt es 30 mal stärker zum Treibhauseffekt bei als Kohlen-
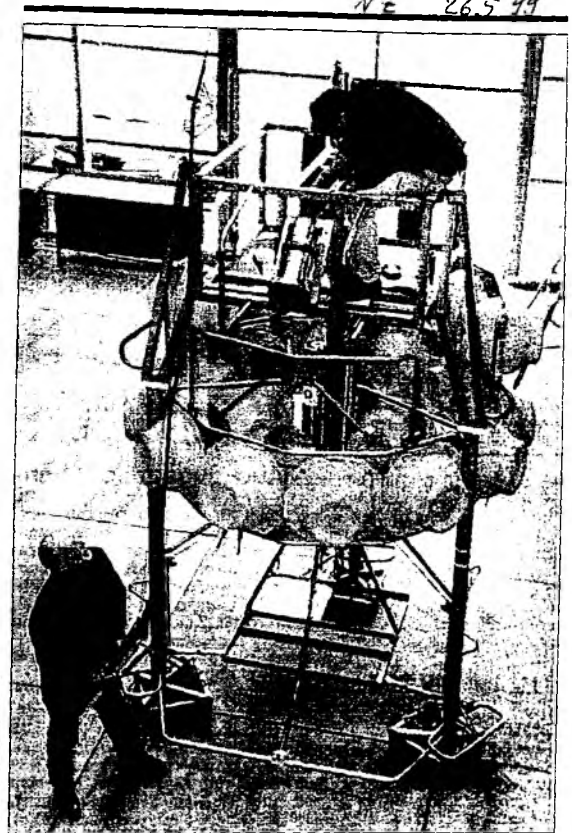
dioxid (CO_2). Zweites Problem: Zerfallenes Methanhydrat bringt unterseeische Hänge zum Abrutschen. Die Folge: verheerende Flutwellen.

Methanhydrate sollen auch hinter mysteriösen Meeresphenomänen wie dem Bermuda-Dreieck stecken. Wenn aufsteigendes Gas das Wasser „verdünnt", kann es die Schiffe nicht mehr tragen; sie gehen unter. Manche Experten sprechen gar von „tickenden Zeitbomen". Mehr als 100 Millionen Dollar wollen die USA und Japan in den nächsten Jahren ausgeben, um das Rätsel zu lösen.

Hamburger Morgenpost 14.7.99

Eisiges Gas aus der Tiefsee

Zwei Mitarbeiter des Geomar Forschungszentrums in Kiel machen ihr Tiefsee-Landersystem reisefertig: Das Gerät soll vor der Küste des US-Bundesstaates Oregon mit Videokamera und Meßsystemen Gasvorkommen eines Gebirges unter dem Meer erkunden. Wasser und Methan aus organischen Ablagerungen haben sich unter hohem Druck und bei niedrigen Temperaturen zu brennbarem Eis verwandelt. Ob die Energien genutzt werden können, ist unklar   Foto: dpa

Während der Expeditionen kommt das von Dr. Olaf Pfannkuche entwickelte Lander-Gerät zum Einsatz: Es soll Proben aus Methan-Quellen entnehmen.   Foto: JKK